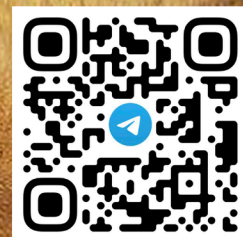


Mining Science and Technology

Горные науки
и технологии

Vol. 9 № 2
2024



<https://mst.misis.ru/>

<https://t.me/MinSciTech>



Activities of the *Mining Science and Technology (Russia) (Gornye nauki i tekhnologii)* international journal are aimed at developing international scientific and professional cooperation in the field of mining.

The journal target audience comprises researchers, specialists in the field of mining, representatives of academic and professional communities.

The journal publishes original papers describing research findings, experience in the implementation of projects in mining industry, review publications.

The journal seeks to develop interdisciplinary areas that contribute to progress in mining, for example, technological and environmental safety, project organization and management in mining industry, development of territories, legal aspects of natural resource use, and other areas studied by researchers and practitioners. The journal always welcomes new developments. Papers are accepted in English or Russian.

EDITOR-IN-CHIEF

Vadim L. Petrov, Prof., Dr.Sci.(Eng.), University of Science and Technology MISIS, Moscow, Russian Federation

DEPUTIES EDITOR-IN-CHIEF

Oleg I. Kazanin, Prof., Dr.Sci.(Eng.), Saint Petersburg Mining University, St. Petersburg, Russian Federation

Svetlana A. Epshtein, Dr.Sci.(Eng.), University of Science and Technology MISIS, Moscow, Russian Federation

EDITORIAL BOARD

Zach Agioutantis, Prof., Ph.D., University of Kentucky, Lexington, Kentucky, USA

Maksim A. Bogdasarou, Prof., Dr.Sci.(Geol. and Min.), Brest State A. S. Pushkin University, Brest, Belarus

Grigory Yu. Boyarko, Prof. Dr. Sci. (Econ.), Cand. Sci. (Geol. and Miner.), National Research Tomsk Polytechnic University, Tomsk, Russian Federation

Xuan Nam Bui, Prof., Dr.Sci., Hanoi University of Mining and Geology, Duc Thang – Bac Tu Liem, Hanoi, Vietnam

Carsten Drenstedt, Prof., Ph.D., Freiberg University of Mining and Technology, Freiberg, Germany

Faramarz Doulati Ardejani, Prof., Ph.D., Colledge of Engineering, University of Tehran, Tehran, Iran

Mikhail S. Ershov, Prof., Dr.Sci.(Eng.), National University of Oil and Gas “Gubkin University”, Moscow, Russian Federation

Akper A. Feyzullaev, Prof., Dr.Sci.(Geol. and Min.), Institute of Geology and Geophysics of the National Academy of Sciences of Azerbaijan, Baku, Azerbaijan

Ochir Gerel, Prof., Dr.Sci.(Geol. and Min.), Geoscience Center, the Mongolian University of Science and Technology, Ulaanbaatar, Mongolia

Zoran Gligorić, Prof., Dr.Sci. (Mining-Underground Mining), University of Belgrade, Belgrade, Republic of Serbia

Monika Hardygora, Prof., Ph.D., Wroclaw University of Technology, Wroclaw, Poland

Nikolae Ilias, Prof., Dr.Sci.(Eng.), University of Petrosani, Petrosani, Romania

Vladislav Kecojevic, Prof., Ph.D., Benjamin M. Statler College of Engineering and Mineral Resources, West Virginia University, Morgantown, West Virginia, USA

Aleksey A. Khoreshok, Prof., Dr.Sci.(Eng.), Gorbachev Kuzbass State Technical University, Kemerovo, Russian Federation

Vladimir I. Klishin, Prof., Dr.Sci.(Eng.), Institute of Coal, Siberian Branch, Russian Academy of Sciences, Kemerovo, Russian Federation

Vladimir N. Koshelev, Prof., Dr.Sci.(Chem.), National University of Oil and Gas “Gubkin University” (Gubkin University), Moscow, Russian Federation

Jyant Kumar, Prof., Ph.D-Geotech.Eng., Indian Institute of Science, Bengaluru, India

Vladimir A. Makarov, Prof., Dr.Sci.(Geol. and Min.), Siberian Federal University, Krasnoyarsk, Russian Federation

Sergey I. Malafeev, Prof., Dr.Sci.(Eng.), Vladimir State University named after Alexander and Nikolay Stoletovs, Vladimir, Russia

Oleg S. Misnikov, Prof., Dr.Sci.(Eng.), Tver State Technical University, Tver, Russian Federation

Valery V. Morozov, Prof., Dr.Sci.(Eng.), University of Science and Technology MISIS, Moscow, Russian Federation

Igor M. Petrov, Dr.Sci.(Eng.), Infomine Research Group LLC, Moscow, Russian Federation

Bakhadirzhan R. Raimzhanov, Prof., Dr.Sci.(Eng.), University of Science and Technology MISIS (branch), Almalyk, Uzbekistan

Bayan R. Rakishev, Prof., Dr.Sci.(Eng.), Kazakh National Research Technical University named after K.I. Satpayev, Alma-Ata, Kazakhstan

Oscar Jaime Restrepo Baena, Prof., Ph.D., National University of Colombia, Medellín, Colombia

Alexander N. Shashenko, Prof., Dr.Sci.(Eng.), National Mining University, Dnipro, Ukraine

Vadim P. Tarasov, Prof., Dr.Sci.(Eng.), University of Science and Technology MISIS, Moscow, Russian Federation

Denis P. Tibilov, Prof., Dr.Sci.(Econ.), Moscow State Institute of International Affairs (University) under the Ministry of Foreign Affairs of Russia, Moscow, Russian Federation

Niyaz G. Valiev, Prof., Dr.Sci.(Eng.), The Ural State Mining University, Ekaterinburg, Russian Federation

Natalia Zhuravleva, Prof., Dr.Sci.(Eng.), West Siberian Testing Center JSC (WSTCenter JSC), Novokuznetsk, Russian Federation

Vera V. Yurak, Assoc. Prof., Dr. Sci. (Econ.), Ural State Mining University, Yekaterinburg; Institute of Economics, Ural Branch of the Russian Academy of Sciences, Yekaterinburg, Russian Federation

EDITORIAL COUNCIL

Yuri G. Agafonov, Assoc. Prof., Cand.Sci.(Eng.), University of Science and Technology MISIS, Moscow, Russian Federation

Michael R. Filonov, Prof., Dr.Sci.(Eng.), University of Science and Technology MISIS, Moscow, Russian Federation

Leonid A. Plaschansky, Prof., Cand.Sci.(Eng.), University of Science and Technology MISIS, Moscow, Russian Federation

Yuri I. Razorenov, Prof., Dr.Sci.(Eng.), Platov South-Russian State Polytechnic University, Novocherkassk, Russian Federation

EXECUTIVE SECRETARY

Daria P. Galushka, University of Science and Technology MISIS, Moscow, Russian Federation

QUARTERLY

FOUNDED in 2016

REGISTRATION

The journal science and applied research journal is registered by the Federal Service for Communication, IT and Mass Communication Control on August 10, 2015. Registration Certificate E-No. ФС77-62652

INDEXATION

Scopus, CAS, EBSCO, DOAJ, РИНЦ, ВИНТИ РАН, Dimensions, BASE, J-Gate, Jisc Library Hub Discover.

FOUNDER AND PUBLISHER



UNIVERSITY MISIS
University of Science and Technology
MISIS

CONTACT

4 Leninsky Prospect, Moscow 119049, Russian Federation

Phone: +7 (495) 955-00-77

e-mail: send@misis.ru



This work is licensed under a
[Creative Commons Attribution 4.0 License](https://creativecommons.org/licenses/by/4.0/).



Деятельность научно-практического журнала «Горные науки и технологии» (Mining Science and Technology (Russia)) направлена на развитие международного научного и профессионального сотрудничества в области горного дела.

Целевая аудитория журнала – исследователи, специалисты в области горного дела, представители академического и профессионального сообществ.

В журнале публикуются оригинальные статьи, описывающие результаты исследований, опыт реализации проектов в горнопромышленном комплексе, обзорные публикации.

Журнал стремится развивать такие междисциплинарные направления, как технологическая и экологическая безопасность, организация и управление проектами в горной промышленности, развитие территорий, правовые аспекты использования природных ресурсов и другие, которые способствуют прогрессу в горном деле и реализуются исследователями и практиками.

ГЛАВНЫЙ РЕДАКТОР

Петров Вадим Леонидович, проф., д.т.н., Университет науки и технологий МИСИС, г. Москва, Российская Федерация

ЗАМЕСТИТЕЛИ ГЛАВНОГО РЕДАКТОРА

Казанин Олег Иванович, проф., д.т.н., Санкт-Петербургский горный университет, г. Санкт-Петербург, Российская Федерация

Эпштейн Светлана Абрамовна, д.т.н., Университет науки и технологий МИСИС, г. Москва, Российская Федерация

РЕДАКЦИОННАЯ КОЛЛЕГИЯ

Агиутантис Зак, проф., д-р наук, Университет Кентукки, г. Лексингтон, Кентукки, США

Богдасаров Максим Альбертович, проф., д.г.-м.н., Брестский государственный университет им. А.С. Пушкина, г. Брест, Беларусь

Боярко Григорий Юрьевич – проф., д.э.н., к.г.-м.н., Национальный исследовательский Томский политехнический университет, г. Томск, Российская Федерация

Буи Суан Нам, проф., д-р наук, Ханойский университет горного дела и технологии, г. Ханой, Вьетнам

Валиев Нияз Гадым оглы, проф., д.т.н., Уральский государственный горный университет, г. Екатеринбург, Российская Федерация

Герел Очир, проф., д.г.-м.н., Центр геолого-геофизических исследований, Монгольский университет науки и технологии, г. Улан-Батор, Монголия

Глигорич Зоран, проф., д-р наук, Белградский университет, г. Белград, Республика Сербия

Дребенштедт Карстен, проф., д-р наук, Технический университет Фрайбургская горная академия, г. Фрайберг, Германия

Дулати Ардежани Фарамарз, проф., д-р наук, Инженерный колледж, Тегеранский университет, г. Тегеран, Иран

Ершов Михаил Сергеевич, проф., д.т.н., Российский государственный университет нефти и газа (национальный исследовательский университет) им. И.М. Губкина, г. Москва, Российская Федерация

Журавлева Наталья Викторовна, проф., д.т.н., АО «Западно-Сибирский испытательный центр» (АО «ЗСИЦентр»), г. Новокузнецк, Российская Федерация

Илиаш Николае, проф., д.т.н., Университет Петрошани, г. Петрошани, Румыния

Кецоджевич Владислав, проф., д-р наук, Институт инженерного дела и минеральных ресурсов им. Бенджамина М. Статлера Университета Западной Вирджинии, г. Моргантаун, Западная Вирджиния, США

Клишин Владимир Иванович, проф., д.т.н., Институт угля Сибирского отделения Российской академии наук, г. Кемерово, Российская Федерация

Кошелев Владимир Николаевич, проф., д.х.н., Российский государственный университет нефти и газа им. И.М. Губкина, г. Москва, Российская Федерация

Кумар Джьянт, проф., д-р наук (геотехнический инжиниринг), Индийский институт науки (Indian Institute of Science), г. Бангалор, Индия

Макаров Владимир Александрович, проф., д.г.-м.н., Сибирский федеральный университет, г. Красноярск, Российская Федерация

Малафеев Сергей Иванович, проф., д.т.н., Владимирский государственный университет имени А.Г. и Н.Г. Столетовых, г. Владимир, Российская Федерация

Мисников Олег Степанович, проф., д.т.н., Тверской государственный технический университет, г. Тверь, Российская Федерация

Морозов Валерий Валентинович, проф., д.т.н., Университет науки и технологий МИСИС, г. Москва, Российская Федерация

Петров Игорь Михайлович, д.т.н., ООО «Исследовательская группа «Инфолайн»», г. Москва, Российская Федерация

Раимжанов Бахадиржан Раимжанович, проф., д.т.н., филиал Университета науки и технологий МИСИС, г. Алмалык, Узбекистан

Ракишев Баян Ракишевич, проф., д.т.н., Казахский национальный исследовательский технический университет им. К.И. Сатпаева, г. Алма-Ата, Казахстан

Рестрепо Баэна Оскар Хайме, проф., д-р наук, Национальный университет Колумбии, г. Медельин, Колумбия

Тарасов Вадим Петрович, проф., д.т.н., НИТУ «МИСиС», г. Москва, Российская Федерация

Тибилов Денис Петрович, проф., д.э.н., Московский государственный институт международных отношений (Университет) Министерства иностранных дел России, г. Москва, Российская Федерация

Фейзуллаев Акпер Акпер оглы, проф., д.г.-м.н., Институт геологии и геофизики (ИГГ) Национальной Академии Наук Азербайджана, г. Баку, Азербайджан

Хорешок Алексей Алексеевич, проф., д.т.н., Кузбасский государственный технический университет им. М.С. Горбачева, г. Кемерово, Российская Федерация

Шашенко Александр Николаевич, проф., д.т.н., Национальный горный университет, г. Днепр, Украина

Хардигора Моника, проф., д-р наук, Вроцлавский технологический университет, г. Вроцлав, Польша

Юрак Вера Васильевна, доц., д.э.н., Уральский государственный горный университет, г. Екатеринбург; старший научный сотрудник, Институт экономики Уральского отделения Российской академии наук (ИЭ УрО РАН), г. Екатеринбург, Российская Федерация

РЕДАКЦИОННЫЙ СОВЕТ

Агафонов Юрий Григорьевич, доц., к.т.н., Университет науки и технологий МИСИС, г. Москва, Российская Федерация

Плащанский Леонид Александрович, проф., к.т.н., Университет науки и технологий МИСИС, г. Москва, Российская Федерация

Разоренов Юрий Иванович, проф., д.т.н., Южно-Российский государственный политехнический университет (НПИ) им. М.И. Платова, г. Новочеркасск, Российская Федерация

Филонов Михаил Рудольфович, проф., д.т.н., Университет науки и технологий МИСИС, г. Москва, Российская Федерация

ОТВЕТСТВЕННЫЙ СЕКРЕТАРЬ

Галушка Дарья Петровна, Университет науки и технологий МИСИС, г. Москва, Российская Федерация

ПЕРИОДИЧНОСТЬ 4 раза в год

ОСНОВАН в 2016 году

РЕГИСТРАЦИЯ

Зарегистрирован Федеральной службой по надзору в сфере связи, информационных технологий и массовых коммуникаций 10 августа 2015 года.

Свидетельство о регистрации Эл № ФС77-62652.

ИНДЕКСИРОВАНИЕ

Scopus, CAS, EBSCO, DOAJ, РИНЦ, ВИНТИ РАН, Dimensions, BASE, J-Gate, Jisc Library Hub Discover.



Журнал открытого доступа.

УЧРЕДИТЕЛЬ И ИЗДАТЕЛЬ



МИСИС Университет науки и технологий
УНИВЕРСИТЕТ НАУКИ И ТЕХНОЛОГИЙ

АДРЕС УЧРЕДИТЕЛЯ И ИЗДАТЕЛЯ

119049, г. Москва, Ленинский проспект, д. 4

КОНТАКТЫ РЕДАКЦИИ

Адрес: 119049, г. Москва, Ленинский проспект, д. 4

Телефон: +7 (495) 955-00-77

e-mail: send@misis.ru



Контент доступен под лицензией
Creative Commons Attribution 4.0 License.



CONTENTS

MINERAL RESOURCES EXPLOITATION

Enhancing the performance of integer models for addressing the long-term production planning problem in open pit mines by decision variable fixation based on parametric analysis of the final pit limit 74

K. Hasozdemir, S.G. Erçelebi

Effect of explosive detonation velocity on the degree of rock pre-fracturing during blasting..... 85

S.V. Khokhlov, Yu.I. Vinogradov, V.A. Makkoev, Z.A. Abiyev

Theoretical aspects of block stone blasting method..... 97

V.N. Kovalevsky, A.V. Mysin, V.I. Sushkova

GEOLOGY OF MINERAL DEPOSITS

Composition and mineralogy of granitoids of the Ob-Zaisan folded region in the context of the prediction of groundwater radioactivity..... 105

V.P. Sukhorukov, A.F. Sukhorukova, D.A. Novikov, A.S. Derkachev

MINING ROCK PROPERTIES. ROCK MECHANICS AND GEOPHYSICS

Determination of deformation modulus and characterization of anisotropic behavior of blocky rock masses 116

O. Ahrami, H. Javaheri Koupaei, K. Ahangari

BENEFICIATION AND PROCESSING OF NATURAL AND TECHNOGENIC RAW MATERIALS

Current trends of improving the efficiency of froth separation of diamond-bearing kimberlites 134

V.V. Morozov, E.G. Kovalenko, G.P. Dvoychenkova, I.V. Pestryak, S.P. Lezova

Enhancing flotation beneficiation efficiency of complex ores using ionometry methods 146

T.A. Yakovleva, A.O. Romashev, G.N. Mashevsky

Comparative processing studies of the Arkachan deposit gold-bearing ores using dry separation and classical wet gravity separation methods 158

A.I. Matveev, I.F. Lebedev, V.R. Vinokurov, E.S. Lvov

SAFETY IN MINING AND PROCESSING INDUSTRY AND ENVIRONMENTAL PROTECTION

Geoenvironmental assessment of different types of cryolithic soils in Western Yakutia under the conditions of diamond-mining operations 170

A.S. Titov, A.S. Toropov

POWER ENGINEERING, AUTOMATION, AND ENERGY PERFORMANCE

Reliability analysis of open-pit power supply system components 183

R.V. Klyuev



СОДЕРЖАНИЕ

РАЗРАБОТКА МЕСТОРОЖДЕНИЙ ПОЛЕЗНЫХ ИСКОПАЕМЫХ

Повышение эффективности целочисленных моделей для решения задачи долгосрочного планирования добычи на открытых горных работах путем установления переменных решений на основе параметрического анализа конечного контура карьера 74

К. Хасоздемир, С. Г. Эрчелеби

Влияние скорости детонации взрывчатых веществ на степень предразрушения горной породы при взрыве 85

С. В. Хохлов, Ю. И. Виноградов, В. А. Маккоев, З. А. Абиев

Теоретические аспекты технологии взрывной отбойки блочного камня 97

В. Н. Ковалевский, А. В. Мысин, В. И. Сушкова

ГЕОЛОГИЯ МЕСТОРОЖДЕНИЙ ПОЛЕЗНЫХ ИСКОПАЕМЫХ

Состав и минералогия гранитоидов Обь-Зайсанской складчатой области в связи с прогнозом радиоактивности подземных вод 105

В. П. Сухоруков, А. Ф. Сухорукова, Д. А. Новиков, А. С. Деркачев

СВОЙСТВА ГОРНЫХ ПОРОД. ГЕОМЕХАНИКА. ГЕОФИЗИКА

Определение модуля деформации и характеристик анизотропного поведения блочных массивов горных пород 116

О. Ахрами, Х. Джавахери Купаи, К. Ахангари

ОБОГАЩЕНИЕ, ПЕРЕРАБОТКА МИНЕРАЛЬНОГО И ТЕХНОГЕННОГО СЫРЬЯ

Современные направления повышения эффективности пенной сепарации алмазосодержащих кимберлитов 134

В. В. Морозов, Е. Г. Коваленко, Г. П. Двойченкова, И. В. Пестряк, С. П. Лезова

Повышение эффективности флотационного обогащения комплексных руд с использованием методов прямой потенциометрии 146

Т. А. Яковлева, А. О. Ромашев, Г. Н. Машевский

Сравнительные технологические исследования золотосодержащей руды месторождения Аркачан методами сухого обогащения и классической мокрой гравитации 158

А. И. Матвеев, И. Ф. Лебедев, В. Р. Винокуров, Е. С. Львов

ТЕХНОЛОГИЧЕСКАЯ БЕЗОПАСНОСТЬ В МИНЕРАЛЬНО-СЫРЬЕВОМ КОМПЛЕКСЕ И ОХРАНА ОКРУЖАЮЩЕЙ СРЕДЫ

Геоэкологическая оценка разных типов почв криолитозоны Западной Якутии в условиях функционирования алмазодобывающих предприятий 170

А. С. Титов, А. С. Торопов

ЭНЕРГЕТИКА, АВТОМАТИЗАЦИЯ И ЭНЕРГОЭФФЕКТИВНОСТЬ

Анализ надежности элементов системы электроснабжения карьеров 183

Р. В. Клюев



MINERAL RESOURCES EXPLOITATION

Research paper

<https://doi.org/10.17073/2500-0632-2023-09-156>

UDC 622.015



Enhancing the performance of integer models for addressing the long-term production planning problem in open pit mines by decision variable fixation based on parametric analysis of the final pit limit

K. Hasozdemir  , S. G. Ercelebi 

Istanbul Technical University, Istanbul, Turkey

 hasozdemir@itu.edu.tr

Abstract

The importance of strategic mine planning to ensure the long-term viability of mining projects has increased significantly because of the limited availability of high-grade ore deposits. Given its high-dimensional and combinatorial nature, developing a precise mathematical optimization technique to solve the entire problem remains challenging, particularly for real-size block models. The primary objective of this study was to propose a method that combines a nested pit strategy with integer programming (IP) models to overcome computational limitations by reducing the problem's complexity, decreasing solution times, and providing insights into alternative production schedules for large-scale open-pit mines. The proposed algorithm strategically fixes the decision variables based on parametric analysis of the ultimate pit limit to simplify the IP model. The approach was applied to various block models from MineLib, and the results were compared with standard IP solutions and findings from related studies using alternative algorithms. Applying the proposed method demonstrated significant reductions in the solution time (up to 95%) and the ability to solve intractable models.

Keywords

open-pit mining, long-term production scheduling, production scheduling, optimization, integer programming, fixing decision variables, pseudoflow

Acknowledgements

The present study is a component of a PhD dissertation focusing on the subject of long-term production planning in open-pit mines. Financial support for this research has been provided by the Scientific Research Projects Unit of Istanbul Technical University.

For citation

Hasozdemir K., Ercelebi S.G. Enhancing the performance of integer models for addressing the long-term production planning problem in open pit mines by decision variable fixation based on parametric analysis of the final pit limit. *Mining Science and Technology (Russia)*. 2024;9(2):74–000. <https://doi.org/10.17073/2500-0632-2023-09-156>

РАЗРАБОТКА МЕСТОРОЖДЕНИЙ ПОЛЕЗНЫХ ИСКОПАЕМЫХ

Научная статья

Повышение эффективности целочисленных моделей для решения задачи долгосрочного планирования добычи на открытых горных работах путем установления переменных решений на основе параметрического анализа конечного контура карьера

К. Хасоздемир  , С.Г. Эрчелеби 

Стамбульский технический университет, г. Стамбул, Турция

 hasozdemir@itu.edu.tr

Аннотация

Важность стратегического планирования горных работ для обеспечения долгосрочной жизнеспособности горных проектов значительно возросла из-за сокращения числа месторождений богатых руд. Учитывая его многомерную и комбинаторную природу, разработка точного метода математической оптимизации для решения всей задачи остается сложной проблемой, особенно для блочных моделей в натуральную величину. Основная цель данного исследования заключалась в том, чтобы предложить метод, сочетающий стратегию вложенных контуров карьера с моделями целочисленного программирования (ЦП/ЦЛП) для преодоления вычислительных ограничений за счет снижения сложности зада-

чи, сокращения времени решения и предоставления информации об альтернативных графиках добычи для крупномасштабных открытых разработок. Предложенный алгоритм стратегически устанавливает переменные решения на основе параметрического анализа конечного (проектного) контура карьера для упрощения ЦП-модели. Этот подход был применен к различным блочным моделям из MineLib, а результаты были сопоставлены со стандартными ЦП-решениями и результатами соответствующих исследований с использованием альтернативных алгоритмов. Применение предложенного метода продемонстрировало существенное сокращение времени решения (на величину до 95%) и возможность решения трудноразрешимых моделей.

Ключевые слова

открытые горные работы, долгосрочное планирование добычи, планирование добычи, оптимизация, целочисленное программирование, установка переменных решения, псевдопоток

Благодарности

Настоящее исследование является составной частью кандидатской диссертации, посвященной теме долгосрочного планирования добычи на открытых горных работах. Финансовую поддержку этому исследованию оказал Отдел научно-исследовательских проектов Стамбульского технического университета.

Для цитирования

Hasozdemir K., Erçelebi S. G. Enhancing the performance of integer models for addressing the long-term production planning problem in open pit mines by decision variable fixation based on parametric analysis of the final pit limit. *Mining Science and Technology (Russia)*. 2024;9(2):74–000. <https://doi.org/10.17073/2500-0632-2023-09-156>

Introduction

Open-pit mining refers to the method of extracting valuable materials from the earth's surface by excavation with the intention of generating financial gain through their subsequent sale. A mining project's economic sustainability is heavily reliant on the careful control of this process. To enhance the manageability of this procedure, the mineral deposit is partitioned into discrete units known as blocks, which are typically modest in size and may not necessarily exhibit cubic dimensions. Each individual block inside the dataset contains distinct properties pertaining to the ore body, including the quantity of ore present, the quantity of waste material, the grade of the valuable mineral contained within, and the anticipated value of this mineral following the process of extraction. Geostatistical approaches are employed to determine these properties. The block model, as depicted in Fig. 1, is a representation of an orebody that has been par-

tioned into discrete blocks. This modeling approach has gained significant traction in the field of computer optimization [1].

Open-pit mine production scheduling (OPMPS) includes determining which blocks, within the final pit limit, should be mined each year and where the blocks should be transported, such as to a mill, trash dump, or stockpile, in order to maximize net present value (NPV) [1]. Long-term production planning for open-pit mine operations plays a key role in the assessment of mining projects. An important contribution in this field is presented in [2], wherein an algorithm developed that utilizes graph theory and dynamic programming to identify the ultimate pit limit that maximizes revenue. Furthermore, it is necessary to take into account various operational limitations when addressing this scheduling problem. One instance of constraints that are commonly referred to as spatial precedence constraints,

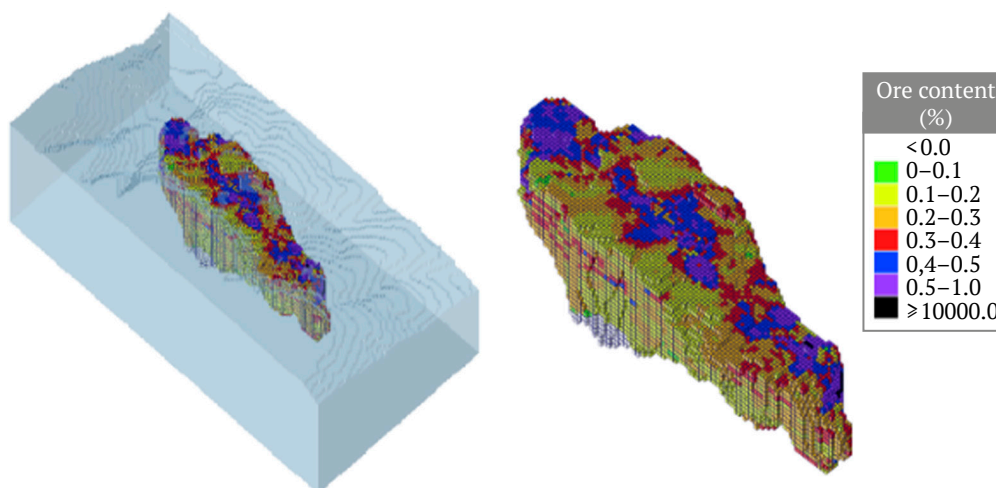


Fig. 1. Example Block Model

geometric sequencing constraints, or wall slope constraints is employed to guarantee the stability of excavated blocks by preventing inward collapse of the deposit. Alternatively, it is imperative that a specific block not be subjected to excavation prior to the removal of the blocks placed above it. Fig. 2 illustrates the implementation of precedence constraints, requiring excavation of blocks 1 to 9 either in earlier stages or concurrently with block 10.

$$\max Z = \sum_{t=1}^T \sum_{n=1}^N \frac{NV_n^t}{(1+r)^t} X_n^t. \quad (1)$$

This article is organized in the following manner: In Section 1, a comprehensive integer programming model is introduced to address the open-pit mining scheduling problem. Section 2 provides an overview of relevant literature to this subject. Section 3 of the paper presents a flowchart outlining the proposed method along with detailed specifications of the sample block models. The numerical outcomes of the proposed methodology are presented in Section 4, where its effectiveness is assessed based on the observed reductions in solution times. The concluding section enumerates the limitations inherent in the proposed methodology and presents prospective possibilities for future academic research.

1. General Integer Programming model of OPMPs problem

The ultimate pit consists of N blocks, and the planning horizon is T time periods. A discounted cash flow of c_i^t units will be obtained by the extraction of block i within the period t , r is the discount rate and A represents the block attributes such as ore tonnage and waste tonnage. Each block i is assigned a value q_i^a for each attribute $a \in A$. u_i^t provides an upper bound on the amount of tonnage that can be excavated in the time period t . Each block i must consider a smaller set of predecessor blocks S_i (see Fig. 2).

Objective Function:

$$\max \sum_{t=1}^T \sum_{n=1}^N \frac{c_i^t (x_i^t - x_i^{t-1})}{(1+r)^t}. \quad (2)$$

Subject to:

$$\sum_{i=1}^N q_i^a (x_i^t - x_i^{t-1}) \leq u_i^t, \quad i=1, \dots, N, t=1, \dots, T, a \in A, \quad (3)$$

$$x_i^{t-1} \leq x_i^t, \quad t=1, \dots, T. \quad (4)$$

$$x_i^t \leq x_i^j, \quad t=1, \dots, T, i=1, \dots, N, j \in S_i, \quad (5)$$

$$x_i^0 = 0, \quad (6)$$

$$x_i^t \in \{0, 1\}, \quad t=1, \dots, T, i=1, \dots, N. \quad (7)$$

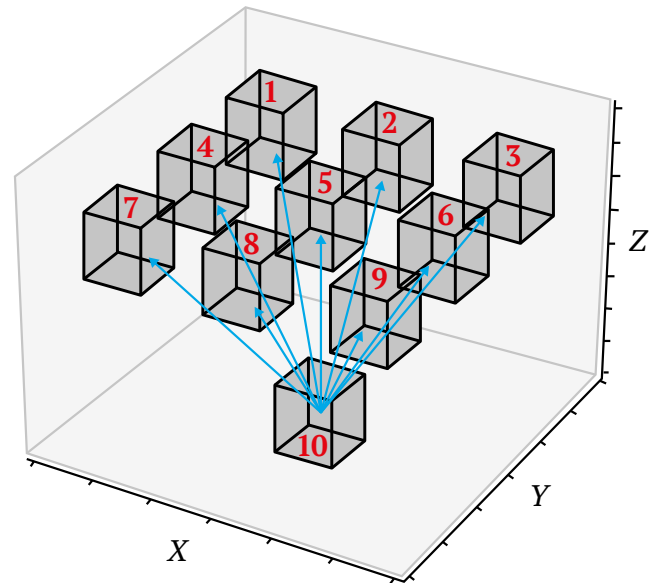


Fig. 2. Representation of precedence constraints

Eq. (2) is the objective function and attempts to maximize the net present value of the mining operation. Eq. (3) enforces the capacity constraints. Eq. (4) enforces the rule that each block must be excavated once and remain excavated. Finally, precedence constraints are enforced using Eq. (5). $x_i^0 = 0$ implies that none of the blocks in the ultimate pit is excavated before the planning horizon in Eq. (6). The decision variables of the model are binary, so they can be 1 if block i is mined in period t and 0 otherwise, Eq. (7). This basic formulation of the OPMPs problem contains NT binary variables. The major challenge in solving OPMPs is that the model instance contains many blocks and time periods, and each block-time period combination has associated binary decision variables to capture the more realistic constraints requiring all previous blocks to be extracted before removing any subsequent blocks. The application of integer models to address the problems of long- and medium-term production planning in open-pit mines is sometimes limited by difficulties such as the inability to find a solution or prolonged time required to find a solution, particularly when dealing with large-scale mineral deposits. This paper proposes a hybrid solution that combines nested pit methodology with ILP as an option to eliminate the aforementioned issues. The aim of the proposed algorithm is to fix the decision variables of the integer programming (IP) model using nested pit limits generated through parametric analysis. This approach yields efficient outcomes and reduces problem complexity. The next section outlines the phases of the proposed algorithm.

2. Literature Review

The conventional approach employed in addressing the OPMPs problem involved dividing the primary problem into smaller sub-problems, which were subsequently addressed individually [3]. The sub-problems, outlined in Fig. 3, include determining the ultimate pit limit, constructing nested pits based on ore selling price and applying a revenue adjustment factor, establishing push-backs as depicted in Fig. 4, and developing a production scheduling plan [4, 5].

Despite the utilization of this approach by the planners thus far, there are limitations as well.

- When the sub-problems are combined, it is possible that the optimal solutions obtained from these sub-problems may not result in an optimal solution for the main problem.

- The time value of money is not considered in the evaluation.

- The use of a fixed cut-off grade in the planning process has a negative impact on the economic reliability of the production schedule.

Pushbacks are a crucial component in the long-term planning process for open-pit mines, as they play a vital role in determining the final design of the mine and the profitability of the operation. They serve as a guide for the temporary production scheduling stage, delineating the start and end points of the extraction process. Moreover, pushbacks ensure the safety of the pit walls, help meet the required ore

production levels, and provide a minimum operational width to accommodate mining equipment and access to the mine for other activities.

The methodology in order to obtain a series of nested pits [6]:

1. A set of blocks denoted as B .

2. Set B represents the final pit of the deposit.

3. Nested pits are generated using a metal price parameterization and an economic block model.

4. Parameterization corresponds to a sequence of N revenue factors $0 < \lambda_1 < \lambda_2 < \dots < \lambda_N \leq 1$, which scales the metal price and each RAF produces a pit.

RAF is a variable which when multiplied with other pit optimisation parameters such as metal price, will produce the different nested pit outlines at different factoring.

In [7], it was determined that the designation of ultimate pit problem can be equivalently framed as the task of identifying the most valuable path within a graph denoted as $G = (S, E, W)$. S is number of nodes, E is number of edges and W is the weight of the edges of the graph (Fig. 5). The problem here is to find a set of nodes (set of tasks) with a maximal value and which respect the precedence relations. Such problem is usually solved using a maximal flow algorithms.

[8] showed that the ultimate pit problem is equivalent to the maximum closure problem, which in turn, can be reduced to the min cut problem. This allows one to use known efficient algorithms for maxi-

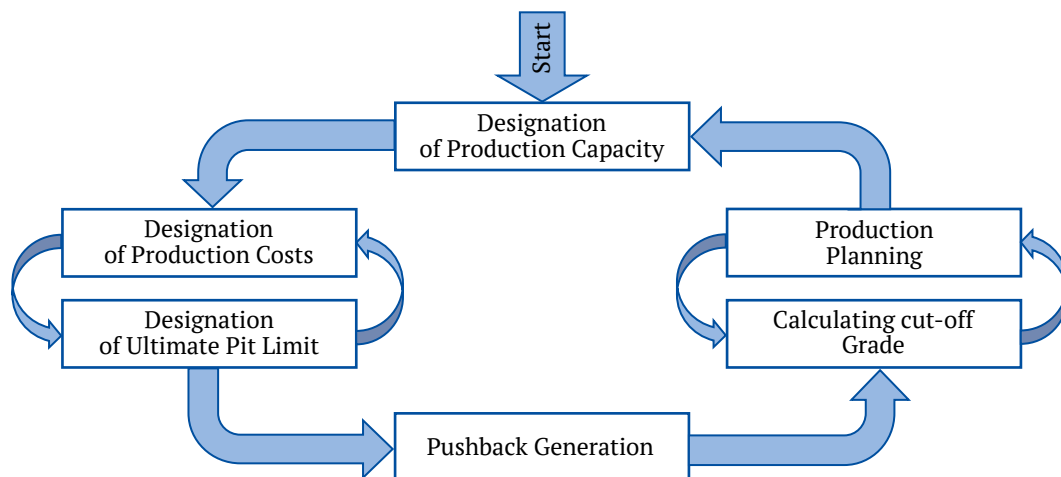


Fig. 3. Schematic view of the production scheduling problem of open pit-mines [3]

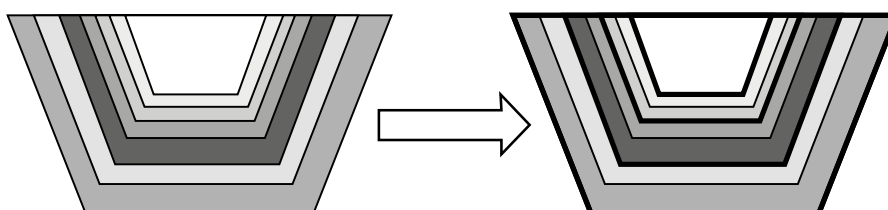


Fig. 4. Pushbacks (left), The chosen pit shells for the long-term schedule (right)

imum flow to find the ultimate pit. The mathematical model of the maximum closure algorithm is given below [9]. Objective function, given in eq. (8), is maximization of the total value of the closure and Constraint (9) identify the precedence constraints. x_i gets the value of 1 if node i is in the closure, 0 otherwise (eq. 10).

$$\max \sum_{i \in N} c_i x_i. \tag{8}$$

Subject to:

$$x_i - x_j \leq 0, \quad j \in Z_i, \quad i \in N; \tag{9}$$

$$x_i \in \{0, 1\}, \quad i \in N, \tag{10}$$

where Z_i is the set of the successors of node i ; c_i is the value of node i .

[10–12] presented a solution to address the pit limit problem (Fig. 6) by utilizing established efficient algorithms for the min cut problem. Their work demonstrates that the LG algorithm can be employed as a network flow algorithm, frequently referred to as the pseudoflow algorithm. The authors demonstrated the process of obtaining an ideal network flow using a succession of normalized trees. The researchers also conducted an analysis of the runtime of the LG method and made enhancements using scaling strategies that differ from those employed in generating push-back designs. Their findings demonstrate that LG can be implemented to operate with a time complexity of $O(mn \log n)$, where m represents the number of arcs and n represents the number of nodes.

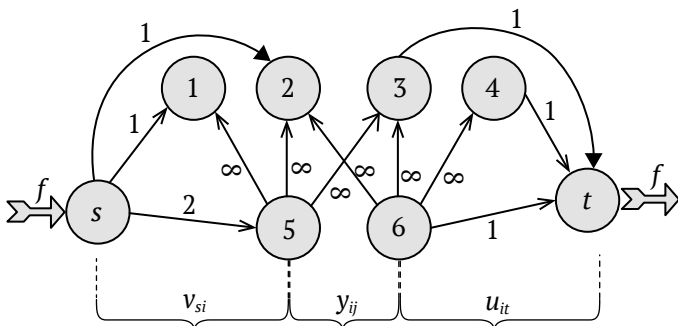


Fig. 5. Network view of the open pit mine (with nodes and edge capacities)

+1	+1	-1	-1
x_1	x_2	x_3	x_4
	+2	-1	
	x_5	x_6	

Fig. 6. Ultimate pit limit (Bold lines)

[13] used the Bienstock-Zuckerberg algorithm in order to improve the Lagrangian relaxation approach that is used in solving the MIP models of the OPMPs problem. [14] proposed a combination of maximum flow and genetic algorithms that try to solve this problem under uncertainty. First, the final pit limit was determined by the maximum flow algorithm on the block model created according to the values obtained from the simulated ore deposits regarding different economic values. Then, the production planning of the blocks within this limit is obtained by the genetic algorithm. They applied penalties for the constraints that were not satisfied by the maximum flow algorithm. They shared their results by applying the proposed model to a copper and a gold mine. Some researchers have attempted to enhance the resilience and adaptability of long-term plans by using stochastic methods to address uncertainties in variables such as ore grades, processing capacities, and market conditions. [15] incorporated geological variability and grade uncertainty into the production scheduling optimization process using conditional simulation and stochastic integer programming (SIP). [16] offered an integrated approach to generate schedules under geological uncertainty for mining complexes with multiple processing and transportation alternatives.

Metaheuristic approaches such as the tabu search, genetic algorithm, bat algorithm, gray wolf algorithm, firefly optimization, and particle swarm optimization are used to solve the OPMPs problem and obtained results are compared with classical methods in [17–20].

3. Proposed algorithm for solution time improvement

The proposed method aims to reach the optimum or near-optimal solutions in a shorter time by narrowing the solution space of the problem by strategically fixing the decision variables of the IP model of the OPMPs problem. The decision process utilized to fix the decision variables in this context is based on nested pits generated by the parametric analysis of the ultimate pit limit. The conventional approach involves representing the economic block model of a mineral deposit as a network based on graph theory. Subsequently, this network is subjected to analysis using maximum flow algorithms to find the ultimate pit limit, which corresponds to the production volume that yields the highest income. The next phase involves subjecting the blocks within the ultimate pit limit to a maximum flow analysis. This analysis entails recalculating their economic values based on the Revenue Adjustment Factor (RAF), resulting in the generation of progressively smaller open pit boundaries. The aforementioned boundaries are commonly referred to as nested pits.

In the procedure outlined above, the selection of the RAF involves incrementing it by 0.01, often within the range of 0.2 to 1, in order to establish an approximate calculation for 80 nested pit limits. Afterward, the calculation of the quantity of ore and waste material, the grade of the valuable mineral, and the economic value resulting from the excavation of these nested pits are performed. Following this computation, the open pit limits providing the annual production capacity are selected to represent the long-term production plan, and a determination is then performed to solve the open pit production planning problem. One significant issue associated with this method pertains to the considerable changes in the open pit limits, which are determined based on the income adjustment factor. Once a certain threshold is reached, these boundaries undergo rapid changes in size. As a result, the quantity of material available between two consecutive limits usually exceeds the annual production capacity by a significant amount. In academic literature, this situation is known as the gap problem. Fig. 8 provides a numerical illustration of this situation. The histogram depicted in Fig. 7 illustrates that the parametric analysis yields a minimum final pit limit of 18 blocks, whereas the nearest second-largest quarry contains 3049 blocks. The gap problem refers to the absence of an appropriate quarry boundary that can be chosen for the initial period while utilizing the conventional planning method.

This paper proposes a hybrid solution that combines the nested pits methodology with IP as an option for reducing the aforementioned issues. The aim of the proposed algorithm is to fix the decision variables of the integer programming (IP) model using the nested pit limits generated through parametric analysis. The act of decision variable fixing in the context of integer programming refers to the pre-termination of certain decision variables, which ulti-

mately dictates the production scheduling of open-pit mining operations within predetermined boundaries. This approach yields efficient outcomes, reducing the problem's model complexity. The next section outlines the phases of the proposed algorithm.

Algorithm

1. Utilization of Hochbaum's pseudoflow algorithm to determine the limit of the ultimate pit.

- The outermost pit shell in Fig. 8 (all blocks within the outermost pit limit, obtained by $RAF = 1$).

- The generation of nested pits by the utilization of parametric analysis on the blocks located within the boundaries of the ultimate pit, employing the RAF (see Fig. 8).

2. Computation of the material quantities within the nested pits, as well as the identification of potential pit shells that can fulfill the intended annual production capacity (see Fig. 8).

- The innermost pit limit is the candidate pit shell for the first period. (Orange blocks, obtained by $RAF = 0.2$). The second pit limit is the candidate pit shell for the second period. (Green blocks, obtained by $RAF = 0.4$).

3. In each time period, the decision variables of the blocks located beyond the limits of the nested pit that have been identified as candidates for that specific period are fixed (Figs. 9, 10).

- For example, for $T = 4$ periods, the x_{i1} variables of the gray blocks are fixed at 0, because the orange blocks represent the candidate pit shell for the 1st period and yield the highest income with a sufficient amount of ore within themselves (Fig. 9). Another example can be seen in Fig. 10. x_{i2} variables of gray blocks are fixed at 0, so blocks that will be excavated during the second period of production will be searched within the green limit because there is sufficient ore for the processing capacity and they yield the highest income.

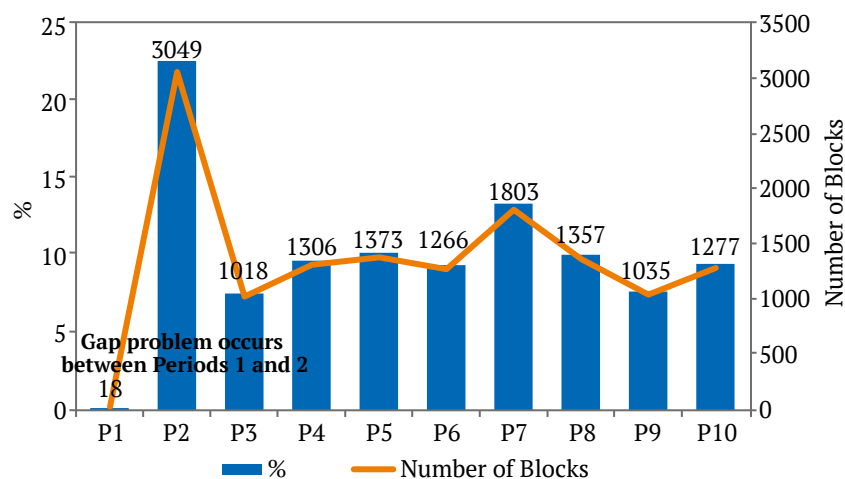


Fig. 7. The Gap Problem is illustrated by the distribution of blocks within nested pit shells

4. A different strategy is implemented to fix variables in the context of ore abundance within a candidate shell over a certain time period. In this procedure, if there is an excess amount of ore within the shell, the decision variables of the blocks within that shell are fixed at 1, as those blocks are expected to be excavated in subsequent periods i.e. x_{i5} variables associated with pink blocks in Fig. 11 are fixed as 1 implying that they are expected to be excavated at the end of $T = 5$).

5. The final process for fixing variables is implemented as follows: if the amount of ore in a candidate shell is less than the ore production capacity, the decision variable for all blocks within that shell is fixed at 1 since these blocks can be excavated within that time frame. (Blue blocks in Fig. 11).

6. Solving the problem with reduced size, which is obtained by fixing the decision variables.

The block models in Table 1 were obtained from MineLib, a widely used dataset in the mining industry.

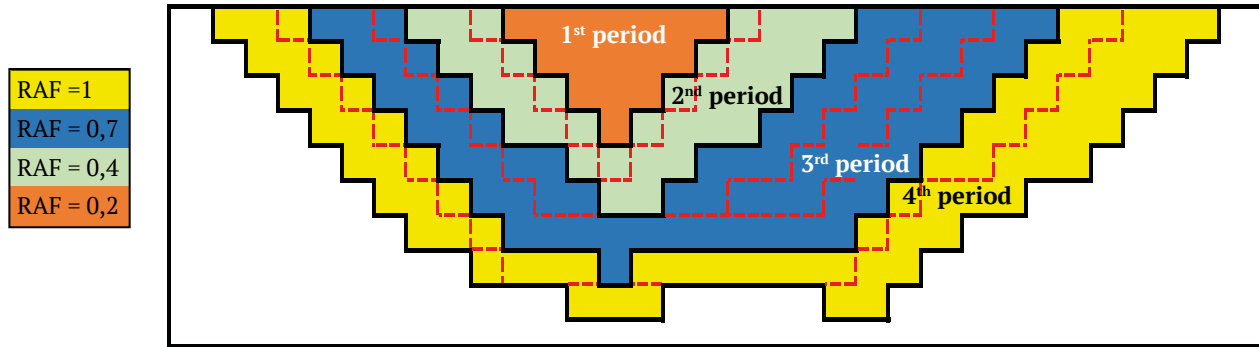


Fig. 8. 2D section of example nested pits (with candidate pit shells for periods)

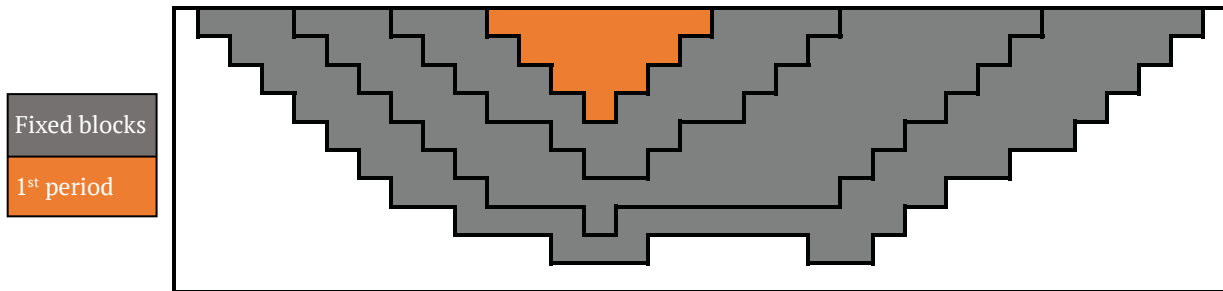


Fig. 9. Example of variable fixing for 1st period

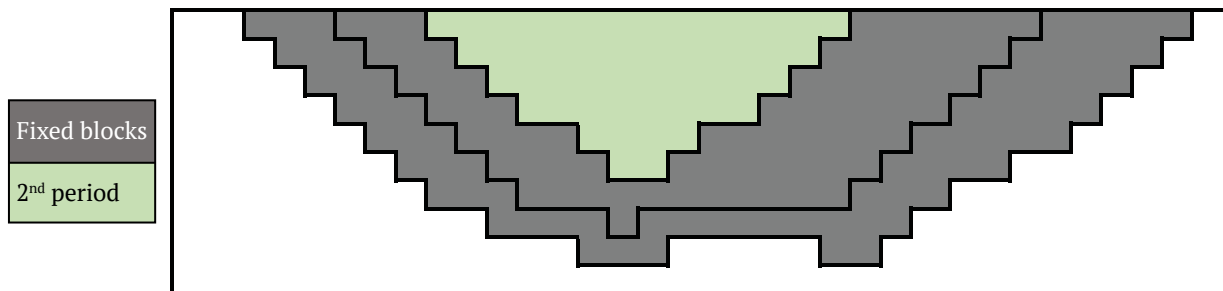


Fig. 10. Example of variable fixing for 2nd period

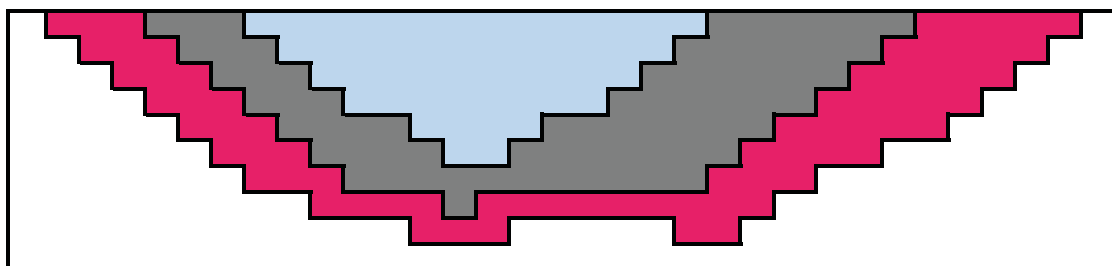


Fig. 11. Variable fixing in the context of ore abundance (pink blocks) and inadequacy of ore (blue blocks)



4. Numerical results obtained by suggested method

The proposed methodology for reducing the solution time of the OPMPs problem is implemented on six different block models obtained from MineLib. MineLib is comprised of various example block models utilized to demonstrate the performance of various algorithms proposed for the solution of the OPMPs problem. The results are given in the following fashion: First, the block models were tried to be solved without any decision variable fixing, and results were tried to be obtained. After that, the proposed method is applied to the same block model, and improvements in solution times are investigated. The GUROBI solver is used for solving the IP models. Optimality gap relaxation is set to %1, and the upper bound for the operating time is set to 36,000 seconds. The GUROBI solver is using the Barrier Method to designate the upper bound of the LP relaxation. Table 2 depicts the numerical results of the suggested method and its comparison with the standard IP model. The acronym “Nstl” denotes the absence of a solution within the designated time limit, whereas “memory” refers to the situation when the computational technique for solving the model surpasses the computer’s available memory capacity. “%inf” indicates that the decrease in solution time could not be measured because the

standard IP model was unable to solve the problem within the given time limit or exceeded the RAM capacity of the PC.

As can be seen from Table 2. By applying the suggested technique to various block models, we were able to observe significant improvements in the duration of the solution time. This demonstrates the effectiveness and practicality of the proposed method in real-world scenarios. In the mean time, some of the problems that can not be solved with the general IP model have been solved with the proposed method which depicts the efficiency of the suggested method. By means of NPV of the solution, there are some decrease on the NPV amount which is a drawback of the suggested methodology. This situation arises due to the limitation of solution alternatives with nested pit boundaries. The decline in net present value (NPV) may be deemed acceptable in the context of solving complex block models of significant scale that are infeasible to solve. An additional limitation of the proposed algorithm is its reliance on the existence of constraints concerning the capacity of ore production. The solutions derived from this methodology may turn out to be unfeasible when there are constraints on the total production capacity. To address this limitation, one potential solution is to incorporate relaxation techniques into the Integer Program-

Table 1

Block model specifications

ID	# of blocks	# of blocks within UPL	# Binary Variables	Ore capacity	Discount Rate	Periods T
zuck_small	9,400	8,752	122,528	20M	10%	14
kd	14,153	13,258	132,580	10M	10%	10
zuck_medium	29,277	29,230	263,880	8M	10%	9
marvin	53,271	5,324	69,212	20M	10%	13
zuck_large	96,821	96,821	968,210	3M	10%	10
mclaughlin	2,140,342	112,687	1,126,687	3.5M	10%	10

Table 2

Numerical Results

ID	Solution time of standard ILP model (sec)	NPV of standard ILP model	Optimality Gap	Solution Time of the suggested algorithm	NPV of suggested algorithm	Optimality Gap	Decrease in solution time
zuck_small	2,688	827.4M	1.79%	110	815.2M	0.60%	-95%
kd	2,806	413.2M	0.15%	177	405.7M	0.98%	-93%
zuck_medium	23,110	721.3M	1.7%	428	706.3M	0.88%	-98%
marvin	1,471	799.5M	0.98%	71	798.3M	0.96%	-95%
zuck_large	Nstl	Nstl	Nstl	2,221	76.9M	0.08%	%inf
mclaughlin	Memory	Memory	Memory	3,332	1,031.2M	0.16%	%inf

ming (IP) model. This would allow for the inclusion of total production capacity limitations within the objective function through the utilization of Lagrange Multipliers. Additionally, it is possible to use various heuristic approaches to ensure compliance with the limitations on total production capacity following the resolution of the integer programming (IP) model using the suggested strategy.

The graphical results of the Marvin block model are displayed in Fig. 12, with the intention of enabling a comparison between the suggested methodology and the traditional IP model. It is apparent that similar results can be attained within a shorter timeframe through variable fixing. The outcomes of the proposed algorithm are additionally compared with the results achieved by the modified TopoSort algorithm in [11] and the Bienstock & Zuckerberg algorithm in [21] as illustrated in Table 3. The TopoSort findings are the most optimal and feasible known outcomes of the relevant block models. The algorithm proposed by Bienstock and Zuckerberg yields a better net present value (NPV); nonetheless, these results are deemed infeasible.

Based on the findings shown in Table 3, the proposed methodology demonstrates notable efficacy in addressing the OPMPs problem while also exhibiting the potential to enhance the maximum achievable NPV for certain block models, as reported in MineLib [22].

Table 3

NPV comparison of the suggested algorithm with related studies

Block Model	TopoSort	Bienstock & Zuckerberg	Suggested Algorithm
mclaughlin	1073,3M	1079,0M	1031,2M
marvin	820,7M	863,4M	798,3M
zuck_medium	615,4M	710,6M	706,3M
kd	396,8M	409,4M	405,7M
zuck_small	788,6M	854,2M	815,2M

Conclusion and future study suggestions

Open-pit mining plays an essential part in the socio-economic progress of nations and the advancement of technology, as it provides the extraction of valuable minerals that serve as the building blocks of these advancements. The achievement of cost-effective mining operations necessitates the implementation of a strategic planning approach. Within this particular context, many researchers have proposed alternative approaches to address the issue of open pit mining production scheduling. The primary aim of this scheduling procedure is to maximize the net present value. The methods represented in this field consist of maximum flow algorithms, linear programming, integer programming, dynamic programming, metaheuristic methods, and simulation techniques.

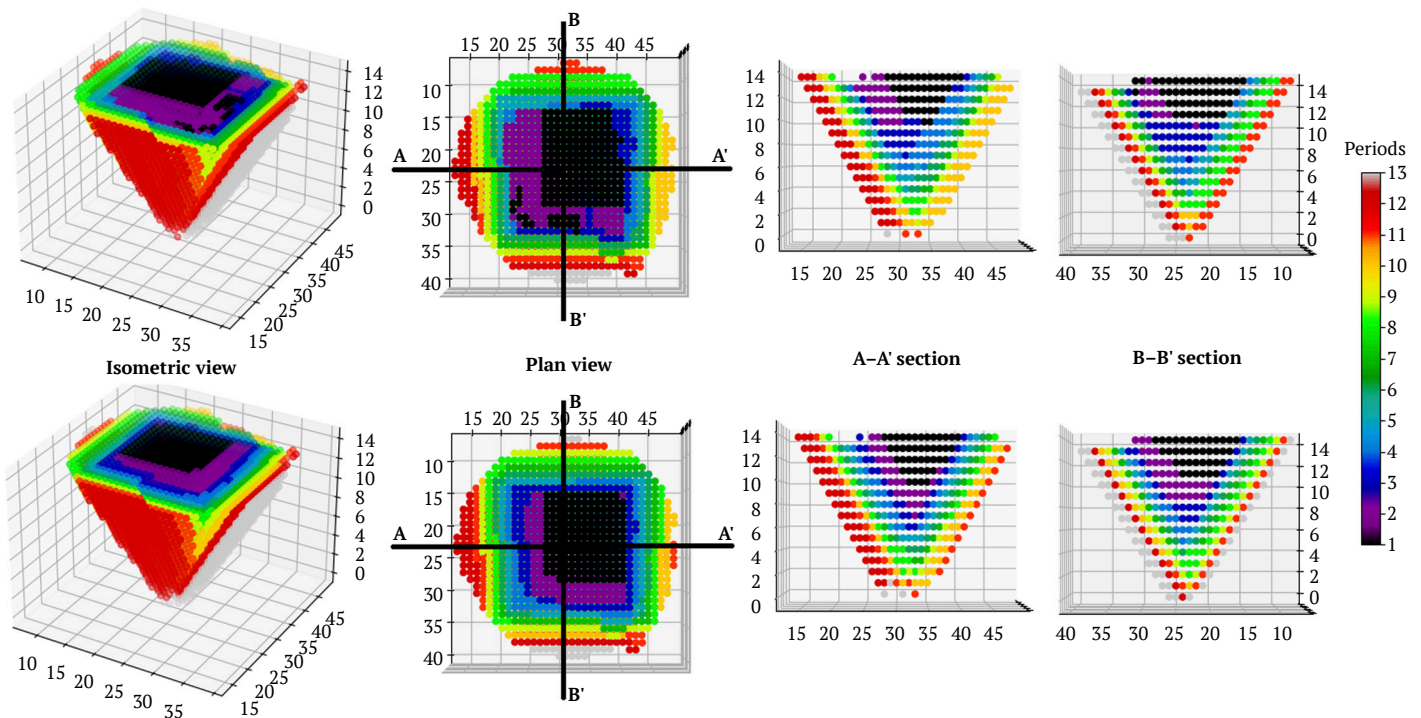


Fig. 12. Example comparison of scheduling results of Marvin block model (conventional IP result (top), IP result with fixed variables (bottom))



While these strategies have proven to be successful in addressing small or medium-sized ore deposits, their efficacy and efficiency are limited when it comes to handling larger mineral deposits. This paper presents a recommended alternative approach aimed at overcoming the challenges associated with the implementation of existing approaches in the context of large mineral resources. Traditionally, the OPMPs problem has been solved by manually picking those that meet the annual production capacity from the nested open pit boundaries generated from the mineral deposit's parametric analysis. The objective of this study is to decrease the problem size by constraining some decision variables of the integer programming model using limits derived from conventional approaches. This approach aims to address the challenges associated with resolving block models of mineral deposits that are either unsolvable or require excessive time to resolve within a limited timeframe. The efficacy of the suggested method has been demonstrated through its application to sample block models in the existing literature. The acquired findings demonstrate that the suggested method not only significantly reduces the solution time by up to 95% but also enables the solving of models that were previously unsolvable due to limited computational resources. Although the decrease in NPV for some models may appear to be a drawback of

this method, it is a significant contribution to the mining industry that various production plan alternatives can be examined in a short period of time based on varying mining capacities and ore sales prices.

Future research possibilities include the incorporation of parameters such as ore grade, vertical rate of advance, and minimum mining width, which should be considered during mining operations, into the planning procedure. The incorporation of operational factors, such as the minimum mining width, can be achieved by integrating them as relevant constraints inside the parametric analysis phase of the proposed method. By using this approach, candidate shells for the periods would meet the given constraints prior to solving the integer programming (IP) model. In addition, further research could explore the effects of techniques employed to meet the constraints of total production capacity. Furthermore, it is worth considering the inclusion of metaheuristic approaches as potential avenues for future research. These methods, although challenging to develop a viable production plan initially, can be explored in subsequent studies where the initial results obtained from the proposed method are utilized and the net present value (NPV) is enhanced through the application of various metaheuristic techniques such as simulated annealing, tabu search, and ant colony optimization.

References

1. Caccetta L., Hill S. An application of branch and cut to open pit mine scheduling. *Journal of Global Optimization*. 2003;27:349–365. <https://doi.org/10.1023/A:1024835022186>
2. Lerchs H., Grossmann I.F. Optimum design of open-pit mines. *Transactions, C.I.M.* 1965;LXVIII:17–24.
3. Dagdelen K., Johnson T.B. Optimum open-pit mine production scheduling by Lagrangian parameterization. In: *Proceedings of the 19th APCOM*. 1984;127–142.
4. Elkington T., Durham R. Integrated open pit pushback selection and production capacity optimization. *Journal of Mining Science*. 2011;47:177–190. <https://doi.org/10.1134/S1062739147020055>
5. Kumral M. Production planning of mines: optimization of block sequencing and destination. *International Journal of Mining, Reclamation, and Environment*. 2012;26(2):93–103. <https://doi.org/10.1080/17480930.2011.644474>
6. Jélvez E., Morales N., Askari-Nasab H. A new model for automated pushback selection. *Computers & Operations Research*. 2020;115:104456. <https://doi.org/10.1016/j.cor.2018.04.015>
7. Tolwinski B., Underwood R. An algorithm to estimate the optimal evaluation of an open-pit mine. In: *Proceedings of the 23rd International Symposium on the Application of Computers and Operations Research in the Mineral Industries*. 1992;399–409.
8. Picard J.C. Maximal closure of a graph and applications to combinatorial problems. *Management Science*. 1976;22(11):1268–1272. <https://doi.org/10.1287/mnsc.22.11.1268>
9. Tachefine B., Soumis F. Maximal closure on a graph with resource constraints. *Computers & Operations Research*. 1997;24(10):981–990. [https://doi.org/10.1016/S0305-0548\(97\)00008-7](https://doi.org/10.1016/S0305-0548(97)00008-7)
10. Chandran B.G., Hochbaum D.S. A computational study of the pseudoflow and push-relabel algorithms for the maximum flow problem. *Operations Research*. 2009;57(2):358–376. <https://doi.org/10.1287/opre.1080.0572>
11. Hochbaum D.S. The pseudoflow algorithm: A new algorithm for the maximum-flow problem *Operations Research*. 2008;56(4):992–1009. <https://doi.org/10.1287/opre.1080.0524>



12. Hochbaum D.S., Chen A. Performance analysis and best implementations of old and new algorithms for the open-pit mining problem. *Operations Research*. 2000;48(6):894–914. <https://doi.org/10.1287/opre.48.6.894.12392>
13. Muoz G., Espinoza D., Goycoolea M. et al. A study of the Bienstock-Zuckerberg algorithm: applications in mining and resource-constrained project scheduling. *Computational Optimization and Applications*. 2018;69(2):501–534. <https://doi.org/10.1007/s10589-017-9946-1>
14. Paithankar A., Chatterjee S. Open-pit mine production schedule optimization using a hybrid of maximum-flow and genetic algorithms. *Applied Soft Computing*. 2019;81:105507. <https://doi.org/10.1016/j.asoc.2019.105507>
15. Ramazan S., Dimitrakopoulos R. Stochastic optimisation of long-term production scheduling for open pit mines with a new integer programming formulation. In: Dimitrakopoulos R. (ed.) *Advances in Applied Strategic Mine Planning*. Springer, Cham; 2018. Pp. 139–153. https://doi.org/10.1007/978-3-319-69320-0_11
16. Montiel L., Dimitrakopoulos R. Optimizing mining complexes with multiple processing and transportation alternatives: An uncertainty-based approach. *European Journal of Operational Research*. 2015;247(1):166–178. <https://doi.org/10.1016/j.ejor.2015.05.002>
17. Alipour A., Khodaiari A.A., Jafari A., Tavakkoli-Moghaddam R. Production scheduling of open-pit mines using genetic algorithms: a case study. *International Journal of Management Science and Engineering Management*. 2020;15(3):176–183. <https://doi.org/10.1080/17509653.2019.1683090>
18. Elsayed S., Sarker R., Essam D., Coello C.C. Evolutionary approach for large-scale mine scheduling. *Information Sciences*. 2020;523:77–90. <https://doi.org/10.1016/j.ins.2020.02.074>
19. Senécal R., Dimitrakopoulos R. Long-term mine production scheduling with multiple processing destinations under mineral supply uncertainty, based on a multi-neighborhood Tabu search. *International Journal of Mining, Reclamation, and Environment*. 2020;34(7):459–475. <https://doi.org/10.1080/17480930.2019.1595902>
20. Tolouei K., Moosavi E., Tabrizi A.H.B. et al. Improving performance of open-pit mine production scheduling problems under grade uncertainty by hybrid algorithms. *Journal of Central South University*. 2020;27(9):2479–2493. <https://doi.org/10.1007/s11771-020-4474-z>
21. Bienstock D., Zuckerberg M. Solving L.P. relaxations of large-scale precedence constrained problems. In: Eisenbrand F., Shepherd F.B. (eds.) *Integer Programming and Combinatorial Optimization. IPCO 2010. Lecture Notes in Computer Science. Vol. 6080*. Springer, Berlin, Heidelberg; 2010. https://doi.org/10.1007/978-3-642-13036-6_1
22. Espinoza D., Goycoolea M., Moreno E., Newman A.N. MineLib: a library of open pit problems. *Annals of Operations Research*. 2013;206:93–114. <https://doi.org/10.1007/s10479-012-1258-3>

Information about the authors

Kursat Hasozdemir – PhD-Student, Research Assistant, Mining Engineering Department, Istanbul Technical University, Istanbul, Turkey; ORCID [0000-0002-2710-9562](https://orcid.org/0000-0002-2710-9562); e-mail hasozdemir@itu.edu.tr

Selamet Gürbüz Ercelebi – Dr. Sci., Professor, Mining Engineering Department, Istanbul Technical University, Istanbul, Turkey; ORCID [0000-0001-8744-885X](https://orcid.org/0000-0001-8744-885X); e-mail ercelebi@itu.edu.tr

Received 11.09.2023
Revised 03.02.2024
Accepted 26.02.2024




MINERAL RESOURCES EXPLOITATION

Research paper

<https://doi.org/10.17073/2500-0632-2023-11-177>

UDC 622.235

**Effect of explosive detonation velocity
on the degree of rock pre-fracturing during blasting**S. V. Khokhlov  , Yu. I. Vinogradov  , V. A. Makkoev   , Z. A. Abiyev  *Empress Catherine II Saint Petersburg Mining University, Saint Petersburg, Russian Federation* s215079@stud.spmi.ru**Abstract**

At many quarries for the extraction of building stone there is a problem of increased output of fines after all stages of crushing and grinding, which leads to a decrease in the economic performance of mining enterprises. The fine fraction is formed by the crushing/grinding of prefractured rock mass. Reducing the intensity and size of the prefracture zones will lead to a solution to the problem at hand. To determine the effect of explosive detonation properties on the degree of structural weakening of a rock mass, studies were conducted to measure the detonation velocity, stresses generated by a blast in the rock mass, as well as laboratory studies of microfracturing by X-ray computer microtomography. The size of the prefracture zones increases from 33 to 77 charge radii with increasing the detonation velocity from 2 to 5.2 km/s. The dependence of the number of microdefects (microfractures) generated by a blast on the velocity of explosive detonation takes the form of an exponent for the near zone and is linear for the distances far from the blast. According to the data of the experiments conducted at short distances (10R), the density of induced microfracturing N is within ≈ 5 thousand pcs/cm³, and with increasing the detonation velocity it increases to ≈ 13.8 thousand pcs/cm³. At medium (40R) and long (70R) distances, N increases from ≈ 750 to $\approx 2,400$ pcs/cm³ and from 0 to ≈ 200 pcs/cm³, respectively. Using explosives with a reduced detonation velocity allows reducing the “surplus” impact on a rock mass and thus reducing the intensity of prefracture in the zone of controlled crushing during a blast. The study allowed obtaining quantitative parameters of the intensity and size of the prefracture zones, which compose the supplement to findings of historical studies on qualitative determination of prefracture.

Keywords


prefracture, crushing to rubble, blast stresses, microfracture, fracture density, detonation velocity, fines yields

For citation

Khokhlov S.V., Vinogradov Yu.I., Makkoev V.A., Abiyev Z.A. Effect of explosive detonation velocity on the degree of rock pre-fracturing during blasting. *Mining Science and Technology (Russia)*. 2024;9(3):85–96. <https://doi.org/10.17073/2500-0632-2023-11-177>

РАЗРАБОТКА МЕСТОРОЖДЕНИЙ ПОЛЕЗНЫХ ИСКОПАЕМЫХ

Научная статья

**Влияние скорости детонации взрывчатых веществ
на степень предразрушения горной породы при взрыве**С. В. Хохлов  , Ю. И. Виноградов  , В. А. Маккоев   , З. А. Абиев  *Санкт-Петербургский горный университет императрицы Екатерины II, г. Санкт-Петербург, Российская Федерация* s215079@stud.spmi.ru**Аннотация**

На многих карьерах по добыче строительного камня присутствует проблема повышенного выхода отсева после всех стадий дробления и измельчения, которая приводит к снижению экономической эффективности горных предприятий. Мелкая фракция образуется вследствие измельчения предразрушенной горной массы. Уменьшение интенсивности и размеров зон предразрушения приведет к решению поставленной проблемы. Для определения влияния детонационных свойств взрывчатых веществ на величину структурного ослабления массива, были проведены исследования по измерению скорости детонации, напряжений, возникающих при взрыве в массиве и лабораторные иссле-



дования микротрещиноватости методом рентгеновской компьютерной микротомографии. Размеры зон предразрушения с ростом скорости детонации с 2 до 5,2 км/с увеличиваются с 33 до 77 радиусов заряда. Зависимость количества вновь образованных взрывом микродефектов от скорости детонации взрывчатых веществ (ВВ) принимает вид экспоненты для ближней зоны и линейна для дальних от взрыва расстояний. По данным проведенных экспериментов, на ближних расстояниях (10R) плотность наведенной микротрещиноватости N находится в пределах ≈ 5 тыс. шт/см³, а с ростом скорости детонации увеличивается до $\approx 13,8$ тыс. шт/см³. На средних (40R) и дальних (70R) расстояниях значение N растёт с ≈ 750 до ≈ 2400 шт/см³ и с 0 до ≈ 200 шт/см³ соответственно. Применяя ВВ с пониженной скоростью детонации, можно снизить «излишнее» воздействие на массив и тем самым уменьшить интенсивность предразрушения в зоне регулируемого дробления при взрыве. В результате исследования получены количественные параметры интенсивности и размеров зон предразрушения, что является дополнением предшествующих работ по качественному определению предразрушения.

Ключевые слова

предразрушение, дробление на щебень, напряжения при взрыве, микротрещина, плотность трещин, скорость детонации, выход мелочи

Для цитирования

Khokhlov S.V., Vinogradov Yu.I., Makkoiev V.A., Abiyev Z.A. Effect of explosive detonation velocity on the degree of rock pre-fracturing during blasting. *Mining Science and Technology (Russia)*. 2024;9(3):85–96. <https://doi.org/10.17073/2500-0632-2023-11-177>

Introduction

The non-metallic materials production segment in the Russian market is an integral part of the mining industry. Crushed stone is the most widely used product of mining and processing of non-metallic building materials, which is used for road construction, production of reinforced concrete, ready-mix concrete, laying and repair of railroad tracks, etc.

In recent years, the volume of crushed stone production reached 22 million m³/year [1, 2]. The economic performance of mining enterprises for the production of crushed stone products directly depends on the volume of quality fractions of crushed stone produced, which is related to the issue of the product quality [3–5].

The problem of increased yield of substandard fines when crushing blasted rock mass exists in crushed stone production at present time [6]. Up to 30% of the final product volume is lost as fines that leads to a decrease in the volume of quality fractions and unsustainable environmental management [7], which is reflected in the growth of areas of fines dumps [8–10].

When material is crushed in crushers, fines is formed during processing of rock mass prefractured by blast [11], since structurally weakened fragments with increased density of microfractures have reduced strength characteristics and tend to crumble into small pieces under relatively small impacts [12, 13].

Changing the detonation characteristics of explosives has a direct effect on the size of the zones and the degree of prefracture. The results of historical tests [14] show that increasing velocity of explosive detonation results in increasing the prefracture zone, in which elastic and strength characteristics of rock

mass properties change with distance from an explosive charge.

Assuming that prefracture is the accumulation of microdefects in a medium, applying the approach to the determination of fracturing and microfracturing based on the multistage fracturing model [15] leads to the need to study the quantitative parameters of microfracturing as a function of detonation velocity.

The purpose of the work is to determine the dependence of the quantitative index of microfracture density on the velocity of detonation of an explosive, which affects the magnitude of stresses occurring in a rock during a blast. An appropriate methodology for establishing this dependence is proposed. The study is necessary to quantify the prefracture parameters and the size of a structural weakening zone.

1. Theoretical treatment

During blast crushing of hard rocks, a zone of wave prefracture is formed [16], within which induced microfracturing increases. The accumulation of microdefects in the volume of both the rock mass and a separately considered piece of the rock mass after the blast leads to structural weakening of the rock and decreasing its strength [11, 12]. A prefracture zone is predominantly developed in hard rocks that adversely affects the economic performance of building stone mining.

Considering the structural weakening of the strength of a rock mass or individual pieces of a rock mass at different distances from a blast, it is necessary to use the multistage model of solid body fracture as a basic model of rock fracture. In accordance with this model, each newly formed defect in a rock mass is predetermined by the presence of smaller defects.

In accordance with this model, each newly formed defect in a rock mass is predetermined by the presence of smaller defects. At the first stage, a process of random quasi-uniform accumulation of first-order defects occurs. It is worth noting that a rock mass, regardless of its structural characteristics, is always an anisotropic medium [17]. The inhomogeneity of a medium, as well as the local differences in the internal loads in a rock mass, leads to the formation of areas of high concentration of first-order defects at the second stage. At the final phase of the stage, when the concentration of first-order defects exceeds a critical threshold level, fusion of the defects (fractures) occurs, which leads to the formation of second-order defects [15]. Accumulation of defects occurs until the moment of rupture – separation of the fragment under study into two or more pieces.

The structural weakening zone is limited to the region of blast-induced microfractures [18]. And the induction of these microfractures (wave prefracture) depends on the magnitude of stresses occurring in a rock [19].

Rock rupture mainly depends on the energy of stress waves [20] propagating in a medium [21, 22]. One of the most important wave characteristics affecting the magnitude of stress is a blast pulse, which predetermines all subsequent stages of the blast development: rock deformation, rock crushing, and rock mass movement. The influence of a blast pulse on the character of rupture is considered in [23, 24].

The findings of historical studies with the blast of the reference explosive Ammonite No. 6ZhV [25] showed that the dependence of the velocity of a rock mass displacement at different distances during the blast on the relative distance has the form of a power function (Fig. 1). It should be noted that the studies covered the conditions of Olenegorsk ferruginous quartzite open pit.

The concept of prefracture refers not only to the part of a rock mass behind the controlled crushing zone, but also to individual rock fragments in the crushing zone after a blast. This is important because these pieces have blast-induced microfracturing, which contributes to structural weakening of the strength of these pieces, and as a result, the yield of substandard fractions when crushing the blasted rock mass into crushed stone increases.

The determination of a rock mass structural weakening magnitude dependence on the stresses caused by a blast will make it possible to determine the size of the prefracture zone and the intensity of fracturing.

2. Research techniques

In determining the parameters of rock prefracture, the method of full-scale experiment was used to determine the stresses generated in a rock during a blast and to measure the detonation velocity of explosives. A laboratory study method was used to investigate the nature of microfracture formation. The methods of statistical data processing and analysis were applied to determine the size of the prefracture zones, as well as for data processing and interpretation [26] and comparison of the study results.

2.1. Stress measurement

The measurement of stresses in a rock, arising during a blast at different distances from the charge, in order to obtain the information about the nature of wave processes during blasting was carried out by an indirect method, by means of performing experimental blasts with recording acceleration of displacement of rock mass particles by measuring transducers. The measurements of accelerations were carried out according to the known method [27–29] with blasting of Ammonite No. 6ZhV, Granulite R, and Emulsolite

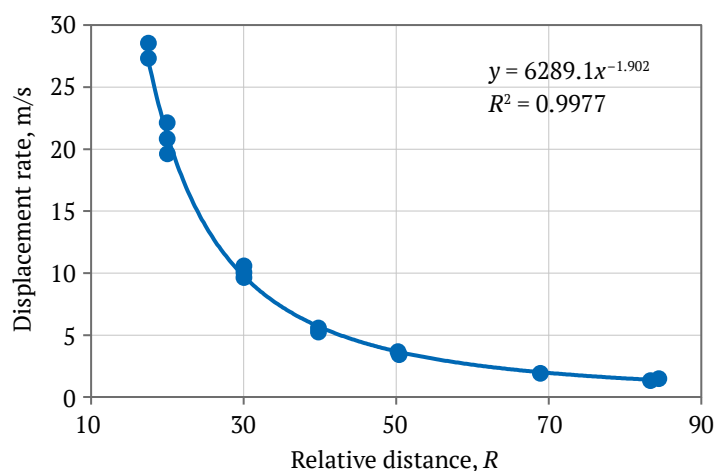


Fig. 1. Graph of rock mass displacement velocity as a function of relative distance [compiled by the authors]

A-20 explosive charges with recording of readings of rock mass particle displacement accelerations at three relative distances from the blast – 10, 40, and 70 radii of the charge.

The study was carried out at a limestone quarry. A schematic of the hole locations for each blast is shown in Fig. 2. Orange indicates a blast hole, blue indicates measurement holes for sensor placement. The given arrangement of holes ensures the accuracy of measurements due to the absence of additional media interfaces between a blast hole and each of the sensors.

Each accelerometer was fixed at the level of the center of an explosive charge. The sensors were fixed in the holes with alabaster with drilling fines added to create an environment as close as possible to the rock mass.

The conversion of accelerations to stresses was accomplished by integrating acceleration values into velocity values. A velocity is taken into account when calculating sound pressure or stress. The sound pressure is represented as the difference between the instantaneous pressure in the wave propagation path and the static pressure proper. The stress wave at each point in the wave field propagates similarly to the particles displacement velocity at the same point. The coupling parameter between pressure and displacement velocity is wave impedance of the medium or its acoustic impedance [30]. The above parameters are related to each other by a relationship:

$$\frac{P}{U} = \rho C, \tag{1}$$

where P – sound pressure, Pa (MPa); U – cparticle displacement velocity, m/s; ρC – acoustic impedance.

The relationship between the stresses occurring in a rock and the displacement velocity under the influence of a seismic explosion wave is established using the method of conversion of the mass veloci-

ty data into the parameters of the resulting stresses through the calculation of the stress in the rock using the following formula:

$$\sigma_0 = \rho_0 C_p U_x, \tag{2}$$

where σ_0 – stresses arising in a rock (pressure of a seismic blast wave), MPa; ρ_0 – material density, kg/m³; C_p – longitudinal wave propagation velocity in a rock mass, m/s; U_x – rock displacement velocity within the measured limits, m/s.

2.2. Detonation velocity measurement

In the field experiments, the detonation velocity at each blast was measured by MREL equipment, namely the DataTrap II VoD Recorder. The measurements were carried out using the resistive method, in which the instrument measures and records the value of the electrical resistance of a special probe cable that decreases as the detonation wave propagates in a charge. The measurement cable is a special coaxial cable with a center conductor and shielding. The cable is placed along the entire length of a blasthole before charging begins. It is mandatory that the cable is in tension when charging an explosive to avoid unreliable results.

Line resistance values are recorded at a frequency of 2.5 MHz. With the known intrinsic resistance of the measuring cable 10.8 Ohm/m, the standard software builds a graph of dependence of distance, m, on time, ms. An example of the graph is shown in Fig. 3.

The detonation velocity is determined by the following formula:

$$D = \frac{\Delta l}{\Delta t}, \tag{3}$$

where D is detonation velocity, m/s; Δl is the distance between the ends of the mean measurement line on the graph, m; Δt is the difference in the time values corresponding to the taken distance values, s.

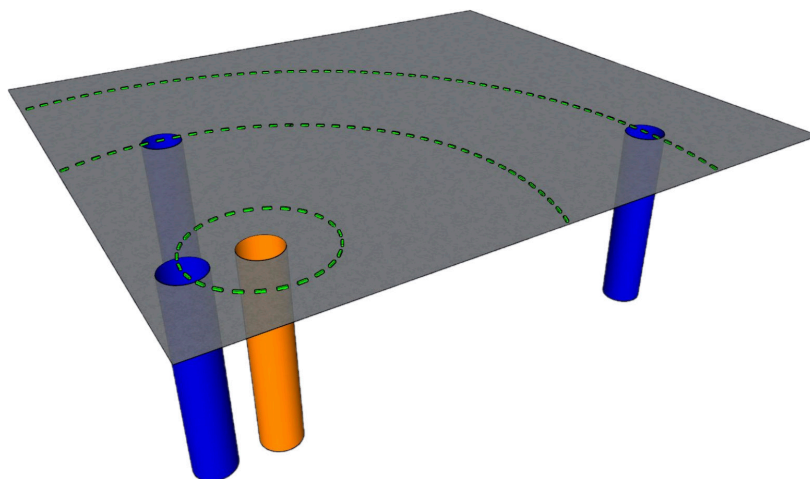


Fig. 2. Hole location scheme [compiled by the authors]

The resistive method of measuring the detonation velocity of explosives can be used to measure the velocity of propagation of detonation waves in explosives if the magnitude of the shock pulse acting on the cable is greater than the quadratic value of the dynamic viscosity coefficient of the material of the inner insulating sheath of the measuring cable [31]. This condition is met if the cable is properly positioned along the length of the explosive charge column.

2.3. Determination of the size of prefracture zones and the degree of microfracturing

After drilling of technological and blasting holes in accordance with the methodology, drilling of geo-technical holes was carried out with sampling (coring) of rock mass [32] before and after blasting. Pre- and post-blast sampling was conducted from holes located at relative distances of 40 and 70 charge radii, as well as at intermediate distances. The recovered samples (specimens) were delivered to laboratories for further laboratory testing.

The method of acoustic emission (AE) analysis was used to determine the pressure (stress) in a rock required to initiate the accumulation stage – microfracture formation. The AE method provides recording time with minimal delay [33], which contributes to obtaining reliable data on the onset of microfracture formation. The approach has performed well not only in static testing [34, 35] but also in sample dynamic loading testing [36, 37].

In the process of stress rupture of rock samples, the distinctive feature is the rupture stadiality [38].

In a rock, being a heterogeneous material, the regularity of stage change is due to the progression of the defect level according to the multistage rupture concept [39]. Researchers [38, 40] distinguish 4 stages of sample strain: I – initial, at which some of the existing defects are closed; II – stage of linear strains, at which the "collapsed" defects are reopened and new first-order defects are formed; III – stage of elasto-plastic strains, at which the process of formation of first-order defects (microfractures) is intensified and the formation of second-order defects begins; IV – prefracture stage, which is caused by the accumulation of macrofractures and precedes the sample rupture [40].

In the above description, the prefracture stage is different from the concept of prefracture in our study, as it is defined in terms of the beginning of imminent sample rupture. In our study, on the other hand, prefractured rock is considered as structurally weakened rock.

In rocks such as marble, limestone, and granite, emission activity, indicating the beginning of the process of microfracture formation, appears at a pressure of 15–38% of the uniaxial compressive strength of the rock [40]. Closely spaced values were given by other authors [41], which demonstrated a value of about 25–30% of the uniaxial compressive strength. The change in the state of a sample in accordance with the decrease in the longitudinal wave velocity begins at stresses of 10–15 MPa [42].

We assume a minimum value of 15% of the rupture pressure for the onset of microfracture formation.

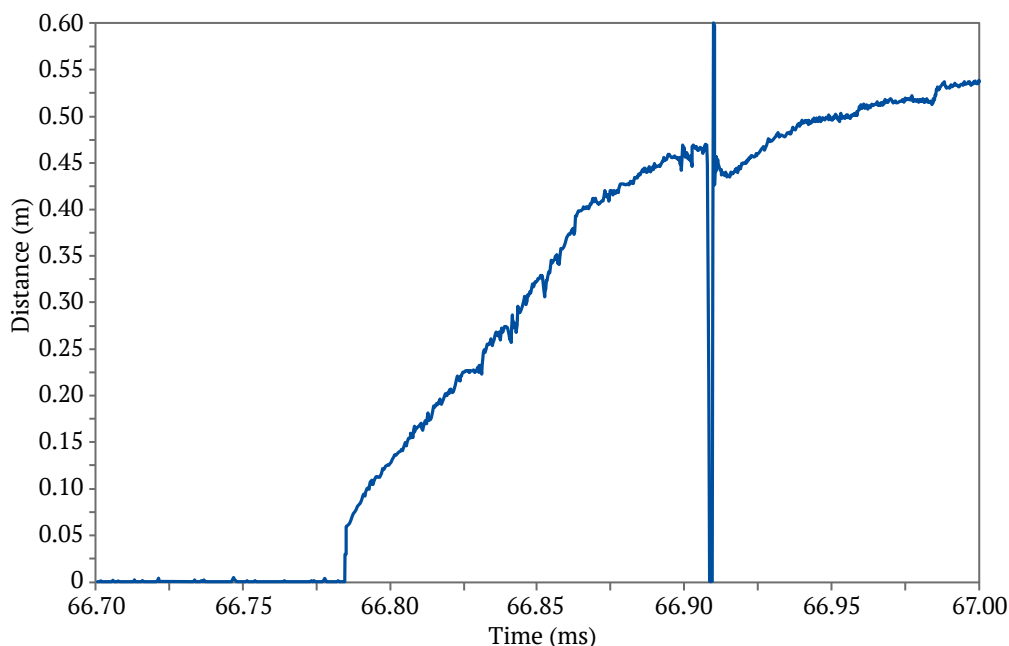


Fig. 3. Graph of distance versus time dependence when measuring detonation velocity [compiled by the authors]

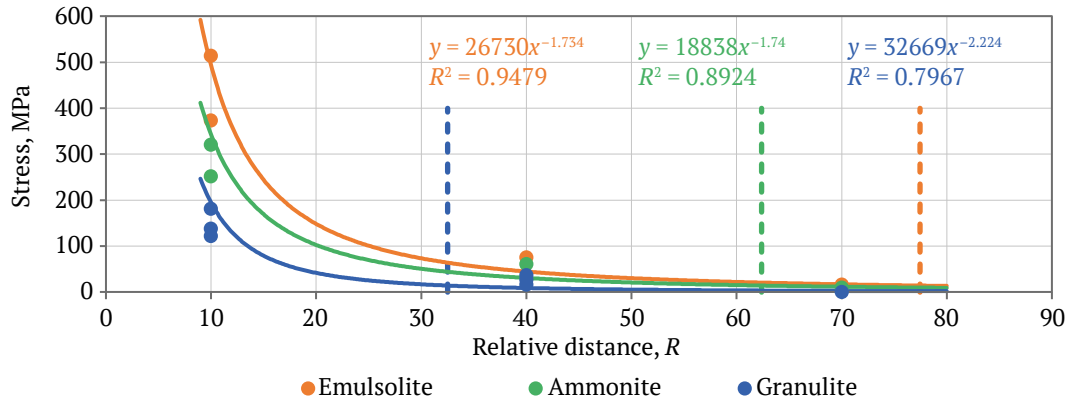


Fig. 4. Graph of stress as a function of distance [compiled by the authors]

While the qualitative determination of the presence of microfractures is necessary to determine the size of the wave prefracture zone, the quantitative parameter is required to justify the degree of prefracture, which is determined by the intensity of fracturing, which is the concentration of microfractures per a certain volume (cm³).

The X-ray computed microtomography method [43] was applied to obtain quantitative characterizations of the sample microfracturing. The reconstruction of binary models of X-ray images allowed the calculation of microfractures per the material volume [44]. SkyScan 1173 tomograph was used for this study and the data were processed using a specialized software.

X-ray computer microtomography data are presented as a set of cross-sections for each sample. The material was taken from the entire sample volume at a layer thickness increment of 20 μm. Since the resolving power of the equipment allows to determine microfractures with a minimum length of 50 μm, and the average limestone grain size is about 0.2 mm [45, 46], the number of intergranular and transgranular microfractures only was taken into account. The concentration of fractures was determined through their density – the number of visible microfractures per unit of area, after which a conversion to fracture density was performed (the number of fractures per unit volume (pcs/cm³)).

3. Findings

When explosive charges were detonated, the accelerations of rock mass displacement at different distances and the detonation velocity at each blast were measured. The average detonation velocities for Granulite, Ammonite, and Emulsolite were 2,000, 4,330, and 5,215 m/s, respectively.

To calculate the stresses, the following parameters were taken into account: ρ₀ – material density,

kg/m³; C_p – longitudinal wave propagation velocity in the rock mass, m/s; U_x – rock displacement velocity within the measured limits [30]. The displacement velocity of rock mass particles was calculated taking into account the stress wave front rise time as a function of the distance.

As shown in Fig. 4, the dependence of blast-induced stresses in a rock on the relative distance, denoted by the value of the radius of an explosive charge, takes the form of a power function. Vertical lines on the graph indicate the boundaries of microfracture formation zones (prefracture zones), which are in the range from 33 (for Granulite) to 77 (for Emulsolite) charge radii. These limits were determined based on the stress values (stress wave pressure) presented in the graph, in accordance with the rock uniaxial compressive strength of 95 MPa. The maximum recorded stress at 10 charge radii is 515 MPa and the minimum one at 70 charge radii is 0.4 MPa.

The dependence of the acceleration pulse rise time on the distance is shown in Fig. 5.

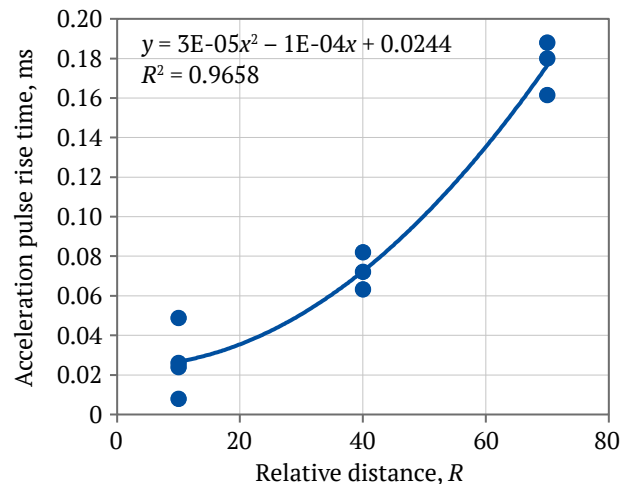


Fig. 5. Graph of acceleration pulse rise time as a function of distance [compiled by the authors]

Samples recovered before and after a blast were scanned to obtain a volumetric model and subsequently calculate fracture densities. The results of the binary models reconstruction for the sample X-ray images are presented in Fig. 6.

The method of calculation of microfracture density allowed determining the difference of their density before and after a blast. Fig. 7 shows an example of processing (quantification of microfracture density data).

According to the experiment data before the blast, the average fracture density was 1,678 pcs/cm³. The present value was taken as relative zero. The dependence of the microfracture density N on the stresses σ occurring in a rock is shown in Fig. 8 and is determined by the following expression:

$$N = 35.389\sigma - 195.49. \quad (4)$$

Based on the data obtained, we plotted the density of microfractures caused by the blast as a function of detonation velocity in limestone rock for various relative distances (Figs. 9–11).

4. Discussion

The obtained dependences are presented based on the parameters of blasts of Ammonite No. 6ZhV, Granulite RP and Emulsolite A-20 for limestone type rock with uniaxial compressive strength of 95 MPa. The different types of explosives with detonation velocities differing by at least 20% were used to allow an objective comparison of the results obtained.

The dependence of stresses in the rock caused by a blast on the relative distance for each type of explosives has the form of a power function that agrees with the data obtained earlier by other authors. The boundary of the prefracture zone in case of the blast of Emulsolite is at 77 radii of the charge from the blast hole and decreases to 33 radii for the blast of Granulite. This confirms the fact of the influence of an explosive detonation velocity on the size of prefracture zones. Beyond these boundaries, no blast-induced microfracturing is observed, as evidenced by the laboratory study on determining microfracture densities

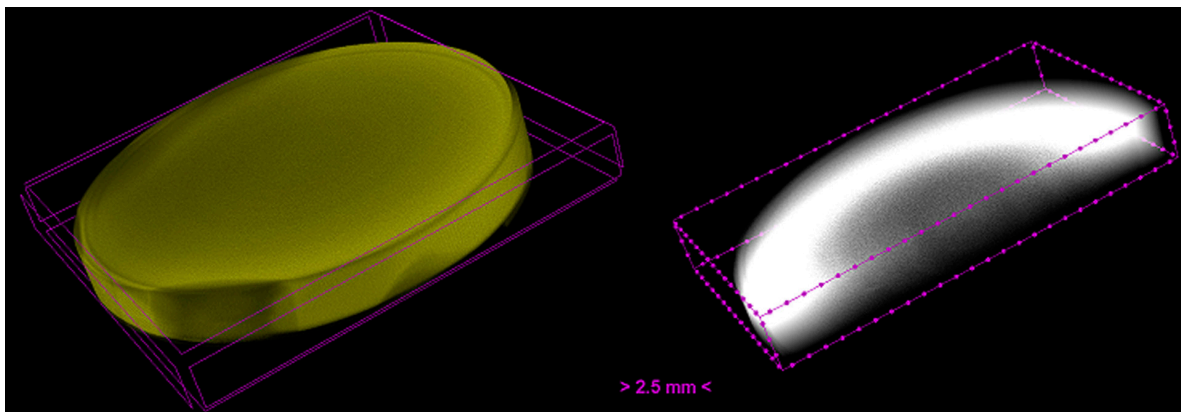


Fig. 6. Sample volumetric model [compiled by the authors]

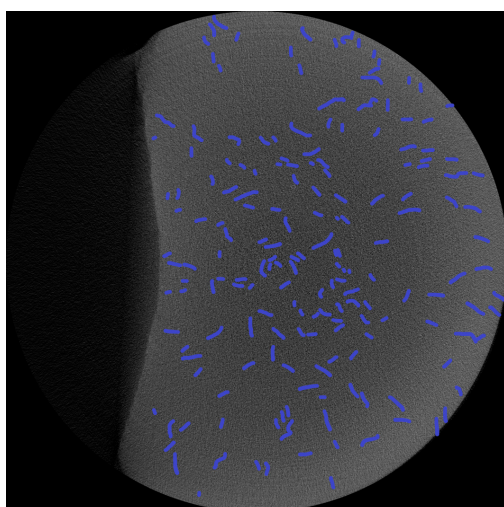


Fig. 7. Microfractures in a sample recovered after a blast at a relative distance of 40R (marked in blue) [compiled by the authors]

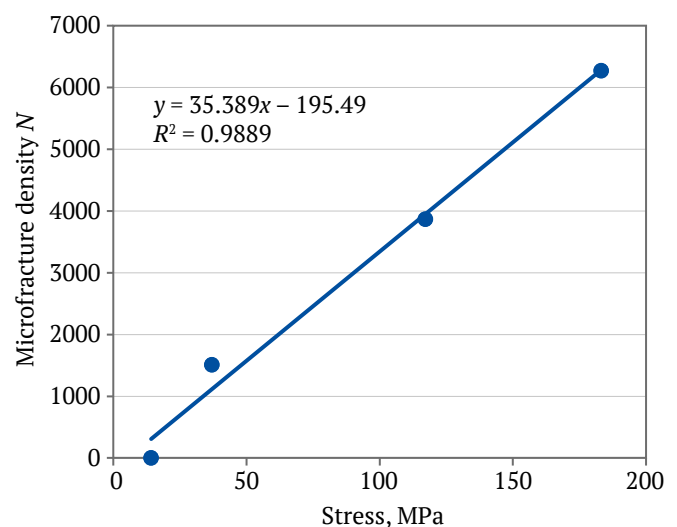


Fig. 8. Graph of the number of fractures in the rock as a function of stress [compiled by the authors]

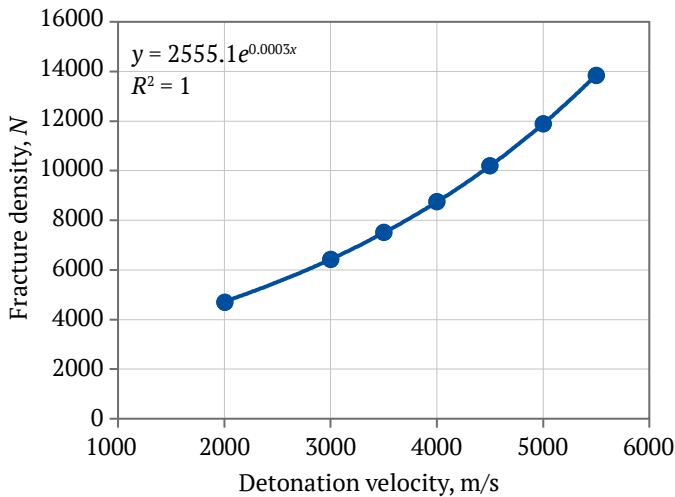


Fig. 9. Graph of the number of fractures as a function of detonation velocity at 10R [compiled by the authors]

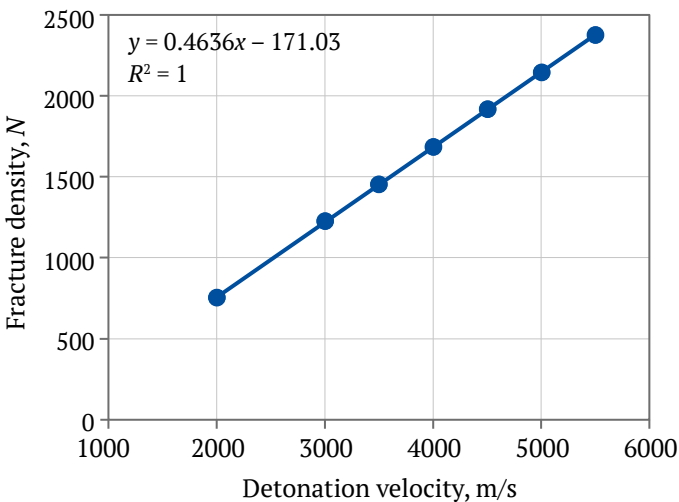


Fig. 10. Graph of the number of fractures as a function of detonation velocity at 40R [compiled by the authors]

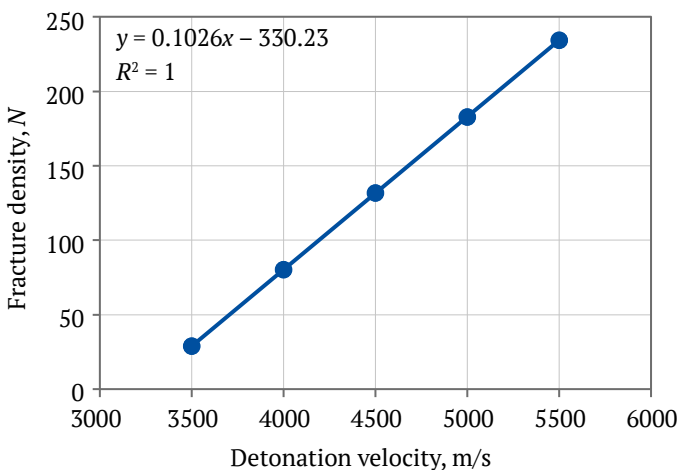


Fig. 11. Graph of the number of fractures as a function of detonation velocity at 70R [compiled by the authors]

at different distances. This allows qualitative determination of prefracture in the limestone rock mass, but most of the study is devoted to quantifying the density of microfractures within the rupture and prefracture zones.

At short distances (10 charge radii), the functions of the dependence of stresses and fracture density on the velocity of explosive detonation have an exponential form, while at medium and long distances (40 and 70 radii), the dependence is linear. This may indicate that the velocity of explosive detonation has the greatest effect on rock prefracture predominantly at short distances. At the same time, the stress pulse rise time increases with increasing the distance. A high-amplitude stress pulse of short duration favors over-crushing of the rock at close distances, but with increasing distance from the blast the stress wave flattens out, leading to better crushing in terms of building stone extraction.

Determination of a quantitative indicator of rock microfracturing is necessary to calculate the degree of wave prefracture of both the whole rock mass and individual pieces after a blast. Undoubtedly, the accumulation of microdefects is stochastic in nature, but an increase in the density of microfractures in the entire volume of the samples was established. The obtained dependence of the microfracture density on the blast-induced stresses arising in a rock has a linear form. In [47-50], it was determined that the magnitude of blast stresses affects the degree of structural weakening of the fragment under consideration that is explained by an increase in fracture density. But in the above studies the authors did not consider quantitative indicators of fracturing, and thus the results of the present study are an addition to the previous studies findings.

Natural microfracturing also affects the strength properties of a rock [51], but in this paper, wave rock prefracture by blasting was considered. The density of natural microfractures was considered as relative zero because the existing microdefects in the rock before a blast affect the stress wave parameters in the rock, and these parameters were actually measured.

Conclusion

When mining hard rock for crushed stone, blast-induced microfracturing has an adverse impact on the quality of the final product.

The results of the experimental studies to determine the qualitative and quantitative parameters of rock prefracture during blast are presented. For instance, when the velocity of explosive detonation increases from 2 to 5.2 km/s, the prefracture zone increases from 33 to 77 charge radii. The dependence of



the number of microdefects (microfractures) generated by a blast on the velocity of explosive detonation takes the form of an exponent for the near zone and is linear for distances far from the blast. According to the data of the experiments conducted at short distances (10R), the density of induced microfracturing N is within ≈ 5 thousand pcs/cm³, and with increasing detonation velocity it increases to ≈ 13.8 thousand pcs/cm³. At medium (40R) and long (70R) distances, N increases from ≈ 750 to ≈ 2400 pcs/cm³ and from 0 to ≈ 200 pcs/cm³, respectively.

It was established that the greatest influence on the shape and duration of the blast pulse is exerted by the velocity of explosive detonation. As the detonation velocity decreases, the peak pressure of the head

part of the pulse decreases, and the duration of its rise increases, while a low-amplitude pulse of long duration contributes to better crushing of a rock mass with the least effect of prefracture.

Using explosives with a reduced detonation velocity allows reducing the “surplus” impact on a rock mass and thus reducing the intensity of prefracture in the zone of controlled crushing during a blast. This is because the individual pieces will be weakened to a lesser extent after a blast and as a result, the yield of undersize when crushing rock into crushed stone will be reduced.

Further consideration of other ways of influencing the degree of structural weakening of a rock within the rupture zone is planned.

References

1. Akhtyamov V.F., Khafizova E.N. Influence of technological non-metallic production wastes on heavy weight concrete properties. *The Russian Automobile and Highway Industry Journal*. 2018;15(2):261–268. (In Russ.) <https://doi.org/10.26518/2071-7296-2018-2-261-268>
2. Khafizova E.N., Akhtyamov V.F., Panchenko I.F., Panchenko D.A. Micro-fine component of stone screening dust in heavy weight cement concrete. *Innovation & Investment*. 2019;(9):261–266. (In Russ.) URL: <https://www.innovazia.ru/upload/iblock/398/gxovlpzi12czrbffn0jydg9ks8se85k/%E2%84%969%202019.pdf>
3. Samukov A.D. Complex recycling of crushed aggregates waste. *Ecology and Industry of Russia*. 2019;23(7):15–19. (In Russ.) <https://doi.org/10.18412/1816-0395-2019-7-15-19>
4. Ding X., Ao Z., Li X. et al. The mechanism of plugging open-pit mine cannon holes and the modification of plugging materials. *Sustainability*. 2023;15(5):4257. <https://doi.org/10.3390/su15054257>
5. Moldovan D.V., Chernobay V.I., Yastrebova K.N. The influence of composite material in the stemming design on its operability. *Mining Informational and Analytical Bulletin*. 2023;(9-1):110–121. (In Russ.) https://doi.org/10.25018/0236_1493_2023_91_0_110
6. Kakharov Z.V., Islomov A.S. Concretes with aggregates from secondary concrete crushing products. *Vestnik Nauki*. 2023;3(5):820–825. (In Russ.)
7. Kornev A.V., Spitsyn A.A., Korshunov G.I., Bazhenova V.A. Preventing dust explosions in coal mines: Methods and current trends. *Mining Informational and Analytical Bulletin*. 2023;(3):133–149. https://doi.org/10.25018/0236_1493_2023_3_0_133
8. Shamaev M.K., Toshtemirov U.T. Extraction of crushed stone and requirements for their quality. *Analytical Journal of Education and Development*. 2022;2(10):131–137. (In Russ.)
9. Ganina A.S., Studenok G.A. Disposal of waste sand from crushing undersizes (fines) in the production of crushed stone. In: *Proceedings of the International Scientific and Practical Conference “Ural Mining School – for Regions”*. Ekaterinburg, April 11, 2022. Ekaterinburg: Ural State Mining University Publ.; 2022. Pp. 390–391. (In Russ.)
10. Korshunov G.I., Karimov A.M., Magamedov G.S., Tyulkin S.A. Reduction of respirable dust-induced impact on open pit mine personnel in large-scale blasting. *Mining Informational and Analytical Bulletin*. 2023;(7):132–144. https://doi.org/10.25018/0236_1493_2023_7_0_132
11. Kameneva E.E., Aminov V.N., Shchukin P.O. Definition of the problem of development and scientific substantiation of technologies for disintegration of overburden and host rocks of different genetic types to obtain building crushed stone. In: *Findings of Research on the Processes of Disintegration of Strong Rocks in Order to Reduce Energy Consumption and Produce Additional Products in the Processing and Beneficiation of Ores and Technogenic Raw Materials*. Collection of scientific papers. Petrozavodsk: VERSO LTD Publ.; 2016. Pp. 3–5. (In Russ.)
12. Tan N., Yang R., Tan Z. Influence of complicated faults on the differentiation and accumulation of in-situ stress in deep rock mass. *International Journal of Minerals, Metallurgy and Materials*. 2023;30(5):791–801. <https://doi.org/10.1007/s12613-022-2528-y>



13. Kovalevich S., Zyryanov I., Chernobay V. Experience of drilling-and-blasting in diamond fields in Yakutia. *Journal of Mining Science*. 2023;58:953–965. <https://doi.org/10.1134/S1062739122060102>
14. Kochanov A.N. Study of parameters of rock mass prefracture zones as a basis for the improvement of blasting technology. *Mining Informational and Analytical Bulletin*. 1996;(5):49–52. (In Russ.)
15. German V.I. Rock failure prediction in mines by seismic monitoring data. *Journal of Mining Sciences*. 2014;(2):99–109. (In Russ.)
16. Moldovan D.V., Chernobay V.I., Sokolov S.T., Bazhenova A.V. Design concepts for explosion products locking in chamber. *Mining Informational and Analytical Bulletin*. 2022;(6–2):5–17. (In Russ.) https://doi.org/10.25018/0236_1493_2022_62_0_5
17. Gospodarikov A.P., Trofimov A.V., Kirkin A.P. Evaluation of deformation characteristics of brittle rocks beyond the limit of strength in the mode of uniaxial servohydraulic loading. *Journal of Mining Institute*. 2022;256:539–548. <https://doi.org/10.31897/PMI.2022.87>
18. Kochanov A.N., Odintsev V.N. Theoretical estimation of microfractured area radius after camouflet explosion. *Explosion Technology*. 2015;(113/70):41–54. (In Russ.)
19. Menzhulin M.G., Shishov A.N., Paramonov G.P., Uvarov A.N. Kinetics of accumulation of induced fracturing in granite under the action of blast loads. *Mining Informational and Analytical Bulletin*. 1999;(1):143–146. (In Russ.)
20. Korshunov V.A., Pavlovich A.A., Bazhukov A.A. Evaluation of the shear strength of rocks by cracks based on the results of testing samples with spherical indentors. *Journal of Mining Institute*. 2023;262:606–618. <https://doi.org/10.31897/PMI.2023.16>
21. Wei M., Dai F., Liu Y., Jiang R. A fracture model for assessing tensile mode crack growth resistance of rocks. *Journal of Rock Mechanics and Geotechnical Engineering*. 2023;15(2):395–411. <https://doi.org/10.1016/j.jrmge.2022.03.001>
22. Alenichev I.A., Rakhmanov R.A. Empirical regularities investigation of rock mass discharge by explosion on the free surface of a pit bench. *Journal of Mining Institute*. 2021;249:334–341. <https://doi.org/10.31897/PMI.2021.3.2>
23. Kabetenov T., Yusupov Kh.A., Rustemov S.T. Rational parameters of blasting, considering action time of explosion-generated pulse. *Journal of Mining Sciences*. 2015;(2):75–81. (In Russ.)
24. Borovikov V.A., Andreev A.A., Efremovtsev N.N. Features of detonation of granulites including low-density polystyrene-containing compositions. *Mining Informational and Analytical Bulletin*. 2007;(6–3):53–62. (In Russ.)
25. Vinogradov Y.I., Artemov V.A. Blasting charge diameter influence on the blasting efficiency. *Journal of Mining Institute*. 2012;198:170–173. (In Russ.)
26. Valkov V.A., Vinogradov K.P., Valkova E.O., Mustafin M.G., Creating highly informative rasters based on laser scanning and aerial photography data. *Geodesy and Cartography*. 2022;83(11):40–49. (In Russ.) <https://doi.org/10.22389/0016-7126-2022-989-11-40-49>
27. Dolzhikov V.V., Ryadinsky D.E., Yakovlev A.A. Influence of deceleration intervals on the amplitudes of stress waves during the explosion of a system of borehole charges. *Mining Informational and Analytical Bulletin*. 2022;(6–2):18–32. https://doi.org/10.25018/0236_1493_2022_62_0_18
28. Artemov V.A., Vinogradova E.Yu., Vinogradov Yu.I., Gendler S.G. Influence of parity between depth of charge placing and weight of explosive on seismoblast waves parameters in near zone of explosion. *Explosion Technology*. 2009;(101/58):303–307. (In Russ.)
29. Menshikov P., Sinizin V., Shemenov V. Main detonation characteristics of explosives determination using the DATATRAP II DATA/VOD RECORDER measuring equipment. *Problems of Subsoil Use*. 2016;(4):112–120. (In Russ.) <https://doi.org/10.18454/2313-1586.2016.04.112>
30. Konurin A.I., Eremenko A.A., Filippov V.N. Assessment features for rock mass conditions under production blasting and geodynamic events. *Mining Informational and Analytical Bulletin*. 2017;(7):153–160. (In Russ.)
31. Ilyakhin S.V., Maslov I.Yu., Bragin P.A. Elementary theory of a measuring cable with a resistive method for measuring velocity of detonation of an explosive. *News of the Ural State Mining University*. 2019;(4):104–108. (In Russ.) <https://doi.org/10.21440/2307-2091-2019-4-104-108>
32. Rodionov V.A., Karpov G.N., Leisle A.V. Methodological approach to the need to assess the explosion and fire hazard properties of sulfide-containing polymetallic ores. *Mining Informational and Analytical Bulletin*. 2022;(6–1):198–213. https://doi.org/10.25018/0236_1493_2022_61_0_198



33. Dong L., Zou W., Li X. et al. Collaborative localization method using analytical and iterative solutions for microseismic/acoustic emission sources in the rockmass structure for underground mining. *Engineering Fracture Mechanics*. 2019;210:95–112. <https://doi.org/10.1016/j.engfracmech.2018.01.032>
34. Potokin A.S., Pak A.K. Study of acoustic and electromagnetic emissions under uniaxial compression of hard rock samples. *Naukosfera*. 2020;(11–2):86–91. (In Russ.) <https://doi.org/10.5281/zenodo.4309468>
35. Rodríguez P., Celestino T.B. Application of acoustic emission monitoring and signal analysis to the qualitative and quantitative characterization of the fracturing process in rocks. *Engineering Fracture Mechanics*. 2019;210:54–69. <https://doi.org/10.1016/j.engfracmech.2018.06.027>
36. Bekher S.A., Popkov A.A. Temporal characteristics of the flow of acoustic emission signals in the development of cracks in glass under shock loading. *Vestnik IzhGTU imeni M. T. Kalashnikova*. 2019;22(1):62–71. (In Russ.) <https://doi.org/10.22213/2413-1172-2019-1-62-71>
37. Hu X., Su G., Chen G. et al. Experiment on rockburst process of borehole and its acoustic emission characteristics. *Rock Mechanics and Rock Engineering*. 2019;52:783–802. <https://doi.org/10.1007/s00603-018-1613-z>
38. Ghasemi S., Khamehchiyan M., Taheri A. et al. Crack evolution in damage stress thresholds in different minerals of granite rock. *Rock Mechanics and Rock Engineering*. 2020;53:1163–1178. <https://doi.org/10.1007/s00603-019-01964-9>
39. Du K., Li X., Tao M., Wang Sh. Experimental study on acoustic emission (AE) characteristics and crack classification during rock fracture in several basic lab tests. *International Journal of Rock Mechanics and Mining Sciences*. 2020;133:104411. <https://doi.org/10.1016/j.ijrmms.2020.104411>
40. Shkuratnik V.L., Novikov E.A., Oshkin R.O. Experimental analysis of thermally stimulated acoustic emission in various-genotype rock specimens under uniaxial compression. *Journal of Mining Sciences*. 2014;(2):69–76. (In Russ.)
41. Oparin V.N., Usol'tseva O.M., Semenov V.N., Tsoi P.A. Evolution of stress–strain state in structured rock specimens under uniaxial loading. *Journal of Mining Sciences*. 2013;(5):3–19. (In Russ.)
42. Viktorov S.D., Kochanov A.N., Odintsev V.N. Pre-destruction of rocks as a stage of fracture process under quasi-static and dynamic loading. *Journal of Mining Institute*. 2007;171:153–157. (In Russ.)
43. Ponomarev A.A., Zavatsky M.D. Methods of application of computer microtomography in geology. *Oil and Gas Studies*. 2015;(3):31–35. (In Russ.) <https://doi.org/10.31660/0445-0108-2015-3-31-35>
44. Koteleva N.I., Valnev V.V., Korolev N.A. Augmented reality as a means of metallurgical equipment servicing. *Tsvetnye Metally*. 2023;(4):14–23. <https://doi.org/10.17580/tsm.2023.04.02>
45. Vettegren V.I., Kuksenko V.S., Shcherbakov I.P. The mechanism and dynamics of rock fracture upon mechanical impact and electric discharge. *Izvestiya, Physics of the Solid Earth*. 2016;52(5):754–769. <https://doi.org/10.1134/S106935131604011X> (Orig. ver.: Vettegren V.I., Kuksenko V.S., Shcherbakov I.P. The mechanism and dynamics of rock fracture upon mechanical impact and electric discharge. *Fizika Zemli*. 2016;(5):134–149. <https://doi.org/10.7868/S0002333716040116>)
46. Yashunsky Yu.V., Novikov I.A., Shkurskii B.B. et al. Authigenic potassium feldspar from upper carboniferous limestone of Moscow Region. *Bulletin of Moscow Society of Naturalists. Geological Series*. 2016;91(6):49–61. (In Russ.)
47. Kochanov A.N., Odintsev V.N. Wave pre-destruction of solid rocks under blasting. *Journal of Mining Sciences*. 2016;(6):38–48. (In Russ.)
48. Kochanov A.N. Some research results in the field of blasting rock rupture. In: *Problems and Prospects of Integrated Development and Conservation of Earth's Subsoil. Collection of articles from the 5th Conference of the International Scientific School of K. N. Trubetskoy, Academician of the Russian Academy of Sciences*. Moscow, November 14–18, 2022. Moscow: IPCON RAS; 2022. Pp. 112–115. (In Russ.)
49. Shevkun E.B., Leshchinskiy A.V., Lysak Yu.A., Plotnikov A. Yu. Long-period delay loosening blasting in open pit mines. *Mining Informational and Analytical Bulletin*. 2020;(10):29–41. (In Russ.) <https://doi.org/10.25018/0236-1493-2020-10-0-29-41>
50. Fan X., Jiang X., Liu Y. et al. Local stress distribution and evolution surrounding flaw and opening within rock block under uniaxial compression. *Theoretical and Applied Fracture Mechanics*. 2021;112:102914. <https://doi.org/10.1016/j.tafmec.2021.102914>
51. Isheisky V.A., Ryadinskii D.E., Magomedov G.S. Increasing the quality of fragmentation of blasting rock mass ased on accounting for structural features of massif in the blast design. *Mining Informational and Analytical Bulletin*. 2023;(9–1):79–95. (In Russ.) https://doi.org/10.25018/0236_1493_2023_91_0_79



Information about the authors

Sergei V. Khokhlov – Cand. Sci. (Eng.), Associate Professor, Department of Explosive Engineering, Empress Catherine II Saint Petersburg Mining University, Saint Petersburg, Russian Federation; ORCID [0000-0003-1040-8328](https://orcid.org/0000-0003-1040-8328), Scopus ID [57199258554](https://scopus.com/authorid/57199258554), ResearcherID [AAG-5849-2019](https://orcid.org/AAG-5849-2019); e-mail khokhlov_sv@pers.spmi.ru

Juriy I. Vinogradov – Cand. Sci. (Eng.), Senior Researcher, Associate Professor, Department of Explosive Engineering, Empress Catherine II Saint Petersburg Mining University, Saint Petersburg, Russian Federation; ORCID [0000-0001-9468-2214](https://orcid.org/0000-0001-9468-2214), Scopus ID [57208625767](https://scopus.com/authorid/57208625767), ResearcherID [AAG-5997-2019](https://orcid.org/AAG-5997-2019); e-mail vinogradov_yui@pers.spmi.ru

Viacheslav A. Makkoev – PhD-Student (Eng.), Department of Explosive Engineering, Empress Catherine II Saint Petersburg Mining University, Saint Petersburg, Russian Federation; ORCID [0000-0003-3656-3625](https://orcid.org/0000-0003-3656-3625), Scopus [57428865400](https://scopus.com/authorid/57428865400); e-mail s215079@stud.spmi.ru

Zaur A. Abiev – Assistant (Eng.), Department of Explosive Engineering, Empress Catherine II Saint Petersburg Mining University, Saint Petersburg, Russian Federation; ORCID [0000-0002-9789-1115](https://orcid.org/0000-0002-9789-1115), Scopus ID [57206657220](https://scopus.com/authorid/57206657220); e-mail Abiev_ZA@pers.spmi.ru

Received 02.11.2023

Revised 08.01.2024

Accepted 18.02.2024



MINERAL RESOURCES EXPLOITATION

Research paper

<https://doi.org/10.17073/2500-0632-2023-12-187>

UDC 622.235

**Theoretical aspects of block stone blasting method**

V. N. Kovalevsky , A. V. Mysin , V. I. Sushkova

Empress Catherine II Saint Petersburg Mining University, Saint Petersburg, Russian Federation s235054@stud.spmi.ru**Abstract**

Block stone excavation is a key aspect of the building materials industry, important for providing construction with durable materials and when giving aesthetic solutions to various structures and design elements. However, when excavating stone (using drilling and blasting), it is necessary to maintain its integrity for further processing and use. The conditions required for applying the method of blasting separation (split off) of stone blocks from hard rock mass were considered, which is important for improving the quality of blasted stone blocks. The rational parameters of stone block blasting with Granilen elastic tubular charges (Granilen ETCs) are presented. An approach to the preliminary assessment of stone block fracturing zone under various explosive loading regimes was determined. The relationship between the consumption of explosives and fracturing of stone blocks at possible blasthole spacing was considered. The mechanism of creating an extended rupture plane in a rock mass was studied. The decisive role of stress waves in the formation of an extended main rupture along the line of blasthole charges was established. It was shown that it is possible to localize the zone of induced fracturing by regulating the conditions for the interaction of stress waves. The results of numerical modeling of stress fields at blasting a single charge and a two-charge Granilen ETC system are presented, which made it possible to assess zones of induced fracturing and the conditions for the formation of a main rupture. Blasting effectiveness increases significantly due to the orientation of the expected stone block separation line parallel to the plane of the best rupture, taking into account the anisotropy of the physical and mechanical properties of granites. The study confirms the feasibility of increasing the yield of commodity blocks when selecting rational blasting parameters.

Keywords

block rock mass, drilling and blasting parameters, directed flow, charge design, blast pulse, blast product pressure, stress diagrams, dynamic strength limit, roughness, induced fracturing

For citation

Kovalevsky V. N., Mysin A. V., Sushkova V. I. Theoretical aspects of block stone blasting method. *Mining Science and Technology (Russia)*. 2024;9(2):97–104. <https://doi.org/10.17073/2500-0632-2023-12-187>

РАЗРАБОТКА МЕСТОРОЖДЕНИЙ ПОЛЕЗНЫХ ИСКОПАЕМЫХ

Научная статья

Теоретические аспекты технологии взрывной отбойки блочного камня

В. Н. Ковалевский , А. В. Мысин , В. И. Сушкова

Санкт-Петербургский горный университет императрицы Екатерины II, г. Санкт-Петербург, Российская Федерация s235054@stud.spmi.ru**Аннотация**

Добыча блочного камня является ключевым аспектом индустрии строительных материалов, важным для обеспечения строительства прочными материалами и при придании эстетических решений различным конструкциям и элементам дизайна. Однако при добыче камня (производстве буровзрывных работ) необходимо сохранить его целостность для последующей обработки и использования. В рамках исследования были рассмотрены условия, необходимые для применения технологии взрывной отбойки блочного камня из скальных горных пород, что актуально для повышения качества отбиваемых камнеблоков. Приведены рациональные параметры взрывной отбойки камнеблоков зарядами эластичными трубчатыми (ЗЭТ) «Гранилен». Определен подход к предварительной оценке зоны нарушения блочного камня при различных режимах взрывного нагружения. Рассмотрена взаимосвязь между расходом взрывчатых веществ (ВВ) и нарушением камнеблоков при возможных расстояниях между шпурами. Исследован механизм создания протяженной плоскости разрыва в массиве горных пород. Установлена определяющая роль волн напряжений при формировании протяженной магистральной трещины по линии шпуровых зарядов. Показана возможность локализации зоны наведенной трещиноватости за счет регулирования условий взаимодействия волн напряжений. Приведены результаты численного моделирования полей напряжений при взрыве одиночных и системы из двух зарядов ЗЭТ «Гранилен», что позволило оценить зоны наведенной трещиноватости и условий формирования магистральной трещины отрыва. Эффективность взрывной отбойки значительно возрастает за счет ориентации ли-



нии предполагаемого отрыва монолита параллельно плоскости наилучшего раскола, учитывая при этом анизотропию физико-механических свойств гранитов. Исследование подтверждает возможности повышения выхода товарных блоков при подборе рациональных параметров взрывной отбойки.

Ключевые слова

блочный массив, параметры буровзрывных работ, направленный расход, конструкция заряда, импульс взрыва, давление продукта взрыва, эпюры напряжений, динамический предел прочности, шероховатость, наведенная трещиноватость

Для цитирования

Kovalevsky V.N., Mysyn A.V., Sushkova V.I. Theoretical aspects of block stone blasting method. *Mining Science and Technology (Russia)*. 2024;9(2):97–104. <https://doi.org/10.17073/2500-0632-2023-12-187>

Introduction

Block stone excavation is a key aspect of the building materials industry, important for providing construction with durable materials and when giving aesthetic solutions to various structures and design elements. However, when excavating stone (using drilling and blasting), it is necessary to maintain its integrity for further processing and use [1].

Some deposits demonstrate high variability in physical and mechanical properties in different parts of a quarry field.

The natural features of natural stone deposits determine the volume of blocks mined and their yield from a rock mass being developed [2]. They are governed by the distances between existing fractures, which vary widely in granite rock masses [3].

The choice of a block stone blasting process flow sheet (PFS) is determined by the structure of rock mass, petrographic features, geometric dimensions of the useful thickness [4].

In this regard, drilling and blasting method in the development of block stone deposits remains in demand at present [5].

As studies [6–8] show, the main parameters of drilling and blasting operations at separation of stone blocks from a rock mass are a blasthole diameter, distance between blastholes, their depth, thickness of a separated stone block, charge type, design, mass, diameter.

The choice of the optimal blasthole spacing depends both on the physical and mechanical properties of a rock and on the initial parameters of the blast pulse: the amplitude of the initial pressure in the blast chamber and the duration of action at the quasi-static stage, necessary for the formation and growth of the main rupture between the blastholes, as well as to ensure the movement of a stone block [9].

In this case, the blasting conditions should ensure the creation of a fracture in the split-off plane with minimal disturbance of the peri-blasthole space [10].

In order to ensure the process of directional fracturing, it is necessary that the pressure of blast products would be greater than the tensile strength of a rock, and, for the preservation of a peripheral rock mass, the pressure of blast products in a blasthole

should not exceed the rock compressive strength [11]. These conditions are achieved by selecting rational blasthole spacing and optimal parameters of a blast pulse [12, 13]. In particular, the use of Granilen ETCs fully allows meeting these requirements [14].

Performing directed fracturing is possible when the pressure of gaseous products in a blasthole exceeds the dynamic tensile strength of a rock, and the preservation of a rock mass in the peri-blasthole zone requires that this pressure does not exceed the compressive strength of the rock [15–17].

The results of the studies presented in [18, 19] indicate that the increase of the radial air gap with respect to the radius of the charge by 3–4 times provides a predominant role of the blast products quasi-static pressure in the directional rupturing. Therefore, a very effective way to control the intensity of the wave and quasi-static stress field can be the regulation of the volumetric concentration of explosive charge energy in a blasthole [20].

The use of Granilen ETCs assumes the creation of the above conditions. The design of Granilen ETCs provides the possibility of regulating the force and time parameters of a blast impulse by changing a charge mass in a blasthole, its length, using the gap between the charge and the blasthole wall, applying stemming, varying blasthole spacing.

The substantiated rational values of blasthole charges parameters allow providing the minimum roughness of faces of a split off stone block and insignificant induced fracturing in the peri-blasthole zone.

Methods and materials

As a rule, separation of a stone block from a rock mass occurs when closely spaced blasthole charges are simultaneously initiated with the detonating cord. In this case, the rock in the plane of location of charges in block perimeter blastholes will be subjected mainly to the action of tensile stresses [21–23].

Consequently, the following conditions must be met in order to split off a block and move it by 0.15–0.3 m [24]:

$$F \geq F_1 + F_2 + F_3, \quad (1)$$

where F is force causing breaking away (separation) and displacement of a stone block, Pa; F_1 is force

leading to split off of a stone block from a rock mass with rupturing area S ($S = BH_{bench}$), Pa, where B is length of a stone block, m; H_{bench} is bench height, m; F_2 is friction force, Pa; F_3 is a force allowing to take into account the layer dip angle, Pa.

Then:

$$F = P_{bp}Nd_{bh}L_{bh}, \quad (2)$$

where P_{bp} is pressure of gaseous blast products in a blasthole, Pa; N is number of blastholes in a row, pcs; d_{bh} is blasthole diameter, m; L_{bh} is blasthole depth, m;

$$F_1 = \sigma_{rupt}^d (BH_{bench} - Nd_{bh}L_{bh}), \quad (3)$$

where σ_{rupt}^d is dynamic tensile strength, Pa;

$$\sigma_{rupt}^d = K_{weak} \cdot K_f \cdot K_i \cdot [\sigma_{rupt}^d], \quad (4)$$

where K_{weak} is a coefficient of structural weakening of a rock mass, $K_{weak} = 0.2-0.4$;

$$K_f \approx \left(\frac{C_p}{C_{p.rm}} \right)^2;$$

K_i is coefficient of impact (for granite = 4–5.7)¹; K_f is acoustic index of fracturing; $C_{p.rm}$ and C_p are P-wave velocities in a rock mass and rock sample, respectively, m/s.

The force which should be applied to overcome the friction between the block and the base as the block moves:

$$F_2 = F_{fr} = f_1 G \cos \alpha, \quad (5)$$

where $f_1 = \text{tg} \alpha$ is friction coefficient; G is rough block of stone weight, kg:

$$G = \rho_{rm} BH_{bench} W, \quad (6)$$

where ρ_{rm} is density of rock mass, kg/m³; W is line of least resistance, m; F_3 is force allowing to account for a layer dip angle, Pa:

$$F_3 = G \sin \alpha. \quad (7)$$

The solution of equations (1)–(7) allows obtaining an expression for calculating the number of blastholes:

$$N = \frac{BH_{bench} [\sigma_{rupt}^d \rho_{rm} W (f_1 \cos a \pm \sin a)]}{d_{bh} L_{bh} (P_{bp} + \sigma_{rupt}^d)}. \quad (8)$$

The length of a split off block

$$B = \frac{N_{bh} + 1}{a}, \quad (9)$$

where a is the distance between blasthole charges, m:

$$a = \frac{d_{bh} (P_{bp} + \sigma_{rupt}^d)}{\sigma_{rupt}^d + \rho_{rm} W (f_1 \cos a \pm \sin a)}. \quad (10)$$

Choosing the type of explosives (in our case, Granilen-2 ETC) and using the Noble-Abel formula [25], we determined the mass of explosive to be blasted in a blasthole volume to create the required pressure of detonation products P_{bp} (11):

$$m_{bl} = \frac{\pi P_{bp} T_0 L_{bh} d_{bh}^2}{4 \cdot 22,4 \cdot 10^{-3} n (P_0 T_{bl} + P_{bp} T_0 \cdot 10^{-3})}, \quad (11)$$

where T_0 is initial temperature, $T_0 = 273$ K; n is the number of moles of gaseous blast products; T_{bl} is temperature of blast products, K; P_0 is atmospheric pressure, Pa, $P_0 = 0.1$ МПа.

During blasting separation of a stone block from a rock mass, ruptures and fractures originate in places where pulse reactions occur, the intensity of which is sufficient for rock rupture and which is determined by the charge design, power, and location in the separated stone block [26–28].

In the presence of a layer rupture, the depth of the placed charge (eccentricity) is determined from the following expression:

$$h = \frac{H^2 + 4W^2}{6H}, \quad (12)$$

where H is height of a rock block, m; W is width (thickness) of a rock block, m.

In case of the absence of a layer rupture, the depth of charge placement is determined from the following expression:

$$h = \frac{H^2 + 4W^2 + HWf'_d}{6(H + Wf'_d)}, \quad (13)$$

where f_d and f'_d are dynamic friction coefficients at the top and bottom vertices of a stone block. For approximate calculations, we can assume $f_d = 0.25$; $f'_d = 0.5$.

The optimal width (thickness) of a stone block is determined from the following expression:

$$W = \sqrt{\left(\frac{3h_{ch} + 6m^2}{H} \right)^2 + 16 \left(2 - \frac{3h_{ch} + 6m}{H} \right) - \frac{3h_{ch} + 6m}{H} f_d}, \quad (14)$$

where h_{ch} is charge height, m; m is underbreak, m.

Based on the above methodology, the parameters of drilling and blasting operations for stone block splitting off using Granilen-2 ETCs were calculated, which are presented in Table 1. Along with the determination of the key D&B parameters, the most important condition for the extraction of high-quality stone blocks is the accuracy of delineation of the separated stone block and ensuring the minimum radius of induced fracturing in the peri-blasthole zone.

¹ Dambaev Zh. G. Physical bases of directional rock blasting and techniques of gentle block stone blasting. [Abstract of Doctoral thesis in Eng. Sci.]. St. Petersburg; 2000. 37 p. (In Russ.)

Table 1

Design D&B parameters for rock block excavation in the presence of bottom rupture ($d_{bh} = 42 \text{ mm}$, $d_{ch} = 15 \text{ mm}$, $l_{bh} = 2.9 \text{ m}$)

Item	Blasthole spacing, m			
	0.3	0.4	0.5	0.6
Charge weight in a blasthole, kg	0.27	0.36	0.45	0.54
Total charge weight, kg	22.4	22.7	22.5	22.7
Number of blastholes	83	63	50	42
Blasthole pressure, MPa	31.0	42.5	55.5	67.0
Expected radius of induced fracturing, m	0.026	0.03	0.035	0.038
Charge length in a blasthole, m	0.75	0.84	1.4	1.7

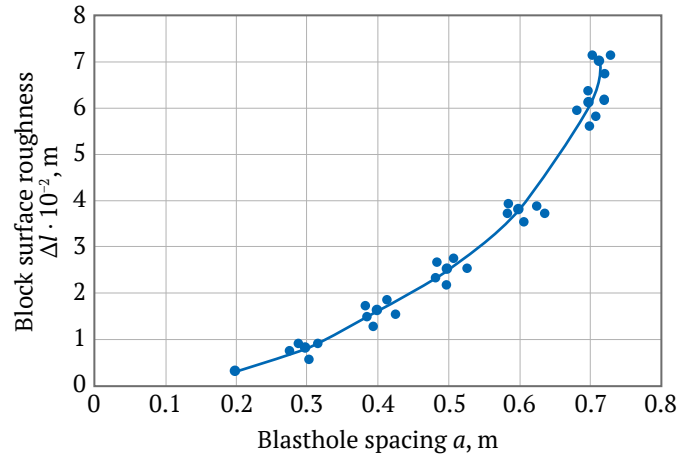


Fig. 1. Block surface roughness as a function of blasthole spacing

The values of these block contour deviations are determined by the charge convergence coefficient equal to

$$n = \frac{a}{W}, \quad (15)$$

where a is blasthole spacing, m; W is width of a stone block, m.

Consequently, the minimum values of a stone block side roughness can be achieved at the optimal value of n .

Based on the results of the tests performed at granite block stone quarries, the dependence of the magnitude of the block contour deviation on blasthole Granilen-2 ETCs spacing was obtained (Fig. 1).

At low-velocity loading mode and interaction of stress waves, an asymmetric stress field is formed around the peripheral (contour) blastholes, which leads to deterministic growth of the main rupture in the split off plane.

Since microfractures are generated by a tensile stress pulse, their surfaces coincide with the radial planes. A contour rupture propagates simultaneously along several structural fractures by fusing microfractures into macrofractures [29]. As a consequence, along the line connecting neighboring charges, the rock mass is weakened by tensile stresses along the contour line, and the main rupture starts to grow between the blastholes, while the growth of side fractures is suspended [30, 31].

The results of studies [25, 32] show that the radius of the zone of induced fracturing in a split off stone block depends both on the size of the charges in the blastholes and the blasthole spacing. The rupture kinetics at directional rupture is determined by both the physical-and-mechanical properties of rocks and the parameters of stresses and pressures

created by the blast products in a charge chamber (blasthole).

When a system of cylindrical charges is blasted, stress waves interact, resulting in a transformation of the stress field.

The approximate method of stress field estimation on the basis of numerical modeling and analytical calculation was used according to the methodology set forth in the studies on the blast of charges with air gap.

As an explosive, Granilen-1 ETCs with charge diameter $d_{ch} = 11 \text{ mm}$ with blast heat $Q = 1550 \text{ kJ/kg}$ was used. The charges were located in blastholes of diameter $d_{bh} = 42 \text{ mm}$ in granite rock mass with rock density $\rho_{rocks} = 2200 \text{ kg/m}^3$, with longitudinal wave velocity $C_p = 6,200 \text{ m/s}$.

The condition of interaction of stress waves providing the main rupture propagation was determined from the expression

$$\sigma_{\varphi_{\max}} \left(\frac{a}{2} \right) = \sigma_{\varphi_1} \left(\frac{a}{2} \right) + \sigma_{\varphi_2} \left(\frac{a}{2} \right) \geq \sigma_{rupt}^{*dyn}, \quad (16)$$

where σ_{φ_1} and σ_{φ_2} are amplitudes of tangential component of stress wave from blasts of neighboring charges, respectively; a – charges spacing, m; σ_{rupt}^{*dyn} – dynamic tensile strength of granite, Pa.

Then [33]:

$$\sigma_{rupt}^{*dyn} = 4\sigma_{rupt}^{st}, \quad (17)$$

where σ_{rupt}^{st} is static tensile strength, $\sigma_{rupt}^{st} = 9.1 \text{ MPa}$, $\sigma_{rupt}^{*dyn} = 36.4 \text{ MPa}$.

This value was taken as the ultimate stress level, below which no main rupture propagation occurred.

The length of a natural microfracture l_0 for granites according to the data of [33] was 0.01–0.03 cm.

The maximum amplitude pressure on a blasthole walls for granites should not exceed 90 MPa [25].

Findings

Figs. 2–4 show the results of calculation of the maximum tangential tensile stresses field when blasting a system of two Granilen-1 ETCs spaced 0.47 and 0.58 m. The charges were initiated simultaneously using a DShE-12 detonating cord passing through the charge channel. The linear densities of charge were 0.14 and 0.16 kg/m.

It follows from the results that the interaction of simultaneously blasted charges leads to a significant

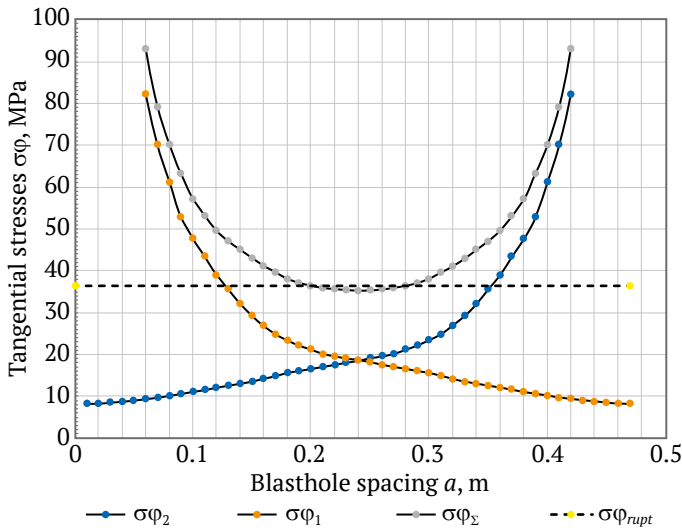


Fig. 2. Individual and total tangential stresses when blasting adjacent charges ($a = 0.47$ m, $q = 0.14$ kg/m): σ_{ϕ_1} and σ_{ϕ_2} are the amplitudes of the tangential component of the stress wave from the first and second charges, respectively, MPa; σ_{ϕ_Σ} is total amplitude of the tangential component of the stress wave from two charges, MPa; σ_{rupt} is maximum permissible value of rupture stress, MPa

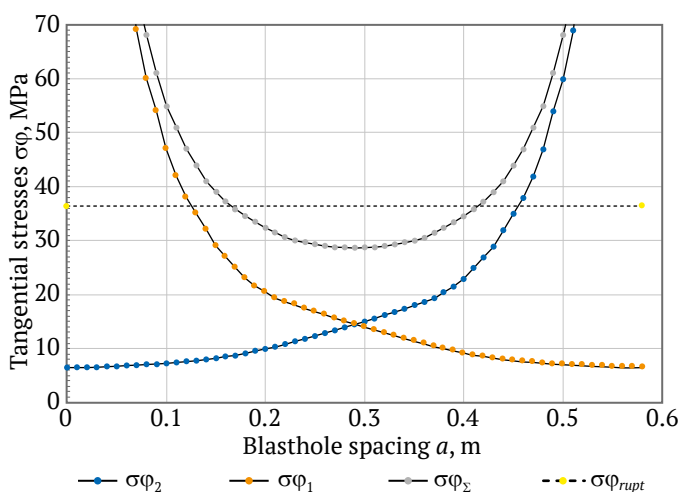


Fig. 3. Individual and total tangential stresses when blasting adjacent charges ($a = 0.58$ m, $q = 0.14$ kg/m): σ_{ϕ_1} and σ_{ϕ_2} are the amplitudes of the tangential component of the stress wave from the first and second charges, respectively, MPa; σ_{ϕ_Σ} is total amplitude of the tangential component of the stress wave from two charges, MPa; σ_{rupt} is maximum permissible value of rupture stress, MPa

change in the stress field in the vicinity of the plane passing through the charges.

It is obvious that if for a single charge the stress continuously decreases with growing distance from the charge, then for interacting charges the stress initially (at first) decreases with growing distance from the charges, and then increases again, reaching a maximum at half the distance between the charges. Fig. 5 shows the calculated dependence of individual tangential tensile stresses at linear charging densities

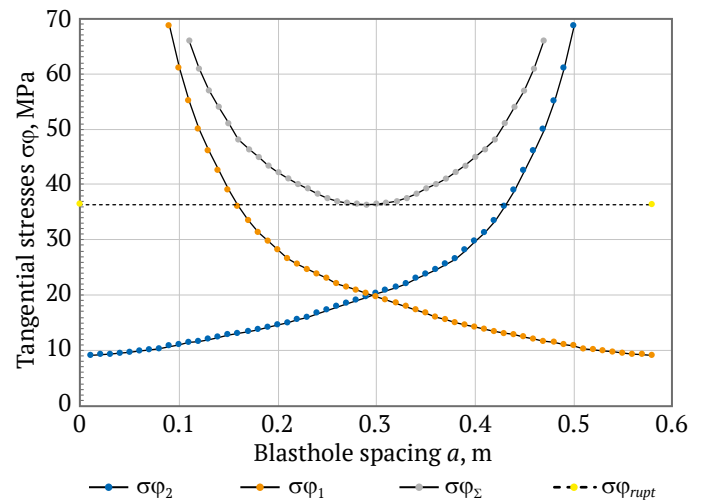


Fig. 4. Individual and total tangential stresses when blasting adjacent charges ($a = 0.58$ m, $q = 0.16$ kg/m): σ_{ϕ_1} and σ_{ϕ_2} are the amplitudes of the tangential component of the stress wave from the first and second charges, respectively, MPa; σ_{ϕ_Σ} is total amplitude of the tangential component of the stress wave from two charges, MPa; σ_{rupt} is maximum permissible value of rupture stress, MPa

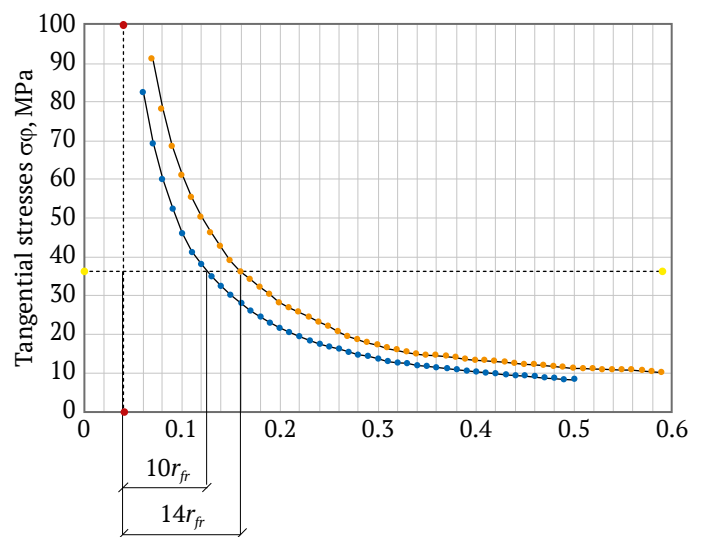


Fig. 5. Zone of induced fracturing at linear charge densities $q_1 = 0.14$ kg/m, $q_2 = 0.16$ kg/m: r_{fr} is radius of fracturing, m; σ_{rupt} is maximum permissible value of rupture stress, MP



$q = 0.14$ and 0.16 kg/m and charge spacing $a = 0.6$ m on the distance from a charge.

The data shown in Fig. 5 allow estimating potential zones of induced fracturing around the blasthole.

The given dependencies allow estimating potential zones of induced fracturing around a blasthole at different charging densities.

Conclusion

It was established that for the most probable propagation of radial main rupture between blasthole charges during stone block mining it is necessary to use the effect of stress wave interaction.

It should be noted that in order to minimize the zone of induced fracturing, the charge amount should be selected so that the tensile stress field in the plane of the rupture does not exceed the tensile strength. The main rupture propagation begins with the arrival of a rarefaction wave reflected from the surface of the separated stone block.

It can also be stated that as the average pressure P_{avr} increases, the length of the main rupture decreases due to the increase in the number of microfractures. Even at the maximum pressure on the blasthole walls, the length of the rupture from an individual blasthole is such that, taking into account the increasing stress intensity factor and the linear system of fractures

propagating between blastholes, the blastholes spacing can be much greater than commonly accepted.

However, at low pressure (small number of fractures), this potential blasthole spacing is not feasible due to the random direction of fracture propagation and hence unpredictability of the rupturing (split off) direction. It is therefore necessary to increase the charge (capacity, blasthole pressure) to increase the number of fractures so that the fractures necessarily propagate along or near the direction of the blasthole line.

With the simultaneous growth of the charge size, the blasthole spacing should be reduced so that the growth of fractures propagating from the blastholes in all directions stops early enough (which happens as soon as the fractures growing in the direction of the blasthole line start to “feel each other”) and the disturbed area around the blastholes is minimized.

Thus, obtaining a directional rupture requires reducing the blasthole spacing and at the same time increasing the blasthole charge within certain limits.

The potential for directional rupture at increased blasthole spacing with reduced charges can be realized by using potential naturally occurring directions/weakeness planes) in a stone (cleavage, layering, etc.), which prevent fracture growth in other directions.

References

1. Careddu N. Dimension stones in the circular economy world. *Resources Policy*. 2019;60:243–245. <https://doi.org/10.1016/j.resourpol.2019.01.012>
2. Paramonov G.P., Kovalevskiy V.N., Mysyn A.V. Determination of the conditions of an effective functioning of elongated cumulative charges in processing the marble stone. *Key Engineering Materials*. 2020;836:19–24. <https://doi.org/10.4028/www.scientific.net/kem.836.19>
3. Borovikov V.A., Vanyagin I.F. About calculation of parameters of stress waves when blasting an elongated charge in rocks. *Vzryvnoe Delo*. 1976;(76/38):74–85. (In Russ.)
4. Skublov S.G., Petrov D.A., Galankina O.L. et al. Th-rich zircon from a pegmatite vein hosted in the Wiborg Rapakivi Granite Massif. *Geosciences*. 2023;13(12):362. <https://doi.org/10.3390/geosciences13120362>
5. Isheisky V.A., Ryadinskii D.E., Magomedov G.S. Increasing the quality of fragmentation of blasting rock mass used on accounting for structural features of massif in the blast design. *Mining Informational and Analytical Bulletin*. 2023;(9–1):79–95. (In Russ.) https://doi.org/10.25018/0236_1493_2023_91_0_79
6. Kovalev A.V. Ways of improving blasting methods of dimensional stone quarrying in intensively fractured rock mass. *Mining Science and Technology (Russia)*. 2018;(1):23–34. (In Russ.) <https://doi.org/10.17073/2500-0632-2018-1-23-34>
7. Pal Roy P. Emerging trends in drilling and blasting technology: concerns and commitments. *Arabian Journal of Geosciences*. 2021;14:652. <https://doi.org/10.1007/s12517-021-06949-z>
8. Sanchidrián J.A., García-Bermudez P., Jimeno C.L. Optimization of granite splitting by blasting using notched holes. *International Journal for Blasting and Fragmentation*. 2000;4(1):1–11. <https://doi.org/10.1080/13855140009408059>
9. Gospodarikov A.P., Revin I.E., Morozov K.V. Composite model of seismic monitoring data analysis during mining operations on the example of the Kukisvumchorrskoye deposit of AO Apatit. *Journal of Mining Institute*. 2023;262:571–580. <https://doi.org/10.31897/PMI.2023.9>



10. Baron L. I., Turchaninov N. A., Klyuchnikov A. B. *Rock disturbance when using blasting by presplitting method*. Leningrad: Nauka Publ.; 1975. 339 p. (In Russ.)
11. Borovikov V. A., Vanyagin I. F. *Blasting methods and technology*. Leningrad: LGI Publ. House; 1985. 92 p. (In Russ.)
12. Ziryayev I. V., Bondarenko I. F., Kovalevich S. V., Kim S. I. Influence of the explosion of a borehole charge with a radial gap on the quality of destruction of diamond-bearing ore. *Mining Informational and Analytical Bulletin*. 2022;(5–2):58–71. (In Russ.) https://doi.org/10.25018/0236_1493_2022_52_0_58
13. Marinin M. A., Evgrafov M. V., Dolzhikov V. V. Production of blasting operations for a given granulometric composition of ore within the framework of the «mine-to-mill» concept: current state and prospects. *Bulletin of the Tomsk Polytechnic University. Geo Assets Engineering*. 2021;332(7):65–74. (In Russ.) <https://doi.org/10.18799/24131830/2021/7/3264>
14. Saadati M., Forquin P., Weddfelt K. et al. On the mechanical behavior of granite material with particular emphasis on the influence from pre-existing cracks and defects. *Journal of Testing and Evaluation*. 2018;46:33–45. <https://doi.org/10.1520/JTE20160072>
15. Zhang Z. X., Chi L. Y., Qiao Y. Fracture initiation, gas ejection, and strain waves measured on specimen surfaces in model rock blasting. *Rock Mechanics and Rock Engineering*. 2021;54:647–663. <https://doi.org/10.1007/s00603-020-02300-2>
16. Borowski G., Smirnov Yu., Ivanov A., Danilov A. Effectiveness of carboxymethyl cellulose solutions for dust suppression in the mining industry. *International Journal of Coal Preparation and Utilization*. 2020;42(8):2345–2356. <https://doi.org/10.1080/19392699.2020.1841177>
17. Cardu M., Saltarin S., Todaro C., Deangeli C. Precision rock excavation: beyond controlled blasting and line drilling. *Mining*. 2021;1(2):192–210. <https://doi.org/10.3390/mining1020013>
18. Leschinsky A. V., Shevkun E. B., Lysak Yu. A. Control of iron ore fragmentation by blasting-way of improvement of processing efficiency. *Mining Informational and Analytical Bulletin*. 2019;(4):41–52. (In Russ.) <https://doi.org/10.25018/0236-1493-2019-04-0-41-52>
19. Darbinyan T. P., Tsymbalov A. A., Zubov V. P., Kolganov A. V. Impact of rock mass jointing on dilution of disseminated copper–nickel ore in Oktyabrsky Mine. *Gornyi Zhurnal*. 2023;(6):19–26. (In Russ.) <https://doi.org/10.17580/gzh.2023.06.03>
20. Moldovan D. V., Chernobay V. I., Yastrebova K. N. The influence of composite material in the stemming design on its operability. *Mining Informational and Analytical Bulletin*. 2023;(9–1):110–121. (In Russ.) https://doi.org/10.25018/0236_1493_2023_91_0_110
21. Protosenya A. G., Belyakov N. A., Bouslova M. A. Modelling of the stress-strain state of block rock mass of ore deposits during development by caving mining systems. *Journal of Mining Institute*. 2023;262:619–627. URL: <https://pmi.spmi.ru/pmi/article/view/15942>
22. Rajaoalison H., Zlotkowski A., Rambolamanana G. Mechanical properties of sandstone using non-destructive method. *Journal of Mining Institute*. 2020;241:113–117. <https://doi.org/10.31897/pmi.2020.1.113>
23. Panasyuk V. B. *Limit equilibrium of brittle bodies with fractures*. Kyiv: Naukova Dumka; 1991. 411 p. (In Russ.)
24. Bychkov G. V., Kokunina L. V., Kazakov S. V. Drilling and blasting method of mining of monoliths and natural stone blocks. *Gornyi Zhurnal*. 2008;(1):45–49. (In Russ.)
25. Blair D. P. Dynamic response of mine pit walls. *International Journal of Rock Mechanics and Mining Sciences*. 2018;106:14–19. <https://doi.org/10.1016/j.ijrmms.2018.04.002>
26. Zubov V. P., Li Yunpeng. Slicing mining of thick gently dipping coal in China: Problems and improvement. *Mining Informational and Analytical Bulletin*. 2023;(7):37–51. (In Russ.) https://doi.org/10.25018/0236_1493_2023_7_0_37
27. Kongar-Syuryun Ch. B., Kovalski E. R. Hardening backfill at potash mines: promising materials regulating stress-strain behavior of rock mass. *Geology and Geophysics of Russian South*. 2023;13(4):177–187. <https://doi.org/10.46698/VNC.2023.34.99.014>
28. Efremov E. I., Kravtsov V. S., Myachina N. N. et al. *Fundamentals of the theory and methods of explosive crushing of rocks*. Kyiv: Naukova Dumka; 1979. 224 p. (In Russ.)
29. Alenichev I. A., Rakhmanov R. A. Empirical regularities investigation of rock mass discharge by explosion on the free surface of a pit bench. *Journal of Mining Institute*. 2021;249:334–341. <https://doi.org/10.31897/PMI.2021.3.2>



30. Elkarmoty M., Colla C., Gabrielli E. et al. A combination of GPR survey and laboratory rock tests for evaluating an ornamental stone deposit in a quarry bench. *Procedia Engineering*. 2017;191:999–1007. <https://doi.org/10.1016/j.proeng.2017.05.272>
31. Nefedov M.A. *Directed destruction of rocks by explosion*. St. Petersburg: St. Petersburg University Publ. House; 1991. 188 p.
32. Meshkov A.A., Afanasyev P.I. *Physical foundations of explosive destruction of rocks*. Monograph. Moscow: Gornaya Kniga; 2021. 124 p.
33. Chertkov V. Ya. Theoretical evaluation of increased microfracturing at block stone blasting. *Fiziko-Tekhnicheskie Problemy Pererabotki Poleznykh Iskopaemykh*. 1983;(1):36–43 (In Russ.)

Information about the authors

Vladimir N. Kovalevskiy – Cand. Sci. (Eng.), Associate Professor, Department of Explosive Engineering, Empress Catherine II Saint Petersburg Mining University, Saint Petersburg, Russian Federation; ORCID [0000-0002-7155-2000](https://orcid.org/0000-0002-7155-2000), Scopus ID [57194598687](https://scopus.com/authorid/57194598687), ResearcherID [AAD-5379-2019](https://orcid.org/AAD-5379-2019); e-mail Kovalevskiy_VN@pers.spmi.ru

Alexey V. Mysin – Cand. Sci. (Eng.), Senior Lecturer at the Department of Geoecology, Empress Catherine II Saint Petersburg Mining University, Saint Petersburg, Russian Federation; ORCID [0000-0001-5968-8290](https://orcid.org/0000-0001-5968-8290), Scopus ID [57196262504](https://scopus.com/authorid/57196262504); e-mail Mysin_AV@pers.spmi.ru

Veronica I. Sushkova – PhD-Student, Department of Explosive Engineering, Empress Catherine II Saint Petersburg Mining University, Saint Petersburg, Russian Federation; ORCID [0000-0003-4247-6499](https://orcid.org/0000-0003-4247-6499), Scopus ID [58121433200](https://scopus.com/authorid/58121433200); e-mail s235054@stud.spmi.ru

Received 06.12.2023

Revised 28.01.2024

Accepted 01.02.2024



GEOLOGY OF MINERAL DEPOSITS

Research paper

<https://doi.org/10.17073/2500-0632-2024-01-208>

UDC 622.03



Composition and mineralogy of granitoids of the Ob-Zaisan folded region in the context of the prediction of groundwater radioactivity

V.P. Sukhorukov^{1,3}  , A.F. Sukhorukova^{2,3}   ✉, D.A. Novikov^{2,3}  , A.S. Derkachev^{2,3}  ¹ V.S. Sobolev Institute of Geology and Mineralogy, Siberian Branch of the Russian Academy of Sciences, Novosibirsk, Russian Federation² A.A. Trofimuk Institute of Oil and Gas Geology and Geophysics, Siberian Branch of the Russian Academy of Sciences, Novosibirsk, Russian Federation³ Novosibirsk State University, Novosibirsk, Russian Federation✉ SukhorukovaAF@ipgg.sbras.ru

Abstract

The presented research is carried out in continuation of the works connected with studying the nature of radioactivity of drainage waters of quarries of Novosibirsk region, performed by the Laboratory of Hydrogeology of Sedimentary Basins of Siberia, INGG SB RAS, which showed that the waters of granite quarries are characterized by significantly higher radioactivity, than waters of other host rocks. The results of detailed mineralogical and geochemical studies of granitoids of the Ob-Zaisan region within the Kolyvan-Tom folded system are presented for the first time. The relevance of the present study is determined by the previously obtained data on high concentrations of uranium, thorium, and radon in drainage water of quarries developed in this territory. The granitoids of the Priobsky (Obsky and Novosibirsk massifs) and Barlak complexes were studied. It was established that the rocks of the complexes differ significantly in the spectrum of accessory minerals, which acted as the concentrators of natural radioactive and rare-earth elements: in the Barlak, in addition to apatite, sphene, and zircon, typical for all phases of the intrusion, fluorite, topaz, rutile, and minerals enriched with rare-earth elements are found: monazite, xenotime, bastnesite, parisite, less often uraninite. It was shown that a wide range of mineral-concentrators of radioactive and rare-earth elements determines higher concentrations of radionuclides in groundwater of the Barlak granitoid complex. Maximum uranium concentrations are one order of magnitude and those of thorium are two orders of magnitude higher in the groundwater of the Barlak granitoid complex compared to those of the Priobsky granitoid complex. The following peak concentrations, mg/dm³, were established in the groundwater of the studied granitoid complexes: ²³⁸U up to 1.40 and ²³²Th up to 2.16 · 10⁻³. One can predict a high background of radionuclides in the groundwater of the Barlak and Priobsky granitoid complexes, within the ranges, mg/dm³: ²³⁸U from 0.1 · 10⁻³ to 1.40 and ²³²Th from 1 · 10⁻⁶ to 2.16 · 10⁻³. Radon ²²²Rn activity in the groundwater ranges 1–50 Bq/dm³ in the contact zones of granitoids with different-aged sedimentary rocks to 600–5,000 Bq/dm³ in the areas of granitoids occurrence.

Keywords

granitoids, mineral-concentrators of radioactive and rare-earth elements, groundwater, radionuclides, ²³⁸U, ²³²Th, ²²²Rn, Novosibirsk region, Western Siberia

Acknowledgements

Field and analytical work on the study of the chemical composition of natural waters was carried out with the financial support of the project of the Ministry of Science and Higher Education of the Russian Federation № FWZZ-2022-0014, and the analytical work on the study of mineralogical, petrographic, and geochemical features of the granitoids of the Ob-Zaisan folded region, with the support of the project № 22-17-20029 of the Russian Science Foundation and the Government of the Novosibirsk region.

For citation

Sukhorukov V.P., Sukhorukova A.F., Novikov D.A., Derkachev A.S. Composition and mineralogy of granitoids of the Ob-Zaisan folded region in the context of the prediction of groundwater radioactivity. *Mining Science and Technology (Russia)*. 2024;9(2):105–115. <https://doi.org/10.17073/2500-0632-2024-01-208>



ГЕОЛОГИЯ МЕСТОРОЖДЕНИЙ ПОЛЕЗНЫХ ИСКОПАЕМЫХ

Научная статья

Состав и минералогия гранитоидов Обь-Зайсанской складчатой области в связи с прогнозом радиоактивности подземных водВ. П. Сухоруков^{1,3}  , А. Ф. Сухорукова^{2,3}   , Д. А. Новиков^{2,3}  , А. С. Деркачев^{2,3}  ¹ Институт геологии и минералогии им. В. С. Соболева СО РАН, г. Новосибирск, Российская Федерация² Институт нефтегазовой геологии и геофизики им. А. А. Трофимука СО РАН, г. Новосибирск, Российская Федерация³ Новосибирский государственный университет, г. Новосибирск, Российская Федерация SukhorukovaAF@ipgg.sbras.ru**Аннотация**

Представленное исследование выполнено в продолжение работ, связанных с изучением природы радиоактивности дренажных вод карьеров Новосибирской области, выполненных лабораторией гидрогеологии осадочных бассейнов Сибири ИНГТ СО РАН, где показано, что воды гранитных карьеров характеризуются существенно более высокими значениями радиоактивности, чем воды других вмещающих пород. Впервые представлены результаты детальных минералогических и геохимических исследований гранитоидов Обь-Зайсанской области в пределах Колывань-Томской складчатой системы. Актуальность настоящего исследования определяется полученными ранее данными о высоких концентрациях урана, тория и радона в дренажных водах разрабатываемых карьеров этой территории. Изучены гранитоиды приобского (Обской и Новосибирский массивы) и барлакского комплексов. Установлено, что породы комплексов существенно различаются спектром аксессуарных минералов, которые выступают концентраторами природных радиоактивных и редкоземельных элементов: в барлакском, помимо апатита, сфена и циркона, характерных для всех фаз внедрения, фиксируются флюорит, топаз, рутил и обогащенные редкоземельными элементами минералы: монацит, ксенотим, бастнезит, паризит, реже уранинит. Показано, что широкий спектр минералов-концентраторов радиоактивных и редкоземельных элементов определяет более высокие концентрации радионуклидов в подземных водах барлакского гранитоидного комплекса. Максимальные концентрации урана на порядок, а тория на два порядка выше в подземных водах барлакского гранитоидного комплекса, по сравнению с приобским. В подземных водах изученных гранитоидных комплексов установлены максимальные концентрации, мг/дм³: ²³⁸U до 1,40 и ²³²Th до 2,16 · 10⁻³. Можно прогнозировать высокий фон радионуклидов в подземных водах барлакского и приобского гранитоидных комплексов в пределах, мг/дм³: ²³⁸U от 0,1 · 10⁻³ до 1,40 и ²³²Th от 1 · 10⁻⁶ до 2,16 · 10⁻³. Активность радона ²²²Rn в подземных водах при этом будет составлять от 1–50 Бк/дм³ в зонах контактов гранитоидов с разновозрастными осадочными породами до 600–5000 Бк/дм³ в областях развития гранитоидов.

Ключевые слова

гранитоиды, минералы-концентраторы радиоактивных и редкоземельных элементов, подземные воды, радионуклиды, ²³⁸U, ²³²Th, ²²²Rn, Новосибирская область, Западная Сибирь

Благодарности

Полевые и аналитические работы по изучению химического состава природных вод выполнены при финансовой поддержке проекта Министерства науки и высшего образования РФ № FWZZ-2022-0014, аналитические работы по изучению минералого-петрографических и геохимических особенностей гранитоидов Обь-Зайсанской складчатой области – при поддержке проекта № 22-17-20029 Российского научного фонда и Правительства Новосибирской области.

Для цитирования

Sukhorukov V. P., Sukhorukova A. F., Novikov D. A., Derkachev A. S. Composition and mineralogy of granitoids of the Ob-Zaisan folded region in the context of the prediction of groundwater radioactivity. *Mining Science and Technology (Russia)*. 2024;9(2):105–115. <https://doi.org/10.17073/2500-0632-2024-01-208>

Introduction

One of the most urgent problems of modern hydrogeochemistry is the study of the phenomenon of radioactivity of natural waters and identification of factors controlling it. It was shown previously that waters of granite quarries are characterized by significantly higher radioactivity in comparison with wa-

ters of other host rocks on the example of drainage waters of quarries of the Novosibirsk region [1] and natural groundwater outlets [2] within the Ob-Zaisan folded zone.

In many countries of the world, including China, India, Turkey, USA, Mexico, Norway, Great Britain, Hungary, Egypt, Asian countries, and others, the pro-



cesses of radionuclide migration in groundwater are actively studied and simulated. The studies in south-eastern Mexico by J.I. Morales-Arredondo et al. have shown that the concentrations of uranium and thorium isotopes in groundwater are low enough not to be dangerous for the population, but it is necessary to control the concentration of radon, which can be high [3]. According to Chinese scientists C. Yu, Z. Song and many others, the weathering processes of granite massifs enhances the dissemination and transfer of uranium and thorium into the aquatic environment. The scientists note the important role of changes in geochemical conditions [4]. P. Baják, K. Csondor, D. Pedretti et al. developed conceptual models of radionuclide mobility in rocks and groundwater that take into account the changing redox conditions in aquifers for the territory of Hungary [5]. S.M. Pérez-Moreno, J.L. Guerrero, F. Mosqueda et al. analyzed the hydrochemical behavior of long-lived natural radionuclides of uranium, thorium and radon in groundwaters of Spain in different geological conditions and performed dose estimates for the ingestion of these radionuclides with water. It was shown that their high concentrations are connected with the granitic base and reductive conditions [6].

Radon activity in water is universally assessed as a potential environmental risk for the population and is determined by radioactive decay of elements of the uranium-radium series. At the same time, there is no direct correlation between uranium concentration in host rocks and radon concentration in groundwater [3].

The results of studies of groundwater radioactivity in different regions show that the maximum concentrations of radionuclides such as uranium and thorium are usually associated with felsic intrusive rocks, in which the average concentrations (according to N.A. Grigoriev) of uranium and thorium are 3.2 and 14.0 g/t, respectively¹. In waters of felsic igneous rocks of the zone of intensive water exchange, uranium concentration ranges $2,0 \cdot 10^{-3}$ to $3 \cdot 10^{-2}$ mg/dm³. The previously obtained data on uranium concentration in water samples allow to classify the groundwater of granitoids of the Ob-Zaisan region according to the classification A.N. Tokarev as uranium waters and, at higher concentrations, even to uranium deposit waters.

For the territory of Novosibirsk and its environs since 2018, the team of the Laboratory of Hydrogeology of Sedimentary Basins of Siberia, INGG SB RAS, has been carrying out work to study the chemical and radionuclide composition, radon levels in ground-

water of various aquifers [7]. The waters both in the zone of granitoids occurrence and beyond its limits, in argillaceous shales and marmorized limestones of Upper Devonian-Lower Carboniferous age, were studied. The occurrences of radon waters Tulinskoye [8] and Kamenskoye [9], and drainage waters of Borok quarry [10] were studied in detail. Data on uranium and thorium concentrations in the groundwater were obtained. At the same time sampling of rocks of water-bearing horizons was carried out for its detailed mineralogical and petrographic investigation.

Consequently, the main purpose of the study is to reveal the relationships between the composition, mineralogy, and spectrum of accessory minerals of the Priobsky and Barlak complexes of granitoids of the Ob-Zaisan folded region and the level of radioactivity of groundwater occurring within them.

Research techniques and subject

The study is based on the collection of geological rock samples and water samples collected by the authors of the paper during field work in 2022–2023 within the Ob-Zaisan folded region from the areas of occurrence of granitoids of the Priobsky and Barlak complexes. The rocks were sampled at 10 sites from Borok, Skala, Novobibeevsky, Gorsky, Tulinsky, Mochishche quarries, outcrops confined to groundwater outlets, and hole cores (Fig. 1).

The microscopic description of 29 petrographic thin sections of granitoids was carried out by the classical method. The determination of petrogenic element concentrations was performed by X-ray fluorescence analysis using a SRM-25 unit at the Center for collective use of scientific equipment for multi-element and isotopic studies of the Siberian Branch of the Russian Academy of Sciences (TsKP MII SB RAS, Novosibirsk). The determination of the concentrations of rare and rare-earth elements in granites was carried out by ICP-MS method using a high-resolution mass spectrometer ELEMENT of Finnigan (Germany) in the TsKP MII SB RAS (Novosibirsk) according to the standard technique.

The accessory mineral paragenesis in the rocks of the Novosibirsk granitoid massif was studied in polished sections by scanning electron microscopy at a MIRA 3 LMU electron scanning microscope (TESCAN ORSAY Holding).

Groundwater collection amounted to 78 samples; pH, Eh, temperature, dissolved O₂ concentration were determined directly at the sites using measuring facilities (Hanna HI9125, oxygen meter AKPM-1-02L) and a field hydrogeochemical laboratory. The measurements of radon concentration in natural waters were carried out using a complex

¹ Geological Dictionary: in 3 vol. Ed. O.V. Petrov; Ed.-comp.: S.I. Andreev et al. Ed. 3rd, reprint and add. St. Petersburg: VSEGEI Publ. House; 2010–2012. (In Russ.)

“Alpharad Plus” in the Laboratory of Hydrogeology of Sedimentary Basins of Siberia, INGG SB RAS. Laboratory study of water chemistry was carried out by titrimetry, ion chromatography, and inductively coupled plasma mass spectrometry in the Topical Research Laboratory of Hydrogeochemistry at the Engineering School of Natural Resources of Tomsk Polytechnic University (TRL of Hydrogeochemistry IShPR TPU).

Geological Setting

Carbonate-volcanogenic-terrigenous deposits of the Middle Devonian-Early Carboniferous age overlain by Quaternary alluvial and subaerial sediments are widespread within the Ob-Zaisan folded region. In the Permian-Triassic time, a granite intrusion intruded them, and granitoids of the Novosibirsk massif were formed. Within the territory of interest, the Priobsky and Barlak granitoid complexes are distinguished.

The Priobsky complex is represented by the petrotypical Obsky and Novosibirsk massifs in the Novosibirsk folded zone (Kolyvan-Tom folded system) and is characterized by a three-phase structure. The first phase is composed of monzonites and quartz monzonites ($\mu P_3-T_1p_1$), with diorites occur-

ring less frequently. The second, main phase is represented by monzogranites ($\epsilon\gamma P_3-T_1p_2$), granosienites, while granites and granodiorites are less common. The third phase includes small bosses and dikes of monzogranites ($\epsilon\gamma P_3-T_1p_3$), monzoleucogranites, and their porphyritic analogs [11].

Two intrusion phases are distinguished within the Barlak complex. The first, main phase is predominantly composed of medium-grained monzoleucogranites ($\epsilon\gamma T_{1-2}b_1$), while leucogranites and monzogranites ($\epsilon\gamma T_{1-2}b_1$) are observed less frequently. The second phase is represented by small bodies and dikes of fine-grained monzoleucogranites ($\epsilon\gamma T_{1-2}b_2$).

In the studied area, granitoids are represented by the second phase of the Priobsky complex (P_3-T_1) and the first phase of the Barlak complex (T_{1-2}).

The multiphase **Priobsky complex** has a relatively simple petrographic composition. Diorites, quartz diorites, and their moderately alkaline analogues constitute the first phase and have limited occurrence. The second phase of the Priobsky complex composes the large Novosibirsk massif, located within the city limits, and is exposed in the Gorsky, Tulinsky, Bugrinsky, Trolleyzny, and Borok quarry areas, as well as the Obsky massif in the Dubrovinsky

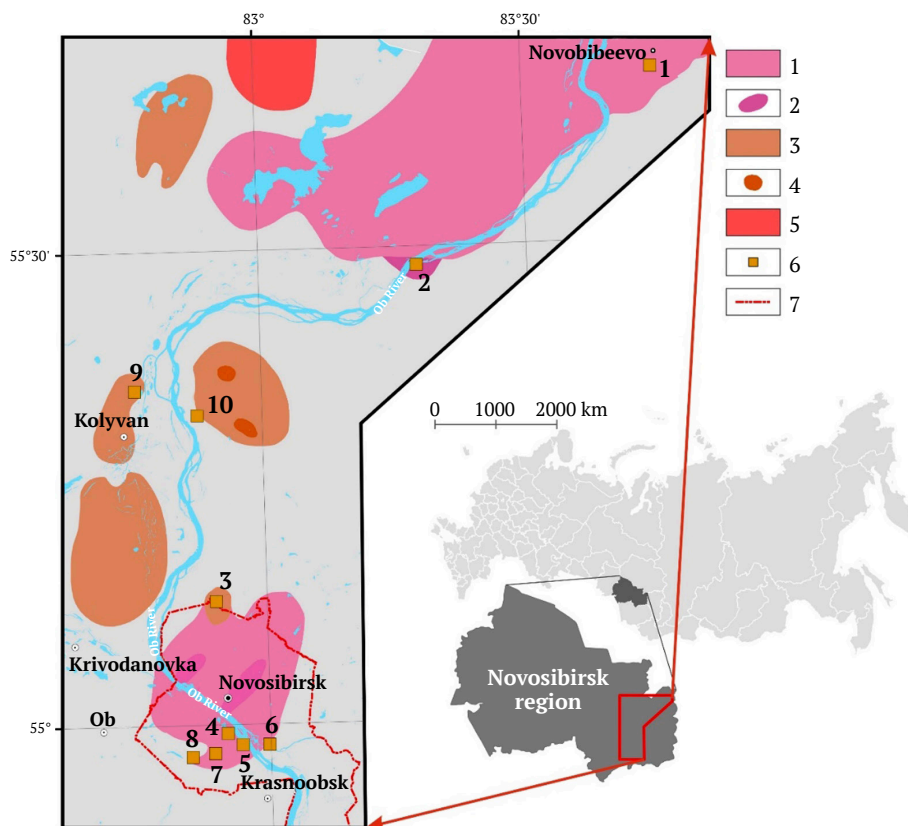


Fig. 1. Location of the study area and rock sampling sites:

- 1 – Priobsky complex, 2nd phase of intrusion; 2 – Priobsky complex, 1st phase of intrusion;
- 3 – Barlak complex, 1st phase of intrusion; 4 – Barlak complex, 2nd phase of intrusion; 5 – Late Permian-Middle Triassic granites;
- 6 – study areas (designations in Table 1); 7 – border of Novosibirsk city

and Novobibeevsky areas (Fig. 2, *a–d*). The sampled rocks of the second phase are represented by biotite and biotite-amphibole granites, monzogranites, and less frequently leucogranites. The biotite-amphibole granites contain about 25% of quartz, 20–35% of K-feldspar and plagioclase, while the content of biotite and hornblende is insignificant, about 2–5 vol.%. Sphene, apatite, and zircon are present as accessory minerals. The structure of the rocks is predominant-

ly equigranular, hypidiomorphic with grain size of 2–3 mm, less often porphyritic with grain size up to 15 mm. At the Novobibeevsky area, the rocks show signs of deformation.

By petrochemical composition the rocks belong to moderately alkaline granites. The silica content varies from 66 to 71 wt.%, rarely up to 75% in leucogranites. The content of Na₂O + K₂O lies in the range of 8.1–9.5 wt.% (Fig. 3, *a*).

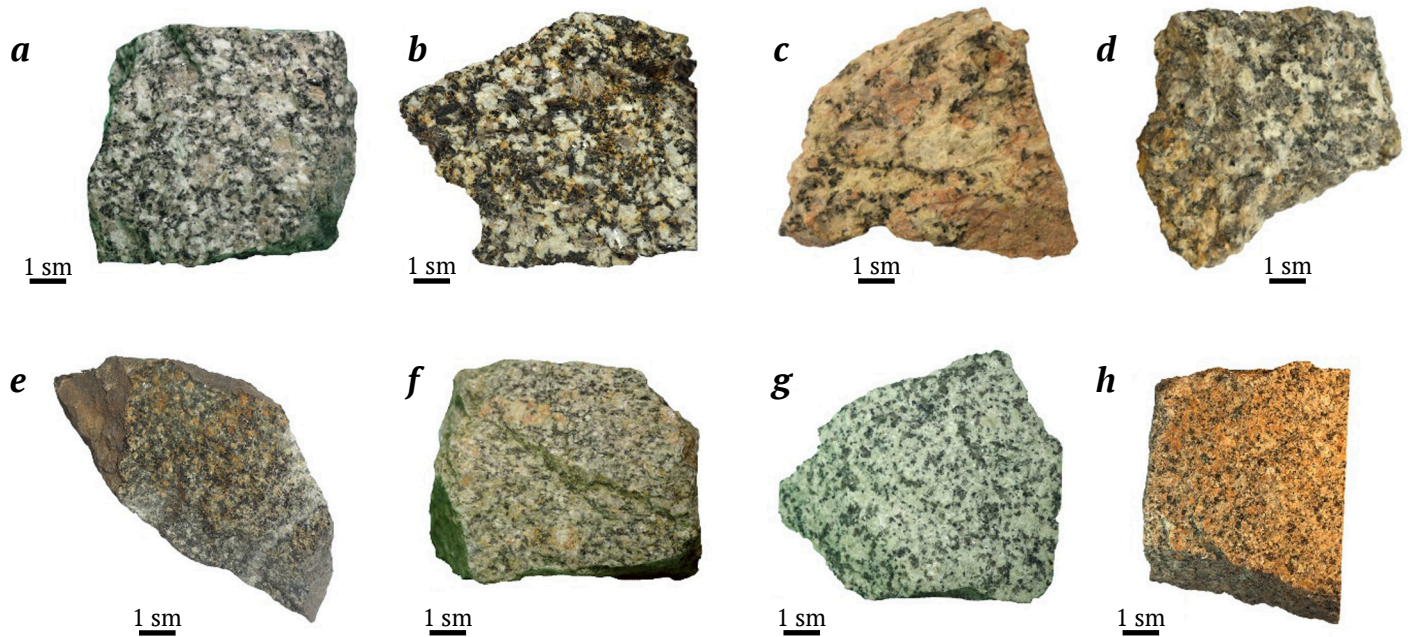


Fig. 2. Main rock types of granitoids of the Ob-Zaisan region:

the Priobsky complex: *a* – biotite-amphibole granite (Borok area); *b* – biotite-amphibole granite (Bugrinsky area); *c* – monzogranite (Gorsky area); *d* – biotite-amphibole granite (Tulinsky area); *e* – pyroxene-amphibole-biotite granodiorite (Dubrovinsky area); *f* – biotite-porphyritic granite (Novobibeevsky area); Barlak complex: *g* – biotite monzogranite (Skala area); *h* – porphyritic leucogranite (Mochishche area)

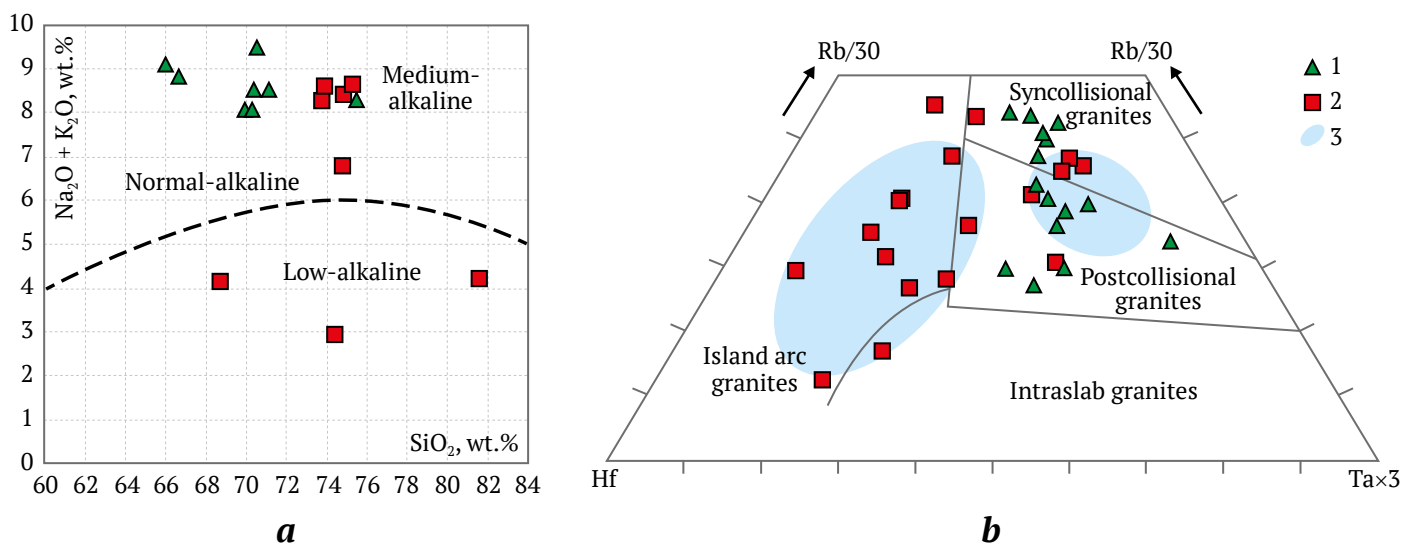


Fig. 3. The composition of granitoids of the Priobsky and Barlak complexes on diagrams: *a* – K₂O/Na₂O–SiO₂ diagrams; *b* – discriminant diagrams. 1 – Priobsky complex; 2 – Barlak complex; 3 – the granitoid complexes occurrence fields (according to A. G. Babin et al. [11])



The **Barlak complex** is characterized by a monotonous composition. It is represented by biotite monzogranites, less frequently by porphyritic leucogranites with yellowish-reddish tints appearing in their coloring within undulose zones due to weathering. Dotted sulfide impregnation and cassiterite are found in quartz veins, while beryl and topaz are found in pegmatites. Ultra-acid granites belong to moderately alkaline potassium granites (rocks of this complex were sampled in the Mochishche quarry, where the massif of granitoids of the Barlak complex intrudes the granites of the second phase of the Priobsky complex, and at the Skala and Bibikha areas (Fig. 2, h, g).

The rocks are represented by biotite monzogranites and less frequently by leucogranites. The rocks contain quartz, 30–35%, K-feldspar and plagioclase, 30–40%, and biotite of 2 to 10%. The structure of the rocks is granitic, hypidiomorphic, can vary from fine-grained (0.5–1 mm) to medium-grained (2–4 mm). Zircon and apatite are found as accessory minerals in granites; in some samples, orthite and monazite occur.

By petrochemical composition, the rocks belong to the moderately alkaline series that is consistent with their high content of K-feldspar, and less frequently to the normal- and low-alkaline series. The content of the sum of $K_2O + Na_2O$ is mainly in the range of 6.5–8.6 wt.%, rarely decreasing to 3–4.3 wt.%. SiO_2 content (69–82 wt.%) of the granites of the Barlak complex distinguishes them from the granites of the Priobsky complex, in which it is mainly at the level of 66–71 wt.% (see Fig. 3, a).

On the discriminant diagrams (Fig. 3, b), the granitoids of the Priobsky complex according to the results of ICP assays of the collected rock samples are located in the field of syncollisional and post-collisional granites, and the granitoids of the Barlak complex, in the field of island arc granites that corresponds to the data of A. G. Babin et al. [11].

Mineralogical and petrographic characterization of rocks

The most widely sampled rocks were the rocks of the Priobsky complex, where a collection of 15 samples was taken from 7 areas, and six rock types were identified. The Barlak complex was studied at three areas in 14 rock samples, and two rock types were identified. Table 1 shows the main rock types that were collected for mineralogical and petrographic study; the general view is shown in the photo table in Fig. 2, and the description is given below.

Priobsky complex rocks

Biotite-amphibole granite (Fig. 4, a). These rocks were sampled within the Novosibirsk massif (Tulinsky, Trolleyny, Bugrinsky, Gorsky areas) and Priobsky massif (Dubrovinsky area).

Its mineralogical composition, rock-forming minerals, %: quartz 25–30, plagioclase 30–45, microcline 23–35, amphibole 2–5, biotite 3–7; accessory minerals: sphene, apatite, zircon (see Fig. 2, a). The rock is formed by idiomorphic crystals of plagioclase and melanitic (mafic) minerals and xenomorphic grains of K-feldspar and quartz located between them. Plagioclase forms prismatic and elongated idiomorphic crystals, often with pronounced faceting, polysynthetic twins, and zonal structure. The grain size is predominantly 1.5–2 mm. Microcline forms xenomorphic grains 2–4 mm in size, located between idiomorphic plagioclase laths. The microcline is characterized by perthitic structures. Quartz forms xenomorphic grains 1–2 mm, the grain shape is isometric or weakly elongated, with irregular boundaries, often with blocky extinction. Hornblende forms idiomorphic crystals of 1–1.5 mm, elongated up to prismatic, occasionally with pronounced faceting. The coloration is dark green to black. Biotite is of tabular habitus 1–2 mm in size, the color is dark brown; the mineral is partially replaced by chlorite. Sphene forms well-faceted rhomboid crystals about 0.5 mm in size or larger grains up to 1 mm without pronounced faceting. Apatite forms long prismatic colorless crystals up to 0.2–0.5 mm in size.

Monzogranite porphyritic (Borok area, Fig. 4, b). The mineral composition, %: quartz about 30, plagioclase 15–20, microcline 45–50, biotite 3–5. Accessory minerals: zircon, apatite, sphene. The structure of the rock is porphyritic, the structure of the rock ma-

Table 1

Main rock types of granitoids of the Ob-Zaisan region

No.	Area	Rock type
Priobsky complex		
<i>Novosibirsk massif</i>		
1	Borok	Biotite-amphibole granite Monzogranite
2	Bugrinsky	Biotite-amphibole granite
3	Gorsky	Monzogranite Leucogranite
4	Tulinsky	Biotite-amphibole granite
5	Trolleyny	Biotite-amphibole granite
<i>Obsky massif</i>		
6	Dubrovinsky	Pyroxene-amphibole-biotite granodiorite Biotite granite Melanocratic diorite Leucogranite
7	Novobibeyeovsky	Biotite porphyritic granite
Barlak complex		
8	Skala	Biotite monzogranite
9	Bibikha	Biotite monzogranite
10	Mochishche	Porphyritic leucogranite

trix is hypidiomorphic. The phenocrysts are formed by crystals of K-feldspar and plagioclase with the sizes ranging from 4 to 8–10 mm. The grain size in the rock matrix is about 1–2 mm. Plagioclase forms elongated crystals, some of which with good faceting, while others have curved, jagged facets. Microcline forms isometric grains with irregular edges. Its phenocrysts demonstrate zones of growing, characterized by abundant quartz inclusions. The microcline is typically perthitic. Biotite is brown, forms individual grains and lenticular clusters. The accessory minerals occur as single grains. Zircon occurs as isometric grains of about 0.1 mm in size; sphene – idiomorphic rhomboid grains in intergrowths with an ore mineral. The secondary alteration is presented by minor sericitization of plagioclase and pelitization of microcline.

Leucogranite – Gorsky and Dubrovinsky areas (Fig. 4, c). Its mineral composition, %: quartz 30–35, plagioclase 35–50, orthoclase 15–30, biotite not more than 2. The accessory minerals are rare and represented mainly by sphene and apatite. At the Dubrovinsky

area, garnet occurs as an accessory mineral of leucogranites. The structure is uniform, granitic. The grain size ranges from 0.5 to 1–2 mm. Plagioclase forms more idiomorphic grains with irregular edges, while orthoclase and quartz form isometric, xenomorphic grains. Biotite is dark brown, wide-tabular, partially replaced by chlorite. Sphene forms rhomboid shape crystals up to 0.5 mm long. Garnet forms isometric crystals, colorless, up to 0.2–0.3 mm in size, evenly distributed in the rock, composes up to 1 vol.% of the rock. The garnet crystals are often with pronounced faceting and rhythmic and zonal structure.

Pyroxene-amphibole-biotite granodiorite – Dubrovinsky area (Fig. 4, d). The rocks are similar in composition and structure to biotite-amphibole granites, but are characterized by a lower quartz content and the presence of an insignificant amount of clinopyroxene. Its mineral composition, %: quartz – 20, plagioclase – 30, microcline – 30, biotite – 10, pyroxene – 3, amphibole – 7. The accessory minerals are represented by significant amounts of apatite (up to 1 vol.% of

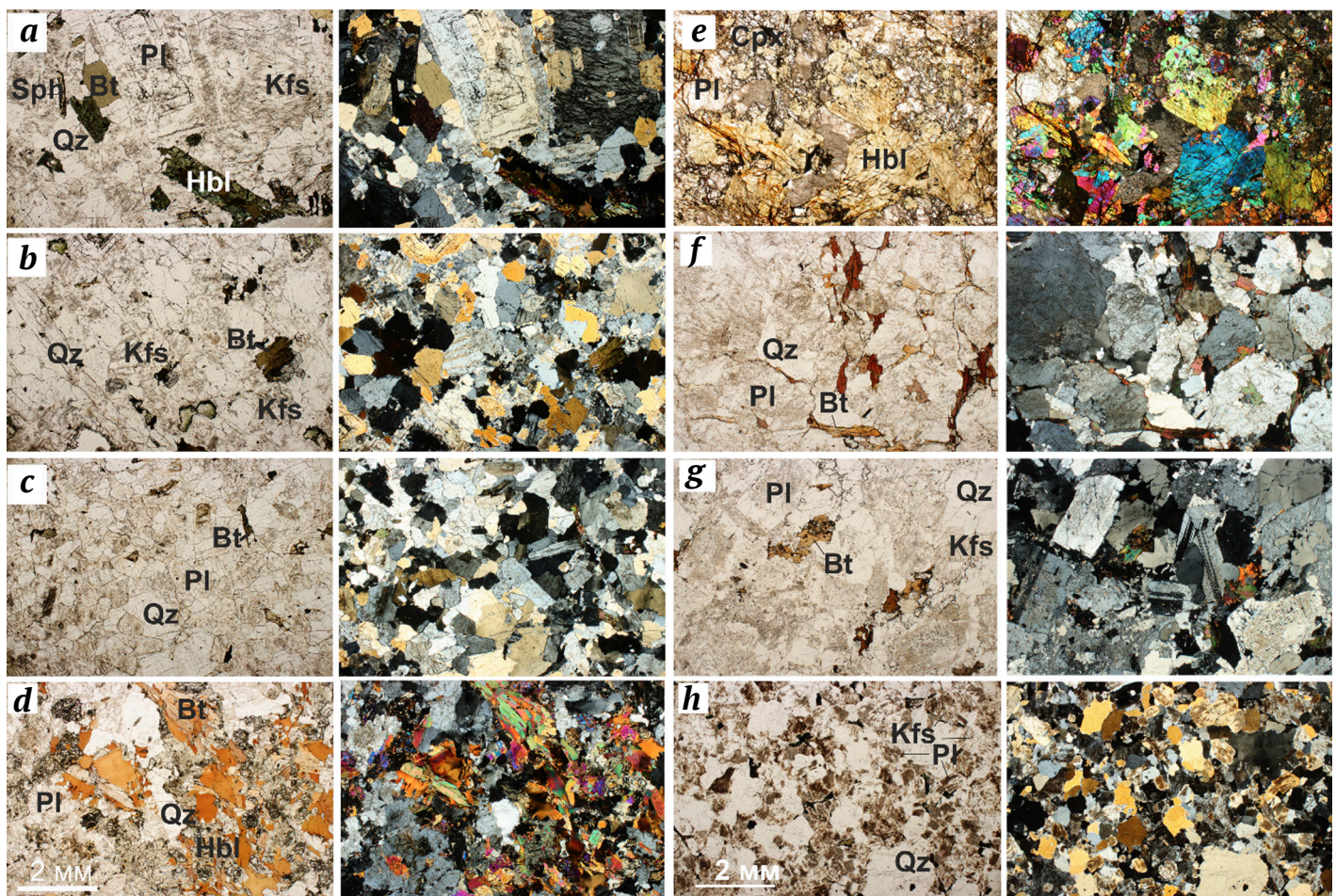


Fig. 4. Microphotographs of granitoids from the sampled massifs (see Table 1):

The Priobsky complex: *a* – biotite-amphibole granite; *b* – monzogranite; *c* – leucogranite; *d* – pyroxene-biotite-amphibole granodiorite; *e* – melanocratic diorite; *f* – biotite granite; The Barlak complex: *g* – biotite monzogranite; *h* – leucogranite. The photos are given on the left with one polar and on the right with crossed polars. All photos are taken at the same scale. The mineral designations: Bt - biotite; Hbl - hornblende; Kfs – K-feldspar; Pl – plagioclase; Qz – quartz, Sph – sphene



the rock), as well as sphene and zircon. The structure of the rock is hypidiomorphic, with the grain size of 1–2 mm. Plagioclase forms partially faceted grains with polysynthetic twins, while microcline and quartz form isometric xenomorphic grains without faceting. Mafic minerals form clusters and spots. Clinopyroxene is colorless, often replaced by a rim of light green amphibole. Biotite is brown to light brown. Apatite forms prismatic crystals up to 0.3–0.5 mm with abundant inclusions of a needle ore mineral. Sphene forms isometric, non-faceted grains up to 0.1 mm in size, while zircon forms faceted grains up to 0.1 mm.

Melanocratic diorite – Dubrovinsky area (Fig. 4, e). Its mineral composition, %: plagioclase – 30, hornblende – 40, clinopyroxene – 20, biotite – 10; accessory minerals: apatite and zircon. The rock structure is hypidiomorphic, the texture is inequigranular. The rock consists mainly of plagioclase and amphibole (the grain size of about 2–3 mm), clinopyroxene (0.3–0.5 mm), and biotite (0.3 mm). Plagioclase forms xenomorphic grains located between amphibole grains and is partially sericitized. Light green colored hornblende forms idiomorphic grains, often faceted. Clinopyroxene forms smaller grains of isometric habitus, located as inclusions in plagioclase; sometimes clusters of such grains surround amphibole. Biotite of light brown color forms growths in the grains of amphibole. Apatite is frequent, forming elongated crystals up to 1 mm in size with abundant inclusions of an ore mineral. Zircon forms faceted crystals up to 0.15 mm in size.

Biotite granite – Dubrovinsky, Novobibeevsky areas (see Fig. 2, f). The mineral composition, %: quartz – 20, biotite – 10, microcline – 15, plagioclase – 55; the accessory minerals: apatite and zircon (Fig. 4, f). The structure of the rock is hypidiomorphic, cataclastic. Porphyritic varieties are common at the Novobibeevsky area. Plagioclase in the rock forms isometric and weakly elongated grains 2–3 mm in size, partly with faceting, while microcline and quartz occur as xenomorphic non-faceted grains. Biotite forms reddish-brown elongated scales 0.5–1 mm, which are often located along the boundaries of quartz and feldspar grains, deformed in places. In porphyritic varieties, phenocrysts are composed of orthoclase, their size is about 10 mm. Apatite forms slightly elongated crystals up to 0.3 mm, the central part of which is grayish due to dust-like impurities. Zircon forms isometric grains up to 0.1 mm in size.

Rocks of the Barlak complex

The Barlak and Kolyvansky massifs are composed of similar composition rocks. They were sampled in the area of Bibikha and Skala settlements respectively. The rocks are represented mainly by equigranular

medium-grained biotite monzogranites. The rocks are biotitic; hornblende is subordinately abundant in leucogranites of the Mochishche boss and in rare cases in monzoleucogranites of the Barlak Massif. In all these rocks, K-feldspar predominates over plagioclase.

Biotite monzogranites – Skala and Bibikha areas (Fig. 4, g). Mineral composition of the rocks, %: quartz – 35, microcline – 30, plagioclase – 25, biotite – 10. The rock structure is granitic. Plagioclase forms idiomorphic crystals of prismatic habitus 0.5–2 mm in size, microcline forms prismatic crystals with irregular edges and poikilitic growths of plagioclase. Quartz forms xenomorphic isometric grains. Biotite is dark brown to black, forms wide tabular scales, often associated with accessory minerals.

Porphyritic leucogranite – Mochishche area (Fig. 4, h). The Mochishche boss located in the edge of the Novosibirsk massif was sampled in the Mochishche quarry. The rocks are represented by porphyritic leucogranite. Its mineral composition, %: quartz – 30, orthoclase – 30, plagioclase – 38, biotite – 2. Accessory minerals: zircon, orthite, apatite. The rock structure is porphyritic, granitic. The phenocrysts are represented by orthoclase 3–4 mm in size. It forms isometric grains with irregular edges, often zoned. In the rock matrix, the grain size is 0.5–1 mm. Plagioclase is idiomorphic and forms prismatic faceted grains, while quartz and orthoclase are xenomorphic. Biotite forms tabular and elongated scales of dark brown to black color, partially or completely replaced by secondary chlorite. Orthite (Fig. 4, g) forms sharply zoned prismatic grains 0.8 mm long. The central part of the grain is light brown, the marginal parts are almost colorless. Zircon is zonal, forms faceted crystals about 0.15 mm in size.

Accessory minerals

Paragenesis of accessory minerals in the studied rocks is represented by a wide range of minerals, most of which can serve as mineral-concentrators of uranium, thorium, and other rare-earth elements, which determines the radioactivity of the rocks themselves and that of fracture-vein groundwater.

The rocks of the Barlak complex are characterized by a wider range of accessory minerals compared to the rocks of the Priobsky complex. The main accessory minerals encountered in the rocks of the Priobsky complex are apatite, sphene, and zircon; they were identified in the Borok, Bugrinsky, Gorsky, Tulinsky, Dubrovinsky, and Novobibeevsky areas and are described in the rock characterization.

In the Kolyvansky massif of the Barlak complex (Skala, Bibikha areas), apatite, sphene, and zircon, widespread in all granitoids of the Ob-Zaisan region,



were also identified as accessory minerals. In addition, fluorite, topaz, and rare earth element-enriched minerals such as monazite and xenotime are characteristic minerals; uraninite is less common. Superimposed greisen mineralization with cassiterite, associated with sericite veins, was also found.

Fluorite forms mainly xenomorphic grains, usually colorless or spotted purple. Topaz occurs in monzogranites, but predominantly is contained in quartz veins and pegmatoidal clusters, in which it forms faceted prismatic crystals up to 1 cm in size. Monazite and xenotime form grains without a clear faceting, zoning is not visible in them, and they often associate with dark brown biotite. Rutile is rare, also occurs in association with biotite, forms small (0.03 mm) oval grains of dark brown color. Uraninite is rare, found in association with monazite in the form of isometric grains in biotite monzogranite in the Skala quarry.

In the Barlak complex within Mochishche area, the following minerals were identified as accessory: fluorite, calcite, rutile, zircon, orthite, and REE-rich minerals: mainly fluorocarbonates bastnesite ((Ce, La, Y) CO₃F) and parisite (CaLa₂(CO₃)₃F₂), while monazite (CePO₄) and xenotime (YPO₄) are less common. Bastnesite forms irregularly shaped grains, mostly without faceting, 30–50 microns in size; parisite occurs as split crystals or clusters of needle-like crystals 20–30 microns in size, sometimes forming inter-

growths with bastnesite. Monazite and xenotime form mainly isometric grains 20–30 microns in size, sometimes also forming intergrowths with parisite, which is consistent with the data of V. I. Sotnikov et al. [12].

Geochemical peculiarities of fracture-vein waters of granitoids

Fracture-vein waters of Upper Paleozoic granites are predominantly neutral and slightly alkaline with pH 6.9–7.8, properly fresh with total salinity of 330 to 690 mg/dm³, characterized mainly by HCO₃ Mg–Ca and SO₄–HCO₃ Na–Mg–Ca composition, have high silicon concentration, from 10 to 23 mg/dm³, averaging at 15 mg/dm³. The medium geochemical parameters range from reducing to oxidizing conditions with Eh ranging from –81.2 to +509.6 mV; O₂ dissolv ranges from 1.62 to 9.91 mg/dm³. The average values of geochemical coefficients for this group are: Ca/Si – 11.49; Mg/Si – 2.48; Na/Si – 1.25; Si/Na – 0.87; Ca/Na – 10.02; Ca/Mg – 4.76; rNa/rCl – 8.79 и SO₄/Cl – 4.35, indicating the accumulation of calcium, magnesium, and proceeding sulfide oxidation processes in the waters. In terms of microcomponent composition, rather high for waters concentrations of Fe, Mn, Zn were identified, averaging, mg/dm³, 1.18; 0.16; 0.02, respectively. At the same time, it should be noted that the microcomponents distribution spectrum in the waters in general has an inherited character when compared with the host granites [7].

Table 2

Radionuclide composition of groundwater of Ob-Zaisan region granitoids

Water sampling location	U · 10 ⁻²	Th · 10 ⁻⁵	Th/U · 10 ⁻⁴	Rn
	mg/dm ³			Bq/dm ³
Priobsky complex				
Borok quarry	0.9–21.3 * 8.3 (9)	0.1–9.6 4.2 (9)	0.97–14.9 3.1 (9)	18–89 53 (9)
Tulinsky quarry	1.2 (2)	0.3–0.7 (2)	2.4–5.7 (2)	2 (1)
Gorsky quarry	1.0–1.2 (2)	0.1–0.15(2)	9.3–10.4 (2)	0 (2)
Bridge-4 (well)	0.7–1.8 1.4 (4)	0.1–1.7 0.6 (4)	0.1–2.5 0.7 (4)	285–597 561 (7)
Hospital-34 (borehole)	1.5–1.7 1.6 (11)	0.05–1.1 0.1 (11)	1.6–9.2 4.1 (11)	98–276 183 (11)
Novobibeevsky quarry	1.0–1.2 1.1 (5)	0.3–3.1 2.0 (5)	2.4–26.6 15.6 (11)	6–39 21 (5)
Novobibeevo settlement (borehole)	11.4	4.2	36.5	429
Chkalovskie Prostory DNG, boreholes	1.1–4.4 3.1 (6)	0.3–1.0 0.5 (6)	0.3–0.9 0.7 (6)	45–141 98 (6)
Barlak complex				
Skala quarry	94–140 118 (4)	3.9–216.3 72.2 (4)	3.3–17.8 5.9 (4)	154–474 334 (4)
Aeroflot horticultural non-commercial partnership (borehole)	30.9–34.8 32.3 (11)	0.1–1.4 0.1 (11)	0.1–0.4 0.1(11)	196–352 272 (13)
Mochishche quarry**	8–29	n/a	n/a	103–630
Yuzhno-Kolyvansky occurrence**	110–250	n/a	n/a	4150–4960

Note: * in the denominator, minimum and maximum values; in the numerator, average values; in parentheses, number of determinations; ** – archive data, n/a – no data available



Groundwater radionuclide composition

Table 2 shows the concentrations of uranium, thorium, and radon in the waters of the Priobsky and Barlak complexes. Peak concentrations of uranium and thorium were measured in waters within the formations of the Barlak complex (areas Skala, Aeroflot, Mochishche), where natural radionuclides are contained in waters within the following ranges, mg/dm³: ²³⁸U from 2.0·10⁻² to 1.4 and ²³²Th from 1 to 216.3·10⁻⁵. ²³²Th/²³⁸U ratio in the waters ranges from 0 to 1.78·10⁻³. ²²²Rn activity ranges from 154 to 630 Bq/dm³, which allows to classify the waters as weakly radon and moderately radon. The waters of the Priobsky complex are characterized by significantly lower radionuclide concentrations, mg/dm³: ²³⁸U from 0.7·10⁻² to 21.3·10⁻² and ²³²Th from 0.1 to 9.6·10⁻⁵. The ²³²Th/²³⁸U ratio in the waters varies between 0 and 36.5·10⁻⁴. The ²²²Rn activity in these waters varies in the range from 6 to 597 Bq/dm³, which allows assigning them to the classes of non-radon to moderately radon waters (according to the N.I. Tolstikhin classification).

According to the data obtained by the team of the Laboratory of Hydrogeology of Sedimentary Basins of Siberia in 2018–2023 [1, 2, 11], in fracture groundwater of argillaceous and calcareous-argillaceous shales the uranium and thorium concentrations are typically lower (in some cases by several orders of magnitude) than in the granitoids. For instance, in the Insky springs waters in clay shales, natural radionuclides are contained in the following ranges, mg/dm³: ²³⁸U from 2.83·10⁻³ to 4.13·10⁻³; ²³²Th from 2.39·10⁻⁶ to 1.16·10⁻⁵, the ratio ²³²Th/²³⁸U in the waters varies from 8.85·10⁻⁴ to 3.61·10⁻³, the activity of ²²²Rn varies from 7 to 149 Bq/dm³. Groundwater in the vicinity of the Verkh-Tula settlement (spring, boreholes) are characterized by even lower radionuclide concentrations in the range, mg/dm³: ²³⁸U from

3.8·10⁻⁶ to 7.2·10⁻³; ²³²Th from 0.1 to 8.0·10⁻⁵, radon activity up to 28 Bq/dm³. Such concentrations are characteristic of the water-bearing complex of wide-spread clay shales.

Conclusion

A detailed study of the composition and mineralogy of granitoids of the Ob-Zaisan folded zone was carried out, and for the first time a wide range of accessory minerals differing in the Priobsky and Barlak complexes was identified. In addition to apatite, sphene, and zircon, which were determined in both complexes, fluorite, topaz, monazite, xenotime, cassiterite, rutile, orthite, and less frequent uraninite and rich in rare-earth elements bastnesite and parisite were identified in the Barlak complex. Waters of the Barlak massif (areas Skala, Mochishche, Aeroflot) are characterized by the highest uranium and thorium concentrations.

It should be noted that on the whole the obtained data are well correlated with radionuclide concentrations in groundwater of the study area (historical data). The concentrations of uranium and thorium in the granitoids are several orders of magnitude higher than those in other water-bearing rocks of the Ob-Zaisan folded region – widespread argillaceous and calcareous shales, as well as intrusions of intermediate composition, limestones, and coals. The obtained data will be further used for modeling of interaction processes in a water-rock system.

One can predict a high background of radionuclides in the groundwater of the Barlak and Priobsky granitoid complexes, within the ranges, mg/dm³: ²³⁸U from 0.1·10⁻³ to 1.40 and ²³²Th from 1.0·10⁻⁶ to 2.16·10⁻⁵. Radon ²²²Rn activity in groundwater ranges 1–50 Bq/dm³ in the contact zones of granitoids with different-aged sedimentary rocks to 600–5,000 Bq/dm³ in the areas of granitoids occurrence.

References

1. Derkachev A.S., Maksimova A.A., Novikov D.A. et al. Nature of radioactivity of quarry drainage waters in the Novosibirsk region. *Mining Science and Technology (Russia)*. 2022;7(3):216–230. <https://doi.org/10.17073/2500-0632-2022-3-216-230>
2. Novikov D.A., Kopylova Yu.G., Sukhorukova A.F. The Inskie Springs: new insights into low-radon waters. *Russian Geology and Geophysics*. 2022;63(12):1424–1441. <https://doi.org/10.2113/RGG20214337>
3. Morales-Arredondo J.I., Hernández M.A.A., Hernández-Mendiola E. et al. Hydrogeochemical behavior of uranium and thorium in rock and groundwater samples from southeastern of El Bajío Guanajuatense, Guanajuato, Mexico. *Environ Earth Science*. 2018;77:567. <https://doi.org/10.1007/s12665-018-7749-z>
4. Yu C., Berger T., Drake H. et al. Geochemical controls on dispersion of U and Th in Quaternary deposits, stream water, and aquatic plants in an area with a granite pluton. *Science of the Total Environment*. 2019;663:16–28.
5. Baják P., Csondor K., Pedretti D. et al. Refining the conceptual model for radionuclide mobility in groundwater in the vicinity of a Hungarian granitic complex using geochemical modeling. *Applied Geochemistry*. 2022;137:105201. <https://doi.org/10.1016/j.apgeochem.2022.105201>



6. Pérez-Moreno S.M., Guerrero J.L., Mosqueda F. et al. Hydrochemical behaviour of long-lived natural radionuclides in Spanish groundwaters. *Catena*. 2020;191:104558. <https://doi.org/10.1016/j.catena.2020.104558>
7. Novikov D.A., Dultsev F.F., Sukhorukova A.F. et al. Monitoring of radionuclides in the natural waters of Novosibirsk, Russia. *Groundwater for Sustainable Development*. 2021;15:100674. <https://doi.org/10.1016/j.gsd.2021.100674>
8. Novikov D.A., Kopylova Yu.G., Pyryaev A.N. et al. Radon-rich waters of the Tulinka aquifers, Novosibirsk, Russia. *Groundwater for Sustainable Development*. 2023;20:100886. <https://doi.org/10.1016/j.gsd.2022.100886>
9. Novikov D.A., Sukhorukova A.F., Korneeva T.V. et al. Hydrogeology and hydrogeochemistry of the «Kamenskoe» field of radon-rich waters (Novosibirsk). *Bulletin of the Tomsk Polytechnic University. Geo Assets Engineering*. 2021;332(4):192–208. <https://doi.org/10.18799/24131830/2021/4/3162>
10. Sukhorukova A.F. Hydrogeological conditions of development and hydrogeochemistry of drainage water of the borok granite quarry. *Bulletin of the Tomsk Polytechnic University. Geo Assets Engineering*. 2022;333(5):209–218. (In Russ.) <https://doi.org/10.18799/24131830/2022/5/3507>
11. Babin G.A., Chernykh A.I., Golovina A.G. et al. *State geological map of the Russian Federation. Scale 1 : 1,000,000 (third generation). Altai-Sayan Series. Sheet N-44. Novosibirsk: Explanatory Note. St. Petersburg: VSEGEI cartographic plant; 2015, 392 p. + 4 incl. (In Russ.)*
12. Sotnikov V.I., Fedoseev G.S., Kungurtsev L.V. et al. [Scientific. Ed. Dr.Sci. (Geol. and Mineral.) O.P. Ivanov] *Geodynamics, magmatism and metallogeny of the Kolyvan-Tom fold zone. Novosibirsk: Publ. House SB RAS, SPC of the JIGGM; 1999. 227 p. (In Russ.)*

Information about the authors

Vasiliy P. Sukhorukov – Cand. Sci. (Geol. and Mineral.), Head of Laboratory, V.S. Sobolev Institute of Geology and Mineralogy, Siberian Branch of the Russian Academy of Sciences, Novosibirsk, Russian Federation; Associate Professor, Novosibirsk State University, Novosibirsk, Russian Federation ORCID [0000-0002-6658-2360](https://orcid.org/0000-0002-6658-2360), Scopus ID [56268382200](https://scopus.com/authorid/56268382200); e-mail svp@igm.nsc.ru

Anna F. Sukhorukova – Cand. Sci. (Geol. and Mineral.), Senior Researcher, A.A. Trofimuk Institute of Oil and Gas Geology and Geophysics, Siberian Branch of the Russian Academy of Sciences, Novosibirsk, Russian Federation; Associate Professor, Senior Researcher, Novosibirsk State University, Novosibirsk, Russian Federation; ORCID [0000-0003-4228-7946](https://orcid.org/0000-0003-4228-7946), Scopus ID [56524401600](https://scopus.com/authorid/56524401600); e-mail SukhorukovaAF@ipgg.sbras.ru

Dmitry A. Novikov – Cand. Sci. (Geol. and Mineral.), Head of Laboratory, A.A. Trofimuk Institute of Oil and Gas Geology and Geophysics, Siberian Branch of the Russian Academy of Sciences, Novosibirsk, Russian Federation; Associate Professor, Leading Researcher, Novosibirsk State University, Novosibirsk, Russian Federation; ORCID [0000-0001-9016-3281](https://orcid.org/0000-0001-9016-3281), Scopus ID [35318389700](https://scopus.com/authorid/35318389700); e-mail NovikovDA@ipgg.sbras.ru

Anton S. Derkachev – Junior Researcher, A.A. Trofimuk Institute of Oil and Gas Geology and Geophysics, Siberian Branch of the Russian Academy of Sciences, Novosibirsk, Russian Federation; Engineer, Novosibirsk State University, Novosibirsk, Russian Federation; ORCID [0000-0001-6101-6573](https://orcid.org/0000-0001-6101-6573), Scopus ID [57223290521](https://scopus.com/authorid/57223290521); e-mail Derkachyovas@ipgg.sbras.ru

Received 17.01.2024

Revised 18.03.2024

Accepted 25.03.2024



MINING ROCK PROPERTIES. ROCK MECHANICS AND GEOPHYSICS

Research paper

<https://doi.org/10.17073/2500-0632-2023-08-143>

UDC 622.02

**Determination of deformation modulus and characterization of anisotropic behavior of blocky rock masses**O. Ahrami¹ , H. Javaheri Koupaei¹   , K. Ahangari²  ¹ Department of Civil Engineering, Science and Research Branch, Islamic Azad University, Tehran, Iran² Department of Mining Engineering, Science and Research Branch, Islamic Azad University, Tehran, Iran h-javaheri@srbiau.ac.ir**Abstract**

The anisotropy in the deformational behavior of blocky rock masses has been comprehensively investigated. The uniaxial deformation modulus was selected as the key parameter. This modulus is generally anisotropic and depends on the loading direction, as well as on the properties of the intact rock, joints, and joint setting. Representative volumes of blocky rock masses were numerically simulated using the discrete element method and were loaded uniaxially in various directions. Subsequently, the failure mode and the deformation modulus were studied for different loading directions and various relative joint settings. A new nonlinear, stress-dependent stiffness matrix for joints was introduced, incorporating the surface conditions of the joints in terms of the Joint Roughness Coefficient (JRC) and the properties of the intact rock materials in terms of the Uniaxial Compressive Strength (UCS). The results of the assessments are presented in the form of rose diagrams, showing variations in the deformation modulus of the blocky rock mass that depend on the joint's JRC, the intact rock's UCS, and the structure of the rock mass in term of the relative joint angle. Also, the expected degree of anisotropy for various joint surface conditions and uniaxial compressive strengths of intact rock were introduced. In the Geological Strength Index (GSI) table, results are classified such that assigning a value to the JRC for each class of joint surface conditions allows for the corresponding deformation modulus and degree of anisotropy. According to this chart, it is deduced that the effect of joint roughness on the deformation modulus of blocky rock masses is greater than that of the intact rock UCS. The results support the hypothesis that a blocky rock mass has a critical strain that is independent of the loading angle (θ) and the orientation of the third joint set (α).

Keywords


deformation modulus, blocky rock mass, anisotropy, joint stiffness matrix, degree of anisotropy, failure mode

For citation

Ahrami O., Javaheri Koupaei H., Ahangari K. Determination of deformation modulus and characterization of anisotropic behavior of blocky rock masses. *Mining Science and Technology (Russia)*. 2024;9(2):116–133. <https://doi.org/10.17073/2500-0632-2023-08-143>

СВОЙСТВА ГОРНЫХ ПОРОД. ГЕОМЕХАНИКА И ГЕОФИЗИКА

Научная статья

Определение модуля деформации и характеристик анизотропного поведения блочных массивов горных породО. Ахрами¹ , Х. Джавахери Купаи¹   , К. Ахангари²  ¹ Кафедра гражданского строительства, научно-исследовательский отдел, Исламский университет Азад, г. Тегеран, Иран² Кафедра горного дела, научно-исследовательский отдел, Исламский университет Азад, г. Тегеран, Иран h-javaheri@srbiau.ac.ir**Аннотация**

Всесторонне изучена анизотропия деформационного поведения блочных массивов горных пород. В качестве ключевого параметра выбран модуль одноосной деформации. В целом он является анизотропным и зависит от направления нагружения, а также от свойств ненарушенной породы, трещин и элементов их залегания. Представительные объемы блочных массивов горных пород были численно смоделированы методом дискретных элементов и одноосно нагружены в различных направлениях. Затем были изучены режим разрушения и модуль деформации для различных направлений нагружения и различных относительных элементов залегания трещин. Внедрена и использована новая нелинейная матрица жесткости трещин в зависимости от напряжения, в которой учитываются состояние поверхности трещин в виде коэффициента шероховатости (JRC) и ненарушенного массива пород в виде пре-



дела прочности при одноосном сжатии (UCS). Результаты оценок представлены в виде роз-диаграмм, демонстрирующих изменение модуля деформации блочного массива горных пород в зависимости от коэффициента шероховатости швов, прочности при одноосном сжатии ненарушенной породы и структуры массива горных пород по относительному углу трещины. Также представлена ожидаемая степень анизотропии для различных условий поверхностных трещин и прочности при одноосном сжатии ненарушенной породы. В таблице геологического индекса прочности (GSI) результаты классифицированы таким образом, что, присвоив значение JRC каждому классу состояния поверхности трещин, можно определить модуль деформации и степень анизотропии, соответствующие значениям GSI. Согласно этой схеме можно сделать вывод, что влияние шероховатости трещин на модуль деформации блочных массивов горных пород больше, чем влияние предела прочности при одноосном сжатии ненарушенной породы. Полученные результаты подтверждают идею о том, что блочный массив имеет критическую деформацию, которая не зависит от угла нагружения θ и направления третьей системы трещин α .

Ключевые слова

модуль деформации, блочный массив горных пород, анизотропия, матрица жесткости трещин, степень анизотропии, режим разрушения

Для цитирования

Ahrami O., Javaheri Koupaei H., Ahangari K. Determination of deformation modulus and characterization of anisotropic behavior of blocky rock masses. *Mining Science and Technology (Russia)*. 2024;9(2):116–133. <https://doi.org/10.17073/2500-0632-2023-08-143>

Highlights

- New nonlinear stress – dependent relations for both normal and shear stiffness of joints have been introduced
- Blocky rock masses are classified based on their joint surface condition and the strength of the intact rock.
- Results are organized in manner analogous to the GSI chart, allowing for the determination of the range of deformation modulus and degree of anisotropy for a specified blocky rock mass with an evaluated GSI.
- The degree of anisotropy in the deformation modulus of blocky rock masses, defined as the ratio of the maximum deformation modulus to the minimum, was determined to be between 1.6 and 2.3, with an average value of 1.88.

Equation Symbols

- σ_n : Normal stress;
- σ_c : Uniaxial Compressive Strength;
- σ_{ci} : Uniaxial Compressive Strength of intact rock;
- σ_{cm} : Uniaxial Compressive Strength of rock mass;
- τ_n : Shear stress;
- τ_f : Peak shear stress;
- τ_{ult} : Ultimate shear stress;
- φ : Friction angle of intact rock;
- φ_j : Friction angle of joint;
- φ_b : Base friction angle of joint;
- a : Empirical constant;
- C : Cohesion parameter of intact rock;
- C_j : Cohesion parameter of joint;
- K : Bulk modulus of intact rock;
- G : Shear modulus of intact rock;
- T : Tensile strength of intact rock;
- T_j : Tensile strength of joint;

- E_i : Intact rock elastic modulus;
- E_m : Deformation modulus of rock mass;
- E_{max} : Maximum deformation modulus of rock mass;
- E_{min} : Minimum deformation modulus of rock mass;
- GSI : Geological strength index;
- JRC : Joint roughness coefficient;
- JCS : Compressive strength of the joint wall;
- UCS : Uniaxial compressive strength;
- K_n : Joint normal stiffness;
- K_s : Joint shear stiffness;
- K_{sn} : Coupling effects of the shear and normal behavior of the joint;
- K_{ns} : Coupling effects of the normal and shear behavior of the joint;
- K_{ni} : Initial joint normal stiffness;
- K_{si} : Initial joint shear stiffness;
- R_f : Failure ratio;
- R_E : Degree of anisotropy deformation;
- U_n : Normal joint relative displacement;
- U_s : Shear joint relative displacement;
- U_{nc} : Maximum joint vertical displacement;
- U : Joint aperture at the beginning of loading;
- U_s^{Peak} : Shear displacement at peak strength;
- D : Disturbance factor.

Introduction

The deformation modulus of rock mass is a fundamental parameter in the geomechanics of tunnels, mining, and other geotechnical rock-supported facilities. The mechanical properties of a rock mass, seen as a fractured medium, are determined by the intact rock, the pattern of relative joint-sets, the geometrical arrangement of the joints, and their mechanical properties. Joint sets, acting as planar discontinuities, confer



scale and direction-dependent mechanical properties. Each joint set introduces anisotropy in the direction of its normal vector. When a rock mass is heavily fractured, the individually imposed anisotropy by the joints in any direction can be considered uniformly distributed, resulting in an isotropic rock mass. Otherwise, even in dimensions larger than the representative elementary volume (REV), where the rock mass can be treated as a continuum, its directional dependence persists.

For rock masses with simple joint settings, analytical relations, such as those proposed by Singh [1], Gerrard [2], Oda [3] and Amadei and Savage [4], are available to evaluate the deformation modulus. An example of such type of relations is the three-dimensional equivalent continuous model presented by Kulhawy [5] for a rock mass with three orthogonal joint sets that displays orthotropic behavior. However, it is impossible to find a closed-form solution for the deformation modulus of rock masses with numerous joint sets or when considering more advanced constitutive behavior for intact rock and joints. It is noteworthy that empirical methods commonly used in rock engineering to evaluate rock mass deformability, such as those presented by Serafim & Pereira [6], Gokceoglu et al. [7], Hoek & Diederichs [8], overlook the effect of rock mass anisotropy and there is a lack of a mathematical platform for creating a behavioral model.

In experimental methods, as the mechanical properties of the rock mass are scale-dependent, the scales of rock samples and test probes seldom correspond proportionally to the actual rock masses. Heuze [9] concluded that the rock mass deformation modulus measured in the field ranges widely between 20 and 60% of the intact rock modulus measured in the laboratory. In-situ tests are costly, time-consuming, and challenging to interpret due to the presence of undefined joints and uncertain boundary conditions. They are often used cautiously as a representative of the extent of the affected rock mass. Furthermore, multiple tests in various directions are necessary to characterize the inherent anisotropy of the rock mass.

Numerical simulations of rock masses as fractured discontinuities generally employ two methodologies. One is the continuum approach, where the impact of discontinuities is implicitly considered through equivalent mechanical properties, as per Singh [1], Agharazi et al. [10]. The other involves numerical solution techniques such as discrete element, finite element, or finite difference methods, in which discontinuities are explicitly simulated. The discrete element method (DEM), introduced by Cundall [11] and further developed by subsequent

researchers [12, 13], is highly regarded for its ability to describe the geometric configurations and constitutive relations of joints and intact rock. Many studies on the mechanical behavior of rock masses have employed discrete element method [14–16].

The present study investigates the anisotropic deformation modulus of blocky rock masses formed by three intersecting joint sets, including two orthogonal sets. This was achieved through discrete element simulations of representative volumes of blocky rock masses.

The critical factor influencing the deformational behavior of a rock mass is the stiffness of its fractures and discontinuities. The stiffness of planar discontinuities, expressed through the normal (K_n) and shear (K_s) components, is crucial for evaluating the stiffness of the rock masses. Definitions that closely reflect actual conditions improve the accuracy of the calculated rock mass deformation modulus. Therefore, efficient relationships that accurately represent nonlinear joint behavior are essential for calculating the rock mass deformation modulus. To this end, a newly inferred nonlinear stress-dependent stiffness matrix for joints has been introduced for the simulations. This matrix accounts for the real nonlinear behavior of joints through their basic parameters, eliminating the need for multiple tests. This study is unique in that directly incorporates the fundamental joint parameters into the calculation of rock mass modulus, enhancing the precision and applicability of the results.

This study aims to present a realistic portrayal of the anisotropic behavior of blocky rock masses by combining numerical simulation with a mathematically-empirical relationship for joint stiffness in a practical manner. It addresses the deformation modulus, failure mechanism, and post-failure behavior for different loading directions, along with summarizing the degree of anisotropy. The deformation moduli are depicted through rose diagrams, illustrating the variability of the blocky rock mass deformation modulus in various directions as a function of the rock mass's intrinsic parameters along. These parameters include the joints JRC, the intact rock's UCS, and the structure of the rock mass in terms of relative joint angle. These diagrams allow for the estimation of the blocky rock mass deformation modulus in different directions without relying on laboratory and in-situ tests or empirical relationships. Furthermore, by consolidating the analysis results into the GSI table, the data were categorized such that assigning a JRC value to each class of joint surface conditions enables the determination of the corresponding deformation modulus and degree of anisotropy for GSI values.

1. Modeling strategy

To examine the state of anisotropy in blocky rock masses, representative volumes were simulated using the discrete element method (via 3DEC software, Itasca 2013¹) and subjected to uniaxial loading in various directions.

For different relative joint settings – representing various blocky rock masses – the failure modes and the deformation moduli were ascertained for different loading directions. The modeling procedure includes: a) defining the geometric configuration of the blocky rock masses; b) applying uniaxial loading to the selected rock mass in various directions; c) specifying the mechanical constitutive behavior of joints and intact rock in a parametric manner; and d) identifying a representative volume for the rock masses. These steps are elaborated on in the subsequent subsections.

1.1. Geometric setting of studied blocky rock masses

The term 'blocky rock mass' usually refers to a rock mass that encompasses three joint sets [17]. In this study, we consider blocky rock masses that include two orthogonal joint sets intersected by a third set, as shown in Fig. 1. In Fig. 1, the third joint set forms an angle (α) with the second joint set, and its strike is perpendicular to the strike of the joint set 1. This study examines rock masses formed by values of $\alpha = 5^\circ, 15^\circ, 30^\circ, 45^\circ, 60^\circ, 75^\circ$ and 90° .

1.2. Loading scheme

To evaluate the anisotropic behavior of the models, a representative volume element of the mass was subjected to uniaxial loading in different directions. This load is applied perpendicular to a plane with

¹ Itasca Consulting Group Inc., 2013. 3DEC 5.00, User's Guide, Itasca Consulting Group, Inc.

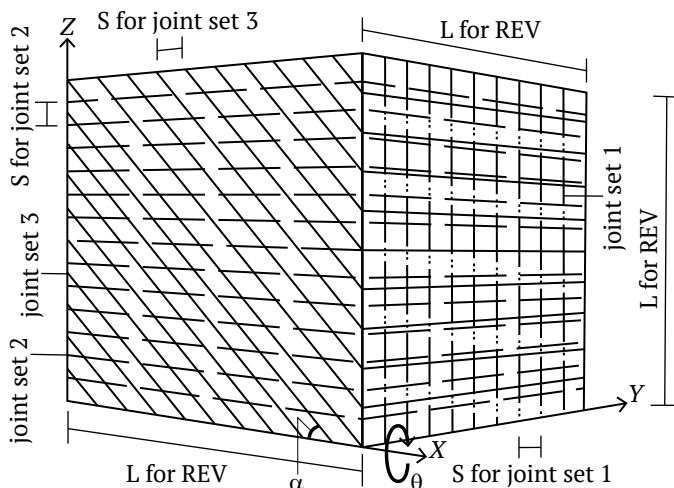


Fig. 1. A blocky rock mass with two orthogonal joint sets intersected by a third joint set forming an angle (α)

a strike parallel to the 'X' axis, deviating from the '-Z' axis by an angle θ .

Fig. 2 depicts the directions of uniaxial loadings on a blocky rock mass with $\alpha = 45^\circ$. As another example, Fig. 3, a illustrates a model of a blocky rock mass with $\alpha = 90^\circ$ and $\theta = 0$, and Fig. 3, b shows a model of a blocky rock mass with $\alpha = 90^\circ$ and $\theta = 45^\circ$.

The 3DEC models are made as cubes with axes aligned with the global coordinates of the software environment, and uniaxial load is consistently applied in the direction of the global vertical axis. To load the mass at an angle θ for each set of joints, the joint planes are rotated around the global x axis by angle θ , as shown in Fig. 1.

1.3. Mechanical properties of joint

A general constitutive equation for the deformation of joints can be expressed as:

$$\begin{pmatrix} \sigma_n \\ \tau_n \end{pmatrix} = \begin{bmatrix} K_n & K_{sn} \\ K_{ns} & K_s \end{bmatrix} \begin{pmatrix} U_n \\ U_s \end{pmatrix}, \quad (1)$$

where σ_n is the normal stress, τ_n is the shear stress, U_n is the normal relative displacement, and U_s is the shear relative displacement of the joint. K_n and K_s are the normal and shear stiffnesses of the joint, respectively, and K_{sn} and K_{ns} are the coupling effects of the shear and normal behaviors of the joint, which have been neglected in this study. To account for a realistic behavior of joint stiffness in the models, new non-linear stress-dependent expressions for the diagonal components of the joint stiffness matrix are introduced in the following subsections. These expressions define the stiffness matrix components as a function of the normal stress to the joint (σ_n) the joint surface condition in terms of the Joint Roughness Coefficient (JRC), and the intact rock material in terms of the Uniaxial Compressive Strength of intact rock (σ_{ci}).

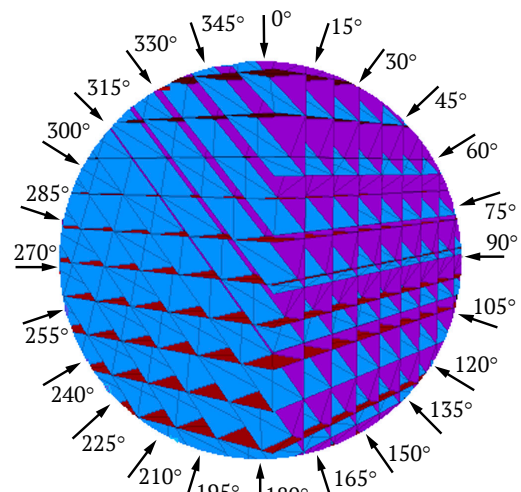


Fig. 2. Directions of Uniaxial Loadings on a blocky rock mass with $\alpha = 45$ degrees

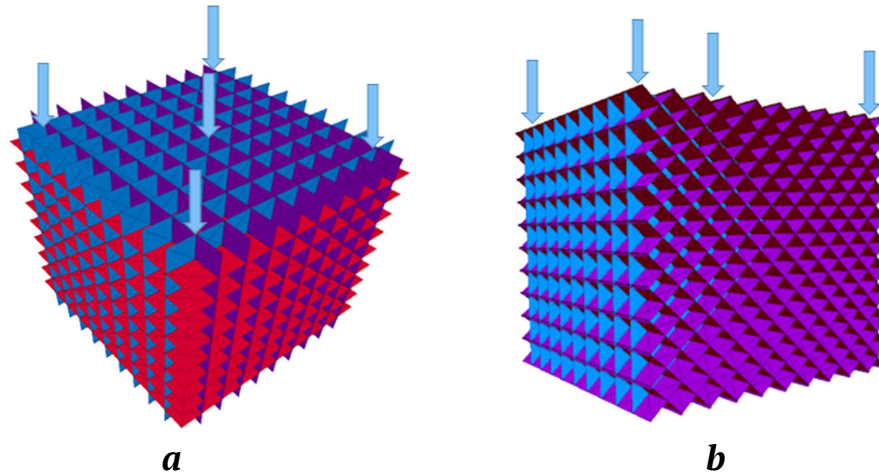


Fig. 3. A blocky rock mass with: a – $\alpha = 90^\circ$ and loading angle $\theta = 0$; b – $\alpha = 90^\circ$ and loading angle by $\theta = 45^\circ$

1.3.1. Normal stiffness

The normal behavior of a joint can be described by the hyperbolic model proposed by Goodman et al. [18] and Bandis et al. [19] as:

$$\sigma_n = \frac{aU_n}{U_{nc} - U_n}, \quad (2)$$

where U_n is the joint vertical displacement, U_{nc} is the maximum joint vertical displacement, and “a” is an empirical constant. Fig. 4 shows a typical normal behavior of joints. From the definition of K_n and Eq. (2):

$$K_n = \frac{d\sigma_n}{dU_n} = \frac{aU_{nc}}{(U_{nc} - U_n)^2}. \quad (3)$$

Thus, the initial joint normal stiffness K_{ni} at the onset of loading, when $U_n = 0$, is:

$$K_{ni} = \frac{a}{U_{nc}}. \quad (4)$$

By solving Eq. (4) for “a” in terms of U_{nc} and K_{ni} , and substituting in Eq. (2) for U_{nc} and then into Eq. (3), K_n becomes:

$$K_n = K_{ni} + \frac{\sigma_n^2}{K_{ni} \left(\frac{\sigma_n U_n}{\sigma_n - K_{ni} U_n} \right)^2} + \frac{2\sigma_n}{\sigma_n - K_{ni} U_n}. \quad (5)$$

Eq. (5) expresses the normal joint stiffness in a specified state of stress and deformation relative to its initial value, K_{ni} which can be evaluated as follow:

Bandis et al. [19] proposed the initial normal stiffness of joints as:

$$K_{ni} = -7.15 + 1.75JRC + 0.02 \left[\frac{JCS}{U} \right]. \quad (6)$$

Here, JRC is the Joint Roughness Coefficient of the joint surface and JCS is the compressive strength of the joint wall expressed in MPa, which can be equated

with the compressive strength of the intact rock (σ_{ci}). The joint aperture U , mm, at the beginning of loading can be estimated by Bandis et al. [19]:

$$U = JRC \left[\frac{0.04\sigma_{ci}}{JCS} - 0.02 \right]. \quad (7)$$

By substituting U from Eq. (7) into Eq. (6), an expression for estimating K_{ni} is derived.

1.3.2. Shear stiffness

The relationship between the relative shear displacement (U_s) and shear stress (τ) can be described by a hyperbolic function [19–21] as:

$$\tau = \left[\frac{1}{K_{si}U_s} + \frac{R_f}{\tau_f} \right]^{-1}, \quad (8)$$

where K_{si} is the initial shear stiffness, τ_f is the shear strength of the joint, R_f is the failure ratio (τ_f/τ_{ult}), and τ_{ult} is the ultimate shear stress. Consequently:

$$K_s = \frac{d\tau}{dU_s} = K_{si} \left[1 + \frac{R_f K_{si} U_s}{\tau_f} \right]^{-2}; \quad (9)$$

$$U_s = \left[\frac{K_{si}}{\tau} - \frac{R_f K_{si}}{\tau_f} \right]^{-1}. \quad (10)$$

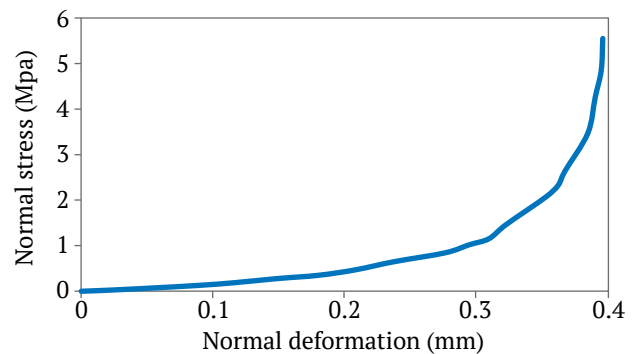


Fig. 4. Typical normal stress-deformation behavior of joints

Table 1

Correlation selection between uniaxial compressive strength and friction angle for intact rock

σ_{ci} , MPa	φ , degree
$\sigma_{ci} < 50$	25
$50 < \sigma_{ci} < 100$	30
$100 < \sigma_{ci} < 250$	35

At the shear strength of a joint, using $\tau = \tau_f$ and $U_s = U_s^{peak}$ from Eq. (10), we get:

$$R_f = 1 - \frac{\tau_f}{K_{si} U_s^{peak}} \quad (11)$$

Following Barton and Choubey [22], the shear displacement at peak strength along a joint is considered to be 0.01 times the length of the joint or fault block; hence, the relative shear displacement, U_s^{peak} is 0.01. From Eq. (11):

$$R_f = 1 - \frac{\tau_f}{0.01 K_{si}} \quad (12)$$

Substituting Eqs. (10) and (12) into Eq. (9), we obtain:

$$K_s = K_{si} \left[1 + \frac{\left(k_{si} - \frac{\tau_f}{0.01} \right) \left(\frac{k_{si}}{\tau} - \frac{k_{si} \left(1 - \frac{\tau_f}{0.01 k_{si}} \right)^{-1}}{\tau_f} \right)^{-2}}{\tau_f} \right] \quad (13)$$

According to Bandis et al. [19]:

$$K_{si} = (-17.19 + 3.86 JRC) (\sigma_n)^{0.783} \quad (14)$$

and following [23–25]:

$$\tau_f = \sigma_n \tan \left[JRC \log \frac{JCS}{\sigma_n} + \varphi_b \right] \quad (15)$$

1.4. Mechanical properties of intact rock

The intact rock is assumed to behave as an isotropic elastic-perfectly plastic material, and the Mohr-Coulomb criterion was adopted as the yield or failure model. The relationship between the elastic modulus, E_i and the uniaxial compressive strength, σ_{ci} , of intact rock was selected from the relationships proposed by Deere & Miller [26]. They proposed correlations between σ_{ci} and Schmidt hammer rebound number ($R_{n(l)}$), and between E_i and $R_{n(l)}$ as:

$$\sigma_{ci} = 6.9 \cdot 10^{(0.0087 \rho R_{n(l)} + 0.16)}, \text{ MPa}; \quad (16)$$

$$E_i = 0.6005 \rho R_{n(l)} - 2.0276, \text{ GPa}, \quad (17)$$

which yields:

$$E_i = 69.023 \log(0.145 \sigma_{ci}) - 13.07, \text{ GPa}, \quad (18)$$

where σ_{ci} is in MPa. Eqs. (16) and (17) have been proposed based on experimental results from 28 lithological units and 3 types of rocks [26].

Poisons' ratio is selected as 0.25.

The cohesion parameter of intact rock, C , is determined as [27]:

$$C = 0.16 \sigma_{ci}. \quad (19)$$

For the friction angle of intact rock, a value is selected as representative for each group variation of σ_{ci} as presented in Table 1, based on typical values of φ for various rocks in [28] and Barton & Choubey [22].

1.5. Representative Elementary Volume of the rock masses

It is recognized that the mechanical behavior of rock masses with a systematic pattern of joints is scale-dependent. Depending on the relative block size (ratio of block size to a characteristic size of the rock mass, e.g. S/L in Fig. 1), rock mass behavior can range from that of intact rock to an asymptotic value at a large scale where the rock mass may be considered a continuum. Cuba [29] suggested that a certain scale, known as the "Representative Elementary Volume" (REV), can be chosen above which the characteristics of the domain remain basically constant. Empirically based relations can be employed to estimating this scale. Schultz [30] recommended a scale of 5 to 10 times the block size or fracture spacing (relative block size = 0.2 to 0.1).

For a cubic volume containing three uniform joint sets with spacing S and dimension L , the minimum relative dimension (L/S) of the REV can be determined through successive analyses of the cube's uniaxial behavior. The chosen volume consists of two orthogonal joint sets intersected by a third set at $\alpha = 45^\circ$, as illustrated in Fig. 1. The results for peak uniaxial strength and uniaxial secant stiffness corresponding to 50 percent of the peak strength E_{50} , are presented in Fig. 5. From this figure, $L/S = 10$ was selected as the REV scale.

2. Validation of the modeling strategy

The validation of the implemented modeling procedure has been conducted through a series of comparisons between existing results and numerical modeling predictions. This includes comparison for: a) simulated variation of uniaxial compressive strength UCS of a rock mass with a single joint set with closed-form solution results (Section 2.1), b) predicted mode of failure of jointed rock masses with experimental modeling results (Section 2.2), and c) predicted anisotropic modulus of rock with a single joint set with experimental modeling results (Section 2.3).

2.1. Simulation of UCS of a rock mass with a single set of joints

Jaeger proposed a closed-form solution for predicting the variation of uniaxial compressive strength of a rock mass with a single joint set in various directions [31]. Fig. 6 compares the UCS from the numerical model of a cylindrical specimen with a single joint set to the solution proposed by Jaeger et al. [31]. The angle of the joints relative to the vertical axis varies from 0° to 90°. In the numerical solution, a cylindrical rock mass sample with a diameter of 2 m and a length of 4 m was loaded to failure. The UCS values are compared in Fig. 6. As shown in Fig. 6, the results closely align with the solution by Jaeger et al. [31]. Details of the intact rock and the joints are provided in the caption of Fig. 6.

2.2. Simulation of experiments on failure modes of jointed rocks

Yang et al. (1998) [32] performed a series of physical model tests to investigate the failure mode and anisotropy of jointed rocks. These models included simulated rock specimens (composed by cement and sand) with one or two non-orthogonal joint sets, as presented in Table 2. Table 2 also provides a compari-

son between the failure states observed in test results reported by Yang et al. (1998) [32] and the outcomes of numerical simulations of these models, which were found to be consistent.

2.3. Simulation of experiments on deformation modulus of jointed rocks

Fig. 7 present a comparison between the experimental deformation modulus from Yang et al. [32] and the results of numerical simulation for a rock mass with a single joint set. The consistency between experimental results and numerical simulation is evident.

3. Results of Simulations

3.1. Anisotropy in rock mass stress-strain behavior and failure mechanism

When a rock mass is subjected to uniaxial loading, the possible failure mechanisms include intact rock failure, failure due to sliding on the joints, and a combination of these two modes. In the analyses, stress-strain curves and modes of failures have been examined. The mechanisms of failure and the post-failure behavior for each loading direction are summarized in Tables 3 and 4.

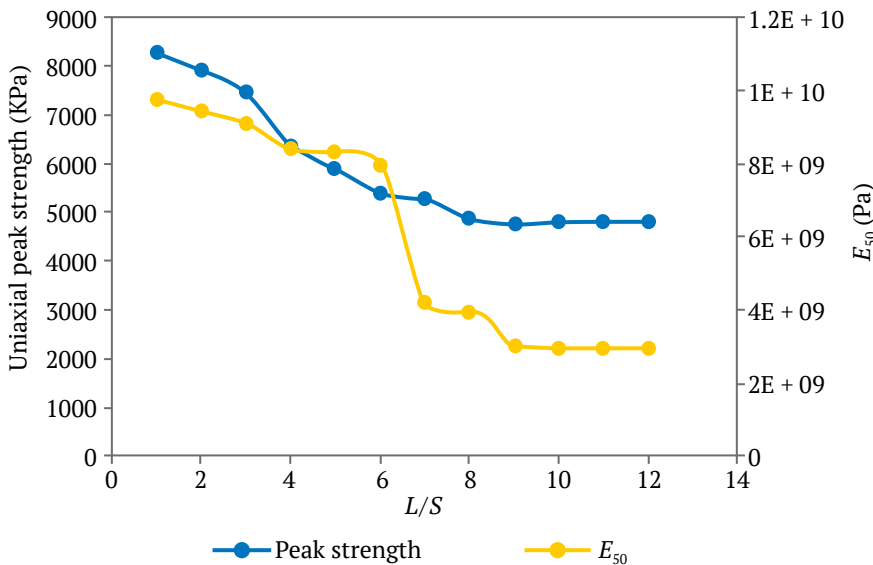


Fig. 5. Variation in uniaxial peak strength and E_{50} for a blocky rock mass ($\alpha = 45^\circ$ in Fig. 1) with L/S ratio (intact rock shear modulus $G = 4$ GPa, intact rock bulk modulus $K = 6.66$ GPa; $\varphi = 25$, $\nu = 0,25$, $c = 2.4$ GPa)

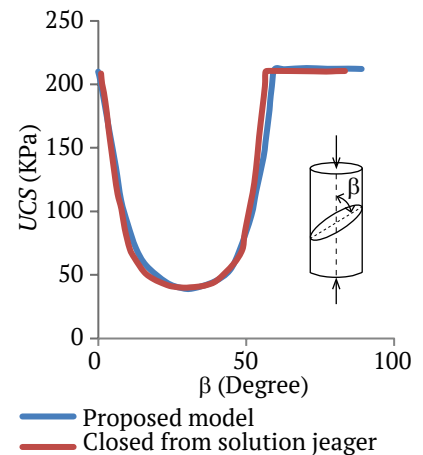


Fig. 6. UCS variation in a rock mass with a single joint set and varied joint inclination. Intact rock parameters: $G = 4.28$ GPa; $K = 1.75$ GPa; $\varphi = 40$; $T = 200$ kPa; Joint parameters: $c_j = 10$ kPa; $\varphi_j = 30$; $T_j = 20$ kPa; $K_n = 15$ GPa/m; $K_s = 12$ GPa/m

Comparison of failure modes in physical and numerical models

Proposed model	Test result	Rock mass with one joint set
dip = 0 dip = 90	Intact rock failure Intact rock failure	Intact rock failure Intact rock failure
Proposed model	Test result	Rock mass with two joint sets
dip = 0/90 dip = 60/-60 (60/120) dip = 40/-40 (40/140)	Intact rock failure Joint sliding Mixed failure (joint sliding + intact rock)	Intact rock failure Joint sliding Mixed failure

Table 2

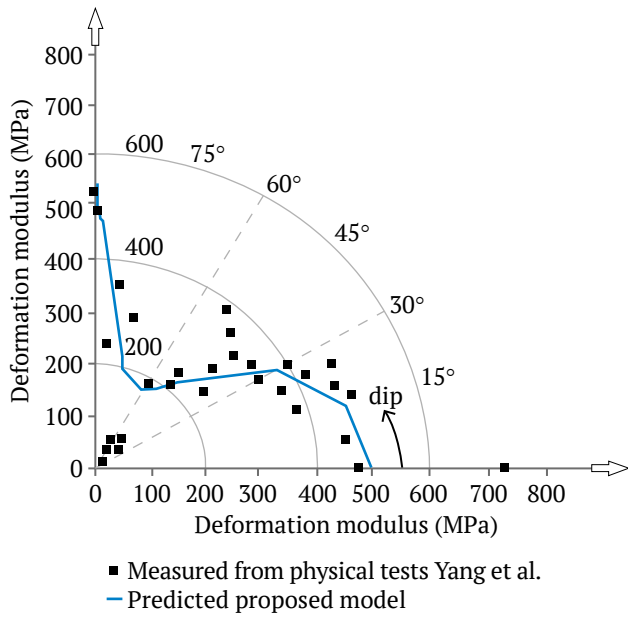


Fig. 7. Experimental vs. numerical simulation deformation modulus comparison from Yang et al. [32] for a rock mass with a single joint set. Fundamental material properties:
 $G = 1.913 \text{ GPa}$; $K = 2.448 \text{ GPa}$;
 $JCS = 7.63 \text{ MPa}$; $\phi = 31$; $\sigma_t = 1.05 \text{ MPa}$; $\nu = 0.19$;
 $U.W. = 1.05 \text{ g/cm}^3$; $\sigma_c = 7.63 \text{ MPa}$

Table 3
Failure mechanisms for the blocky rock masses shown in Fig. 1

θ	α						
	5	15	30	45	60	75	90
0°	IRF + JS	IRF + JS	IRF + JS	JS	JS	IRF + JS	IRF
15°	IRF + JS	IRF + JS	JS	JS	IRF + JS	IRF + JS	IRF + JS
30°	JS	JS	JS	JS	JS	JS	JS
45°	JS	JS	JS	JS	JS	JS	JS
60°	JS	JS	JS	JS	JS	JS	JS
75°	IRF + JS	IRF + JS	JS	JS	JS	IRF + JS	IRF + JS
90°	IRF + JS	IRF + JS	IRF + JS	JS	JS	IRF + JS	IRF

Note: IRF: Intact rock failure; JS: Joint sliding

Table 4
Post-failure behavior of blocky rock masses shown in Fig. 1

θ	α						
	5	15	30	45	60	75	90
0°	P & B	P & B	S & B	P & S	P & S	P & B	P & B
15°	P & B	P & S	S	S	S & B	S & B	S & B
30°	P & S	S	S	S	P & S	P & S	S
45°	P & S	S	S	S	S	S	P & S
60°	P & S	S	P & S	S	S	S	S
75°	P & B	P & B	S	S	S	P & B	P & B
90°	P & B	P & B	S & B	P & S	P & S	P & B	P & B

Note: P: Perfect plastic; S: Softening; B: Brittle

For instance, in the case of poor rock ($0 < JRC < 4$ and $\sigma_{ci} < 25 \text{ MPa}$) by selecting $\sigma_{ci} = 15$ and $JRC = 2$ as mean values, Fig. 8 shows how axial stress-strain curves vary with the relative uniaxial loading direction α . σ_{ci} represents the UCS of the intact rock. For each curve, the mode of failure has also been indicated in the Figure.

When the loading direction is perpendicular to or parallel with the planes of the joints, ($\theta = 0$ or $\theta = 90$) and ($\alpha = 0$ or $\alpha = 90$), failure of the blocky rock mass occurs due to the failure in the rock material. In other cases, failure of the rock mass occurs due to the sliding on the joints or as a combination of sliding on the joints and failure of the intact rock. When the direction of loading varies from 15 to 75° ($15 \leq \theta \leq 75$), failure in the blocky rock mass occurs due to the sliding on the joints. In this case, the uniaxial strength of the rock mass, σ_{cm} , is between 0.35 to 0.45MPa ($\sigma_{cm} < 0.03\sigma_{ci}$). When θ varies from 0° to 15° or from 75° to 90° ($0 < \theta < 15$ or $75 < \theta < 90$), failure occurs as a combination of the failure of the intact rock and sliding on the joints. In this case, σ_{cm} varies from 0.8 to 1.4MPa ($\sigma_{cm} < 0.1\sigma_{ci}$). For the case of fair-quality blocky rock mass ($4 < JRC < 8$ and $50 < \sigma_{ci} < 100$), when the failure occurs due to the sliding on the joints, $\sigma_{cm} < 0.05\sigma_{ci}$; and when failure occurs as a combination of failure of the intact rock and sliding on the joints, $\sigma_{cm} < 0.16\sigma_{ci}$. For good-quality blocky rock masses ($8 < JRC < 12$ and $100 < \sigma_{ci} < 250$), when failure occurs due to the sliding on the joints, $\sigma_{cm} < 0.14\sigma_{ci}$ and when it occurs as a combination of the failure of the intact rock and sliding on the joints, $\sigma_{cm} < 0.4\sigma_{ci}$. Fig. 9 shows a subset of these results for brevity.

It is important to note that when failure in the blocky rock mass occurs due to sliding on the joints (at $\theta = 30$, $\theta = 45$, and $\theta = 60$), the yield strain ranges from 0.2 to 0.4 and is independent of the loading angle (θ) and the direction of the third joint set (α). When samples undergo softening after peak stress, phenomena such as block rotation within the mass and the formation of a zigzag pattern on the fracture surface are observed.

3.2. Anisotropy in deformation modulus of blocky rock masses

The deformation modulus is considered a function of the characteristics of the joints and intact rock, as well as the direction. Blocky rock masses were classified based on the joints condition by JRC as ($0 < JRC < 4$, $4 < JRC < 8$, $8 < JRC < 12$, $12 < JRC < 16$, $16 < JRC < 20$) and the UCS of the intact rock as ($\sigma_{ci} < 25 \text{ MPa}$, $25 < \sigma_{ci} < 50 \text{ MPa}$, $50 < \sigma_{ci} < 100 \text{ MPa}$, $100 < \sigma_{ci} < 250 \text{ MPa}$). The deformation modulus for each group is calculated for different α directions. Results of these calculations are presented in a polar coordinate system introduced in Fig. 10.

In this system, angle θ (defined in Fig. 1) is measured in the positive trigonometric direction from 0° to 90° , and the value of the deformation modulus is indicated in the radial direction from the center. In these charts, the deformation modulus is expressed in GPa. In Fig. 10, the curve represents the range $16 < JRC < 20$ and $50 < \sigma_{ci} < 100$ MPa at $\alpha = 30^\circ$. Each point on this curve, which attributes a modulus value E to θ in 5° increments, is calculated as follows:

- for a specific value of θ ;
- for σ_{ci} ranging from 50 to 100MPa in 5 steps (60, 70, 80, 90, 100MPa);
- for JRC from 16 to 20 in 4 steps (17, 18, 19, 20);

– an E is calculated for each pair of JRC and σ_{ci} , and their mean value is attributed to the θ value.

Figs. 11 to 14 display the results. In these figures, each curve corresponds to a specific value of α . From these figures, by knowing the rock mass structure (α), joint conditions (based on JRC), and intact rock properties (represented by σ_{ci}), the deformation modulus of the rock mass can be extracted from the curves for different loading directions. For example, in Fig. 10, for a rock mass with two orthogonal joint sets and a third joint set at $\alpha = 30$, if the condition of joint is very good, ($16 < JRC < 20$), and $50 < \sigma_{ci} < 100$ MPa, the deformation modulus at $\theta = 15^\circ$ is 39 GPa.

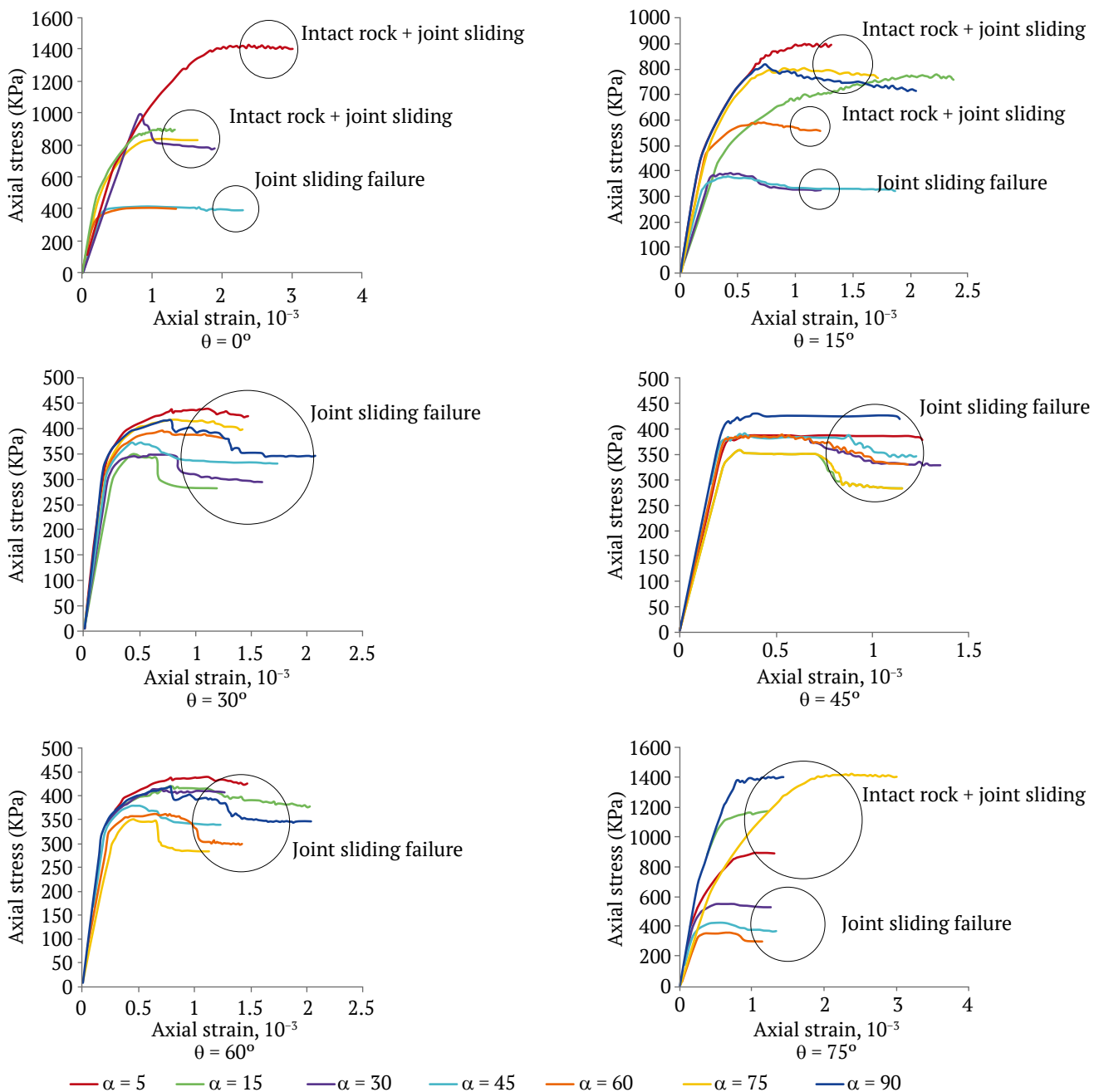


Fig. 8. Stress-strain curve comparison for different directions of third joint set (α) at different loading angles (θ) for poor quality blocky rock mass ($JRC = 2$ and $\sigma_{ci} = 15$ MPa)

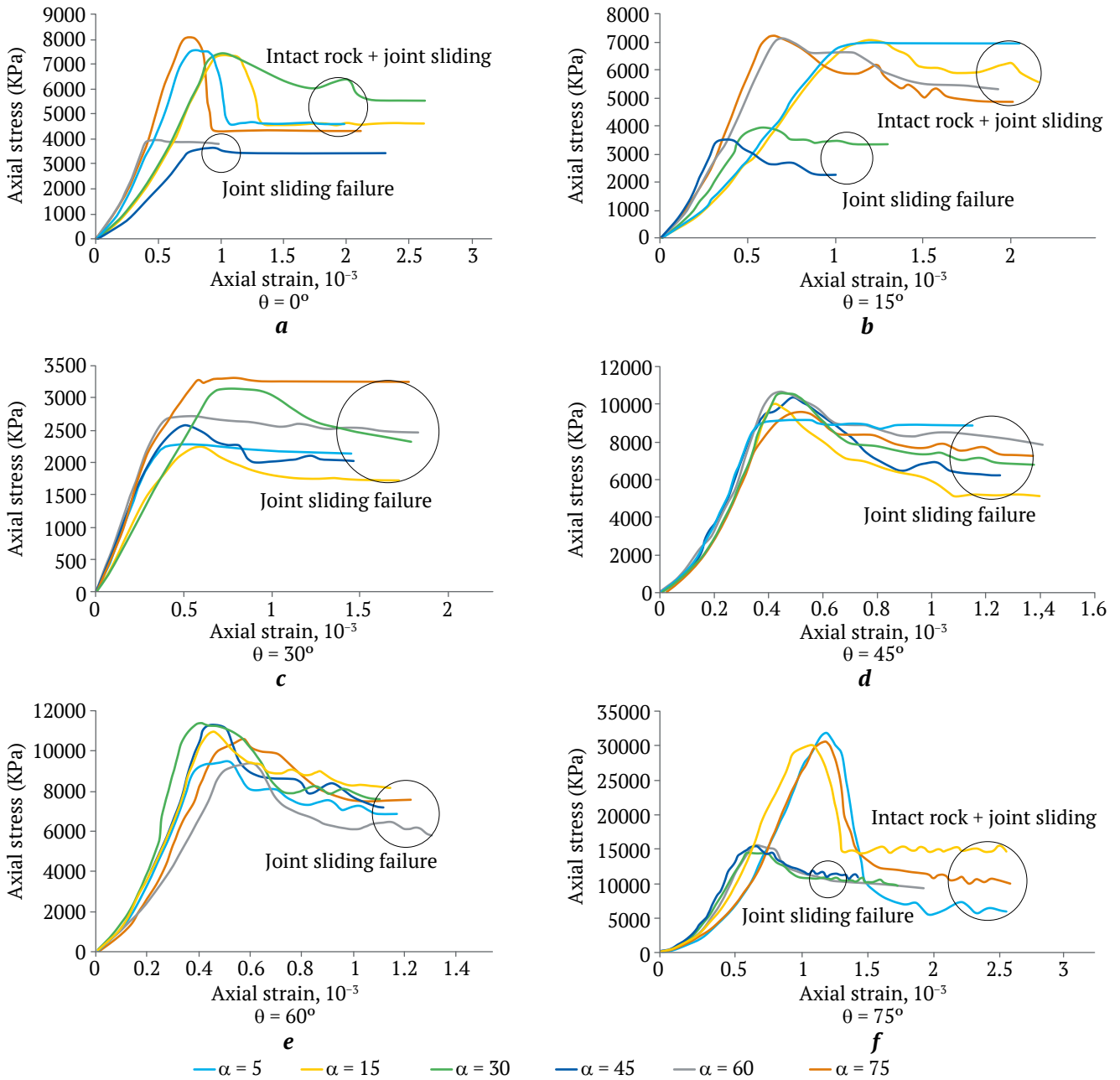


Fig. 9. Stress-strain curve comparison for different directions of the third joint set (α) at different loading angles (θ):
 a, b, c, for fair quality blocky rock mass ($JRC = 8$ and $\sigma_{ci} = 80$ MPa);
 d, e, f, for good quality blocky rock mass ($JRC = 12$ and $\sigma_{ci} = 150$ MPa)

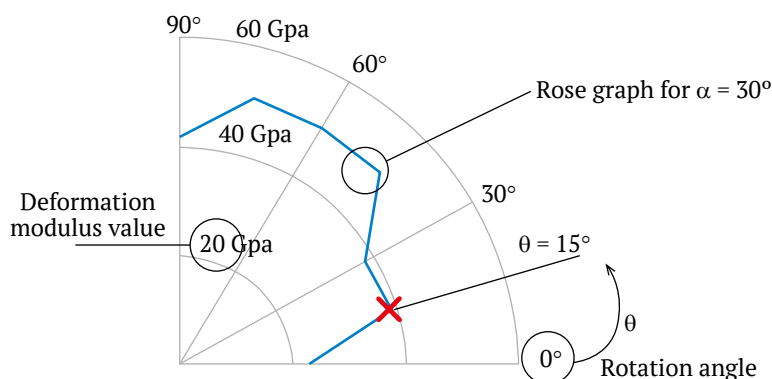


Fig. 10. Polar coordinate representation of blocky rock mass deformation modulus as a function of angle θ (curve shown for $16 < JRC < 20$, $50 < \sigma_{ci} < 100$ MPa, and $\alpha = 30^\circ$)

3.3. Indexing anisotropy in blocky rock masses

An anisotropy index (R_E), defined as the ratio of the maximum deformation modulus (E_{max}) to the minimum deformation modulus (E_{min}), can be expressed as:

$$R_E = \frac{E_{max}}{E_{min}} \quad (20)$$

R_E has been calculated for each curve in Figs. 11 to 14, and the results are presented in Fig. 15. For exam-

ple, in Fig. 15, *a*, the first column shows that $R_E = 1.64$ corresponds to the anisotropy of a blocky rock mass with $\alpha = 5^\circ$, $0 < JRC < 4$ and $\sigma_{ci} < 25$ MPa. This is the mean value of R_E 's calculated for pairs of (JRC, σ_{ci}) as $JRC = 1, 2, 3, 4$ and $\sigma_{ci} = 5, 10, 15, 20, 25$ MPa. For each column, the values are displayed as bars above it. The magnitude of anisotropy index for a blocky rock mass can be expected to be between 1.6 and 2.3 ($1.6 \leq R_E \leq 2.3$), with an average value of 1.88.

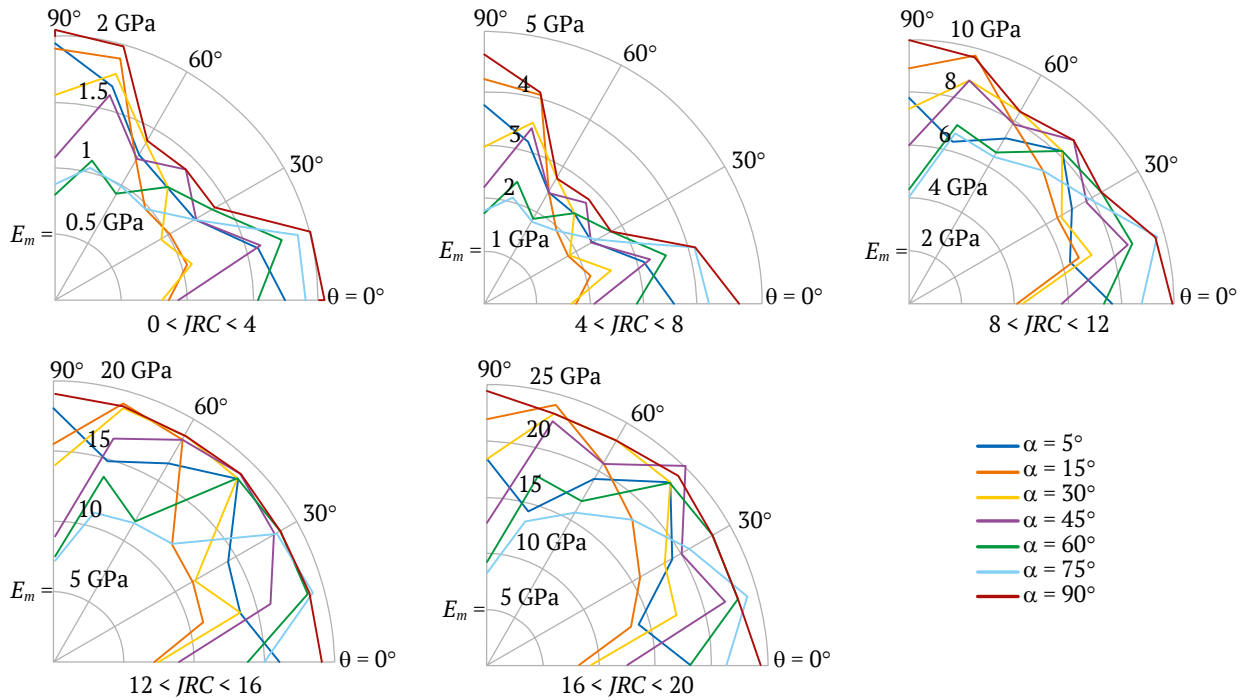


Fig. 11. Deformation modulus of blocky rock masses for $\sigma_{ci} < 25$

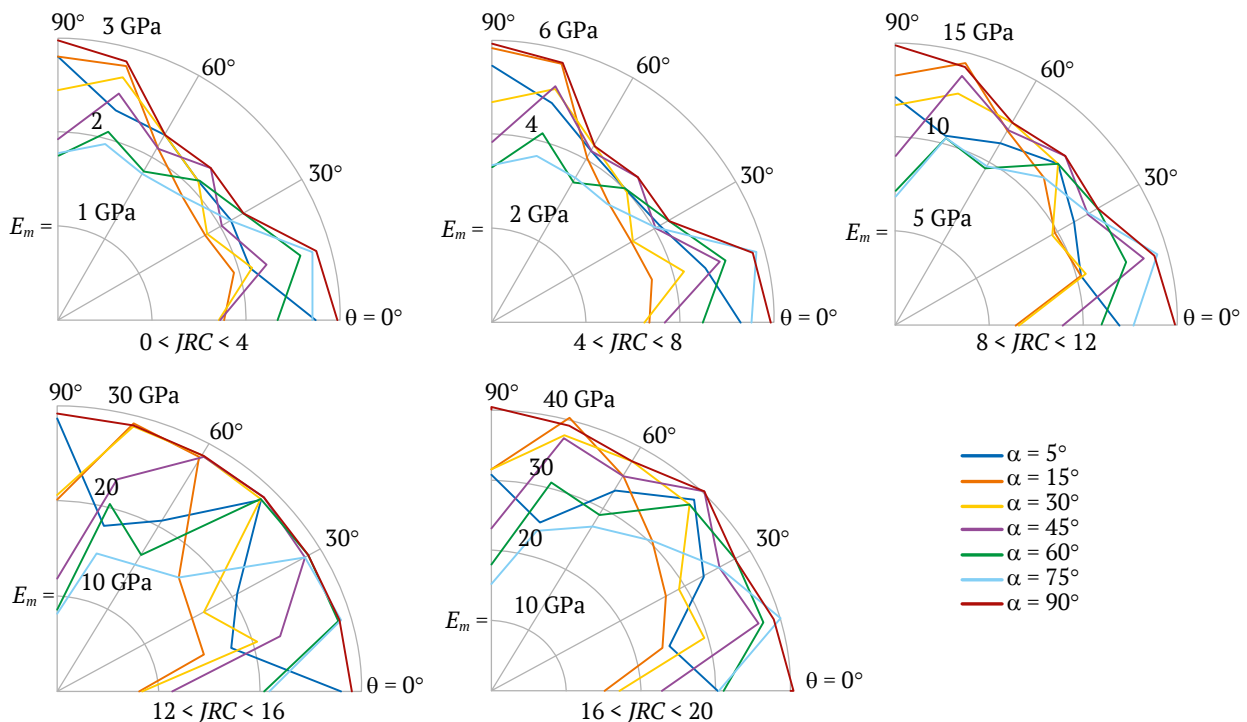


Fig. 12. Deformation modulus of blocky rock masses for $25 < \sigma_{ci} < 50$

3.4. Comparison of results with empirical relationships

For further evaluation of the results presented in Figs. 11 to 14, the range of variation of the deformation modulus for each class of blocky rock masses is presented and compared with corresponding results from empirical relationships in Tables 5. In this table, the classification of blocky rock masses is based

on the surface condition of the joints, similar to the *GSI* table by Hoek [17]. For each class of rock mass (with specified range of *JRC*), E_m values calculated for different ranges of σ_{ci} , were compared, and maximum and minimum values are presented in the table.

Table 5 assigns range of *GSI* values for each class of rock mass based of *JRC* values, in analogy with the *GSI* table by Hoek [17].

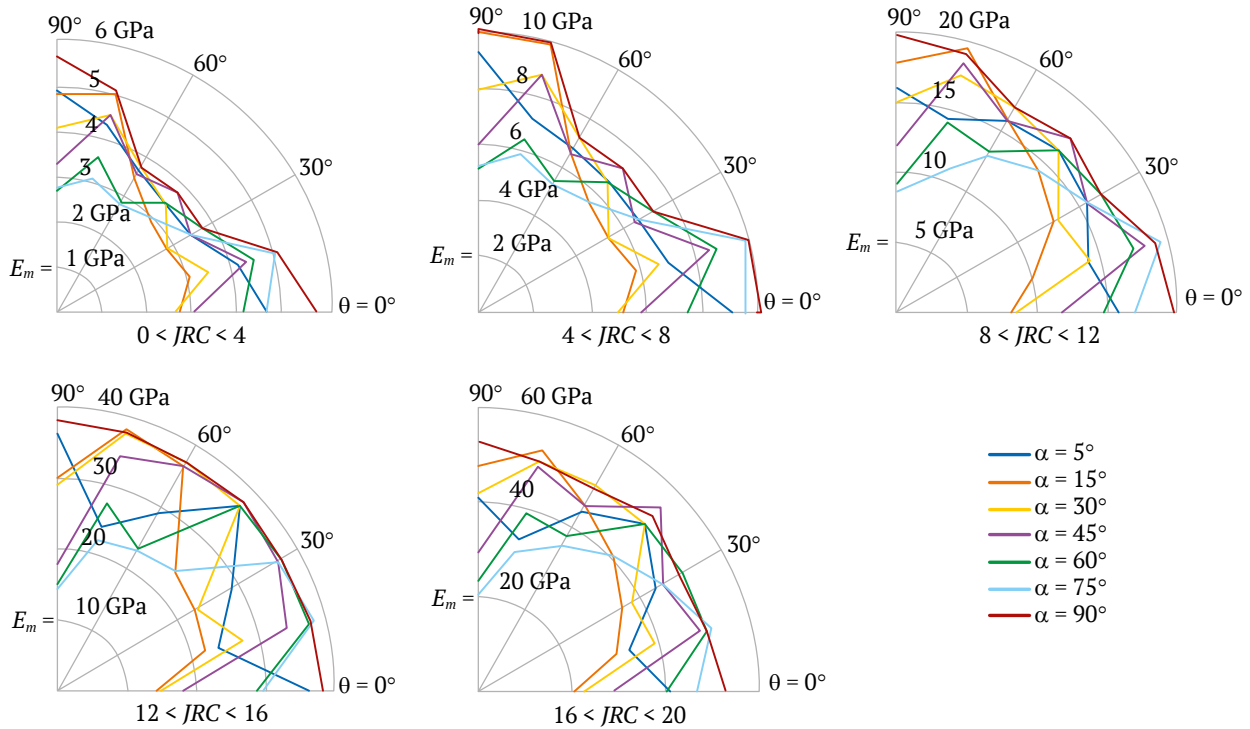


Fig. 13. Deformation modulus of blocky rock masses for $50 < \sigma_{ci} < 100$

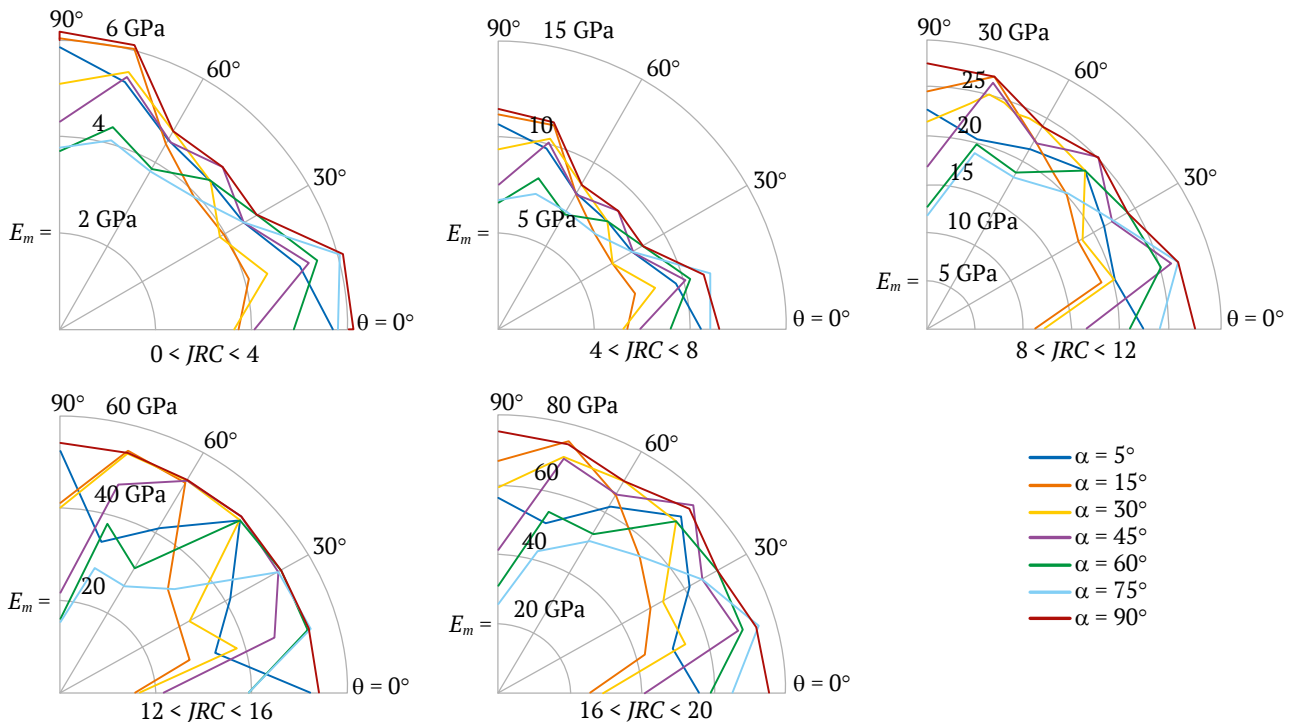


Fig. 14. Deformation modulus of blocky rock masses for $100 < \sigma_{ci} < 250$

A comparison in Table 5 shows that the relation proposed by Hoek and Diederichs [8] with a disturbance factor (D) of 0 (“ D ” is zero for an undisturbed state, 0.5 for partially disturbed, and 1 for fully disturbed states) shows the best match with the numerical simulation results. This is graphically presented in Fig. 16. The modulus values obtained from the relation proposed by Serafim & Pereira [6] are higher than those in the

current study, but the values from Gokceoglu et al. [7] are lower compared to the results of the current simulations. Also, the deformation modulus from Sonmez [36] and Carvalho [35] are high when compared to the results of the current research for blocky rock mass with weak joints. However, for strong joints, the modulus values are lower, indicating a very high safety factor for weak joints and a very low one for strong joints.

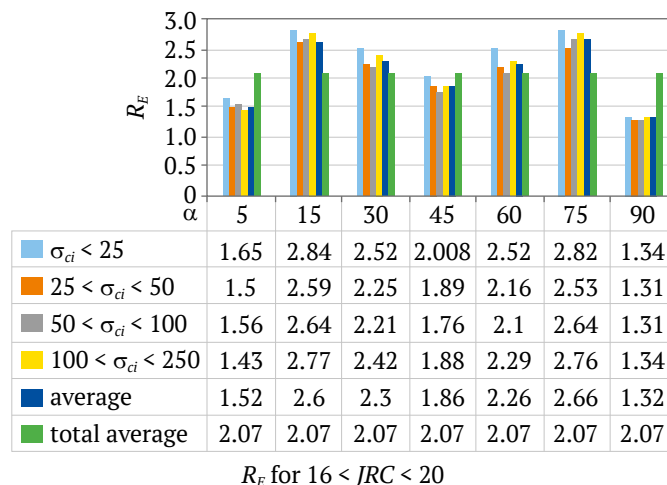
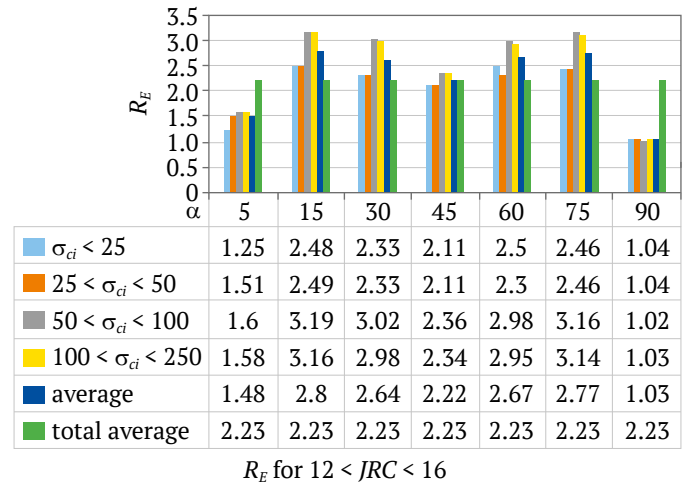
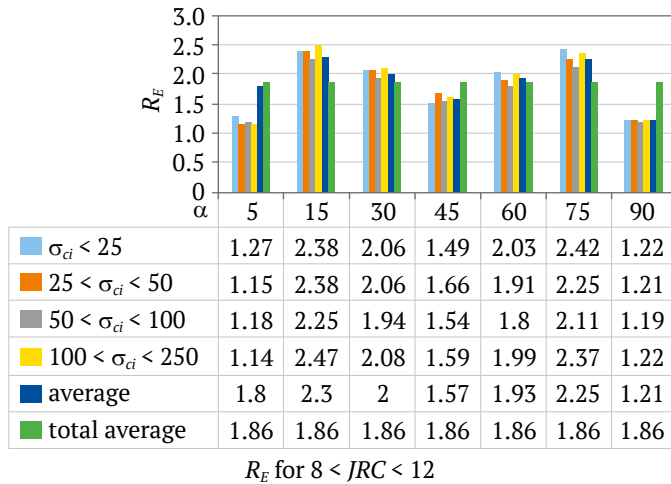
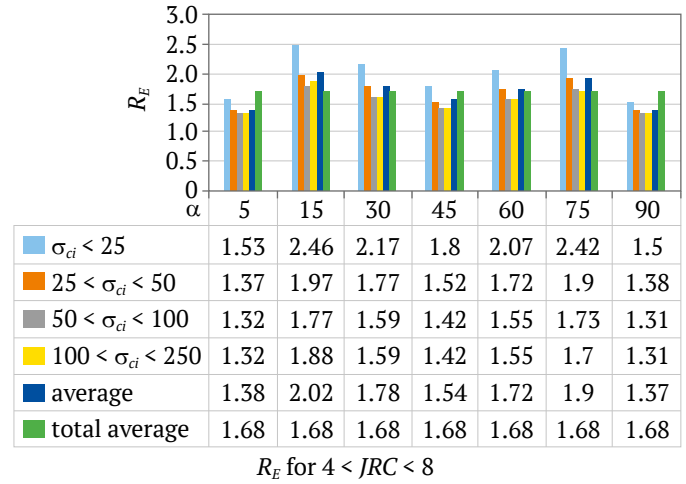
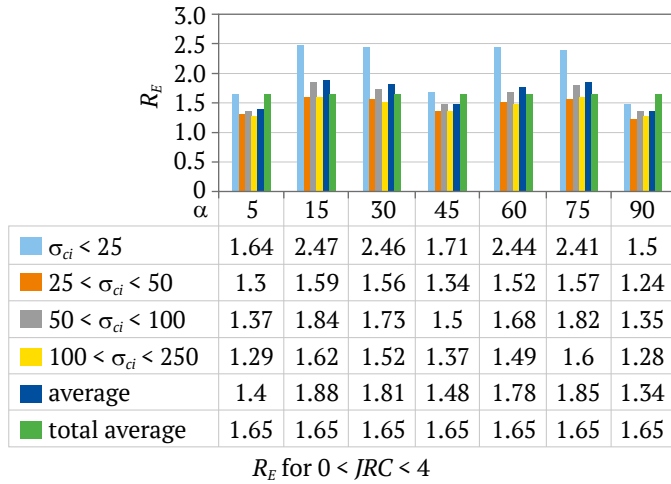


Fig. 15. Anisotropy index, R_E , in blocky rock masses

3.5. Deformation modulus and anisotropy index of blocky rock masses as a function of GSI

The results of the calculation of deformation modulus, E_m , and the anisotropy index, R_E , of blocky rock masses can be summarized in a GSI table as shown in Fig. 17. The JRC values relate to the surface quality of the joints in this table.

Figs. 11 to 14 show that when JRC is assumed to be constant in each column of the GSI table, an increase in one interval in σ_{ci} results in an average eight-fold increase E_m . On the other hand, for a specific value of σ_{ci} , an increase in JRC by one interval causes an average 24-fold increase in the deformation modulus.

It can be inferred that the effect of the quality of the joints is greater than the strength of the intact rock on the deformation modulus of blocky rock masses.

For example, according to Table 6, at a fixed interval of $50 < \sigma_{ci} < 100$, an increase in the JRC from 0 to 20 results in the deformation modulus increasing from an average of 2.5GPa to 50GPa, which is a 20-fold increase. For $8 < JRC < 12$, an increase in σ_{ci} from $\sigma_{ci} < 25$ MPa to $\sigma_{ci} < 250$ MPa results in the average deformation modulus for the rock mass in-

creasing from 4 GPa to 27.5 GPa. This represents an approximate 6.8-fold increase. Based on this observation, joint roughness affects the deformation modulus about three times more than the intact rock's UCS .

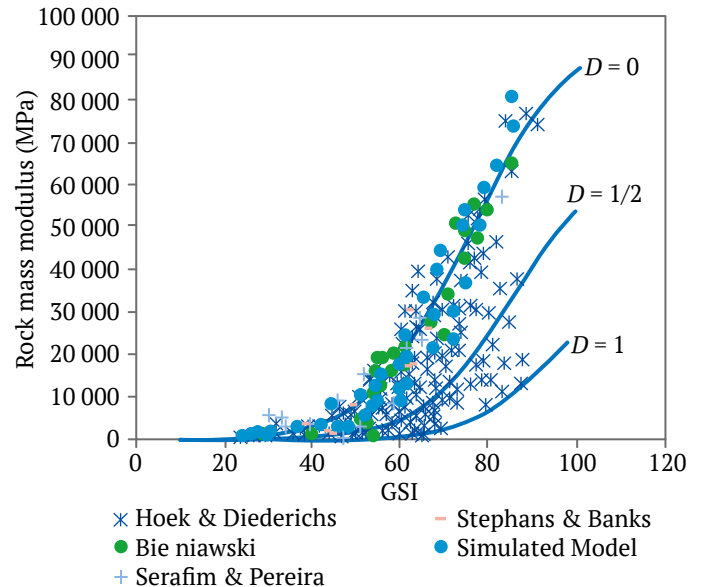


Fig. 16. Comparative analysis of rock mass deformation modulus from empirical formulas versus numerical simulation

Table 5

Comparative evaluation of deformation modulus for blocky rock masses (E_m) using empirical formulas and numerical simulation

Joint surface condition	Poor	Very poor	Very good	Good	Fair	Reference
JRC	0 < < 4	4 < < 8	8 < < 12	12 < < 16	16 < < 20	
<i>Deformation modulus (GPa)</i>						
Numerical simulation	0.79–6.2	1.6–11.5	4–27.5	7–54.2	8–75.5	–
GSI	25–45	35–55	45–65	55–75	65–85	–
$10^{(RMR - 10)/40}$	3.16–10	5.6–17.7	10–31.6	17.7–56.2	31.6–100	[6]
$2RMR - 100$	–	–	–	0–60	40–80	[33]
$0.1451e^{0.654 GSI}$	0.744–2.752	1.43–5.29	2.75–10.18	5.29–19.58	10.18–37.66	[7]
$0.0736e^{0.755 RMR}$	0.7–3.2	1.5–6.8	3.2–14.5	6.8–30.9	4.5–65.7	[7]
$0.33e^{0.064 GSI}$	1.63–5.87	3.1–11.14	5.87–21.14	11.14–40.1	21.14–76.04	[34]
$E_r S^{1/4}$	6.22–10.85	8.21–14.32	10.85–18.91	14.32–24.96	18.91–32.96	[35]
$E_i(S^{\alpha})^{0.4}$	8.61–14.49	11.37–18.38	14.49–22.95	18.38–28.76	22.95–35.85	[36]
$D = 0; 10^5 \left(\frac{1 - D/2}{1 + e^{(75 + 25D - GSI)/11}} \right)$	1.05–6.13	2.56–13.96	6.13–28.73	13.96–50	28.73–71.42	[8]
$D = 0.5; 10^5 \left(\frac{1 - D/2}{1 + e^{(75 + 25D - GSI)/11}} \right)$	0.254–1.54	0.629–3.71	1.54–8.59	3.71–18.23	8.59–33.27	[8]
$D = 1; 10^5 \left(\frac{1 - D/2}{1 + e^{(75 + 25D - GSI)/11}} \right)$	0.055–0.334	0.135–0.823	0.334–1.96	0.823–4.68	1.96–10.21	[8]

$$GSI = RMR - 5, \quad s = \exp\left(\frac{GSI - 100}{9}\right)$$

<p>Geological Strength Index (<i>GSI</i>)</p> <p>From the description of structure and surface conditions of the rock mass, pick an appropriate box in this chart. Estimate the average value of <i>GSI</i> from the contours. Do not attempt to be too precise. Quoting a range of <i>GSI</i> from 36 to 42 is more realistic than stating that <i>GSI</i> = 38</p>		<p>Surface conditions</p> <p>Very Good Very rough and fresh unweathered surfaces</p> <p>Good Rough, maybe slightly weathered or iron stained surfaces</p> <p>Fair Smooth and / or moderately weathered and altered surfaces</p> <p>Poor Slickensided or highly weathered surfaces or compact coatings with fillings of angular fragments</p> <p>Very poor Slickensided and highly weathered surfaces with soft clay coatings or fillings</p>				
<p>Structure</p>		<p>Decreasing surface quality →</p>				
	<p>Intact / Massive – intact rock specimens or massive in-situ rock masses with very few widely spaced discontinuities</p>	90			N/A	N/A
	<p>Blocky – very well interlocked undisturbed rock mass consisting of cubical blocks formed by three orthogonal discontinuity sets</p>	80				
		70				
		65–85	55–75	<i>GSI</i> 45–65	35–55	25–45
		16–20	12–16	<i>JRC</i> 8–12	4–8	0–4
		8–75.5	7–54.2	<i>E_m</i> 4–27.5	1.6–11.5	0.79–6.2
		2.1	2.2	<i>R_E</i> 1.8	1.6	1.6

Fig. 17. Deformation modulus, E_m , anisotropy index, R_E and JRC for blocky rock masses in the GSI chart

Table 6

Rock mass deformation modulus as a function of JRC and σ_{ci}

<i>GSI</i>	25–45	35–55	45–65	55–75	65–85	<p>8-fold increase in deformability modulus on average</p>
<i>JRC</i>	0–4	4–8	8–12	12–16	16–20	
σ_{ci}	Deformation of modulus (GPa)					
$\sigma_{ci} < 25$	0.79–1.75	1.6–4	4–10	7–19	8–23	
$25 < \sigma_{ci} < 50$	1.75–2.8	2.75–6	7–14.5	8–29	17–40	
$50 < \sigma_{ci} < 100$	2.5–5	5.2–10	8–19.5	15–38	20–50	
$100 < \sigma_{ci} < 250$	3.7–6.2	6.7–11.5	12–27.5	18–54.2	22–75.5	
<p>24-fold increase in deformability modulus on average</p>						

Conclusion

A systematic investigation of anisotropy in the deformation behavior of blocky rock masses is carried out using discrete element simulations. The rock mass consists of two orthogonal joint sets intersected by a third. The third joint set forms a variable angle with the second joint set, and its strike is perpendicular to that of joint set 1. Elements with representative volumes of the masses were uniaxially loaded in different directions.

New nonlinear stress-dependent relations for the normal and shear stiffness of joints have been introduced and used in the simulations. JRC and intact rock UCS serve as independent variables in these relations. It was determined that joint normal and shear stiffness coefficients significantly influence the overall deformation behavior of the rock mass. Notably, the effect of normal stiffness on the rock mass deformation modulus is approximately twice that of shear stiffness. Additionally, it was observed



that the roughness of the joints has a much greater impact on the deformation modulus than the UCS of the intact rock.

An important consideration is the potential presence of thin layers on the joints. In this research, the effects of joint fillers are reflected in the JRC as illustrated in the first row of Table 6. However, the adhesion and friction coefficient on the joint surfaces, which can significantly influence simulation results due to the presence of thin layers, are not detailed. In this context, Voznesenskii et al. [37], conducted comprehensive research discussing the significant impact of thin layers of carbonaceous clays on the contact cracking resistance between different rocks.

Numerical investigations indicated that a mass with $L/S \geq 10$ can be considered as a REV for a blocky rock mass when evaluating the deformation modulus and failure modes.

The deformation modulus, failure mode, and post-failure behavior of the blocky rock masses were evaluated for various relative loading and joint an-

gles. The degree of anisotropy for the deformation modulus (due to the fracture systems), represented by the anisotropy index R_E , was deduced as $1.6 \leq R_E \leq 2.3$, with an average value of 1.88 in blocky rock masses.

When the mode of failure is characterized by “slipping on the joints”, the yield strain ranges from 0.2 to 0.4, independent of the loading angle and the direction of the third joint set.

Results are presented in the form of polar curves showing variations in the blocky rock mass deformation modulus, which depend on the joints' JRC , the intact rock's UCS , and the rock mass structure in terms of the relative joint angle. These curves facilitate the estimation of the blocky rock mass deformation modulus in different directions without the need for laboratory and in-situ tests or empirical relationships.

In the GSI table, results are categorized such that assigning a JRC value to each class of joint surface conditions allows for the determination of corresponding deformation modulus and degree of anisotropy for GSI values.

References

1. Singh B. Continuum characterization of jointed rock masses: Part I – The constitutive equations. *International Journal of Rock Mechanics and Mining Sciences & Geomechanics Abstracts*. 1973;10(4):311–335. [https://doi.org/10.1016/0148-9062\(73\)90041-7](https://doi.org/10.1016/0148-9062(73)90041-7)
2. Gerrard C.M. The equivalent elastic properties of simplified and jointed rock masses. In: Beer G., Brooker J.R., Carter J.P. (Eds.) *Proceedings of the 17th International Conference on Computer Methods and Advances in Geomechanics*. May 6–10, 1991. Cairns, Australia. Rotterdam: A. A. Balkemam, Brookfield; 1991. Pp. 333–337.
3. Oda M. An experimental study of the elasticity of mylonite rock with random cracks. *International Journal of Rock Mechanics and Mining Sciences & Geomechanics Abstracts*. 1988;25:59–69.
4. Amadei B., Savage W.Z. Effect of joints on rock mass strength and deformability. In: Hudson J.A. (Ed.) *Comprehensive Rock Engineering – Principle, Practice and Projects*. Vol. 1. Oxford, UK: Pergamon; 1993. Pp. 331–365.
5. Kulhawy F.H. Geomechanical model for rock foundation settlement. *Journal of the Geotechnical Engineering Division*. 1978;104(2):211–227. <https://doi.org/10.1061/AJGEB6.0000582>
6. Serafim J.L., Pereira J.P. Consideration of the geomechanical classification of Bieniawski. In: *Proceedings of the International Symposium on Engineering Geology and Underground Construction*. Vol. 1. September 12–15, 1983. Lisbon, Portugal; 1983. Pp. 33–44.
7. Gokceoglu C., Sonmez H., Kayabasi A. Predicting the deformation moduli of rock masses. *International Journal of Rock Mechanics and Mining Sciences*. 2003;40(5):701–710. [https://doi.org/10.1016/S1365-1609\(03\)00062-5](https://doi.org/10.1016/S1365-1609(03)00062-5)
8. Hoek E., Diederichs M.S. Empirical estimation of rock mass modulus. *International Journal of Rock Mechanics and Mining Sciences*. 2006;43(2):203–215. <https://doi.org/10.1016/j.ijrmms.2005.06.005>
9. Heuze F. E. Scale effects in the determination of rock mass strength and deformability. *Rock Mechanics*. 1980;12:167–192. <https://doi.org/10.1007/BF01251024>
10. Agharazi A., Derek Martin C., Tannant D. A three-dimensional equivalent continuum constitutive model for jointed rock masses containing up to three random joint sets. *Geomechanics and Geoengineering*. 2012;7(4):227–238. <https://doi.org/10.1080/17486025.2012.714476>
11. Cundall P. A. A computer model for simulating progressive large scale movements in blocking rock systems. In: *Proceedings of the Symposium of the International Society on Rock Mechanics*. France. 1971.



12. Lemos J.V., Hart R.D., Cundall P.A. A generalized distinct element program for modeling jointed rock mass. In: Stephansson O. (Ed.) *Proceedings of the International Symposium on Fundamentals of Rock Joints*. 15–20 September 1985. Bjorkiden, Sweden; 1985. Pp. 335–343.
13. Cundall P.A. Formulation of a three-dimensional distinct element model – Part I. A scheme to detect and represent contacts in a system composed of many polyhedral blocks. *International Journal of Rock Mechanics and Mining Sciences & Geomechanics Abstracts*. 1988;25(3):107–116. [https://doi.org/10.1016/0148-9062\(88\)92293-0](https://doi.org/10.1016/0148-9062(88)92293-0)
14. Kulatilake P.H.S.W., Wang S., Stephansson O. Effect of finite size joints on the deformability of jointed rock in three dimensions. *International Journal of Rock Mechanics and Mining Sciences & Geomechanics Abstracts*. 1993;30(5):479–501. [https://doi.org/10.1016/0148-9062\(93\)92216-D](https://doi.org/10.1016/0148-9062(93)92216-D)
15. Min K.B., Jing L. Numerical determination of the equivalent elastic compliance tensor for fractured rock masses using the distinct element method. *International Journal of Rock Mechanics and Mining Sciences*. 2003;40(6):795–816. [https://doi.org/10.1016/S1365-1609\(03\)00038-8](https://doi.org/10.1016/S1365-1609(03)00038-8)
16. Ivars D.M., Pierce M.E., Darcel C. et al. The synthetic rock mass approach for jointed rock mass modelling. *International Journal of Rock Mechanics and Mining Sciences*. 2011;48(2):219–244. <https://doi.org/10.1016/j.ijrmms.2010.11.014>
17. Hoek E., Brown E.T. Practical estimates of rock mass strength. *International Journal of Rock Mechanics and Mining Sciences*. 1997;34(8):1165–1186. [https://doi.org/10.1016/S1365-1609\(97\)80069-X](https://doi.org/10.1016/S1365-1609(97)80069-X)
18. Goodman R.E., Taylor R.L., Brekke T.L. A model for the mechanics of jointed rock. *Journal of the Soil Mechanics and Foundations Division*. 1968;94(3):637–659. <https://doi.org/10.1061/JSFEAQ.0001133>
19. Bandis S.C., Lumsden A.C., Barton N.R. Fundamentals of rock joint deformation. *International Journal of Rock Mechanics and Mining Sciences & Geomechanics Abstracts*. 1983;20(6):249–268. [https://doi.org/10.1016/0148-9062\(83\)90595-8](https://doi.org/10.1016/0148-9062(83)90595-8)
20. Duncan J.M., Chang C.Y. Nonlinear analysis of stress and strain in soil. *Journal of the Soil Mechanics and Foundations Division*. 1970;96(5):1629–1655. <https://doi.org/10.1061/JSFEAQ.000145>
21. Priest S.D. *Discontinuity analysis for rock engineering*. London etc.: Chapman & Hall; 1993.
22. Barton N., Choubey V. The shear strength of rock joints in theory and practice. *Rock Mechanics and Rock Engineering*. 1977;10:1–54. <https://doi.org/10.1007/BF01261801>
23. Barton N.R. Review of a new shear strength criterion for rock joints. *Engineering Geology*. 1973;7(4):287–332. [https://doi.org/10.1016/0013-7952\(73\)90013-6](https://doi.org/10.1016/0013-7952(73)90013-6)
24. Barton N.R. The shear strength of rock and rock joints. *International Journal of Rock Mechanics and Mining Sciences & Geomechanics Abstracts*. 1976;13(9):255–279. [https://doi.org/10.1016/0148-9062\(76\)90003-6](https://doi.org/10.1016/0148-9062(76)90003-6)
25. Barton N.R., Bandis S.C. Review of predictive capabilities of JRC-JCS model in engineering practice, In: Barton N., Stephansson O. (Eds.) *Proceedings of the International Symposium on Rock Joints*. November 1990, Loen, Norway. Rotterdam: Balkema; 1990. Pp. 603–610.
26. Deere D.U., Miller R.P. *Engineering classification and index properties for intact rock*. Technical Report No. AFWL-TR-65-116. Air Force Weapons Laboratory (WLDC). Kirtland Air Base, New Mexico; 1966.
27. Robertson A. The interpretation of geological factors for use in slope theory. In: *Planning Open Pit Mines, Proceeding of the Symposium on the Theoretical Background to the Planning of Open Pit Mines with Special Reference to Slope Stability*. August 29–September 4, 1970, Johannesburg, South Africa. A.A. Balkema; 1970. Pp. 55–71.
28. Goodman R.E. *Introduction to Rock Mechanics*. 2nd Edition. New York: John Wiley & Sons Ltd.; 1989.
29. Cuba A. *Personal Communication*. 1990.
30. Schultz R.A. Relative scale and the strength and deformability of rock masses. *Journal of Structural Geology*. 1996;18(9):1139–1149.
31. Jaeger J.C., Cook N.G.W., Zimmerman R.W. *Fundamentals of rock mechanics*. Oxford: Blackwell Publishing Ltd.; 2007.
32. Yang Z.Y., Chen J.M., Huang T.H. Effect of joint sets on the strength and deformation of rock mass models. Effect of joint sets on the strength and deformation of rock mass models. *International Journal of Rock Mechanics and Mining Sciences*. 1998;35(1):75–84. [https://doi.org/10.1016/S1365-1609\(98\)80024-5](https://doi.org/10.1016/S1365-1609(98)80024-5)
33. Bieniawski Z.T. Determining rock mass deformability: experience from case histories. *International Journal of Rock Mechanics and Mining Sciences & Geomechanics Abstracts*. 1978;15(5):237–247. [https://doi.org/10.1016/0148-9062\(78\)90956-7](https://doi.org/10.1016/0148-9062(78)90956-7)
34. Hoek E. *Practical Rock Engineering*. Revision version. 2004.



35. Carvalho J. *Estimation of rock mass modulus*. Personal communication. 2004.
36. Sonmez H., Gokceoglu C., Ulusay R. Indirect determination of the modulus of deformation of rock mass based on the GSI system. *International Journal of Rock Mechanics and Mining Sciences*. 2004;41(5):849–857. <https://doi.org/10.1016/j.ijrmms.2003.01.006>
37. Voznesenskii A.S., Osipov Yu.V., Ushakov E.I. et al. Effect of weak inclusions on the fracture toughness of interfaces between various rocks. *Engineering Failure Analysis*. 2023;146:107140. <https://doi.org/10.1016/j.engfailanal.2023.107140>

Information about the authors

Omid Ahrami – PhD-Candidate, Department of Civil Engineering, Science and Research Branch, Islamic Azad University, Tehran, Iran; ORCID [0009-0008-5551-9500](https://orcid.org/0009-0008-5551-9500); e-mail omid.ahrami@gmail.com

Hossein Javaheri Koupaei – Assistant Professor, Department of Civil Engineering, Science and Research Branch, Islamic Azad University, Tehran, Iran; ORCID [0000-0003-3745-0913](https://orcid.org/0000-0003-3745-0913); Scopus ID [57215596931](https://scopus.com/authorid/57215596931); e-mail h-javaheri@srbiau.ac.ir

Kaveh Ahangari – Professor, Department of Mining Engineering, Science and Research Branch, Islamic Azad University, Tehran, Iran; ORCID [0000-0001-9462-7303](https://orcid.org/0000-0001-9462-7303), Scopus ID [36130116400](https://scopus.com/authorid/36130116400); e-mail ahangari@srbiau.ac.ir

Received 17.08.2023

Revised 01.02.2024

Accepted 15.02.2024



BENEFICIATION AND PROCESSING OF NATURAL AND TECHNOGENIC RAW MATERIALS

Research paper



<https://doi.org/10.17073/2500-0632-2023-07-136>

UDC 622.765.4

Current trends of improving the efficiency of froth separation of diamond-bearing kimberlites


V. V. Morozov¹   , E. G. Kovalenko²  , G. P. Dvoychenkova^{3,4}  ,
I. V. Pestryak¹  , S. P. Lezova¹  

¹ University of Science and Technology MISIS, Moscow, Russian Federation

² Yakutniproalmaz Institute, ALROSA, Mirny, Russian Federation

³ Institute for Problems of Integrated Subsoil Development, Russian Academy of Sciences, Moscow, Russian Federation

⁴ Mirny Polytechnical Institute under the North-Eastern Federal University named after M.K. Ammosov (MPTI (f) SVFU),
Mirny, Russian Federation

 dchmggu@mail.ru

Abstract

Along with the introduction of new froth separation sections at new and existing enterprises, the basis for increasing the output of small diamonds is the reduction of their losses at the existing froth separation sections. The results of the studies of diamond surface composition under conditions of technogenic hydrophilization made it possible to establish the influence of the effects of crystallization of carbonate and silicate mineral films and the fixation of sludge fractions on the hydrophobicity and floatability of diamonds. It was proposed to use combined regimes of conditioning of ore and recycled water to increase floatability of diamonds, providing removal of hydrophilizing coatings and restoration of natural hydrophobicity of diamonds. The application of methods of acoustic, thermal, electrochemical, and reagent treatment of water-mineral disperse systems, as well as their combinations to increase floatability and reduce losses of hydrophilic diamonds in the process of froth separation was considered and substantiated.

Based on the study of the effect of the temperature factor in the preparation and froth separation processes, the optimal temperature regime of froth separation cycle operations was substantiated, providing the use of the heat consumed for thermal treatment of the initial diamond-containing material at a temperature of 85–90°C to maintain the required temperature in the conditioning operations with a collector and immediately in the froth separation and flotation operations.

It was shown that the regulation of phase composition of an apolar collector by additives of low- and medium-molecular fractions provides increase of its collecting ability due to transition of asphaltene-resin fraction into adhesion-active form and occurrence of processes of the collector autodispersing in aqueous phase.

On the basis of the statistical analysis of froth separation process indicators depending on changing the share of recycled water in the processes the reason for worsening the indicators (performance) was determined, which consisted in a significant increase in the concentration of sludges. The optimum degree of recycled water use (85%) was determined, which ensures decreasing the used collector consumption by 8% without decreasing diamond recovery and concentrate quality.

Keywords

diamonds, kimberlites, coatings, conditioning, hydrophobization, collector, froth separation, closed-loop water recycling, ALROSA

For citation


Morozov V.V., Kovalenko E.G., Dvoychenkova G.P., Pestryak I.V., Lezova S.P. Current trends of improving the efficiency of froth separation of diamond-bearing kimberlites. *Mining Science and Technology (Russia)*. 2024;9(2):134–145. <https://doi.org/10.17073/2500-0632-2023-07-136>



ОБОГАЩЕНИЕ, ПЕРЕРАБОТКА МИНЕРАЛЬНОГО И ТЕХНОГЕННОГО СЫРЬЯ

Научная статья

Современные направления повышения эффективности пенной сепарации алмазосодержащих кимберлитов

В. В. Морозов¹   , Е. Г. Коваленко²  , Г. П. Двойченкова^{3,4}  ,И. В. Пестряк¹  , С. П. Лезова¹  ¹ Университет науки и технологий МИСИС, г. Москва, Российская Федерация² Институт «Якутнипроалмаз» АК «АЛРОСА» (ПАО), г. Мирный, Российская Федерация³ Институт проблем комплексного освоения недр РАН (ИПКОН РАН), г. Москва, Российская Федерация⁴ Мирнинский Политехнический институт – филиал Северо-Восточного федерального университета им. М. К. Аммосова (МПТИ (ф) СВФУ), г. Мирный, Российская Федерация dchmggu@mail.ru

Аннотация

Наряду с внедрением новых отделений пенной сепарации на новых и действующих предприятиях ресурсом повышения выпуска мелких алмазов является снижение их потерь на действующих переделах пенной сепарации. Исследование состава поверхности алмазов в условиях техногенной гидрофилизации позволило установить влияние эффектов кристаллизации пленок карбонатных и силикатных минералов, а также закрепления шламовых фракций на уменьшение гидрофобности и флотиремости алмазов. Предложено использовать для повышения флотиремости алмазов комбинированные режимы кондиционирования руды и оборотной воды, обеспечивающие удаление гидрофилирующих покрытий и восстановление природной гидрофобности алмазов. Рассмотрено и обосновано применение способов акустической, тепловой, электрохимической и реагентной обработки водно-минеральных дисперсных систем, а также их комбинаций для повышения флотиремости и снижения потерь гидрофильных алмазов в процессе пенной сепарации.

На основании исследования влияния температурного фактора в процессах подготовки и пенной сепарации обоснован оптимальный температурный режим операций цикла пенной сепарации, использующий тепло, расходуемое для тепловой обработки исходного алмазосодержащего продукта при температуре 85–90 °С, для поддержания требуемой температуры в операциях кондиционирования с собирателем и непосредственно в операциях пенной сепарации и флотации.

Показано, что регулирование фазового состава аполярного собирателя добавками низко- и среднемолекулярных фракций обеспечивает повышение его собирательной способности за счет перевода асфальтен-смолистой фракции в адгезионно-активную форму и протекания процессов автодиспергирования собирателя в водной фазе.

На основании статистического анализа показателей процесса пенной сепарации в условиях изменения доли направляемой в технологические процессы оборотной воды определена причина снижения показателей, заключающаяся в существенном возрастании концентрации шламов. Определена оптимальная степень замыкания водооборота (85%), обеспечивающая снижение расхода применяемого собирателя на 8% без уменьшения извлечения алмазов и снижения качества концентратов.

Ключевые слова

алмазы, кимберлиты, покрытия, кондиционирование, гидрофобизация, собиратель, пенная сепарация, замкнутый водооборот, АК «АЛРОСА»

Для цитирования

Morozov V.V., Kovalenko E.G., Dvoychenkova G.P., Pestryak I.V., Lezova S.P. Current trends of improving the efficiency of froth separation of diamond-bearing kimberlites. *Mining Science and Technology (Russia)*. 2024;9(2):134–145. <https://doi.org/10.17073/2500-0632-2023-07-136>

Introduction

One of the promising areas for increasing the output of fine diamond size classes at ALROSA's enterprises is their extraction from kimberlites using a method of froth separation developed at ALROSA under the guidance of PhD M.N. Zlobin [1, 2]. The importance of the froth separation and flotation process is due to the fact that it enables achieving beneficia-

tion of –2 + 0.5 mm size class, to which more than 40% of the total quantity of diamonds in the ore belong, which constitute up to 10% of the value of all commercial products.

Along with the introduction of new froth separation sections at new and existing enterprises, the basis for increasing the output of small diamonds is the reduction of their losses at the existing froth separa-



tion sections, which currently reach 20%. The losses are primarily caused by hydrophilic mineral coatings present on a diamond surface, formed under conditions of hypergenic processes in a deposit or due to technogenic hydrophilization [3, 4]. A promising way to remove hydrophilizing coatings and restore the natural hydrophobicity of diamonds is using a combination of different types of physical and physico-chemical methods of treatment, the most effective of which are thermal, acoustic treatment of pulp, and electrochemical treatment of recycled water [5, 6]. At the same time, a necessary condition for achieving a positive result is to ensure a selective regime of diamond hydrophobization, which is achieved by using dispersing agents for sludges and agent-regulators of crystallization of hydrophilizing coatings [7].

Another important trend in increasing the efficiency of the froth separation cycle is optimization of the composition of collectors, which are presented by various petroleum products [8, 9]. This solves the problems of both increasing diamond recovery and reducing the consumption and, consequently, the cost of reagents. An important condition for increasing diamond recovery is a reasonable selection of the temperature conditions of the processes of conditioning a diamond-containing product with collectors and the processes of froth separation and flotation as such [9].

The selected directions of improving the process of froth separation and flotation allow achieving maximum performance with the correct selection of the process parameters, taking into account the mechanism of interaction of mineral surface with ionic-molecular components of the pulp liquid phase and with a collector, as well as changes in the composition of the aqueous phase under conditions of closed-loop water circulation [10, 11]. Therefore, the main scientific goal of the research was to establish the regularities of changes in surface properties and floatability of diamonds when using different types of conditioning of water-disperse systems in the processes of froth separation and flotation of diamond-bearing kimberlites.

1. Research techniques

The elemental composition of the surface mineral coatings on diamonds was analyzed using the method of scanning X-ray electron spectrometry at a JSL-5610LV Jeol scanning electron microscope [12]. The information on the mineralogical composition of the solid phase was obtained by analyzing the data of infrared spectrophotometry in the wave number range of 400–4000 cm^{-1} using a Specord 75 IR instrument [13].

An improved technique of measuring the three-phase wetting contact angle of a collector drop on minerals using an OCA 15EC instrument was used to study the effect of a collector composition and preparation regimes on the collector fixation and hydrophobicity of diamonds and kimberlite minerals [14].

The method of combined optical microscopy was used to study the phase composition and structure of the collectors [15]. The images of a thin layer of the petroleum products were obtained by a Micromed-3-LUM microscope. Visiometric analysis and determination of size distribution of grains of asphaltene-resin and paraffin fractions were carried out using VideoTesT 4.0 program package¹. The peculiarity of the applied technique is the possibility to determine the mass fraction of both asphaltenes and petroleum resins in a collector in the form of solid formations.

The collecting properties of the studied collectors in relation to diamonds were tested using a frothless flotation cell, Hallimond tube [16]. For laboratory studies of the process of diamond-containing kimberlite product froth separation, a froth separator equipped with a conditioner with reagent dosers, a unit for electrochemical treatment of recycled water, and a steam generator were used. The initial material with the coarseness of 0.5 to 2 mm, which was taken from the feed of the froth separation cycle, diamond-containing gravity concentrate, was used in the research.

To determine the regularities of interaction of the collector with minerals, the methods of extraction-spectral analysis of the collector distribution between the liquid and solid phases of the flotation system were used [17].

Scaled-up tests of the froth separation process were carried out at a LFM-001C automated unit of the Yakutniproalmaz Institute using closed-loop water cycle. The reagent regime used was consistent with the plant reagent regime. In the scaled-up tests, conditioning of a sample with a collector for two minutes was performed after pretreatment. A prepared sample of diamond-containing material was fed onto the separator froth bed. The resulting froth and cell products were dewatered on a sieve. The separated aqueous phase was returned to the recycled water tank. Diamonds were extracted from the froth separation products after drying them for weighing and recovery calculation.

¹ VideoTesT-Master (Structure) 4.0: specification. Saint Petersburg 2002, 15 p.



2. Restoration of natural hydrophobicity and floatability of hydrophilized diamonds

In order to select the conditions for preventing technogenic hydrophilization of diamonds, special studies were conducted, and quantitative regularities of formation of hydrophilizing coatings on their surface were determined. For this purpose, surface composition studies were carried out while ageing a sample in desludged and non-desludged recycled water. The surface composition was determined by scanning X-ray electron spectroscopy. At the same time, the floatability of diamonds was determined by flotation of a sample weighing 200 mg with grain size of 0.5 to 1 mm in a frothless flotation unit for 4 min at a total air consumption of 50 ml. Prior to flotation, conditioning of the diamond sample in a collector emulsion was carried out.

To reproduce the conditions of formation of technogenic mineralization occurring at the contact of diamonds with mineralized aqueous phase in sample preparation operations, the prepared sample before conditioning with a collector was pre-aged in recycled water in an open container for 180 min.

The tests results showed that ageing diamonds in the process water of the processing plant No. 3 of the Mirny Mining and Processing Complex leads to a continuous increase in the mass fraction of mineral coatings on the surface of diamond crystals (Fig. 1) and a decrease in the diamond floatability (Fig. 2).

The high rate of changing surface composition and decreasing floatability allows concluding that the initial cause of diamond hydrophilization is the crystallization of carbonate and silicate mineral films [6]. The comparison of the dependences shows that ageing diamonds in non-desludged pro-

cess water leads to a significantly more intensive (4–5.5 times) increase in the concentration of mineral coatings on the diamond surface (see Fig. 1) and a significant decrease in the floatability of minerals (by 10.1%, see Fig. 2). The most probable mechanism of technogenic hydrophilization of diamonds is fixation of sludge fractions on the surface of floating minerals hydrophilized by mineral films.

To solve the problem of restoring the natural hydrophobicity and floatability of diamonds, taking into account the significant contribution of sludges, the application of acoustic activation was considered [18, 19]. Taking into account the results of our own earlier studies [5, 6, 9], it was proposed to use combined regimes, including the application of both acoustic and thermal treatment to increase the floatability of diamonds.

The tests were performed with diamond-containing samples at a laboratory froth separator. The diamonds were extracted from selected kimberlite samples of +0.5–2 mm grain size at an X-ray luminescence separator. The diamond-free samples of kimberlite products were then averaged and divided into 30 g subsamples. 20 diamond crystals were added to each subsample. A prepared subsample in the presence of sodium hexametaphosphate was treated with a collector (F-5 bunker fuel oil and butyl aerofloat at consumptions of 1,000 and 25 g/t, respectively) and fed to the froth separator. The frothing agent, methylisobutylcarbinol (MIBC), was fed into the aqueous phase of the froth separation process.

In the course of the laboratory tests at the froth separation unit, an initial subsample was heated and aged at a temperature of 60–95 °C for 1 min. Then acoustic (ultrasonic) treatment was carried out at an

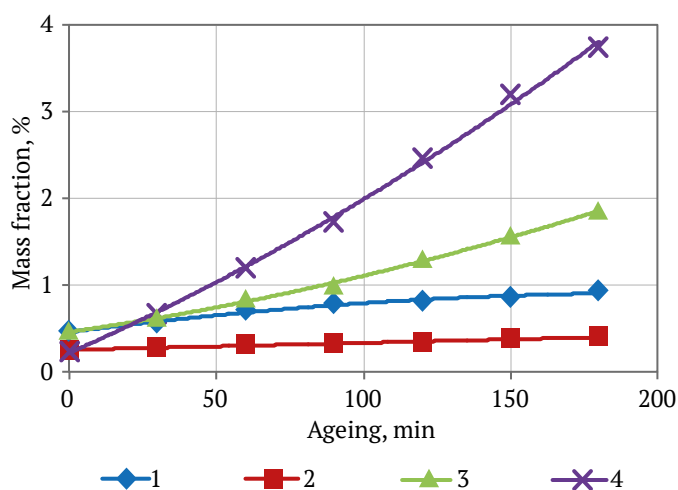


Fig. 1. Changes in the mass fraction of elements of mineral coatings on the surface of diamonds when they are aged in desludged (1, 2) and non-desludged (3, 4) recycled water: 1, 3 – calcium; 2, 4 – silicon

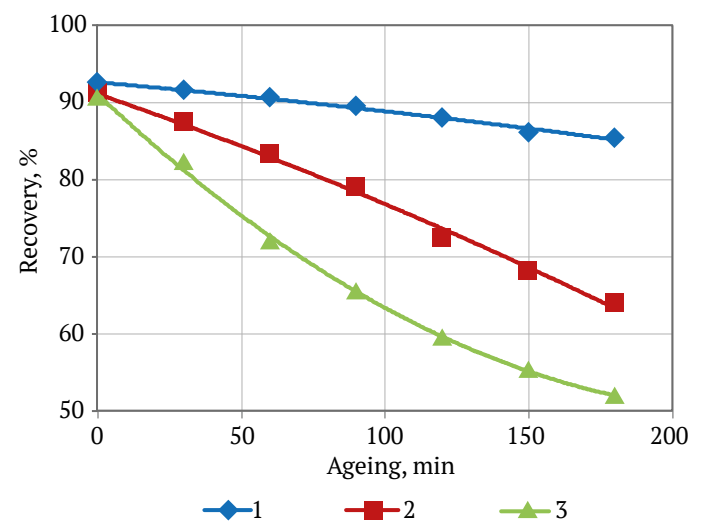


Fig. 2. Recovery of diamonds in frothless flotation after ageing them in low-salinity (1), desludged (2) and non-desludged (3) high-salinity recycled water

IL 100–6/1 unit for 1–2 min. After removal of excess water phase with sludge fraction, reagents (the fuel oil and aerofloat) were added to the subsample and agitated for two minutes.

The prepared subsample was fed to the froth bed of the laboratory separator. The concentrate (froth product) and tailings (cell product) obtained in the froth separation process were dewatered. The separated aqueous phase was returned to the recycled water tank. Diamonds were extracted from the froth separation products after drying them for weighing and recovery calculation.

The results of the analysis showed that the joint application of thermal and ultrasonic treatment led to a 1.8–4.2-fold decrease in the proportion of diamond surface with mineral coatings. The earlier studies showed that the maximum increase in diamond recovery was achieved with the use of a combination of ultrasonic treatment and heating a sample to 85–90 °C [20].

The study of reagent methods of intensifying diamond desludging by conditioning of froth separation feed also showed the effectiveness of using sodium polyphosphate, oxyethylene diphosphonic acid (OEDP), and sodium metasilicate. The results of X-ray-electron spectral analysis showed that the use of dispersing agents allowed to reduce the surface concentration of mineral contaminant compo-

nents by 1.3–1.5 times and promotes the removal of sludges from the diamond surface. Good results were achieved with the simultaneous application of ultrasonic scrubbing and additions of oxyethylene diphosphonic acid to the aqueous phase at a consumption of 500 g/m³ [20]. The maximum positive effect was achieved when ultrasonic, thermal, and reagent treatment processes were used together. The results of the tests showed that the combination of ultrasonic (UST) and thermal treatment of the initial feed with the addition of oxyethylene diphosphonic acid (OEDP) or sodium polyphosphate provided an increase in diamond recovery by 7.5% with a significant decrease in the yield of kimberlite into the concentrate (Table 1).

A significant effect on hydrophobization and increase of floatability of diamonds is provided by electrochemical conditioning of recycled water [6, 21]. To assess the effect of a combination of factors (changing diamond hydrophobicity and the saturation of the aqueous phase of the pulp with gas), a test was conducted to determine the collector retentivity in relation to diamond crystals of flotation size (+0.6–1 mm). In the test, a droplet of the fuel oil interacted with a subsample of diamond crystals (100 mg) at the bottom of a glass cuvette and then recycled water were added. The fuel oil droplet concentrated at the aqueous phase–air interface and floatated diamonds fixed at the fuel oil–aqueous phase interface (Fig. 3, a).

Table 1

Effect of ultrasonic and thermal treatment and additives of oxyethylidene diphosphonic acid (OEDP) and sodium polyphosphate on froth separation outcomes

No.	Processing conditions			Recovery to concentrate, %	
	UST duration, sec.	Temperature, °C	Dispersing agent concentration, mg/L	Diamonds	Kimberlite
Using OEDP					
1	–	24	–	82.5	0.86
2	60	24	100	90.0	0.40
3	60	85	200	90.0	0.33
Using sodium polyphosphate					
4	60	24	100	80.0	0.44
5	60	85	200	90.0	0.36

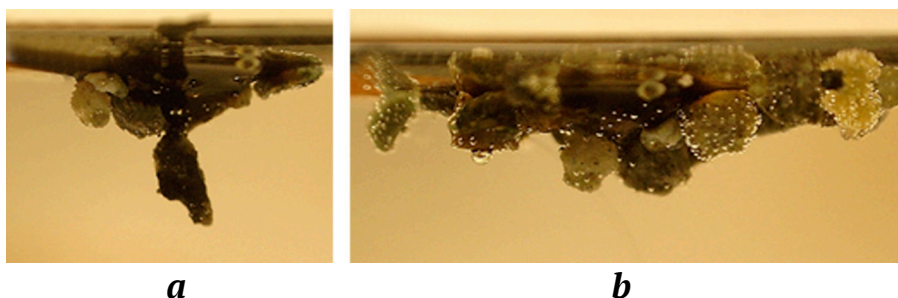


Fig. 3. An aggregate of a F-5 bunker fuel oil droplet and diamonds on the surface of recycled water: a – in ordinary recycled water; b – in recycled water after electrochemical conditioning

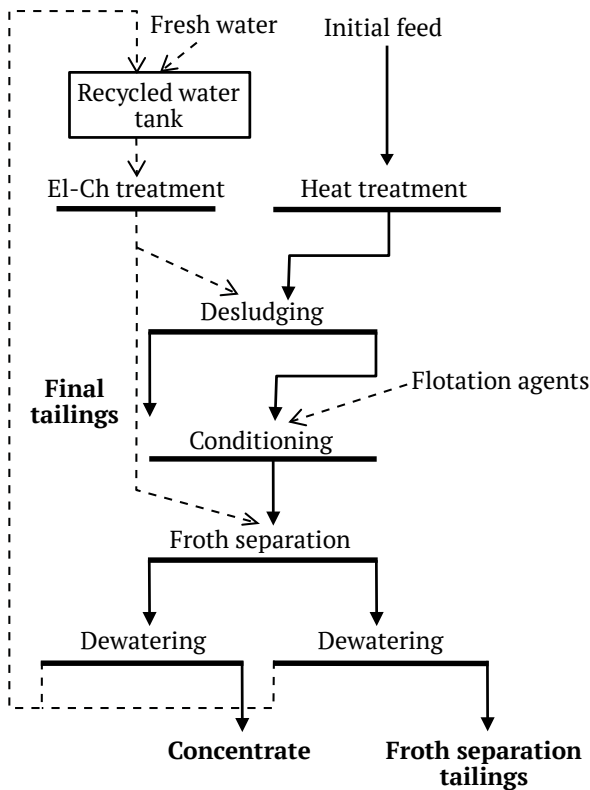


Fig. 4. Scheme for preparation of diamond-containing product for froth separation process, including thermal treatment of ore pulp and electrochemical treatment of recycled water

The results of observations showed that when using recycled water that has undergone electrochemical conditioning, a droplet of the fuel oil spreads to a greater extent along the interface between the aqueous phase and air, and a 40–50% greater number of diamond crystals are fixed on it (Fig. 3, b). At the same time, a large number of gas microbubbles are observed on the surface of diamonds, which indicates the saturation of the treated water with gas phase and the tendency of the gas phase to form bubbles on the surface of diamond crystals.

To evaluate the effectiveness of the combination of the thermal and electrochemical conditioning, a scheme was tested, including heating of the froth separation feed before the flotation reagents conditioning operation and the subsequent use of the accumulated heat in the operations of the froth separation feed conditioning with the reagents and properly the froth separation process (Fig. 4).

The flotation tests were carried out using electrochemical conditioning of recycled water. Electrochemical conditioning was carried out in a diaphragmless electrolyzer at a current density of 100 A/m² and an electricity consumption of 1.5 kWh/m³. To clarify the mechanism of the electrochemical conditioning

effect on diamond properties, tests with hydrophobic and technogenically-hydrophilized diamonds were performed. Hydrophilization of diamonds was carried out by ageing them in sludge-containing recycled water of the froth separation cycle in contact with air for three hours.

The analysis of the developed regime testing at the laboratory froth separation unit showed that when using the combined thermal and electrochemical treatment (at a temperature of 85–90 °C), the diamond recovery (82.5%) is noticeably higher than the recovery when using these treatment methods separately (58.5% and 69%, Table 2). The yield of kimberlite into the concentrate remained stable in all tests (0.47–0.6%) [20].

The analysis of the conducted studies outcomes showed that floatability of hydrophilic diamonds after thermal and electrochemical treatment increased by 49% and became comparable with the recovery of naturally hydrophobic diamonds. This result allows concluding that the reason for the increase in floatability of diamonds is the restoration of their natural hydrophobicity due to the removal of hydrophilizing films. The observed increase in the recovery of naturally hydrophobic diamonds (up to 18%) indicates the manifestation of the effect of additional aeration of the medium by electrolysis gases, which is typical for the conditions of application of electrolysis products (see Fig. 3) and, possibly, due to other effects, for example, an increase in the activity of a collector.

Selection of temperature regime of conditioning of diamond-containing product with collector

The temperature of a medium in the preparatory and basic process operations is an important parameter of froth separation cycle [9, 17]. To determine the rational thermal regime, wetting contact angle measurements were performed on diamonds and kimberlite in the temperature range of 14 to 60 °C.

Table 2

Effect of temperature on wetting contact angles of diamonds and kimberlite by a droplet of collector in aqueous medium

No.	Medium temperature, °C	Wetting contact angle on minerals, deg. (minimum–maximum/average)	
		Diamond	Kimberlite
1	14	91–95/93	Breakaway
2	24	92–97/94.5	Breakaway
3	30	94–101/97.5	Breakaway
4	40	94–100/97.0	Breakaway
5	50	91–96/93.5	Piecewise, 40–75/57.5
6	60	90–93/91.5	Piecewise, 45–75/60



The influence of temperature on the adhesive activity of a collector to the surface of a diamond and kimberlite in aqueous medium was assessed by measuring the wetting contact angles using a special technique, including the application of a droplet of F-5 fuel oil to the wetted surface of a mineral and the subsequent rise in the liquid level in the cuvette, described in detail in [9]. The results showed that the wetting contact angle, which characterizes the hydrophobicity of a diamond and its tendency to interact with a collector, increases in the temperature range of 14–40 °C and decreases with further temperature increase (Table 2). The fixation of the collector on the surface of kimberlite is observed fragmentarily and manifests itself at temperatures above 40 °C.

When the thermal conditioning of the initial feed of the froth separation cycle is carried out at 80–90 °C, the temperature in the subsequent operation of conditioning with reagents is 25–30 °C, and in the froth separation operation, 20–22 °C. The higher medium temperature in the conditioning and froth separation operations with the use of thermal conditioning relative to the medium temperature in the control test (14 °C) is provided by the heat energy expended in the initial feed thermal conditioning operation. The froth separation tests confirmed the results of the tests on studying the effect of temperature on the adhesive activity of a collector in relation to diamonds and showed that maintaining the medium temperature in the operation of conditioning the diamond-containing product with the collector up to 30–40 °C led to an increase in diamond recovery by 6.2–7.3% (Table 3).

The obtained results (achieving the maximum positive effect at a temperature of 40 °C) showed that in order to achieve the best outcomes, it is advisable, along with thermal conditioning of the froth separation cycle feed, to conduct additional pulp heating in the operation of conditioning of the froth separation feed. At the same time, the required temperature regime of the froth separation and flotation operation (24 to 28 °C) is to be maintained [9].

Table 3

Effect of medium temperature in the collector conditioning operation on diamond and kimberlite recovery in the froth separation operation

No.	Medium temperature, °C	Flotation recovery, %	
		Diamond	Kimberlite
1	14 (without thermal conditioning)	79.1	1.7
2	24	83.6	1.7
3	30	85.3	1.7
4	40	86.4	1.6
5	50	85.0	1.6

The efficiency of the selected temperature regime of the froth separation process was tested on a LFM-001C automated froth separation unit of the Yakutniproalmaz Institute. In the tests, the initial diamond-containing product was heat treated at a temperature of 85 °C. Due to the accumulated heat, the temperature of the medium in the operation of conditioning with the collector was 34–40 °C, and in the froth separation operation, 24 °C. The tests results showed that the diamond recovery to the concentrate achieved at thermal conditioning of the initial feed and subsequent increase of the medium temperature in conditioning and froth separation operations exceeded the corresponding recovery values in the control test at the medium temperature in conditioning and froth separation operations of 14 °C by 3.5%.

Thus, according to the results of scaled-up studies conducted at the automated unit, the temperature regime of the froth separation cycle operations for the processing plants of Alrosa was recommended, which implied maintaining the temperature in the heat treatment operation of the initial feed at 85–90 °C, in the conditioning operation with the collector, at 30–40 °C, and in the froth separation operation, at 20–24 °C.

Optimization of collector fractional composition

Fuel oils used in diamond flotation are not optimal collectors. This is due to the fact that GOSTs and TU for petroleum products determine their composition and properties to satisfy the requirements of consumers, which are power engineering and transportation facilities. Earlier studies have shown that F-5 and M-40 fuel oils contain a large amount of inactive resin-asphaltene fraction present as crystallized solids [9].

In order to increase the collecting ability of M-40 and F-5 fuel oils, it was proposed to transfer the resin-asphaltene fraction from the coarse-dispersed state to the form of colloidal or molecular solution by adding light ends of petroleum refining [17]. To determine the collector structure formation regularities at its dilution and the subsequent selection of the fractional composition, the modified M-40 fuel oil was studied using the method of combined optical microscopy. The technique application allows to diagnose the presence of crystalline and colloidal forms of insoluble components, for example, the fraction of petroleum resins and asphaltenes in a petroleum product [22, 23].

The studies carried out by optical microscopy method using a Micromed-3-LYuM microscope in combined lighting regime showed that the resins and asphaltenes are present in the dispersed state (black crystals and aggregates) and in the form of solution in medium- and low-molecular components (areas with yellow–green glow).

The analysis of the results showed that dilution of M-40 fuel oil with diesel oil cut (DOC) by 20 and 30% results in dispersing of the aggregates of asphaltene crystals and their dissolution with formation of fine-dispersed and dissolved forms (Fig. 5).

To determine the efficiency of fixing the collector on diamonds, the technique of UV-spectral analysis of the distribution of a collector between the liquid and solid phases of the flotation system was used, including operations of extraction of organic substances from the components of the aqueous dispersed system diamond – aqueous phase, measurement of concentrations, and the collector balance calculation [17].

The collecting properties of the studied collectors in relation to diamonds were tested using a frothless flotation cell, Hallimond tube. The diamonds of the coarseness of 0.5 to 1 mm, which were taken from diamond-containing gravity concentrate, were used in the research.

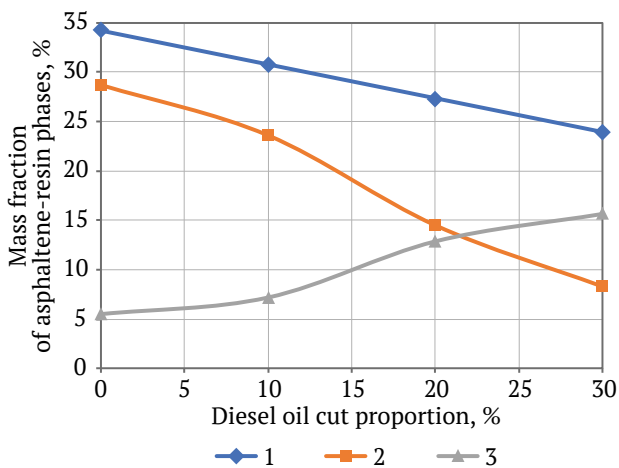


Fig. 5. Change of mass fraction of asphaltene-resin phases at dilution of M-40 fuel oil with diesel oil cut:
 1 – calculated; 2 – in solid form according to the results of visometric analysis; 3 – in dissolved and emulsion forms (as a difference of the first two values)

Table 4
Amount of fixed collector and recovery of diamonds to concentrate in Hallimond tube frothless flotation of diamonds

No.	Collector used	Share of collector fixed on diamonds, %	Diamond recovery into concentrate, %
1	M-40 fuel oil	45	68.4
2	M-40 fuel oil + 20% DOC	61	78.6
3	M-40 fuel oil + 20% DOC + DEK (KSM-1)	82	92.2
4	M-40 fuel oil + 20% DOC + EMK (KSM-2)	87	92.5
5	M-40 fuel oil + 20% DOC + DMK (KSM-3)	80	88.7

The research results showed that the compound collector, obtained by dilution of M-40 fuel oil by 20% DOC, demonstrated the best process performance: an increase in the proportion of collector fixed on the surface of diamonds by 16%, and a significant increase in their floatability (Table 4, test 2).

Another effective approach to modify the characteristics of the collector is the addition of reagents to its composition, providing autodispersing of the collector in aqueous phase. It was confirmed that the use of ketone additives (DEK – diethyl ketone, EMK – ethyl methyl ketone, DMK – dimethyl ketone) in the compound M-40 fuel oil-based collector composition provided an increase in the proportion of the collector fixed on diamonds from 45 to 87% (Table 5, tests 3, 4, 5). The proportion of collector fixed on kimberlite minerals increases insignificantly in this case.

The results of the flotation tests showed (see Table 4) that the maximum recovery of diamonds using the compound of M-40 fuel oil and aliphatic ketones was achieved in the area of mass fraction of ketones of 8–20%.

Collectors KSM-1 and KSM-2, which are compounds of M-40 fuel oil, diesel oil cut, and ketones, were also tested at a LFM-001S froth separation unit, operating in close to industrial regime (collector consumption of 1000 g/t, butyl aerofloat consumption of 50 g/t, a frothing agent consumption of 150 g/t). Bench test results showed that in the temperature range of 14–24°C, the diamond recovery reached 90–95% with a selectivity of 82.2–89.25% [17]. The comparison of the flotation tests results showed that the use of KSM-1 and KSM-2 collectors allowed achieving the recovery of 90% at half less consumption of the collector (Fig. 6). This is very important in terms of both reducing costs for flotation agents and decreasing environmental impact.

Selection of water recycling scheme parameters in froth separation cycle

The proportion of recycled water in a water consumption in the froth separation cycle is a key parameter determining the level of accumulation of soluble salts, sludges, and flotation reagents in the aqueous phase of beneficiation processes [24, 25].

The main reason for worsening froth separation performance at increasing the share of recycled water in the total water balance is the process of sludge accumulation. An increase in the share of recycled water leads to an increase in the concentration of sludge, which is due to the deterioration of conditions and decreasing efficiency of the recycled water clarification operation.

On the other hand, increasing the share of recycled water increases residual concentrations of

collector by 25–40%. This not only does not worsen flotation performance, but also reduces reagent consumption by 10–15%.

The results of the regression analysis showed that sludge concentration is the most significant adverse factor leading to lower diamond recovery, which results from a significantly stronger negative association (PCC = -0.56, Table 5) compared to the association with other parameters (PCC = -0.31–0.32, Table 5).

The results of the regression analysis are confirmed by a comparative analysis of the dependence of sludge accumulation and diamond recovery to the concentrate on the proportion of recycled water in the froth separation cycle. As can be seen from Fig. 7, when the proportion of recycled water reaches 85%, a gradual increase in the concentration of sludge in recycled water and a decrease in diamond recovery are observed. Therefore, the proportion of recycled water in the water balance in the froth separation cycle of 85% was established as the maximum permissible value (Fig. 7).

The increase in the proportion of recycled water from 70 to 85% recommended based on the findings of the present research was tested and implemented when modernizing the scheme of the froth separation cycle at Processing Plant No. 3 of Mirny Mining and Processing Complex. The task of reducing the concentration of sludge in recycled water was achieved with the use of single-stage clarification of the -2+1 mm coarseness initial feed thickening overflow and final tailings of the froth separation. The results of the tests showed the feasibility of reducing the collector consumption by 7% with the proportion of recycled water of 85% while maintaining diamond recovery and concentrate quality at the same level (Table 6).

To increase the proportion of recycled water in the water balance of the froth separation cycle up to 90% (in order to reduce the consumption of flotation agents), it is necessary to use effective methods to decrease the concentration of sludge in recycled water. This result can be achieved by using a two-stage scheme for clarification of the recycled water or by adding coagulants or flocculants that do not adversely affect the froth separation process. Reduction of sludge concentration

by 20–30%, achieved through the application of a two-stage clarification scheme, will allow increasing the proportion of recycled water up to 90% without reducing diamond recovery and achieving a total reduction in reagent consumption by 11%.

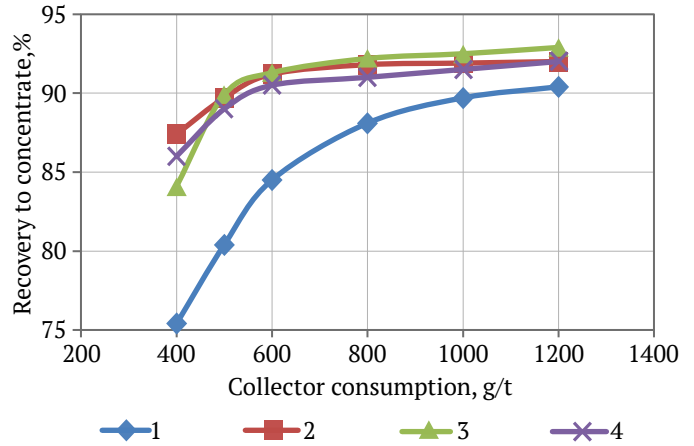


Fig. 6. Diamond recovery in froth separation with the use of collectors:

1 – M-40 fuel oil; 2 – KSM-1 collector; 3 – KSM-2 collector; 4 – KSM-3 collector

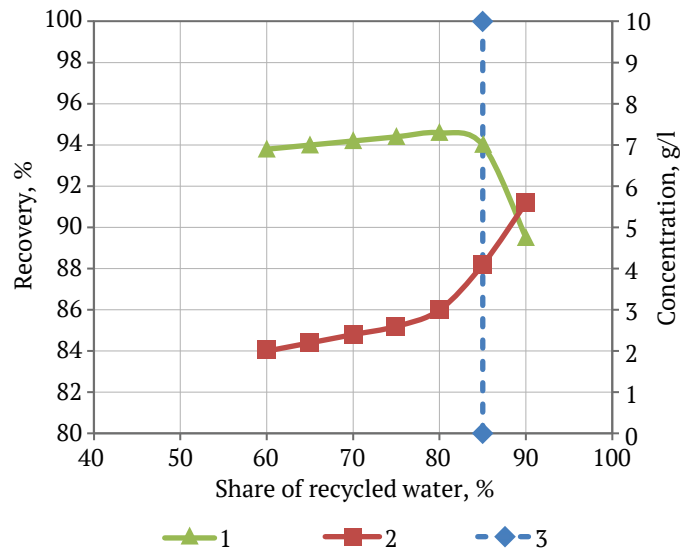


Fig. 7. Effect of the proportion of recycled water in the water balance of froth separation cycle on: 1 – sludge concentration and 2 – diamond recovery; 3 – limiting value of the proportion of recycled water

Pair correlation coefficients (PCC) between diamond recovery and parameters of recycled water of froth separation cycle

Table 5

Recycled water parameters	Diamond recovery, %			PCC between diamond recovery and recycled water parameters
	Minimum	Maximum	Medium	
Proportion of recycled water	65	90	74	-0.31
Salinity, g-ion/l	0.4	0.6	0.47	-0.32
Sludge concentration, g/l	3.1	5.8	4.0	-0.56



Table 6

Froth separation cycle indicators when changing recycled water proportion

Recycled water proportion, %	Collector consumption, g/t		Diamond recovery into concentrate, %	Kimberlite yield into concentrate, %
	F-5 bunker fuel oil	Butyl aerofloat		
Single-stage desludging				
70	1,100	25	87.9	0.65
75	1,050	23.5	87.9	0.64
85	1,020	22.8	87.8	0.63
90	970	21.5	85.8	0.62
Two-stage desludging				
85	1,020	22.8	87.9	0.60
90	970	21.5	87.8	0.60

Conclusions

It was shown that technogenic hydrophilization of diamonds is caused by the processes of crystallization of films of carbonate and silicate minerals and fixation of sludge fractions on the hydrophilized surfaces of diamonds. It was proposed to use combined regimes of conditioning of ore and recycled water using acoustic, thermal, electrochemical, and reagent treatment to increase diamond recovery, providing an increase in floatability of hydrophilic diamonds by 30–35% by reducing or preventing their hydrophilization and removal of sludges.

A rational temperature regime of froth separation cycle is proposed, including thermal treatment of the initial feed and assuming the use of heat consumed in the cycle to increase the temperature of the medium in the operations of conditioning with the collector and froth separation of a size class beneficiated. The feasibility of reducing diamond losses due to maintaining the optimal thermal regime by 3.5% was established.

It was shown that an effective way to increase the performance of froth separation is the modification of phase composition of fuel oils by additives of low- and medium-molecular fractions, which ensured the transition of asphaltenes and oil resins into an adhesive-active form, as well as provided autodispersing the collector in the aqueous phase. Tests of KSM-1 and KSM-2 reagents with additives of alkyl ketones confirmed their greater efficiency in comparison with F-5 bunker fuel oil.

The optimum proportion of recycled water (85%) was determined, which was achieved by applying a water recycling scheme including single-stage clarification of the initial feed thickening overflow and final tailings of the froth separation cycle, providing an 8% reduction in collector consumption while maintaining diamond recovery and concentrate quality at a high level. Application of a two-stage clarification scheme is proposed to reduce the concentration of sludge in water and increase the proportion of recycled water use.

References

1. Zlobin M.N. *The state and some ways of development of the technology of enrichment of diamond-containing raw materials at the "Alrosa" enterprise*. Moscow: Almazy; 2002. Pp. 59–63. (In Russ.)
2. Zlobin M.N. Technology of hard grained flotation during beneficiation of diamond-bearing ores. *Gornyi Zhurnal*. 2011;(1):87–89. (In Russ.)
3. Goryachev B.E. *Technology of diamond-bearing ores*. Moscow: MISIS; 2010. 326 p. (In Russ.)
4. Makhachev A.F., Larionov N.P., Savitsky V.B. New trends in developing the processes of diamond-bearing resources at ALROSA's enterprises. *Gornyi Zhurnal*. 2005;(7):65–68 (In Russ.)
5. Chanturia V.A., Dvoichenkova G.P., Koval'chuk O.E. Surface properties of diamonds recovered from metasomatically modified kimberlites during processing. *Fiziko-Tekhnicheskiye Problemy Razrabotki Poleznykh Iskopaemykh*. 2015;(2):138–149. (In Russ.)
6. Kovalenko E.G., Dvoichenkova G.P., Polivanskaya V.V. Joint scientific basis of heat and electrochemical treatment to improve foam separation of diamond ore. *Nauchnyy Vestnik MGGU*. 2014;(3):67–80. (In Russ.)



7. Zhang J., Kouznetsov D.L., Yu M. et al. Improving the separation of diamond from gangue minerals. *Minerals Engineering*. 2012;36–38:168–171. <https://doi.org/10.1016/j.mineng.2012.03.015>
8. Liu L., Cheng G., Yu W., Yang Ch. Flotation collector preparation and evaluation of oil shale. *Oil Shale*. 2018;35(3):242–253. <https://doi.org/10.3176/oil.2018.3.04>
9. Morozov V.V., Kovalenko E.G., Dvoichenkova G.P., Chut-Dy V.A. Selection of Temperature regimes for conditioning and flotation of diamond-bearing kimberlite with compound collectors. *Mining Science and Technology (Russia)*. 2022;7(4):287–297. <https://doi.org/10.17073/2500-0632-2022-10-23>
10. Westhuyzen P., Bouwer W., Jakins A. Current trends in the development of new or optimization of existing diamond processing plants, with focus on beneficiation. *Journal of The Southern African Institute of Mining and Metallurgy*. 2014;114:537–546.
11. Di Feo A., Mortazavi S., Langley S. The Effects of Water Recycling on Flotation at a North American Concentrator, Part 1. *Journal of Minerals and Materials Characterization and Engineering*. 2020;8(4):37–45. <https://doi.org/10.4236/jmmce.2020.84016>
12. Mikhlin Yu. X-ray Photoelectron Spectroscopy in Mineral Processing Studies. *Applied Sciences*. 2020;10(15):5138. <https://doi.org/10.3390/app10155138>
13. Thompson J.M. *Infrared spectroscopy*. Pan Stanford Publ.; 2018. 196 p.
14. Huhtamäki T., Tian X., Korhonen J.T., Ras R.H.A. Surface-wetting characterization using contact-angle measurements. *Nature Protocols*. 2019;15:2259. <https://doi.org/10.1038/s41596-018-0047-0>
15. Alekseenko V.V., Voronov D.V., Katashevstev M.D., Pakhomovskiy A.N. Study of emulsion granulometric composition by means of an optical microscope and a method for automated recognition of objects in digital photos. *Proceedings of Irkutsk State Technical University*. 2015;(2):99–104. (In Russ.)
16. Farrokhrouz M., Haghi H. The application of hallimond tube for floatability study of pure galena from nakhlak mine. In: *13th Conference on Environment and Mineral Processing*. Part 1. Ostrava, Czech Republic; 2009. Pp. 89–96.
17. Morozov V.V., Kovalenko E.G., Dvoichenkova G.P. et al. Selection of collector composition and temperature conditions for diamond foam separation. *Journal of Mining and Metallurgy*. 2022;58A(1):21–28. <https://doi.org/10.5937/JMMA2201021M>
18. Khmelev V.N., Khmelev S.S., Golykh R.N., Barsukov R.V. Increasing the efficiency of ultrasonic cavitation treatment of viscous and dispersed liquid media. *Polzunovskiy Vestnik*. 2010;(3):321–325 (In Russ.)
19. Makhachev A.F. Increasing the performance of collecting agents in diamond flotation on the basis of vibrojet magnetic activation. In: *Proceedings of the International Conference “Scientific Basis and Practice of Processing of Ores and Technogenic Raw Materials”*. Yekaterinburg; 2018. Pp. 122–126. (In Russ.)
20. Kovalenko E.G., Dvoichenkova G.P., Morozov V.V. Selection and justification of water-mineral system conditioning regimes in beneficiating diamond-bearing kimberlites. In: *Current Problems of Complex and Deep Processing of Mineral Raw Materials of Natural and Technogenic Origin. Plaksin Readings – 2022*. Vladivostok: 2022. Pp. 102–105. (In Russ.)
21. Chanturia V.A., Trofimova E.A., Bogachev V.I., Dikov Y.P. Nanoformations on the surface of natural diamonds. *Mining Informational and Analytical Bulletin*. 2009;(S14):35–41. (In Russ.)
22. Pivovarova N.A., Kirillova L.B., Takaeva M.A. et al. On the properties and structure of petroleum dispersed systems. *Vestnik of Astrakhan State Technical University*. 2008;(6):138–143. (In Russ.)
23. Ganeeva Y.M., Yusupova T.N., Romanov G.V. Asphaltene nano-aggregates: structure, phase transitions and effect on petroleum systems. *Russian Chemical Reviews*. 2011;80(10):993–1008. <https://doi.org/10.1070/RC2011v080n10ABEH004174> (Orig. ver.: Ganeeva Y.M., Yusupova T.N., Romanov G.V. Asphaltene nano-aggregates: structure, phase transitions and effect on petroleum systems. *Uspekhi Khimii*. 2011;80(10):993–1008. (In Russ.))
24. Pestryak I.V. Modeling and analysis of physicochemical processes in recirculating water conditioning. *Journal of Mining Science*. 2015;51(4):811–818. <https://doi.org/10.1134/S1062739115040189> (Orig. ver.: Pestryak I.V. Modeling and analysis of physicochemical processes in recirculating water conditioning. *Fiziko-Tekhnicheskiye Problemy Razrabotki Poleznykh Iskopayemykh*. 2015;(4):143–150. (In Russ.))
25. Michaux B., Hannula J., Rudolph M., Reuter M.A. Study of process water recirculation in a flotation plant by means of process simulation. *Minerals Engineering*. 2020;148:106181. <https://doi.org/10.1016/j.mineng.2020.106181>



Information about the authors

Valery V. Morozov – Dr. Sci. (Eng.), Professor of Department General and Inorganic Chemistry, University of Science and Technology MISIS, Moscow, Russian Federation; ORCID [0000-0003-4105-944X](https://orcid.org/0000-0003-4105-944X), Scopus ID [7402759618](https://scopus.com/authorid/7402759618); e-mail dchmggu@mail.ru

Evgeny G. Kovalenko – Cand. Sci. (Eng.), Chief Engineer, “Yakutniproalmaz” Institute AC “ALROSA”, Mirny, Republic of Sakha (Yakutia), Russian Federation; Associate Professor, Polytechnic Institute (branch) North-Eastern Federal University named after M. K. Ammosov, Mirny, Republic of Sakha (Yakutia), Russian Federation; ORCID [0000-0002-0320-0839](https://orcid.org/0000-0002-0320-0839), Scopus ID [57200340844](https://scopus.com/authorid/57200340844); email kovalenkoeg@alrosa.ru, kovalenkoeg@gmail.ru

Galina P. Dvoichenkova – Dr. Sci. (Eng.), Leading Researcher, Institute of Problems of Integrated Development of Mineral Resources of the Russian Academy of Sciences, Moscow, Russian Federation; Professor, Polytechnic Institute (branch) North-Eastern Federal University named after M. K. Ammosov, Mirny, Republic of Sakha (Yakutia), Russian Federation; ORCID [0000-0003-3637-7929](https://orcid.org/0000-0003-3637-7929), Scopus ID [8837172700](https://scopus.com/authorid/8837172700); e-mail dvoigp@mail.ru

Irina V. Pestryak – Dr. Sci. (Eng.), Head of the Department of General and Inorganic Chemistry, Associate Professor, University of Science and Technology MISIS, Moscow, Russian Federation; ORCID [0000-0002-1745-6579](https://orcid.org/0000-0002-1745-6579), Scopus ID [55577597700](https://scopus.com/authorid/55577597700); e-mail spestryak@mail.ru

Svetlana P. Lezova – Senior Lecturer of the Department of General and Inorganic Chemistry, University of Science and Technology MISIS, Moscow, Russian Federation; ORCID [0000-0001-8354-8802](https://orcid.org/0000-0001-8354-8802), Scopus ID [57206659544](https://scopus.com/authorid/57206659544); e-mail svlezova@mail.ru

Received 17.07.2023

Revised 07.08.2023

Accepted 18.09.2023



BENEFICIATION AND PROCESSING OF NATURAL AND TECHNOGENIC RAW MATERIALS

Research paper

<https://doi.org/10.17073/2500-0632-2023-08-145>

UDC 622.7.09




Enhancing flotation beneficiation efficiency of complex ores using ionometry methods

T. A. Yakovleva¹ , A. O. Romashev¹   , G. N. Mashevsky²  

¹ *Empress Catherine II Saint Petersburg Mining University, Saint Petersburg, Russian Federation*

² *NOVOMEK Group of Companies, St. Petersburg, Russian Federation*

 romashev_ao@pers.spmi.ru

Abstract

Flotation beneficiation plays a leading role in the processing most ores. The efficiency of this process is ensured by the correct selection of operating modes, which involves choosing the most selective reagents and determining their optimal consumption. Despite the significance of this issue, the classic approach to determining beneficiation parameters involves testing followed by the processing of the results obtained and the determination of the reagent consumption. However, such studies do not reveal the essence of the physicochemical processes occurring within the pulp, and the results of testing one sample may not correspond to the optimum when the properties of the sample change.

The purpose of this work is to develop and implement a methodological approach to the study of ore flotation beneficiation using ionometry methods. The data obtained from ion-selective sensors significantly deepen our insight into the transformations occurring during the flotation process and allow for consideration of possible adverse factors that hinder effective process progression.

To achieve this goal, a comparative analysis of two approaches to flotation beneficiation testing was performed using complex sulfide ores as examples. In the first stage, a flotation beneficiation study was conducted through D-optimal factor testing, which included 20 individual tests to determine the optimal consumption of modifying reagents, yielding qualitative indicators. In the second stage, flotation tests were conducted using electrochemical monitoring with pH, Ag₂S, Pt, and membrane electrodes. A universal flowchart for flotation studies with ion-selective sensors has been developed, facilitating the application of this approach to various ores. The implementation of the results from this comparative analysis has led to a 7.8% increase in beneficiation efficiency while reducing reagent consumption. Additionally, the insights gained into the electrochemical processes occurring allowed for assumptions about the adverse factors affecting flotation outcomes. In conclusion, a model for the potential application of this approach at existing enterprises was proposed, including the implementation of an “intelligent assistant” for flotation operators based on the developed electrochemical models.

Keywords

flotation, flotation beneficiation, complex ores, ionometry methods, ionometry, optimization, electrodes, dressability, simulation, reagents, testwork design, pH, Ag₂S, Pt electrodes

Funding

The work was carried out within the framework of a grant from the Russian Science Foundation (project No. 23-47-00109).

For citation


Yakovleva T. A., Romashev A. O., Mashevsky G. N. Enhancing flotation beneficiation efficiency of complex ores using ionometry methods. *Mining Science and Technology (Russia)*. 2024;9(2):146–157. <https://doi.org/10.17073/2500-0632-2023-08-145>



ОБОГАЩЕНИЕ, ПЕРЕРАБОТКА МИНЕРАЛЬНОГО И ТЕХНОГЕННОГО СЫРЬЯ

Научная статья

Повышение эффективности флотационного обогащения комплексных руд с использованием методов прямой потенциометрии

Т.А. Яковлева¹ , А.О. Ромашев¹   , Г.Н. Машевский²  ¹ Санкт-Петербургский горный университет императрицы Екатерины II, г. Санкт-Петербург, Российская Федерация² Группа компаний «НОВОМЭК», г. Санкт-Петербург, Российская Федерация romashev_ao@pers.spmi.ru

Аннотация

Флотационное обогащение играет ведущую роль при переработке большинства типов руд. Эффективность данного передела в большей степени обеспечивается правильным подбором режимов работы, выбором наиболее селективных реагентов и определением их оптимального расхода. Несмотря на очевидную важность данного вопроса классическим подходом к определению данных параметров является постановка плана эксперимента с последующей обработкой полученных результатов. Между тем проведение подобного рода исследований не раскрывает сущности физико-химических процессов, происходящих в пульпе, а результаты, полученные на одном образце, могут не соответствовать оптимальному при изменении исходных характеристик пробы.

Целью данной работы является разработка и реализация методического подхода с использованием методов прямой потенциометрии при исследовании руд на обогатимость флотационным методом. Получаемые данные от ионоселективных сенсоров позволяют в значительной мере расширить картину происходящих в процессе флотации преобразований и учесть возможные негативные факторы, препятствующие эффективному протеканию процесса.

Для реализации поставленной цели проведен сравнительный анализ двух подходов к постановке опытов по флотационному обогащению на примере комплексных сульфидных руд. На первом этапе проведено исследование по флотационному обогащению при помощи постановки D-оптимального факторного эксперимента, включающего 20 опытов по подбору оптимальных расходов реагентов-модификаторов с получением качественных показателей. На втором этапе поставлены опыты по флотации с применением электрохимического контроля с помощью рН, Ag₂S, Pt и мембранных электродов. В результате разработана универсальная блок-схема проведения флотационных исследований с ионоселективными сенсорами, позволяющая реализовать данный подход на различных рудах. Полученные результаты позволили интенсифицировать процесс обогащения, повысив его эффективность на 7,8 %, при сокращении расхода подаваемых реагентов. Помимо этого, полученные данные позволили выявить ряд негативных факторов, влияющих на результат. В заключение предложена модель для реализации данного подхода на предприятиях, включающая внедрение «интеллектуального помощника» оператора флотации на основе инициализированных электрохимических моделей.

Ключевые слова

флотация, флотационное обогащение, комплексные руды, методы прямой потенциометрии, ионометрия, оптимизация, электроды, обогащение, моделирование, реагенты, планирование эксперимента, рН, Ag₂S, Pt-электроды

Финансирование

Работа выполнена в рамках гранта РНФ (проект № 23-47-00109).

Для цитирования

Yakovleva T.A., Romashev A.O., Mashevsky G.N. Enhancing flotation beneficiation efficiency of complex ores using ionometry methods. *Mining Science and Technology (Russia)*. 2024;9(2):146–157. <https://doi.org/10.17073/2500-0632-2023-08-145>

Introduction

The processing of mineral raw materials with low grade of commercially valuable components poses challenges for industrial enterprises aiming to modernize production. Currently, most enterprises address the problem of replenishing losses in

concentrate production by increasing the volume of ore processed [1]. Additionally, efforts to increase or replenish the concentrate produced often result in the neglect of integrated subsoil usage, compromising the achievement of sustainable development goals in the mineral sector [2, 3].



Applying a more flexible approach through the use of modern automation technologies, as opposed to extensive method, enables the simultaneous resolution for both economic and, more importantly, environmental issues [4]. In the modernization of technologies at processing plants, researchers typically focus on optimizing the costliest stage, ore preparation [5]. While these efforts are crucial in reducing the final costs of the products obtained, the challenges of enhancing the comprehensiveness and depth of processing are predominantly addressed by intensifying the main stage: the flotation process [6–8].

In the contemporary practice of flotation beneficiation, the variability of the processed raw materials, especially due to ore heterogeneity, is one of the adverse factors affecting process performance [9]. This variability complicates the automatic control of the flotation process and the of dosing flotation reagents, thereby deteriorating both the qualitative and quantitative process indicators [10].

The selection of a reagent regime when studying ores for flotation dressability also poses challenges. Typically, this involves a step-by-step determination of the optimal consumption of each reagent type to establish the optimum conditions, or it involves applying various optimum plans. Although these methods are well-established, they require significant effort to conduct the testwork. For example, the commonly used Box-Behnken design necessitates 17 tests (in the simplest case, without repetitions). An alternative is the use of ionometry, measuring and recording electrode potentials. This approach, while established in electrochemical research, lacks a generally accepted methodology for its application in selecting reagent regimes and requires further refinement.

Therefore, the purpose of this work is to develop and test a methodological approach for studying flotation using ionometry.

To achieve this goal, we compared two approaches to designing tests for initial study of raw material dressability. The first, traditional approach uses a methodology to develop an optimal testwork plan, taking proposed flotation reagents' consumption values as predictors (calculated in grams per tonne) to find the conditions providing the best quality indicators. The second approach utilizes ion-selective sensors (electrodes).

Theory

The flotation process, from the standpoint of automatic control and regulation, can be conditionally divided into three consecutive stages. The first stage, ore pulp preparation (ore grinding, adding water

and modifying reagents, and the interaction of the ore with the reagents in the pulp), encapsulates the physicochemical essence of flotation. The second stage, the hydrodynamic one, includes the automatic stabilization of airflow rate and pulp level in a flotation machine, as well as other actuators controlling the process. The third stage involves adjusting the froth layer characteristics, where the secondary beneficiation of the processed raw materials occurs [11]. The first stage is of particular interest as it is the primary contributor to producing high-quality concentrate.

One approach to automatic process control involves studying the electrochemical properties of the flotation pulp. The importance of optimizing flotation based on ionometry was recognized as early as 1933–1934 when Wark and Cox first researched the relationship between the wetting contact angle and the pH value [5]. Their work also notes that pH is an important parameter in flotation processes. Over the years, pH remained the sole electrochemical parameter recognized in ore flotation dressability studies. However, analyzing additional parameters, such as electrode potentials, can uncover implicit dependencies and enhance overall process efficiency by creating digital twins of a particular processing stage or an entire plant flow sheet [12–14]. Recent publications have addressed this topic. For example, papers [15, 16] describe a “Digital Plant” project implementation: using the bulk flotation area of the Talnakh processing plant, a digital twin of an operator was created – a system that simulates the actions of an operator, stabilizes the flotation process, and performs control actions in real time [15]. Works [17, 18] emphasize the use of ion-selective electrodes for electrochemical pulp monitoring. The data obtained allowed for the investigation of electrochemical corrosion processes and the formation of coordination compounds of BtX with metals. After analyzing this data, the informative value of film membrane ion-selective EM electrode potentials was demonstrated. The investigation into the kinetics of potential shifts of a film membrane electrode within the decopperization and deironing circuit for rougher zinc concentrate at the Uchaly processing plant revealed substantial deviation of the electrode's potential values into negative territory. These deviations did not match the actual concentrations of free xanthate ions in the pulp. The markedly negative potential recorded by film membrane electrode indicate the formation of complexes between xanthate ions and zinc cations. Additionally, patent [19] describes a pioneering practical shift from establishing control measures on “g/t” to applying mass



ratios of pulp components that form sulfoxide complex, acting as depressants for Ni and Fe. Here, bisulfite ions were employed as sulfoxide depressants, with a maintained mass balance between iron ions, thiosulfate ions, and bisulfite ions in the pulp’s liquid phase. This industrial innovation highlights the potential for iron sulfite complex formation within the pulp, which can strongly adhere to the surface of nickel and pyrrhotite (sulfides) as hydrophilic anions, resulting in their depression.

While electrode use in enhancing flotation processes is not novel, the application of such knowledge to ore dressability studies is notably lacking, especially given the absence of a standardized methodological approach. The literature reviewed focuses on operational technologies, underlining the critical need to bridge this knowledge gap.

Research Materials and Techniques

Complex copper ores, comprised: 0.75% Cu, 23.48% Fe, 2.49% S, 64.61% SiO₂, were chosen for this study. The mineralogical composition of the sample used in the research is presented in Table 1.

Preliminary tests were carried out to determine the optimal grinding duration for the initial sample to achieve the liberation of mineral components, targeting a yield of 65% for the -0.071 mm grain size class. These tests were performed in a laboratory mill, MShL-7, with a ball load constituting 40% of the volume (9 kg) and a rotational speed set to 80% of the critical speed. The kinetic studies indicated that the required grinding time to reach the desired grain size was 12 min and 10 s.

Flotation beneficiation tests were conducted using a 3-L cell pneumatic-mechanical flotation machine from Vektis Minerals LLC. The material, immediately after grinding, was introduced to the cell where it interacted with flotation reagents according to a test plan.

The reagents employed included: CaO as a medium regulator, Na₂S as a depressant (sulfidizer), and BtX (butyl potassium xanthate) as a collector. The tests protocol was as follows: the initial subsample with a grain size of -2.0 mm was milled to achieve 65% passing -0.071 mm, during which dry medium regulator (CaO) was also incorporated. Subsequently, the 1st rougher flotation was carried out with the addition of Na₂S and BtX reagents, along with a constant T-80 frother dosage of 40 g/t. While the purpose of this research was not the selection and comparison of various reagents – although such an evaluation is extremely pertinent in the current economic climate – approach described below can be adapted for that purpose as well.

After the test, the beneficiation products were dried and analyzed using an EDX-8000P energy-dispersive X-ray fluorescent spectrometer, capable of detecting elements from C to U, manufactured by Shimadzu. Sample preparation for measurements involved obtaining a representative subsample weighing 5 ± 1 g followed by comminution.

During flotation beneficiation, the pulp’s electrochemical properties were monitored using a laboratory setup (Fig. 1), consisting of an array of electrodes connected to an EMF-16 Precision Electrochemistry Interface for real-time data acquisition redox and ion-selective electrodes (supporting up to 16 channels).

The following ion-selective sensors (electrodes) were used to examine the feedstock’s electrochemical properties: a pH electrode for assessing hydrogen ions concentration in the pulp/water [20]; an Ag₂S-electrode [21]; an EM – membrane electrode [22]; and an Pt electrode to determine the medium’s redox potential [23]. In line with the developed methodology’s requirements for electrochemical measurements, the ion-selective electrodes were calibrated to establish the electrochemical model

Table 1

Mineralogical composition of the sample

Mineral	Mass fraction of mineral in samples, %	Mineral	Mass fraction of mineral in samples, %
Ore minerals		Nonmetallic minerals	
Pyrite, marcasite	2.27	Calcite	32–35
Chalcopyrite	2.55	Garnet	19–20
Arsenopyrite	1.58	Chlorite	15–16
Magnetite	1.05	Microcline	10–11
Limonite	0.40	Pyroxene	3–4
Fahl ore	0.21	Kaolinite	2–3
Bornite	0.11	Quartz	2–3

necessary for diagnosing xanthate consumption and selecting the appropriate electrode set¹ [24, 25].

The electrodes' performance was gauged by calculating the slope of the electrode function, which for a singly charged component should be 59 ± 5 , in accordance with the Nernst equation [26–28].

Calibration of pH electrodes followed a standard procedure, using buffer solutions and accounting for the temperature of the medium under examination.

¹ Romashev A.O., Yakovleva T.A., Gatiyatullin B.L. Computer program No. 2023680109. A program for selecting ion-selective sensors based on calibration data. Application submission: 2023-09-14, patent publication: 26.09.2023.

Results and Discussion

The initial phase of our flotation beneficiation research was conducted using a “classical” method, where we assembled a matrix for a three-factor D-optimal experiment [29]. This types of designs are widely used in various scientific disciplines for their superior capability in assessing the nonlinear impacts of factors [30–32]. The structure and design of the D-factor experiment are shown in Fig. 2 and Table 2, respectively. The consumptions of the aforementioned reagents were selected as predictors, and the consumption intervals were chosen based of an analysis of literature sources and operation experience

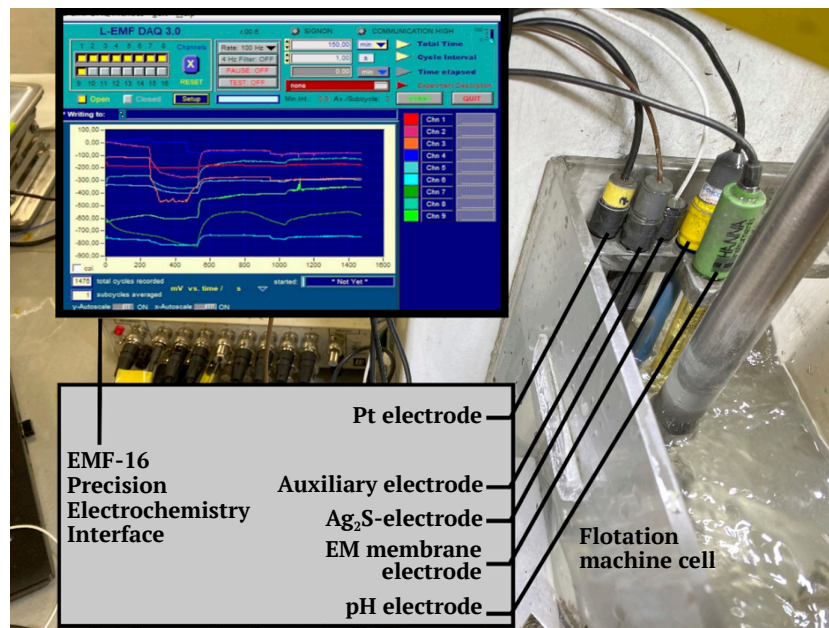
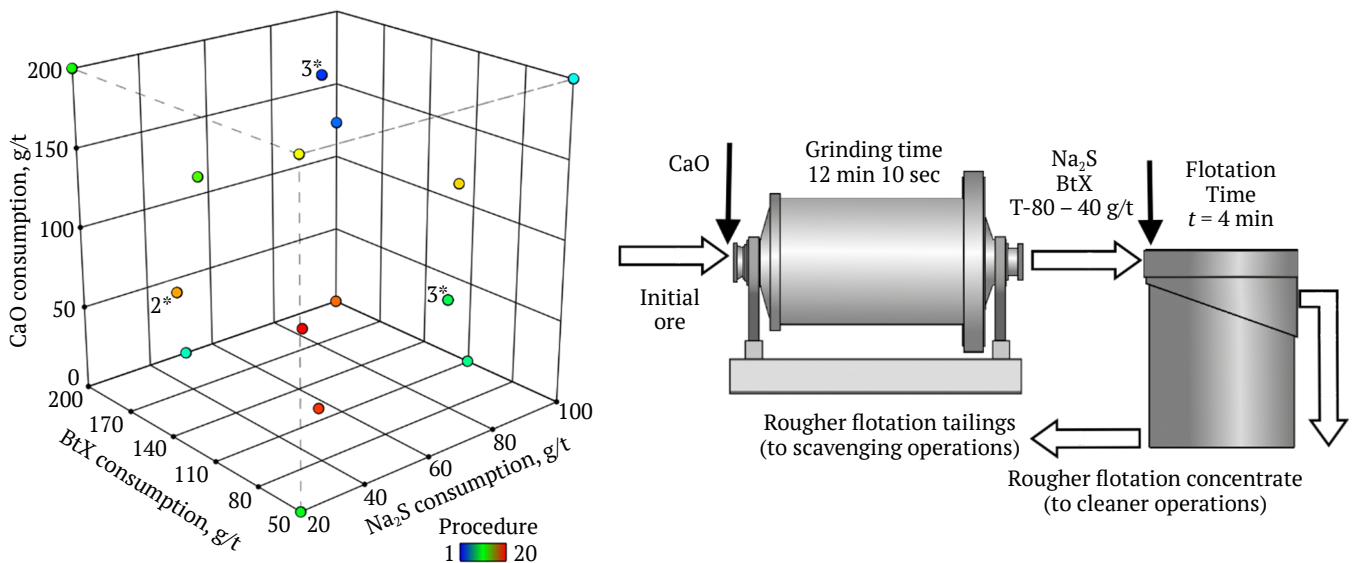


Fig. 1. Laboratory setup for monitoring electrochemical parameters in a flotation machine cell (compiled by the authors)



* The number indicates the repetitions at a given point

Fig. 2. Matrix of the D-factor experiment and flowchart for the series of tests (compiled by the authors)



Table 2

Testwork design and outcomes

Factor	Reagent	UoM	Minimum	Maximum	Min. level	Max. level	Average	STDEV
A	Na ₂ S	g/t	20.00	100.00	-1 ↔ 20.00	+1 ↔ 100.00	58.25	30.06
B	BtX	g/t	50.00	200.00	-1 ↔ 50.00	+1 ↔ 200.00	117.81	58.27
C	CaO	g/t	0.00	200.00	-1 ↔ 0.00	+1 ↔ 200.00	104.85	75.38

from similar enterprises. As an optimization criterion, the Hankok–Luyken efficiency criterion for copper was used. This criterion serves as a technological optimization measure because it includes qualitative beneficiation indicators and generally reflects the degree of current beneficiation expertise relative to the maximum potential experience, the so-called case of “ideal” beneficiation. A total of 20 flotation tests were carried out (including repetitions in central points) within the prescribed consumption ranges of the experiment plan. From the products of each test, three representative samples were taken to analyze qualitative indicators, and the arithmetic mean of these three measurements was considered the final result. It should be noted that this work only addressed the rougher flotation stage, omitting additional flotation operations needed to produce standard products.

Our statistical analysis for model adequacy showed an insubstantial effect of CaO consumption on flotation efficiency (Fig. 3), with no marked efficiency improvement upon increasing its usage. The local peaks arise from the influence of other factors. Hence, it is judicious to assign a zero consumption level for this reagent for the samples under scrutiny.

The analysis of the response surface of the efficiency of the beneficiation process, as a function of the consumption of Na₂S and BtX, allows us to conclude that there is a local peak under the given test conditions (Fig. 4).

To find the optimal consumption corresponding to the point of the local peak, the gradient search method was used, suitable for analyzing complex nonlinear dependencies. The solution found enabled the establishment of the consumptions for CaO, Na₂S, and BtX at 0, 49.64, and 103.48 g/t, respectively. According to the resulting model, the beneficiation efficiency at these parameters is 74.34%.

To confirm the data obtained, an additional series of tests were carried out using the determined consumption values, and the averaged results (with each experiment was repeated 3 times) are presented in Table 3. The copper recovery to the concentrate of the 1st rougher flotation was 75.8%, with a copper grade of 16.20% and a beneficiation efficiency of 72.81%, which had a relative error of 2.05% compared to the model data.

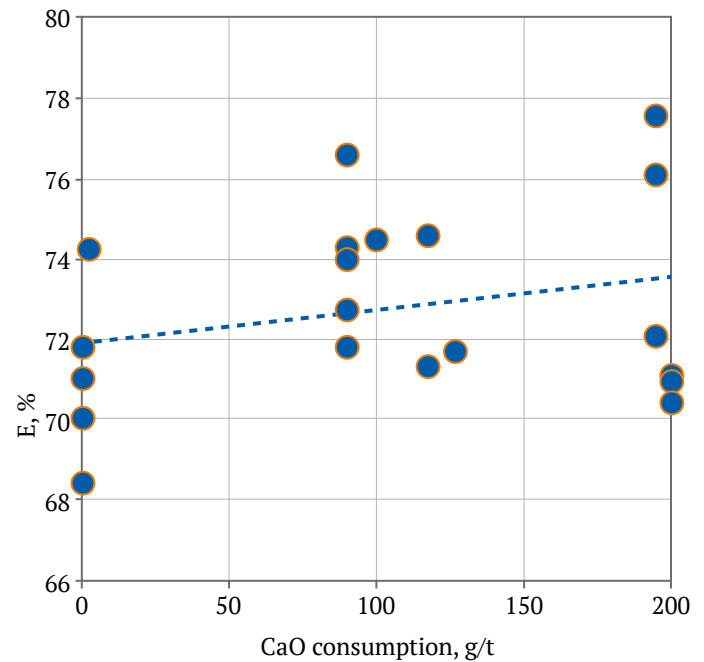


Fig. 3. Effect of CaO consumption on beneficiation efficiency (compiled by the authors)

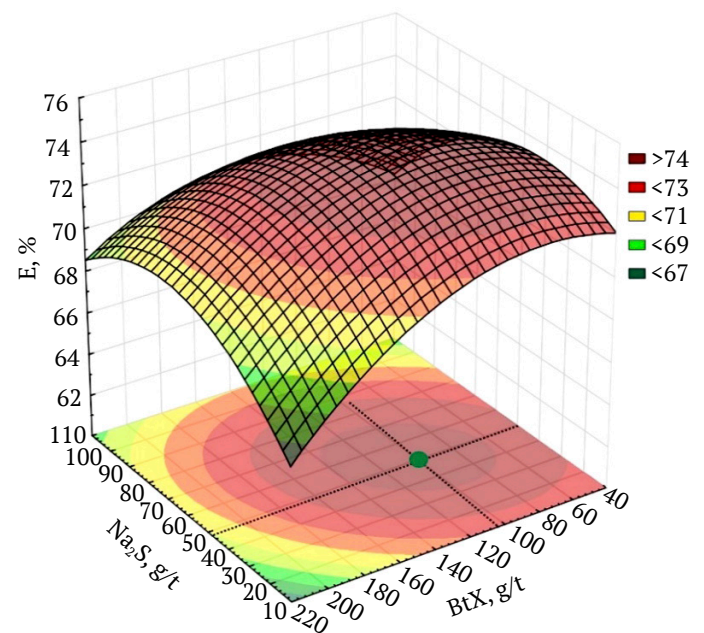


Fig. 4. Response surface of the beneficiation process efficiency as a function of Na₂S and BtX consumption, based on results from the D-factor experiment (compiled by the authors)

The second stage of the research involved dressability tests with electrochemical parameter monitoring. A generalized flowchart of the research using ion-selective sensors is depicted in Fig. 5. This flowchart is divided into three stages. Stages 1 and 2 are conducted during the initial examination of a sample prior to flotation beneficiation. The information obtained at these stages first allows for the identification of the most sensitive electrode pairs (stage 1) and secondly determines the target values for the argentite electrode potential and the stabilization time. The selection technique is more fully described in [27] and [33].

Within the framework of this flowchart, tests to investigate the electrochemical properties of the initial pulp were conducted. The schematic of these tests is shown in Fig. 6.

The method for investigating the electrochemical properties of ore pulp entails studying the kinetics of changes in the electrochemical parameters of the pulp, using a multisensor potentiometric system that monitors the potentials of electrodes installed directly in the pulp [27]. Then, an indicator (xanthate) is introduced into the resulting pulp both with and without preliminary aeration (Fig. 6, *b* and *a*, respectively).

Table 3

Results of open flotation tests at varying consumptions of selected reagents

Product	Yield, %	Percentage, %				Recovery, %			
		Cu	Fe	S	SiO ₂	Cu	Fe	S	SiO ₂
1st rougher flotation concentrate	3.54	16.05	20.16	15.00	47.31	75.8	3.04	21.33	2.59
Waste tailings	96.46	0.18	23.60	2.03	65.25	24.2	96.96	78.67	97.41
Ore	100.00	0.75	23.48	2.49	64.61	100	100.00	100.00	100.00

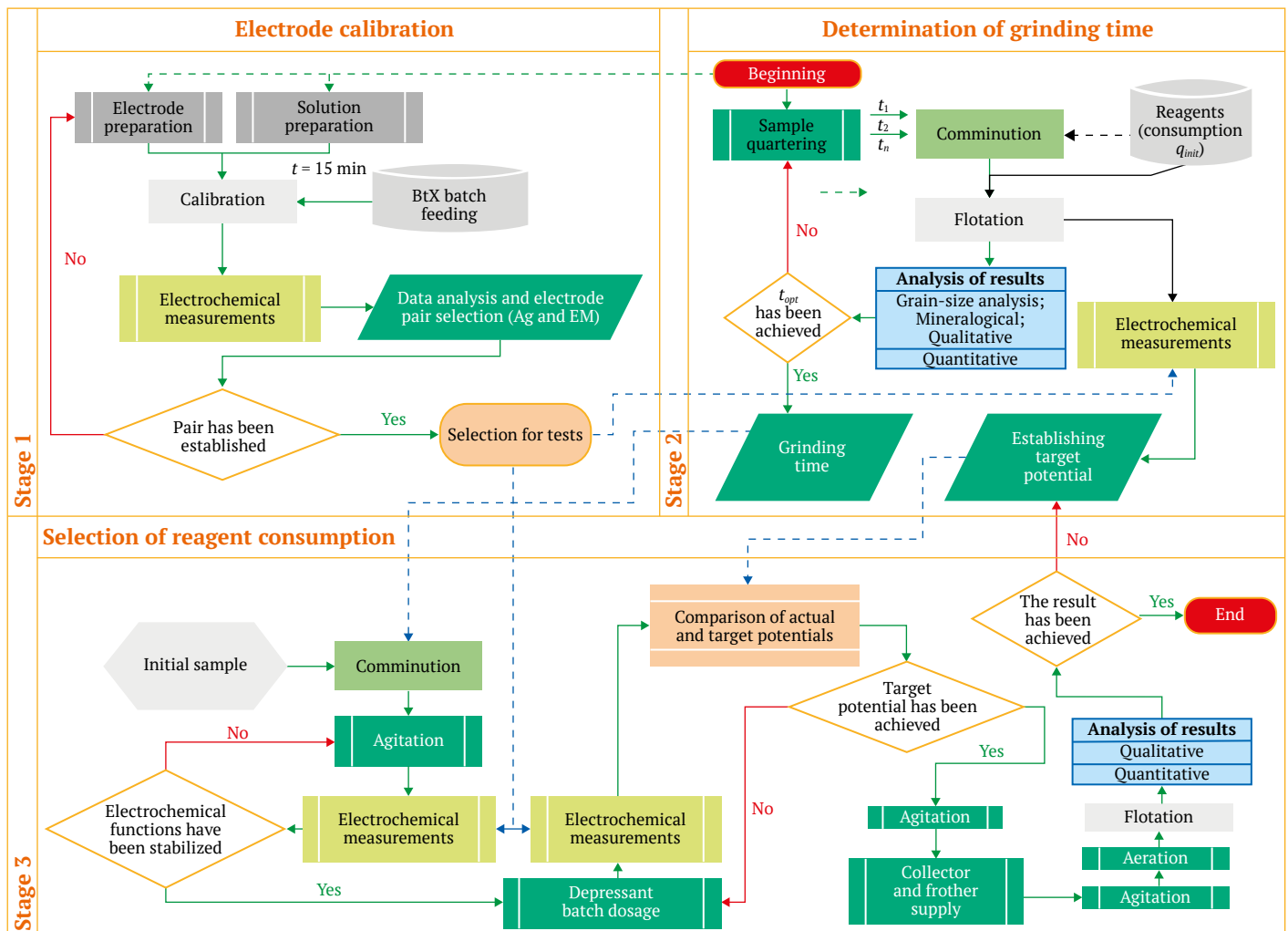


Fig. 5. Flowchart of flotation studies with ion-selective sensors (compiled by the authors)

Based on the obtained potentiograms of the absolute electrochemical potentials and diagnostic models, conclusions were drawn about the main components of the pulp that adversely or positively impact performance of the technological process. The results of the tests investigating the initial electrochemical parameters of the pulp are illustrated in Fig. 7.

After mixing the initial sample pulp, the potentials of the Mo, Pt, and Ag₂S electrodes shifted to the negative zone (Fig. 7, a, b). The potentiograms show a sharp increase in potential values during pulp aeration (point 3 in Fig. 7, a, b), which could be attributed

to redox processes occurring [27]. The significantly negative potential of the Ag₂S electrode upon mixing the initial pulp (after grinding) (point 1 in Fig. 7, a, b) suggests the presence of complexation processes, corroborated by changes in the kinetics of the film (membrane) ion-selective EM electrode potential. The Ag₂S electrode readings, during aeration tests (point 3, Fig. 7, a, b), indicate that Cu²⁺ cations enter the pulp, binding the initial xanthate portions (i.e., xanthate binds to copper cations). Therefore, the incremental addition of Na₂S could depress mineral surfaces and neutralize (mitigate) this adverse effect.

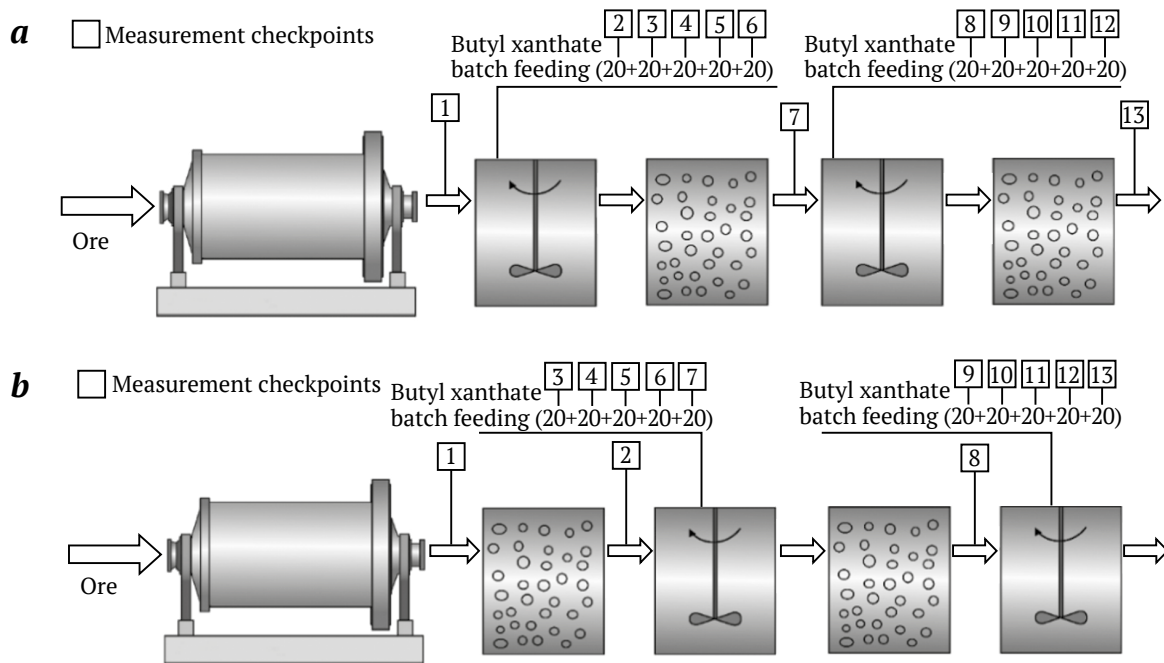


Fig. 6. Flow chart of a series of tests: a – without aeration; b – with preliminary aeration (compiled by the authors)

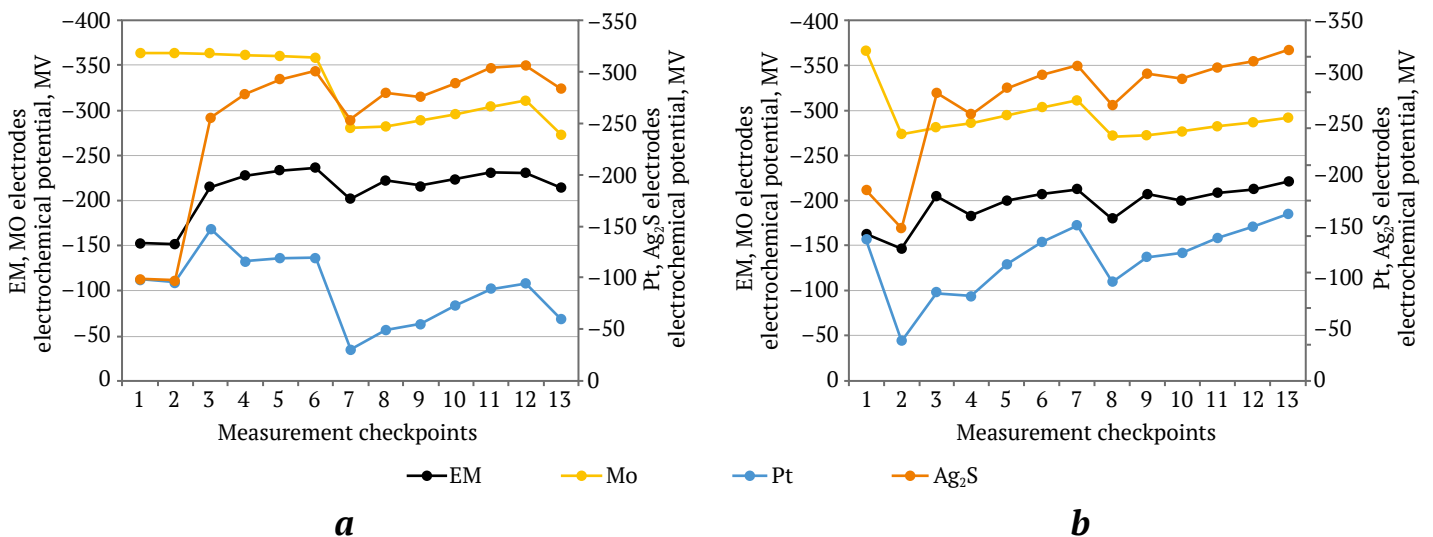


Fig 7. Results of tests investigating initial electrochemical parameters: a – without aeration; b – with preliminary aeration (compiled by the authors)

Table 4

Results of open flotation tests at Ag_2S potential maintained at -450 mV

Product	Yield, %	Percentage, %				Recovery, %			
		Cu	Fe	S	SiO ₂	Cu	Fe	S	SiO ₂
1st rougher flotation concentrate	3.12	19.89	19.62	15.18	36.67	83.13	2.61	19.03	1.77
Waste tailings	96.88	0.13	23.6	2.08	65.51	16.87	97.39	80.97	98.23
Ore	100.00	0.75	23.48	2.49	64.61	100.00	100.00	100.00	100.00

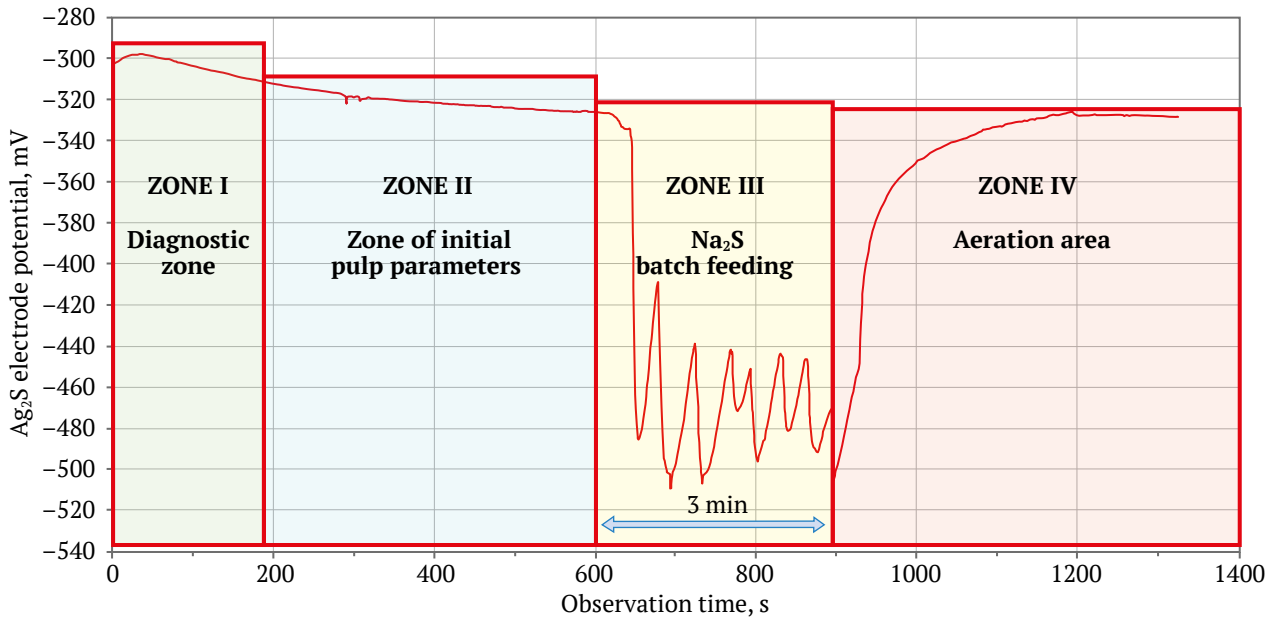


Fig. 8. Potentiogram displaying the kinetics of changes in Ag_2S electrode potential (compiled by the authors)

The results of this test are presented in Fig. 8 and Table 4. In Fig. 8, four zones of electrode function readings are discernible. Zone I shows a flattening of the electrode function. In Zone II, monitoring of the initial pulp parameters revealed the Ag_2S electrode potential in negative zone at -320 to -330 mV, likely due to soluble elements in the ore generating Fe^{2+} ions in the pulp. During Zone III, the Na_2S reagent was titrated for three minutes [33], a technique employed to sustain the Ag_2S electrode potential at -450 mV [27]. In Zone IV, xanthate and air were introduced.

The batched reagent consumptions were as follows: Na_2S – 15 g/t and BtX – 100 g/t. The test results showed that the 1st rougher flotation concentrate grade increased from 16.05 to 19.89% Cu, while the Cu content in the tailings decreased from 0.26 to 0.18%. Consequently, Cu recovery rose by 7.37%. The beneficiation efficiency reached 80.61%, which was 7.8% higher than the target value obtained from the experimental design.

These results imply that the beneficiation flowchart for this raw material might effectively comprise only three operations: 1st and 2nd rougher flotations, as well as a scavenging flotation, since the 1st rougher flotation already achieves substantial recovery of sulfides into bulk concentrate.

Conclusion

The studies conducted have validated the effectiveness of ionometry methods for investigating ore dressability. By adjusting reagent feed and concurrently monitoring electrode potentials, we achieved a 7.8% increase in beneficiation efficiency within a single operation.

The research and the methodology introduced for examining the electrochemical properties of pulp enable rapid identification and management adverse factors affecting flotation, leading to enhance process quality indicators. The reducing in investigation time and the possibility of indirect real-time monitoring are also of notable importance. This method can serve



as a blueprint for a production process, placing monitoring points throughout the production flowchart, and permits the real-time analysis of industrial beneficiation processes and, with provision for on-the-fly adjustment reagents feeding points in the flotation process. A significant benefit of systems based on ion-selective sensors is their capability to deliver operational control data with minimal delay. The information and diagnostic models generated can help

to minimize the influence of human error and reduce production costs through optimal reagent dosing. Looking ahead, the rapid advancement of artificial intelligence systems promises the development of self-learning systems employing neural network technology. These systems could function as an “interactive assistant”, offering real-time mode-adjustment recommendations with zero lag, leading to significant costs savings and significant economic benefits.

References

1. Litvinenko V.S., Petrov E.I., Vasilevskaya D.V. et al. Assessment of the role of the state in the management of mineral resources. *Journal of Mining Institute*. 2023;259:95–111. <https://doi.org/10.31897/pmi.2022.100>
2. Yurak V.V., Dushin A.V., Mochalova L.A. Vs sustainable development: scenarios for the future. *Journal of Mining Institute*. 2020;242:242–247. <https://doi.org/10.31897/pmi.2020.2.242>
3. Tsyglianu P.P., Romasheva N.V., Fadeeva M.L., Petrov I.V. Engineering projects in the Russian fuel and energy complex: actual problems, factors and recommendations for development. *Ugol'*. 2023;(3):45–51. (In Russ.) <https://doi.org/10.18796/0041-5790-2023-3-45-51>
4. Romasheva N.V., Babenko M.A., Nikolaichuk L.A. Sustainable development of the Russian Arctic region: environmental problems and ways to solve them. *Mining Informational and Analytical Bulletin*. 2022;(10–2):78–87. https://doi.org/10.25018/0236_1493_2022_10_2_78
5. Aleksandrova T.N., Afanasova A.V., Kuznetsov V.V., Aburova V.A. Selection of copper–nickel sulfide ore flotation parameters based on floatability ranking of flotation components. *Mining Informational and Analytical Bulletin*. 2022;(1):131–147. (In Russ.) https://doi.org/10.25018/0236_1493_2022_1_0_131
6. Vasilyeva M.A., Volchikhina A.A., Morozov M.D. Re-backfill technology and equipment. *Mining Informational and Analytical Bulletin*. 2021;(6):133–144. (In Russ.) https://doi.org/10.25018/0236_1493_2021_6_0_133
7. Zhou C., Zhao Y., Liu C. et al. Fluidization expansion of novel generation dense medium and flow regime transition in gas–solid separation fluidized bed. *Fundamental Research*. 2023. <https://doi.org/10.1016/j.fmre.2023.02.008>
8. Afanasova A.V., Aburova V.A., Prokhorova E.O., Lushina E.A. Investigation of the influence of depressors on flotation-active rock-forming minerals in sulphide gold-bearing ore flotation. *Mining Informational and Analytical Bulletin*. 2022;(6–2):161–174. (In Russ.) https://doi.org/10.25018/0236_1493_2022_6_2_161
9. Aleksandrova T.N. Key directions in processing carbonaceous rocks. *Journal of Mining Institute*. 2016;220:568–572. <https://doi.org/10.18454/pmi.2016.4.568>
10. Aleksandrova T.N., O'Connor C. Processing of platinum group metal ores in Russia and South Africa: current state and prospects. *Journal of Mining Institute*. 2020;244:462–473. <https://doi.org/10.31897/pmi.2020.4.9>
11. Boduen A. Ya., Petrov G. V., Kobylansky A. A., Bulaev A. G. Sulfide leaching of high-grade arsenic copper concentrates. *Obogashchenie Rud*. 2022;(1):14–19. (In Russ.) <https://doi.org/10.17580/or.2022.01.03>
12. Nikolaeva N.V., Aleksandrova T.N., Chanturiya E.L., Afanasova A.V. Mineral and technological features of magnetite-hematite ores and their influence on the choice of processing technology. *ACS Omega*. 2021;6(13):9077–9085. <https://doi.org/10.1021/acsomega.1c00129>
13. Zhang D., Gao X. A digital twin dosing system for iron reverse flotation. *Journal of Manufacturing Systems*. 2022;63:238–249. <https://doi.org/10.1016/j.jmsy.2022.03.006>
14. Ohenoja M., Koistinen A., Hultgren M. et al. Continuous adaptation of a digital twin model for a pilot flotation plant. *Minerals Engineering*. 2023;198:108081. <https://doi.org/10.1016/j.mineng.2023.108081>
15. Bendaouia A., Abdelwahed E.H., Qassimi S. et al. Digital Transformation of the Flotation Monitoring Towards an Online Analyzer. In: *Smart Applications and Data Analysis. SADASC 2022. Communications in Computer and Information Science*. Springer, Cham. 2022;1677. https://doi.org/10.1007/978-3-031-20490-6_26



16. Abrarov A.D., Datsiev M.S., Chikildin D.E., Fedotov D.N. Optimization of bulk flotation process at Talnakh Concentrator based on machine learning algorithms. *Tsvetnye Metally*. 2022;(2):87–93. (In Russ.) <https://doi.org/10.17580/tsm.2022.02.11>
17. Aleksandrova T.N., Ushakov E.K., Orlova A.V. Method of complex copper–zinc ore typification using neural network models. *Mining Informational and Analytical Bulletin*. 2020;(5):140–147. (In Russ.) <https://doi.org/10.25018/0236-1493-2020-5-0-140-147>
18. Aleksandrova T., Nikolaeva N., Kuznetsov V. Thermodynamic and experimental substantiation of the possibility of formation and extraction of organometallic compounds as indicators of deep naphthogenesis. *Energies*. 2023;16(9):3862. <https://doi.org/10.3390/en16093862>
19. Mashevskiy G. N., Petrov A. V., Lyyra M. et. al. Development of new series of Outotec products for electrochemical control of flotation process. *Tsvetnye Metally*. 2010;(2):93–95. (In Russ.)
20. Göktepe F. Effect of pH on pulp potential and sulphide mineral flotation. *Turkish Journal of Engineering and Environmental Sciences*. 2002;26(4):309–318.
21. Horwood C., Stadermann M. Evaluation of a Ag/Ag₂S reference electrode with long-term stability for electrochemistry in ionic liquids. *Electrochemistry Communications*. 2018;88:105–108. <https://doi.org/10.1016/j.elecom.2018.02.005>
22. Tatarnikov A.V., Sokolskaya I., Shneerson Ya.M. et al. Treatment of platinum flotation products. *Platinum Metals Review*. 2004;48(3):125–132. <https://doi.org/10.1595/003214004X483125132>
23. Liao L.W., Li M.F., Kang J. et al. Electrode reaction induced pH change at the Pt electrode/electrolyte interface and its impact on electrode processes. *Journal of Electroanalytical Chemistry*. 2013;688:207–215. <https://doi.org/10.1016/j.jelechem.2012.08.031>
24. Balatovic M. *Handbook of flotation reagents: chemistry, theory and practice. Flotation of Sulfide Ores*. Elsevier; 2007. 445 p. <https://doi.org/10.1016/b978-0-444-53029-5.x5009-6>
25. Woodcock J.T., Jones M.H. Chemical environment in Australian lead-zinc flotation plant pulps: II, Collector residualism metals in solution, and other parameters. In: *Proceedings of the Australasian Institute of Mining and Metallurgy*. 1970;235:61–76.
26. Titov D.V. Applying geophysical methods to assessing the technological properties of ores of sulfide polymetallic deposits. *Izvestiya Tomskogo Politekhnikeskogo Universiteta*. 2006;309(4):40–47. (In Russ.)
27. Yakovleva T.A., Romashev A.O., Mashevskiy G.N. Digital technologies for optimizing the dosing of flotation reagents during flotation of non-ferrous metal ores. *Mining Informational and Analytical Bulletin*. 2022;(6–2):175–188. (In Russ.) https://doi.org/10.25018/0236_1493_2022_62_0_175
28. Vidal-Iglesias F.J., Solla-Gullón J., Rodes A. et al. Understanding the Nernst equation and other electrochemical concepts: an easy experimental approach for students. *Journal of Chemical Education*. 2012;89(7):936–939. <https://doi.org/10.1021/ed2007179>
29. Tan S.Y., Chia V.Y.Y., Hölttä-Otto K., Anariba F. Teaching the Nernst equation and faradaic current through the use of a designette: an opportunity to strengthen key electrochemical concepts and clarify misconceptions. *Journal of Chemical Education*. 2020;97(8):2238–2243. <https://doi.org/10.1021/acs.jchemed.9b00932>
30. Napier-Munn T.J. *Statistical methods for mineral engineers – How to design experiments and analyse data*. Queensland, Australia: Julius Kruttschnitt Mineral Research Centre; 2014. 627 p.
31. Goos P., Jones B., Syafitri U. I-optimal design of mixture experiments. *Journal of the American Statistical Association*. 2016;111(514):899–911. <https://doi.org/10.1080/01621459.2015.1136632>
32. Mancenido M.V., Pan R., Montgomery D.C., Anderson-Cook C.M. Comparing D-optimal designs with common mixture experimental designs for logistic regression. *Chemometrics and Intelligent Laboratory Systems*. 2019;187:11–18. <https://doi.org/10.1016/j.chemolab.2019.02.003>
33. Mashevskiy G.N., Ushakov E.K., Yakovleva T.A. Digital technology for optimizing the sodium sulphide dosage during copper ore flotation. *Obogashchenie Rud*. 2021;(3):18–23. (In Russ.) <https://doi.org/10.17580/or.2021.03.04>
34. Aleksandrova T., Nikolaeva N., Kuznetsov V. Thermodynamic and experimental substantiation of the possibility of formation and extraction of organometallic compounds as indicators of deep naphthogenesis. *Energies*. 2023;16(9):3862. <https://doi.org/10.3390/en16093862>
35. Aleksandrova T.N., Prokhorova E.O. Modification of properties of rock-forming minerals during flotation. *Mining Informational and Analytical Bulletin*. 2023;(12):123–138. (In Russ.) https://doi.org/10.25018/0236_1493_2023_12_0_123



Information about the authors

Tatyana A. Yakovleva – PhD-Student of the Department of Mineral Processing, Empress Catherine II Saint Petersburg Mining University, Saint Petersburg, Russian Federation; ORCID [0000-0003-4834-0429](https://orcid.org/0000-0003-4834-0429); e-mail iakovleva@gmail.com

Artyem O. Romashev – Cand. Sci. (Eng.), Associate Professor of the Department of Mineral Processing, Deputy Head of the Department of Mineral Processing, Empress Catherine II Saint Petersburg Mining University, Saint Petersburg, Russian Federation; ORCID [0000-0003-3210-8000](https://orcid.org/0000-0003-3210-8000), Scopus ID [56330093400](https://scopus.org/authorid/56330093400); e-mail Romashev_AO@pers.spmi.ru

Gennady N. Mashevsky – Dr. Sci. (Eng.), Technology Advisor, NOVOMEK Group of Companies, Saint Petersburg, Russian Federation; ORCID: [0009-0008-9038-8665](https://orcid.org/0009-0008-9038-8665), Scopus ID [56290154600](https://scopus.org/authorid/56290154600); e-mail gennadii.mashevskii@novomek.ru

Received 24.08.2023

Revised 17.01.2024

Accepted 20.01.2024



BENEFICIATION AND PROCESSING OF NATURAL AND TECHNOGENIC RAW MATERIALS

Research paper

<https://doi.org/10.17073/2500-0632-2023-10-168>

УДК 622.7:622.34(001)[571.76]

**Comparative processing studies of the Arkachan deposit gold-bearing ores using dry separation and classical wet gravity separation methods**

A. I. Matveev , I. F. Lebedev ✉, V. R. Vinokurov , E. S. Lvov

*Federal Research Center “Yakutsk Research Center of the Siberian Branch of the Russian Academy of Sciences”
N.V. Chersky North Mining Institute, Siberian Branch of the Russian Academy of Sciences, Yakutsk, Russian Federation*✉ ivleb@mail.ru**Abstract**

The use of dry methods of processing and beneficiation of mineral raw materials is one of the promising areas, as this approach to concentrate production is less energy-consuming, less labor-intensive, and economically beneficial. The paper presents experimental studies on preliminary dry separation of Arkachan deposit ores to determine the quality of beneficiation of the separation products. The studies on dressability were carried out on pilot plants for dry ore processing and beneficiation: combined impact crusher DKD-300, centrifugal mill TsMVU-800, pneumatic separator POS-2000. Processing of the obtained separation products by pneumatic separation and screening according to the sequential flow chart of crushing and grinding was carried out in laboratory conditions at a gravity concentration table SKO-0.5. The GRG test was performed at an ITOMAK-0.1 centrifugal concentrator using a sequential grinding circuit. The GRG test showed that for more efficient gravity separation of gold, up to total gold recovery of 73.91%, the degree of grinding up to 80% passing 0.071 mm was required, allowing obtaining a gravity concentrate graded at 70.28 g/t gold.

Keywords

crusher, mill, pneumatic separator, dry separation, screening, grinding, concentrator, gold, recovery, performance

Acknowledge

The study was performed within the framework of the state assignment of the Ministry of Science and Higher Education of the Russian Federation (Project No. 0297-2021-0022, EGISU Research and Development Center No. 122011800089-2) with the use of the equipment of the TsKP of the FRC YaSC SB RAS (grant No. 13.TsKP.21.0016).

For citation

Matveev A. I., Lebedev I. F., Vinokurov V. R., Lvov E. S. Comparative processing studies of the Arkachan deposit gold-bearing ores using dry separation and classical wet gravity separation methods. *Mining Science and Technology (Russia)*. 2024;9(2):158–169. <https://doi.org/10.17073/2500-0632-2023-10-168>

ОБОГАЩЕНИЕ, ПЕРЕРАБОТКА МИНЕРАЛЬНОГО И ТЕХНОГЕННОГО СЫРЬЯ

Научная статья

Сравнительные технологические исследования золотосодержащей руды месторождения Аркачан методами сухого обогащения и классической мокрой гравитации

А. И. Матвеев , И. Ф. Лебедев ✉, В. Р. Винокуров , Е. С. Львов

*Федеральный исследовательский центр «Якутский научный центр Сибирского отделения Российской академии наук»
Институт горного дела Севера им. Н.В. Черского Сибирского отделения Российской академии наук,
г. Якутск, Российская Федерация*✉ ivleb@mail.ru**Аннотация**

Использование сухих технологий переработки и обогащения минерального сырья является одним из перспективных направлений, так как данный способ производства концентрата менее энергозатратен, менее трудоемок и экономически выгоден. В работе приведены экспериментальные работы по предварительному сухому обогащению руд месторождения Аркачан для определения качества обо-



гашения продуктов разделения. Исследования на обогатимость проводились на опытных установках сухого метода переработки и обогащения руд: дробилке комбинированного ударного действия ДКД-300, центробежной мельнице ЦМВУ-800, пневмосепараторе ПОС-2000. Обработка полученных продуктов разделения пневмосепарацией и грохочением по последовательной схеме дробления и измельчения проводилась в лабораторных условиях на гравитационном концентрационном столе СКО-0,5. GRG-тест проходил на центробежном концентраторе ИТОМАК-0,1 по последовательной схеме измельчения. Анализ проведенного GRG-теста показал, что для более приемлемых условий гравитационного обогащения золота – до 73,91 % – необходима степень измельчения до 80 % класса –0,071 мм, для получения гравитационного концентрата с содержанием 70,28 г/т золота.

Ключевые слова

дробилка, мельница, пневмосепаратор, сухое обогащение, классификация, измельчение, концентрат, золото, извлечение, эффективность

Финансирование

Работа выполнена в рамках государственного задания Министерства науки и высшего образования Российской Федерации (тема № 0297-2021-0022, ЕГИСУ НИОКТР № 122011800089-2) с использованием оборудования ЦКП ФИЦ ЯНЦ СО РАН (грант №13.ЦКП.21.0016).

Для цитирования

Matveev A. I., Lebedev I. F., Vinokurov V. R., Lvov E. S. Comparative processing studies of the Arkachan deposit gold-bearing ores using dry separation and classical wet gravity separation methods. *Mining Science and Technology (Russia)*. 2024;9(2):158–169. <https://doi.org/10.17073/2500-0632-2023-10-168>

Introduction

Reducing the cost of finished products by applying the most economically advantageous processes and technologies of mineral processing and beneficiation is one of the urgent tasks in the mining and processing industry. One of the promising areas is the use of dry methods of mineral raw materials beneficiation, as this approach to concentrate production has a number of significant advantages.

The purpose of this work is conducting experimental studies on preliminary dry separation of the Arkachan deposit ores and assessing the quality of the separation products with the recovery of gold from the pneumatic separation concentrate and tailings by gravity separation methods.

The ore samples from the Arkachan deposit by material composition are lumpy ore material of –150+40 mm in particle size, with veins of quartz-carbonate, quartz-carbonate-sulfide, quartz-goethite, and quartz-limonite composition.

The technology of the tests on dry ore separation provides for treatment of the separation products for maximum recovery of free gold from the products and correct accounting in determining the qualitative and quantitative indicators of the separation processes [1–3].

The technology involves two interrelated processes:

- ore preparation (crushing and grinding) to release and recover free gold up to 50 microns [4–6];
- pneumatic separation to produce concentrates with a high grade of free gold at a particle size of up to 100 microns.

The tested technology provides for the use of crusher DKD-300¹ [7, 8] based on the technique of multiple impact action [9, 10] with productivity up to 15 tph, centrifugal mill TsMVU-800² with productivity up to 6 tph, and pneumatic separator POS-2000 with productivity up to 6 tph.

Classical wet gravity separation was carried out using the GRG test methodology, which involves sequential release and recovery of gold as an ore is ground in stages. The GRG test consists of three successive stages of mineral disintegration and three stages of beneficiation.

For the comparative characterization of these two technologies, optimal crushing process parameters of crushing and grinding apparatuses, fractional compositions of crushing and grinding products, release of gold-bearing minerals from the ore matrix, the results of the studies on dry beneficiation of the crushed fraction using POS-2000 pneumatic separator with the determination of the recovery of gold-bearing minerals by pneumatic separation, the degrees of reduction were determined and used [11, 12]. The quality of beneficiation and

¹ Matveev A.I., Vinokurov V.P., Grigoriev A.N., Monastirev A.M. Patent No. 2111055 of the Russian Federation. Combined impact crusher. Published on 20.05.1998.

² Matveev A.I., Grigoriev A.N., Filippov V.E. Patent No. 2150323 7 B02 C 13/20. Counter Impact Centrifugal Pulverizer. SB RAS North Mining Institute. Published on 06/10/2000; Matveev A.I., Vinokurov V.R., Grigoriev A.N. Patent No. 2746502 B02C 7/00. Vertical Centrifugal Pulverizer. Federal State Budgetary Institution of Science Federal Research Center Yakutsk Research Center of the Siberian Branch of the Russian Academy of Sciences. Published on 14.04.2021.



the separation products was determined by particle size class. The technological assessment was given and the feasibility of using dry ore separation for obtaining gold concentrates at the preliminary stage of beneficiation were substantiated [13, 14].

General methodology of the performed studies on ore sample processing

The experimental sample processing was carried out in conjunction with basic sequential processing of an ore sample weighing at least 500 kg. A small portion of the initial sample was retained for umpire analytical studies.

The tests were carried out according to the flow chart, providing for the sequential processing of ore at the DKD-300 crusher, TsMVU-800 mill, and POS-2000 pneumatic separator (Fig. 1).

For end-to-end testing, the initial sample after each crushing cycle was separated by screening into particle size classes of +5 mm, -5+3 mm and -3+0 mm.

The +5 mm particle size classes formed in the crushing process were subjected to successive staged crushing at a DKD-300 crusher, and the number of crushing cycles was determined by sufficient degree

of mass loss of +5 mm size classes after the latest crushing cycle.

The crushing products of -5 + 3 mm and -3 + 1 mm particle size classes were ground at a TsMVU-800 centrifugal mill. The grinding products were separated at POS-2000 pneumatic separator to obtain concentrate and tailings. For the end-to-end tests, grinding and pneumatic separation were performed sequentially.

The pneumatic separation concentrates were screened to separate into two particle size classes: -1 mm and +1 mm. The resulting -1 mm class was further concentrated at a SKO-0.5 table, then at a Moseley analyzer for free gold recovery by finishing (magnetic separation and washing in bromoform).

The -3+0 mm particle size class obtained after primary crushing was also screened to separate the +1 mm particle size class, which was sent for regrinding with following pneumatic separation. The screening products of +1 mm and -1 mm particle size classes were subjected to pneumatic separation at the POS-2000 to obtain concentrate and tailings.

Free gold was separated from the pneumatic separation concentrates using Moseley analyzer finishing, magnetic separation, and bromoform washing.

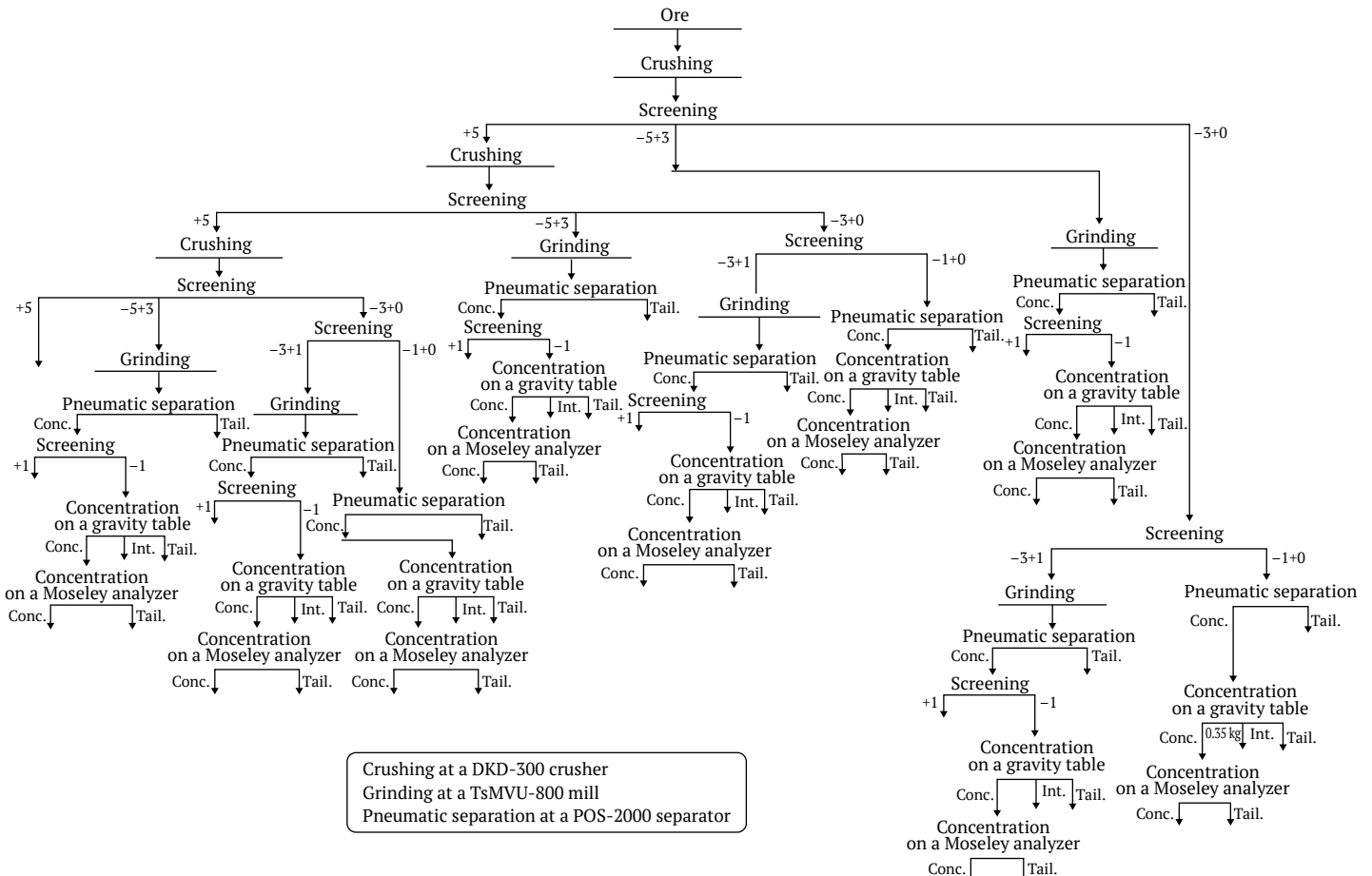


Fig. 1. Flow chart of sample processing: Conc. – concentrate; Tail. – tailings, Int. – intermediates

All crushing and grinding products were subjected to particle size distribution analysis with appropriate sampling, and the separation products from the pneumatic separation, concentration table, and Moseley analyzer were analyzed by fire assay or atomic adsorption method for residual gold grade after complete recovery of free gold particles.

Based on the conducted research results, the qualitative and quantitative indicators of the sample processing flow chart were calculated. The quality of pneumatic separation was determined after analyzing the processing products taking into account the recovered amount of free gold.

As the final step, a balance calculation of the processing products in terms of gold grade and recovery by processing cycle (crushing-grinding-pneumatic separation) and for throughout sample processing was performed.

Methodology of the GRG test for assessing the gravity dressability of the gold-bearing ore

A study of the initial ore sample by GRG test was carried out to determine the deposit ore gold dressability based on the use of a Knelson centrifugal concentrator [15–17]. The GRG test technique is based on the sequential recovery of released gold by grinding stage, i.e. as gold is released, and excludes overgrinding and comminution of coarse gold particles [18, 19]. The GRG test involves three consecutive cycles of mineral disintegration and corresponding three cycles of subsequent beneficiation [20, 21].

The GRG test specifies the grinding degrees of the test materials:

Stage 1 – up to 100% passing 1 mm (P100 –1 mm);

Stage 2 – up to 80% passing 0.315 mm (P80 –0.315 mm);

Stage 3 – 88% passing 0.071 mm (P88 –0.071 mm).

At the first stage of grinding, DAU-250 active impact crusher was used, whose technical characteristics are given in Table 1.

The initial mass of a sample taken for the test was 65 kg, which was milled and beneficiated to produce concentrate and tailings.

The second stage received the ground tailings of the first stage, the third stage received the ground tailings of the second stage; the grinding was carried out at a MSHL-120 laboratory ball mill. General drawing of the laboratory ball mill is shown in Fig. 2, and its technical characteristics are given in Table 2.

The beneficiation was carried out at an ITO-MAK-0.1 centrifugal concentrator (Fig. 3). This centrifugal concentrator is a Russian analog of a Knelson

concentrator; technological characteristics of these facilities are comparable under equal operating conditions. Technical characteristics of the ITOMAK-0.1 are given in Table 3.

The flow chart of the GRG test using the DAU-250, MSHL-120, ITOMAK-0.1 facilities is presented in Fig. 4.

Table 1

Technical characteristics of DAU-250 crusher

Parameter	Value
Max. particle size of feed material, mm	100
Relieve slot, mm	1–10
Motor power, kW	7.5
Motor speed, rpm	960–1,490
Feed throughput, tph	1.0
Weight with electric motor, t	0.8



Fig. 2. Laboratory MSHL-120 ball mill

Table 2

Technical characteristics of MSHL-120

Parameter	Value
Drum volume, l	120
Feed material particle size, mm, max	8
Drum speed, rpm	48–60
Final product particle size, mm	–0.071
Ball load, kg	Up to 80
Diameter of balls, mm, within	20–80
Installed power, kW	1.5
Operating mode	Intermittent, continuous
Grinding method	Dry

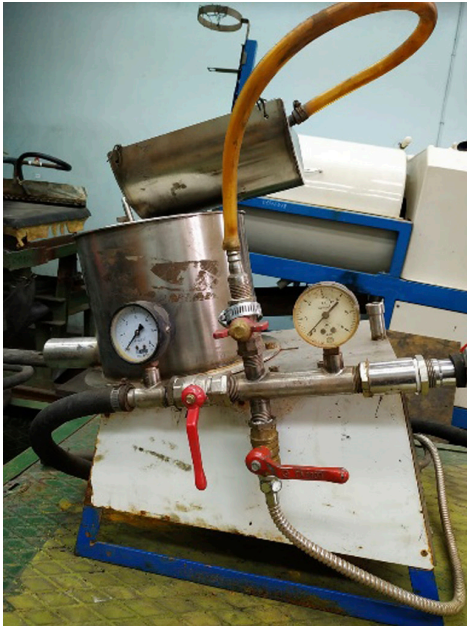


Fig. 3. ITOMAK-0.1 centrifugal concentrator

Table 3

Technical characteristics of ITOMAK-0.1

Parameter	Value
Motor power, W	250
Three-phase AC mains supply voltage*, V	380±38
Solid sludge capacity, kg/h	100
Slurry capacity, m ³ /h	0.37
Maximum flushing water consumption, m ³ /h	2.5
Feed material particle size (for alluvium), mm, max	2.0
Feed material particle size (for ore), mm, max	0.5
Slurry solid content, %	Up to 75
Concentrate volume, ml, max	120
Facility weight, kg, max	55
Overall facility dimensions, mm, L×W×H, max	550×350×780

Results of Arkachan deposit ore metallurgical sample investigations involving crushing, grinding, and pneumatic separation

According to the methodology of the conducted researches the tested flow chart of sample processing represents consecutive operations of gold release by staged crushing, grinding, and pneumatic separation of crushed materials passing 3 mm, carried out directly in the DKD-300 crusher, TsMVU-800 mill, and POS-2000 pneumatic separator.

The tests were carried out according to the flow chart presented in Fig. 1, according to the general methodology, providing sequential crushing of ore in the crusher.

A total of three crushing cycles were performed at a DKD-300 crusher during the sample processing (Table 4).

As shown in Table 4, the maximum degree of crushing by cycle was 9.35.

Grinding of ore samples was carried out in a centrifugal step mill TsMVU-800 according to the flow chart shown in Fig. 1. The crushing and screening products of the -5+3 mm and -3+1 mm particle size classes (Tables 5, 6) comprised the grinding feed. All the grinding products were subjected to pneumatic separation in POS-2000 pneumatic separator.

As can be seen from the results obtained (see Table 5), when grinding the particle size classes -3+1 mm, the minimum fineness number was 2.01 mm and the maximum one was 2.17 mm. When grinding coarser classes of -5+3 mm, the fineness number ranged from 3.05 to 3.59 mm (see Table 6), being significantly higher. This is due to the peculiarity of impact grinding in centrifugal mills, where

Table 4

Particle size distributions of the DKD-300 crusher crushing products

Particle size class (mm)	Yield, %		
	1 st cycle	2 nd cycle	3 rd cycle
-0.071	3.57	2.44	2.18
-0.1+0.071	1.99	0.62	0.76
-0.2+0.1	2.82	1.66	2.27
-0.315+0.2	1.15	1.07	1.47
-0.63+0.315	3.61	1.93	2.58
-1+0.63	4.92	2.86	3.44
-2+1	8.78	5.92	7.22
-5+2	22.93	32.07	37.40
-10+5	14.59	24.63	23.03
-20+10	21.23	22.44	17.34
-40+20	8.83	4.34	2.31
+40	5.59	0.00	0.00
Degree of crushing	9.35	2.28	2.02

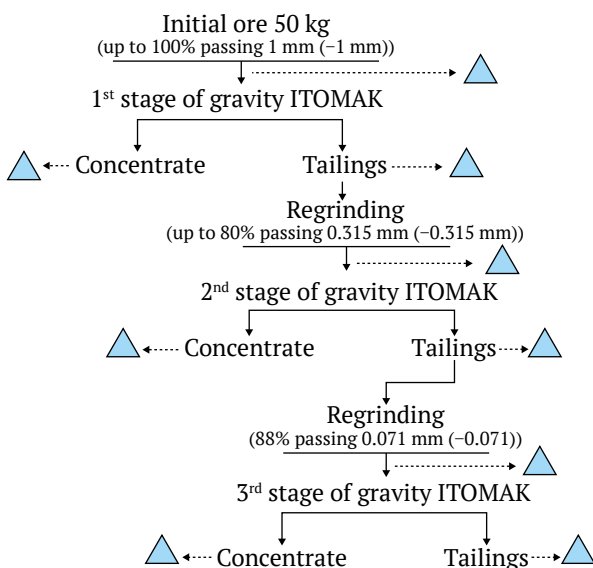


Fig. 4. GRG test design



the effect of the mass of a broken piece manifests itself. The more massive and coarser a particle, the greater the energy of dynamic impact when the particles collide with the mill's working bodies; correspondingly, the higher the fineness number.

POS-2000 pneumatic separator was tested in two operating modes. The first mode consisted in the sequential combined operation with centrifugal mill TsMVU-800, and the second one, in separate pneumatic separation of passing 1 mm screening products. The resulting pneumatic separation concentrate was divided into two classes, -1 mm and +1 mm. The particle size class -1 mm was concentrated at a SKO-0.5 concentration table to produce a rough concentrate. The table concentrate was further processed in a Moseley analyzer until a "primary concentrate" – ultra concentrate – was obtained.

Gold grade in the +1 mm particle size classes and in the pneumatic separation tailings was determined by fire assay.

In the second mode of operation, i.e. at pneumatic separation of screening products of -1 mm particle size class, the obtained pneumatic separation concentrate was also concentrated at the SKO-0.5 concentration table to assess the quality of separation. The concentrate was then processed at a Moseley table to separate the primary gold concentrate.

The beneficiation results at three different pneumatic separator productivities after processing the separation products by concentration at the SKO and at the Moseley analyzer with the corresponding results of gold grades assays in the separation products are shown in Table 7.

The highest gold recovery, 35.25%, was observed at the lowest productivity, 1.8 tph (i.e. in the most quiet option of separation), but the rational level of productivity in this case was 3 tph. The gold grade in the pneumatic separation tailings is higher than in the concentrate in all cases, indicating the transfer of fine and bound gold into the tailings.

Table 5

Particle size distributions of -3+1 mm particle size class crushing cycles products

Particle size class (mm)	1 st cycle		2 nd cycle		3 rd cycle	
	Initial	After grinding	Initial	After grinding	Initial	After grinding
-0.071+0	0.00	4.11	0.00	4.10	0.00	2.64
-0.1+0.071	0.00	2.85	0.00	2.25	0.00	2.58
-0.2+0.1	0.00	14.24	0.00	14.13	0.00	15.10
-0.315+0.2	0.00	9.49	0.00	8.71	0.00	7.82
-0.5+0.315	0.00	9.18	0.00	10.39	0.00	10.57
-1+0.5	0.00	26.58	0.00	28.35	0.00	31.26
-1.6+1	64.06	25.95	68.66	25.61	70.35	24.73
-2.5+1.6	19.93	7.59	17.31	6.46	16.40	5.29
-3.2+2.5	16.01	0.00	14.03	0.00	13.25	0.00
Grinding degree	-	2.17	-	2.15	-	2.01

Table 6

Particle size distribution characteristics of grinding of crushing cycle products of -5+3 mm particle size class

Particle size class (mm)	1 st cycle		2 nd cycle		3 rd cycle	
	Initial	After grinding	Initial	After grinding	Initial	After grinding
-0.071+0	0.00	16.71	0.00	10.25	0.00	8.74
-0.1+0.071	0.00	6.48	0.00	4.30	0.00	4.14
-0.2+0.1	0.00	15.46	0.00	14.75	0.00	14.25
-0.315+0.2	0.00	7.23	0.00	9.22	0.00	9.20
-0.5+0.315	0.00	5.49	0.00	8.81	0.00	8.05
-1+0.5	0.00	13.72	0.00	18.03	0.00	17.24
-1.6+1	0.00	16.71	0.00	17.83	0.00	20.00
-2.5+1.6	0.00	6.73	0.00	6.35	0.00	6.90
-3.2+2.5	78.97	11.47	86.52	9.22	74.40	10.34
-5+3.2	21.04	0.00	13.48	1.23	25.60	1.15
Grinding degree	-	3.59	-	3.34	-	3.05



Results of the GRG test

GRG test was conducted with the initial ore sample weighing 65 kg at the ITOMAK-0.1 centrifugal concentrator in the following modes: solid sludge productivity – 100 kg/h; pulp productivity – 0.37 m³/h; maximum consumption of flushing water – 2.5 m³/h.

The solids content in the slurry fed to gravity separation was 25–30%. This test was performed in three stages. At the 1st stage, ore sample weighing 65 kg was crushed in the impact crusher DAU-250 to 100% passing 1.0 mm, and the crushed ore was passed through ITOMAK-0.1 concentrator. Next, the tailings of the first stage were re-ground to 80% passing 0.315 mm and processed at the ITOMAK concentrator. At the 3rd stage, the tailings of the 2nd stage were re-ground to 88% passing 0.071 mm. During the process at all stages, samples were taken from the tailings for particle size distribution analysis. All gravity concentrates and tailings of the ITOMAK centrifugal concentrator were sampled for particle size distribution determination as well as for gold fire assay.

The initial 65 kg sample was initially crushed to a particle size of –1 mm. For determining initial gold distribution by size class, sieving was carried out on sieves with mesh 0.63, 0.5, 0.315, 0.2, 0.1, 0.071 mm. From each resulting particle size class, subsamples were taken for fire assay. Based on the results of the assay, a table of gold distribution by particle size class was compiled (Table 8). The table shows that gold is unevenly distributed by size class. The highest gold grades were found in the fine –0.2 mm particle size classes, while the highest proportion of gold was contained in the –0.2+0.1 mm and –0.071 mm classes, 27.35% and 23.46%, respectively.

Beneficiation of this sample in the ITOMAK centrifugal concentrator produced concentrate weighing 2.573 kg and tailings weighing 61.327 kg. The resulting products were screened into particle size classes: –1+0.63 mm; –0.63+0.5 mm; –0.5+0.315 mm; –0.315+0.2 mm; –0.2+0.1 mm; –0.1+0.071 mm; –0.071 mm. The material from each particle size class was subjected to fire assay. The assay results and gold distribution in the first stage are presented in Table 9.

Table 7

Pneumatic separation results

No.	Product	Productivity, tph	Weight, g	Yield, %	Gold grade		Recovery E, %
					g	g/t	
	POS-9-1 separation		54,950	100.00	0.91	16.61	100.00
1	POS-9-1 concentrate	6	16,600	30.21	0.29	17.47	31.76
2	POS-9-1 tailings		30,107.5	54.79	0.55	18.20	60.02
3	POS-9-1 losses		8,242.5	15.00	0.08	9.10	8.22
	POS-9-2 separation			52,500	100.00	0.88	16.73
1	POS-9-2 concentrate	3	22,200	42.29	0.30	13.65	34.50
2	POS-9-2 tailings		22,425	42.71	0.38	17.10	43.66
3	POS-9-2 losses		7,875	15.00	0.19	8.55	21.83
	POS-9-3 separation		43,050	100.00	0.59	13.75	100.00
1	POS-9-3 concentrate	1.8	16,600	38.56	0.21	12.57	35.25
2	POS-9-3 tailings		19,992.5	46.44	0.33	16.50	55.75
3	POS-9-3 losses		6,457.5	15.00	0.05	8.25	9.00

Table 8

Distribution of gold by particle size class in the initial sample of –1.0 mm particle size

Particle size class (mm)	Yield, %	Weight, g	Au Grade (g/t)	Au proportion, %
–1+0.63	32.20	20,575.8	2.12	14.74
–0.63+0.5	6.80	4345.2	3.52	5.17
–0.5+0.315	13.20	8,434.8	3.78	10.77
–0.315+0.2	9.00	5751	3.48	6.76
–0.2+0.1	12.30	7,859.7	10.3	27.35
–0.1+0.071	6.30	4,025.7	8.64	11.75
–0.071+0	20.20	12,907.8	5.38	23.46
Total	100	63,900	4.63	100.00



The table shows that in the 1st stage of gravity separation of ore crushed to -1 mm particle size class, high proportions of gold belonged to the concentrates in the finer particle size classes (-0.2+0.1 mm; -0.1+0.071 mm; -0.071 mm), with a noticeable redistribution of gold into these classes with a total proportion of 83.72% in the -0.2 mm particle size class. As for tailings, all particle size classes showed roughly similar gold grades, but the coarse classes +0.2 mm demonstrated higher gold grades. The highest grade was found in -0.315+0.2 mm class, 8.8 g/t. This may be due to the presence of unreleased gold in these size class.

Further, the tailings obtained at the 1st stage of gravity separation were further milled in the laboratory ball mill (see Fig. 2) to 80% passing 0.315 mm and became the feed for the 2nd stage of gravity separation at the ITOMAK.

From this product, a 1,000 g subsample was taken for sieving and sampling for gold fire assay. The assay results and gold distribution are presented in Table 10.

As can be seen from the results presented in Table 10, after grinding the tailings of the 1st stage of gravity separation to 80% passing 0.315 mm, the residual

gold grade in the tailings of the first stage of concentration is redistributed evenly by size class. The gold grades range from 3.44 g/t (-0.5+0.315 mm class) to 6.66 g/t (for -0.1+0.071 mm class). The highest proportion of redistributed gold was found in the -0.2+0.1 and -0.071 mm classes, 26.19 and 25.79%, respectively.

The crushed tailings were sent to Stage 2 gravity separation at the ITOMAK concentrator. The concentrate weighing 2,210 kg and tailings weighing 57.117 kg were obtained. The obtained products were subjected to particle size analysis by particle size class: +0.315 mm; -0.315+0.2 mm; -0.2+0.1 mm; -0.1+0.071 mm; -0.071 mm. Gold grades were determined for each size class of each product obtained. The results are presented in Table 11.

The data presented in Table 11 shows that the proportion of gold in the concentrate (particle size class) passing 0.071 mm is 38.33%, while the maximum proportion of gold in the tailings belongs to the particle size class 0.2+0.1 mm and amounts to 30.98%. This is due to the fact that the ore is hard-dressable to a certain extent in terms of gold release, just as in the case of crushing the ore to -1 mm particle size, grinding to -0.315 mm did not release much of the gold present in the ore.

Table 9

Results of the GRG test Stage 1

Particle size class (mm)	Concentrate				Tailings			
	Yield, %	Weight, g	Au Grade (g/t)	Au distribution, %	Yield, %	Weight, g	Au Grade (g/t)	Au proportion, %
-1+0.63	21.72	558.93	13.0	3.35	12.30	7,543.22	4.12	9.64
-0.63+0.5	17.07	439.09	8.80	1.78	8.80	5,396.78	5.20	8.70
-0.5+0.315	17.02	438.03	21.6	4.36	12.60	7,727.20	5.08	12.18
-0.315+0.2	13.89	357.42	41.1	6.78	13.40	8,217.82	8.80	22.43
-0.2+0.1	21.39	550.45	115	29.20	22.60	13,859.90	4.96	21.32
-0.1+0.071	4.70	120.91	284	15.84	9.40	5,764.74	4.96	8.87
-0.071+0	4.20	108.18	775	38.68	20.90	12,817.34	4.24	16.86
Total	100	2573	84.24	100	100	61,327.00	5.26	100

Table 10

Particle size distribution and gold grades and proportions in ground tailings from Stage 1 gravity separation at ITOMAK concentrator

Particle size class (mm)	Yield, %	Weight, g	Au Grade (g/t)	Au proportion, %
-0.5+0.315	20.00	12,065.4	3.44	14.24
-0.315+0.2	17.10	10,315.917	4.40	15.58
-0.2+0.1	26.80	16,167.636	4.72	26.19
-0.1+0.071	13.20	7,963.164	6.66	18.20
-0.071+0	22.90	13,814.883	5.44	25.79
Total	100	60,327	4.83	100.00



The tailings obtained after the 2nd stage of gravity separation were ground to 88% passing 0.071 mm using the laboratory ball mill. As with the feed for the 2nd stage gravity separation at ITOMAK, the ground tailings became the feed for the 3rd gravity separation stage at the ITOMAK. A sample weighing 517 g was taken from the crushed tailings and subjected to particle size distribution analysis. The gold grade was assayed in each obtained particle size class.

As can be seen from the table, after grinding the tailings of the 2nd stage of gravity concentration to 88% passing 0.071 mm, most of the contained gold (89.27%) goes to the -0.071 mm particle size class.

The ground tailings were sent to Stage 3 gravity separation in the ITOMAK concentrator. A concentrate weighing 1.479 kg and tailings weighing 55.121 kg were obtained. Gold grades were assayed in each size class of each product obtained. The results are presented in Table 13.

Table 14 summarizes the GRG test results for the three ITOMAK gravity separation stages.

The table shows that the maximum gold content in the concentrate is in the -0.071 mm size class,

and the minimum value of gold content is in the tailings, while the distribution of gold in the concentrate and in the tailings is almost the same, with the maximum value belonging to the finer class passing 0.071 mm.

The test results established the initial ore grade at 8.44 g/t, which is consistent with the value for sample #1 (trench 500) obtained from through sample processing.

The highest gold recovery was achieved at the 1st stage of gravity separation (ore ground to -1 mm particle size class), in which 40.20% of released free gold were recovered into the concentrate, with 38.68% of which belonged to -0.071 mm particle size class. This indicates that gold contained in the ore is mainly represented by fine free gold particles of less than 71 microns in size that is confirmed by the test results presented in Table 9.

Grinding of tailings of the 1st stage to 80% passing 0.315 mm made it possible to extract additionally into concentrate 14.46% of released gold, which is also mainly represented by particle size class -0.071 mm and amounts to 38.33% (see Table 11).

Table 11

Results of the GRG test Stage 2

Particle size class (mm)	Concentrate				Tailings			
	Yield, %	Weight, g	Au Grade (g/t)	Au proportion, %	Yield, %	Weight, g	Au Grade (g/t)	Au proportion, %
-0.5+0.315	12.66	279.79	12.7	4.71	5.54	3,164.28	4.56	4.73
-0.315+0.2	32.97	728.64	21.1	20.38	18.90	10,795.11	7.80	27.58
-0.2+0.1	38.30	846.43	23.2	26.03	29.05	16,592.49	5.70	30.98
-0.1+0.071	8.92	197.13	40.4	10.56	16.43	9,384.32	4.40	13.53
-0.071+0	7.15	158.02	183	38.33	30.08	17,180.79	4.12	23.19
Total	100	2,210	34.14	100	100.00	57,117.00	5.34	100

Table 12

Particle size distribution and gold grades in the ground tailings of the 2nd stage of gravity separation at the ITOMAK concentrator

Particle size class (mm)	Yield, %	Weight, g	Au Grade (g/t)	Au distribution, %
-0.1+0.071	12.00	6,792	4.00	10.73
-0.071+0	88.00	49,808	4.54	89.27
Total	100	56,600	4.48	100.00

Table 13

Results of the GRG test Stage 3

Particle size class (mm)	Concentrate				Tailings			
	Yield, %	Weight, g	Au Grade (g/t)	Au proportion, %	Yield, %	Weight, g	Au Grade (g/t)	Au proportion, %
-0.1+0.071	32.14	475.35	35.40	16.19	11.46	6,316.87	2.32	11.29
-0.071+0	67.86	1,003.65	86.80	83.81	88.54	48,804.13	2.36	88.71
Total	100	1,479	70.28	100.00	100	55121.00	2.36	100



Table 14

Summary table of GRG test results

Product	Yield, %	Weight, g	Au Grade (g/t)	Au distribution (Au proportion), %
Stage 1 – 100% passing 1 mm				
Concentrate 1	4.03	2,573.00	84.24	40.20
Tailings 1	95.97	61,327.00	5.26	59.80
Feed (ore)	100.00	63,900.00	8.44	100.00
Stage 2 – 80% passing 0.315 mm				
Concentrate 2	3.73	2,210	34.14	19.82
Tailings 2	96.27	57,117	5.34	80.18
Feed (tailings 1)	100	59,327	6.42	100.00
Stage 3 – 88% passing 0.071 mm				
Concentrate 3	2.61	1,479	70.28	44.46
Tailings 3	97.39	55,121	2.36	55.54
Feed (tailings 2)	100	56,600	4.13	100.00
Total				
Concentrate 1	4.19	2,573.00	84.24	38.57
Concentrate 2	3.60	2,210.00	34.14	14.46
Concentrate 3	2.41	14,79.00	70.28	20.88
Tailings 3	89.80	55,121.00	2.36	26.08
Feed – ore	100.00	61,383.00	8.79	100.00

When the 2nd stage tailings were milled to 88% passing 0.071 mm, 20.88% of the released gold was additionally recovered into the concentrate, which is also mostly in the –0.071 mm particle size class and amounts to 83.81% (see Table 13).

Thus, the results of the standard GRG test showed the following: from the ore milled to 100% passing 1 mm, 38.57% of gold are recovered into the concentrate; from the tailings of the 1st stage after regrinding to 80% passing 0.315 mm, 14.46% of gold are recovered into the concentrate.

The total recovery to the gravity concentrate obtained after the first and second stages of grinding was 53.03%. Grinding of 2nd stage gravity separation tailings to 88% passing 0.071 mm enabled obtaining additionally a gravity concentrate 3 containing 70.28 g/t gold at a recovery of 20.88%. The total gold recovery into the three gravity concentrates (1+2+3) amounted to 73.91%.

Discussion of the test results

Au grade in ore samples from Arkachan deposit provided for the study, namely, sample No.1 (trench 500), 7.95 g/t and No.2 (trench 600), 11.28 g/t was redetermined based on the results of processing and balance calculations.

Ore quality in terms of gold grade in the tested samples is high, but in contrast to the data of the geological report, the polydispersity of gold is not

confirmed, i.e. we are talking only about dispersed gold particles passing 100 µm or impregnated gold, presumably in pyrite. For this ore the existing technology of dry separation is inefficient, as the applied technology of dry grinding in a step centrifugal mill does not release such dispersed gold; in addition, the process of pneumatic separation doesn't provide required beneficiation, despite the fact that the process of gold release and its redistribution into fine particle size classes is observed to some extent.

A detailed study of the feasibility of pneumatic dry ore separation requires more thorough post-fine grinding studies at the laboratory level rather than at the bulk test level.

The processing of the pneumatic separation products by gravity separation methods showed the feasibility of gold recovery, which requires a high degree of grinding, 80% passing 0.071 mm. This conclusion is confirmed by historical GRG tests performed in TsNIGRI.

Conclusions

The research on the processing of the Arkachan deposit ore samples for assessing efficiency of dry separation technology to obtain highly concentrated gold-containing products allowed establishing the following:

– the experimental studies and balance calculations determined the gold grade in the studied



samples: in sample No. 1 (trench 500), 7.95 g/t and in sample No. 2 (trench 600), 11.28 g/t, with gold in the samples occurs in finely dispersed form (less than 100 μm) and impregnated in mineral, presumably in pyrite;

– the studies of the crushing process in DKD-300 in cyclic mode show quite a high result in terms of crushing degree in the initial ore sample: for sample No. 1 (trench 500) in the first cycle – 9.35, in the second cycle – 2.28, in the third cycle – 2.02; for sample No. 2 (trench 600) the crushing degrees were 9.23, 2.89, and 2.16 in the corresponding cycles;

– the studies of the grinding process of the crushing products passing 5 mm in the TsMVU-800 centrifugal mill showed that the grinding is generally effective for obtaining the bulk of the ore in fraction passing 1 mm in two cycles; the total yield of the control particle size class -0.071 mm for the size class $-5+3$ mm is 27.5%, for the size class $-3+1$ mm, 16.2%, which corresponds to the indicators of conventional coarse grinding;

– the release of gold (unlocking intergrowths) is confirmed by redistribution and selective concentration of gold into -3 mm particle size classes in the crushing processes with a degree of concentration of 1.51 for sample No. 2 (trench 600) and 1.52 for sample No. 1 (trench 500), as well as redistribution of gold into -0.071 mm class in the grinding processes and in the GRG test;

– the beneficiation of gold by pneumatic separation in the POS-2000 failed due to too coarse grinding at the TsMVU-800 centrifugal mill;

– the GRG test showed that for more efficient gravity separation of gold, up to 73.91%, the degree of grinding up to 80% passing 0.071 mm is required, allowing obtaining a gravity concentrate graded at 70.28 g/t gold;

– dry beneficiation as applied to the ores of Arkachan deposit is technologically inefficient. Additional laboratory studies of pneumatic separation processes at high degree of ore materials grinding are required.

References

1. Yusupov T.S. Improvement of dissociation of rebellious minerals. *Journal of Mining Science*. 2016;52(3):559–564. <https://doi.org/10.1134/S1062739116030825> (Orig. ver.: Yusupov T.S. Improvement of dissociation of rebellious minerals. *Fiziko-Tekhnicheskiye Problemy Razrabotki Poleznykh Iskopayemykh*. 2016;(3):143–149. (In Russ.))
2. Sotoudeh F., Nehring M., Kizil M.S., Knights P. Integrated underground mining and pre-concentration systems; a critical review of technical concepts and developments. *International Journal of Mining, Reclamation and Environment*. 2020;35(3):153–182. <https://doi.org/10.1080/17480930.2020.1782573>
3. Lakshmanan V.I., Ojaghi A., Gorain B. Beneficiation of gold and silver ores. In: Lakshmanan V., Gorain B. (eds) *Innovations and Breakthroughs in the Gold and Silver Industries*. Springer, Cham; 2019. https://doi.org/10.1007/978-3-030-32549-7_4
4. Levanskii E.I., Levanskii A.E., Garabagiu A.A. Energy-saving rotor-centrifugal mills for the grinding of bulk and lumpy materials. In: *Resource- and energy-saving technologies in the Chemical and Petrochemical Industry. Materials of the International Scientific and Technical Conference*. Minsk: BSTU; 1998. Pp. 36–38. (In Russ.)
5. Klushantsev B.V., Kosarev A.I., Muizemnek Yu.A. Crushers. *Designs, calculation, peculiarities of operation*. Moscow: Mashinostroenie Publ.; 1990. 320 p. (In Russ.)
6. Revnivitsev V.I., Gaponov G.V., Zarogatsky L.P. et al. *Selective desintegration of minerals*. Revnivitsev V.I. (Eds.) Moscow: Nedra Publ.; 1988. 285 p. (In Russ.)
7. L'vov E.S., Matveev A.I. Studying the formation of particle size distribution and disclosure of minerals in ore crushing mill using multiple dynamic action DCD-300. *Mining Informational and Analytical Bulletin*. 2014;(10):112–116. (In Russ.)
8. Matveev A.I., L'vov E.S., Osipov D.A. Use of the combined impact crusher DKD-300 in the dry concentration scheme at Zarnitsa kimberlite pipe. *Journal of Mining Sciences*. 2013;(4):107–115. (In Russ.)
9. Matveev A.I., L'vov E.S., Zaikina A.V. Dissociation of gold ore from Gurbey deposit under impact effects. *Journal of Mining Sciences*. 2021;(2):141–151. (In Russ.)
10. Matveev A.I., L'vov E.S. Disintegratability procedure for geomaterials in multiple impact crushing. *Journal of Mining Sciences*. 2020;(2):137–143. (In Russ.)
11. Nunna V., Hapugoda S., Eswarappa S.G. et al. Evaluation of dry processing technologies for treating low grade lateritic iron ore fines. *Mineral Processing and Extractive Metallurgy Review*. 2022;43(3):283–299. <https://doi.org/10.1080/08827508.2020.1837127>



12. Tripathy S.K., Banerjee P.K., Suresh N. et al. Dry high-intensity magnetic separation in mineral industry – a review of present status and future prospects. *Mineral Processing and Extractive Metallurgy Review*. 2017;38(6):339–365. <https://doi.org/10.1080/08827508.2017.1323743>
13. Chelgani S.Ch., Neisiani A.A. *Dry mineral processing*. Springer Cham; 2022. 156 p. <https://doi.org/10.1007/978-3-030-93750-8>
14. Shishkin S.F., Dzyuzer V. Ya., Shishkin A.S. Air Classification of Sands for the Glass Industry. *Glass and Ceramics*. 2001;58(11):370–373. <https://doi.org/10.1023/A:1014997923206>
15. Surimbayev B.N., Kanaly E.S., Bolotova L.S., Shalgymbayev S.T. Assessment of gravity dressability of gold ore – GRG test. *Mining Science and Technology (Russia)*. 2020;5(2):92–103. <https://doi.org/10.17073/2500-0632-2020-2-92-103>
16. Brochot S. Sampling for metallurgical test: how the test results can be used to estimate their confidence level. In: *XXVIII International Mineral Processing Congress*. September 11–15, 2016. Québec City Convention Center, Québec City, Canada.
17. Myrzaliev B.M., Nogaeva K.A., Molmakova M.S. Determination of Jamgyr deposit ore gravity concentration feasibility. *Proceedings of Irkutsk State Technical University*. 2018;22(10):153–165. (In Russ.) <https://doi.org/10.21285/1814-3520-2018-10-153-165>
18. Koppalkar S., Bouajila A., Gagnon C., Noel G. Understanding the discrepancy between prediction and plant GRG recovery for improving the gold gravity performance. *Minerals Engineering*. 2011;24(6):559–564. <https://doi.org/10.1016/j.mineng.2010.09.007>
19. Laplante A.R. *A Standardized Test to Determine Gravity Recoverable Gold*. 2000. Available from: <http://knel-onrussian.xplore.com/sites/knelsongravity/files/reports/report21s.pdf> [Accessed: 07.03.2020].
20. Laplante A.R., Dunne R.C. The Gravity recoverable gold test and flash flotation. In: *Proceeding 34th Annual Meeting of the Canadian Mineral Processors*. January 22–24, 2002. Ottawa, Canada. Available from: <http://seprosys-tems.com/language/wp-content/uploads/2016/09/laplante.pdf> [Accessed: 10.03.2020].
21. Surimbayev B., Bolotova L., Esengaraev E., Mazyarkina L. The study of gravity separation of gold-bearing ores of the Raigorodok deposit. *Industry of Kazakhstan*. 2017;101(2):40–42 (In Russ.)

Information about the authors

Andrey I. Matveev – Dr. Sci. (Eng.), Head of the Laboratory, Federal Research Center “Yakutsk Research Center of the Siberian Branch of the Russian Academy of Sciences” N.V. Chersky North Mining Institute, Siberian Branch of the Russian Academy of Sciences, Yakutsk, Russian Federation; ORCID [0000-0002-4298-5990](https://orcid.org/0000-0002-4298-5990); e-mail andrei.mati@yandex.ru

Ivan F. Lebedev – Cand. Sci. (Eng.), Senior Researcher, Federal Research Center “Yakutsk Research Center of the Siberian Branch of the Russian Academy of Sciences” N.V. Chersky North Mining Institute, Siberian Branch of the Russian Academy of Sciences, Yakutsk, Russian Federation; ORCID [0000-0003-1116-8872](https://orcid.org/0000-0003-1116-8872); e-mail ivleb@mail.ru

Vasiliy R. Vinokurov – Researcher, Federal Research Center “Yakutsk Research Center of the Siberian Branch of the Russian Academy of Sciences” N.V. Chersky North Mining Institute, Siberian Branch of the Russian Academy of Sciences, Yakutsk, Russian Federation; ORCID [0000-0001-5698-7922](https://orcid.org/0000-0001-5698-7922); e-mail vaviro@mail.ru

Evgenii S. Lvov – Researcher, Federal Research Center “Yakutsk Research Center of the Siberian Branch of the Russian Academy of Sciences” N.V. Chersky North Mining Institute, Siberian Branch of the Russian Academy of Sciences, Yakutsk, Russian Federation; ORCID [0000-0002-3843-0714](https://orcid.org/0000-0002-3843-0714); e-mail lvoves@bk.ru

Received 11.10.2023

Revised 01.02.2024

Accepted 15.02.2024







SAFETY IN MINING AND PROCESSING INDUSTRY AND ENVIRONMENTAL PROTECTION

Research paper

<https://doi.org/10.17073/2500-0632-2023-12-188>

UDC 550.424:504.064.2:631.4

**Geoenvironmental assessment of different types of cryolithic soils in Western Yakutia under the conditions of diamond-mining operations**A. S. Titov¹ , A. S. Toropov²   ¹ ECOSTANDARD Technical Solutions LLC, Moscow, Russian Federation² Lomonosov Moscow State University, Moscow, Russian Federation torop990@gmail.com**Abstract**

The problems of geoenvironmental consequences of mining operations are especially acute in the arctic and subarctic regions, where the spread of permafrost significantly reduces the buffering capacity of landscapes. The article presents data on the content of heavy metals in the soil cover of the transient zone between the middle taiga and north taiga landscapes of Western Yakutia under the conditions of mining operations and assesses the resistance of different types of soils to heavy metals pollution. Field and laboratory works were carried out in August 2022. The heavy metals content was determined by atomic absorption spectrometry. Specialized software was used for analysis, such as MS Excel 2013, Statistica 12.0, and QGIS 3.26.1. Calculation of organic forms of heavy metals in soil solutions was performed using the NICA-Donnan model. In the course of studies, the structure of the soil cover in the Nakyn kimberlite field in the conditions of the mining industrial complex operation was determined and a sketch map of the soil cover of the territory was compiled. The geochemical series of the studied heavy metals is as follows according to the degree of concentration of heavy metals in cryolithic soils: Pb > Zn > Ni > Cu > Cd > As > Hg. Positive correlations between humus and Cd, Pb, Zn, as well as the occurrence of synergism in the Pb–Cd, Zn–Pb, Zn–Cu pairs were revealed. The soils organic matter enhances migration of heavy metals. The man-made input of Ni and Zn in cryolithic soils will lead to increase of mobile fraction. Cd is more mobile in pale-yellow carbonate and cryogenic soils. The regional background level of heavy metals for these types of soils was calculated, which can be used in future works when the intensity of mining operations increases.

Keywords

heavy metals, soil pollution, taiga-frozen soils, cryogenic soils, diamond mining, Nyurba kimberlite field, arsenic (As), cadmium (Cd), mercury (Hg), lead (Pb), copper (Cu), nickel (Ni), zinc (Zn), Western Yakutia, speciation, geochemistry, thermodynamic modeling, NICA-Donnan.

Acknowledgments

The authors thank the team of the testing laboratory of ECOSTANDARD Technical Solutions LLC for providing containers, reagents and performing analytical studies, as well as the management of ECOSTANDARD Technical Solutions LLC for arranging the field work. The work on the study of migration forms of heavy metals was supported by the RSF grant No. 23-27-00140.

For citation

Titov A. S., Toropov A. S. Geoenvironmental assessment of different types of cryolithic soils in Western Yakutia under the conditions of diamond-mining operations. *Mining Science and Technology (Russia)*. 2024;9(2):170–182. <https://doi.org/10.17073/2500-0632-2023-12-188>

ТЕХНОЛОГИЧЕСКАЯ БЕЗОПАСНОСТЬ В МИНЕРАЛЬНО-СЫРЬЕВОМ КОМПЛЕКСЕ И ОХРАНА ОКРУЖАЮЩЕЙ СРЕДЫ

Научная статья

Геоэкологическая оценка разных типов почв криолитозоны Западной Якутии в условиях функционирования алмазодобывающих предприятийА. С. Титов¹ , А. С. Торопов²   ¹ ООО «ЭКОСТАНДАРТ «Технические решения», г. Москва, Российская Федерация² Московский государственный университет им. М.В. Ломоносова, г. Москва, Российская Федерация torop990@gmail.com**Аннотация**

Проблемы геоэкологических последствий горнодобывающих предприятий стоят особенно остро в арктических и приарктических районах, где распространение вечной мерзлоты значительно сокращает буферные способности ландшафтов. В статье представлены данные о содержании тяжелых



металлов в почвенном покрове переходной зоны от среднетаежных к северотаежным ландшафтам Западной Якутии в условиях функционирования горнодобывающего производства и предложены подходы к оценке устойчивости разных типов почв к загрязнению тяжелыми металлами. Полевые и лабораторные работы проведены в августе 2022 г. Определение содержания тяжелых металлов проводилось методом атомно-абсорбционной спектрометрии. Для анализа использовалось специализированное программное обеспечение – MS Excel 2013, Statistica 12.0, QGIS 3.26.1. Расчет органических форм нахождения тяжелых металлов в почвенных растворах выполнен с помощью модели NICA-Donnan. В ходе исследования определена структура почвенного покрова Накынского кимберлитового поля в условиях функционирования горнопромышленного комплекса и составлена карта-схема почвенного покрова территории. Геохимический ряд изученных тяжелых металлов по степени концентрирования тяжелых металлов в почвах криолитозоны: $Pb > Zn > Ni > Cu > Cd > As > Hg$. Выявлены положительные зависимости между гумусом и Cd, Pb, Zn, а также проявление синергизма в парах Pb–Cd, Zn–Pb, Zn–Cu. Органическое вещество почв усиливает миграцию тяжелых металлов. Технологическое поступление в почвы криолитозоны Ni и Zn приводит к росту доли их подвижных форм. В пацево-карбонатных и криоземах в большей степени подвижен Cd. Рассчитан региональный фоновый уровень тяжелых металлов для данных типов почв, который может быть использован в будущих работах при увеличении интенсивности горнодобывающих работ.

Ключевые слова

тяжелые металлы, загрязнение почв, таежно-мерзлотные почвы, криозёмы, алмазодобыча, нюрбинское кимберлитовое поле, мышьяк (As), кадмий (Cd), ртуть (Hg), свинец (Pb), медь (Cu), никель (Ni), цинк (Zn), Западная Якутия, формы миграции, геохимия, термодинамическое моделирование, NICA-Donnan

Благодарности

Авторы благодарят коллектив испытательной лаборатории ООО «ЭКОСТАНДАРТ «Технические решения» за предоставление тары, реагентов и выполнение аналитических исследований, а также руководство ООО «ЭКОСТАНДАРТ «Технические решения» за организацию полевых работ. Работа по изучению миграционных форм тяжелых металлов выполнена при поддержке гранта РФФ 23-27-00140.

Для цитирования

Titov A. S., Toropov A. S. Geoenvironmental assessment of different types of cryolithic soils in Western Yakutia under the conditions of diamond-mining operations. *Mining Science and Technology (Russia)*. 2024;9(2):170–182. <https://doi.org/10.17073/2500-0632-2023-12-188>

Introduction

Large industrial complexes influence the change in physical and chemical parameters of cryolithic soils [1], affect the functioning of the soil cover directly and determine the intensity of its man-made pollution [2]. Man-made pollution of soils spreads along the prevailing wind direction over considerable distances by atmospheric transfer of pollutants formed during the operation of heavy machinery [3] and dusting processes [4]. The territories of the permanent allotment are almost completely transformed [5], natural landscapes are converted into man-made ones, and beyond its boundaries local areas characterized by the increased content of chemical elements may be formed [6].

The location of large industrial complexes in subarctic regions, where the soil profile is thin, the drainage of the territory is poor, and permafrost rocks are widespread, requires a deeper study of the geoenvironmental consequences of mineral extraction [7], as they have a negative impact on the ability of soils to self-restore. This is also noted by a number of authors [8].

The above factors make it necessary to study heavy metals in the soil cover of the cryolithic zone near operating industrial complexes to form a da-

tabase for complex geoenvironmental research and monitoring [9]. The relevance of the study of the natural environment geochemical features in the Far East of the Russian Federation, also in the conditions of active cryogenic processes, is emphasized by the availability of recent studies in such regions [10].

The research was conducted in the Nyurba District of the Republic of Sakha (Yakutia) within the Nakyn kimberlite field (NKF) [11] (Fig. 1). The purpose of the study was to analyze the features and distribution patterns of the gross content along with the assessment of migration features associated with the organic matter of heavy metals (HM) in cryolithic soils under the conditions of diamond mining operations.

To achieve this goal the following tasks were set and solved: to conduct field geoenvironmental studies in the territory under consideration and soil sampling, to determine the main chemical indicators and the actual content of HM in soils, to determine the main distribution patterns of HM depending on chemical indicators and the soil type, to establish the forms of occurrence of HM in water extracts, and to calculate the background values of the gross content of Cd, Hg, Ni, Cu, Zn, Pb, and As for further studies.

The NKF is located within the Siberian platform composed of metamorphic rocks of the Archean age, overlain by a thick sedimentary cover of the V–J age. In terms of the regional tectonic structure, the NKF is located at the junction of the Nepsko-Botuobinsky antecline, the Syugdzhersky saddle and the Vilyui syncline. The relief of the territory is denudational. It is represented by a slightly sloping plain, which is structurally confined to the macroslope of the Markha-Khannya-Nakyn interfluvium. The absolute elevations are 220–248 m.

The climate of the area is extreme continental. The northwestern wind direction prevails (27%), although calms dominate (36%). The territory is dissected by a ravine and gully network. The main water artery is the Dyakhtar-Yuryage River (a tributary of the Markha River). The soil cover belongs to the group of taiga-frost soils. According to geobotanical zoning the territory belongs to the boreal vegetation kingdom of the Central Siberian province with the predominance of *Larix Gmelinii* (Rupr.) [11].

Objects and methods of research

Field work was carried out in 2022 on the territory of transitional landscapes of the Markha-Khannya-Nakyn interfluvium (Fig. 2). A part of the research was carried out within the sanitary protection zone (SPZ) of the mining complex, and a part outside the SPZ, in the ratio of 40/60. To determine the content of heavy metals in the soil cover of the adjoining territory, test sites with the soil structure survey points were allocated. Soil by-pits were arranged throughout the territory, and soil sections were studied at the sites

with different biotopes to the depth of permafrost occurrence. The test sites were arranged, considering the wind rose: a half of the test sites was arranged on the leeward side, and the other half on the windward side. The main sources of possible soil cover pollution at this location are the site of immediate field development and its infrastructure.

Sampling and sample transportation were carried out in accordance with the methods generally accepted in the geoenvironmental studies¹. A total of 54 samples were collected at 27 sampling locations in the surveyed area.

The gross content of the following heavy metals was determined in the collected samples: Cd, Hg, Ni, Cu, Zn, Pb, and As by atomic absorption spectrometry using the Kvant-Z spectrometer. The physical and chemical parameters were determined by potentiometric method (pH), the content of organic matter was determined by colorimetry according to I.B. Tyurin, the particle-size distribution was defined in field conditions according to Kachinsky, and laboratory studies were performed by sieve analysis. The quantitative data obtained were processed using the Microsoft Excel 2013, Statistica 12.0 software, and cartographic material was compiled using the Quantum GIS 3.26.1 software.

¹ All-Union instruction on soil surveys and compilation of large-scale soil maps of land use, GOST 17.4.4.02 "Nature protection. Soils. Methods for sampling and preparation of soil for chemical, bacteriological, helminthological analysis".

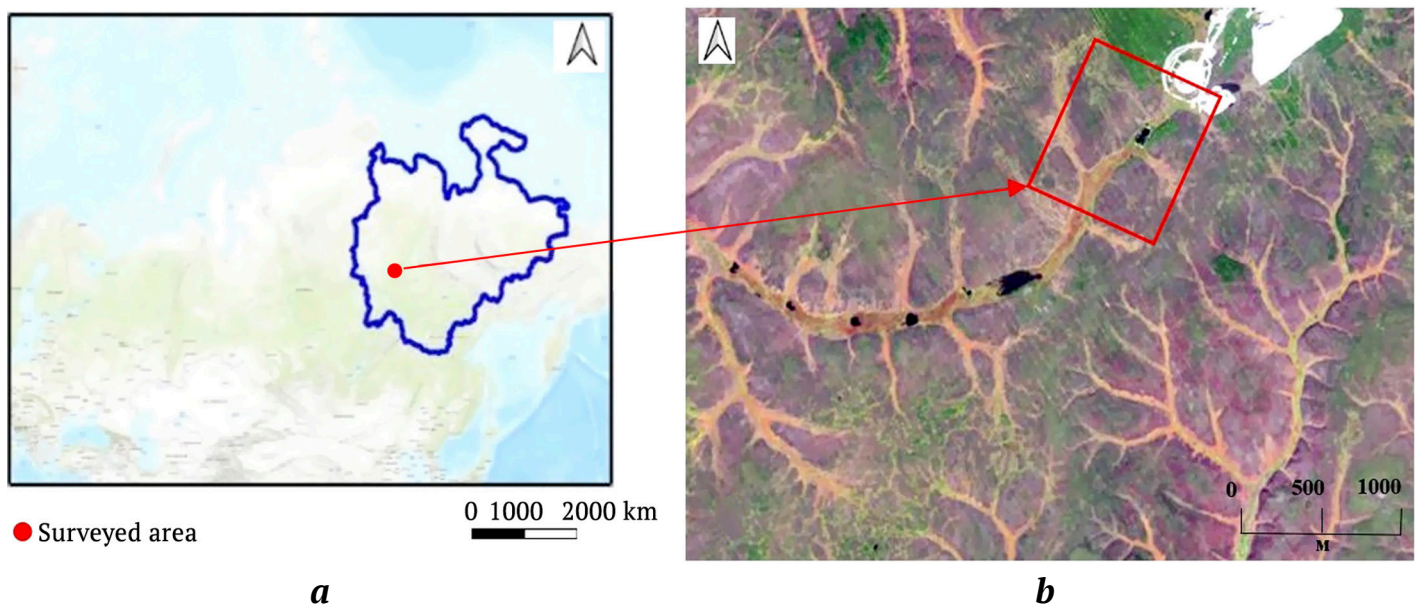


Fig. 1. Sketch map of the studied area: *a* – relative to the Russian Federation; *b* – satellite image of the surveyed area in R–G–B

The standard calculation of the total pollution indicator – Z_c [12] was used for integral assessment:

$$Z_c = \sum (K_{c_i} + \dots + K_{c_n}) - (n - 1),$$

where K_{c_i} is the coefficient of concentration of the i -th component; n is the number of the summed K_{c_i} ,

$$K_{c_i} = \frac{C_i}{C_b},$$

where C_i is the actual content of the element; C_b is the background content of the element.

The ranking has been adopted conditionally in accordance with the current RD: 16 – permissible; 16–32 – moderately dangerous; 32–128 – dangerous; ≥ 128 – extremely dangerous [12].

The migration patterns of elements in the water-soluble fraction (1 : 10) of soils were calculated using the Minteq 3.1 complex, taking into account pH, the main anions and cations, and the dissolved organic carbon concentrations according to the NICA-

Donnan model with the fulvic acids to humic acids ratio of 1 : 8.

To assess the environmental state of soils it is customary to use the reference (background) content of various elements in them, but to date, extensive background studies for the gross content of HM for this area or in similar conditions have not been conducted. A comparison is proposed based on our own background studies, $n = 5$.

Results and discussion

Cryogenic soils, pale-yellow carbonate soils and peat-bog soils are common within the surveyed area (Fig. 3).

High-frost homogeneous cryogenic soils (Fig. 4, *a*) are up to 42 cm thick, structureless, running. The particle-size distribution is close to light loams, and the permafrost surface is undulate. The upper levels are weakly acidic, neutralized with depth, and the soil acidity is in direct correlation with organic matter, which is typical for such soils [13].



a



b

Fig. 2. Soil cover research: *a* – preparation for test pit drive; *b* – test pit drive

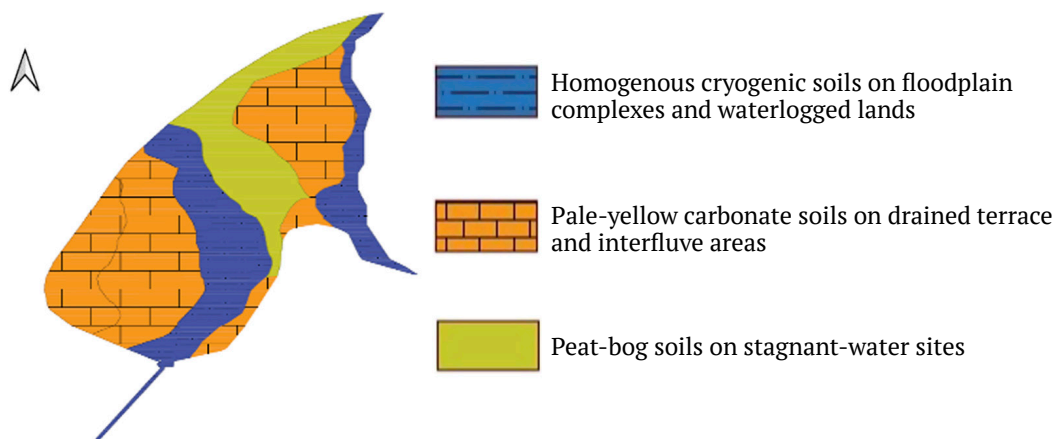


Fig. 3. Schematic map of soil conditions of the surveyed area (1 : 5000)

Peat-bog soils (Fig. 4, *b*) have been formed within oligotrophic bogs and in areas of local depressions. These soils are developed to a depth of 40 cm, and the lower level is waterlogged.

Pale-yellow carbonate soils (Fig. 4, *c*) are dominant in the surveyed area and occupy up to 69% of the territory. This type of soil has a greater profile thickness – up to 64 cm, has been formed on sandy-light loamy substrate in the old bed of the Dyakhtar Yuryage River, and the permafrost layer is under alluvial sediments.

Cryogenic soils occupy mainly slightly sloping areas of the Dyakhtar-Nakyn interfluvium and are formed on cryogenic landforms (Fig. 5, *a* – boolgunyakhs, weakly polygonal relief). The subtype is homogeneous thin high-frost cryogenic soils. They are diagnosed mainly by cryoturbation traces within the profile [14].

Peat-bog soils (Fig. 5, *b*) are confined to the Dyakhtar-Yuryage River valley (Fig. 5, *b*). The studies showed that soil groupings have a relatively homogeneous structure and thickness. The vegetation cover is homogeneous, with *Larix Gmelinii* as the dominant species in the stand, and the *Betula Alba* (Roth.) birch as an admixture; the state of the stand in interfluvial and terrace complexes is suppressed, with dechromation and, less often, defoliation observed; in floodplain complexes it is satisfactory [15].

Pale-yellow carbonate soils (Fig. 5, *c*). They are formed both on solid masses of *Larix Gmelinii* and on forest edges covered mainly with shrubby species – cowberry *Vaccinium vitis-idaea* (L.) Avror., blueberry *Vaccinium uliginosum* (L.), waterberry *Empetrum nigrum* (L.), on extensive thickets of cladonia *Cladonia stellaris* (Opiz.) Pouzar&Vezda and *Cladonia rangiferina* (L.) Weber&Wigg (Fig. 5, *c*).

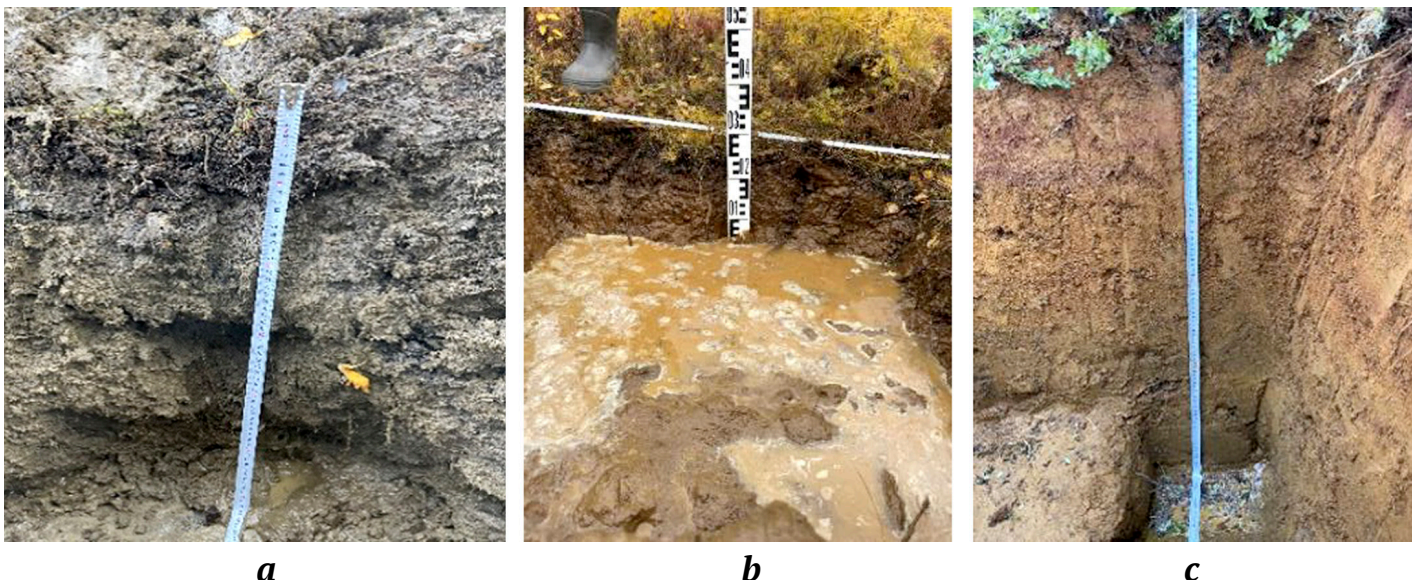


Fig. 4. Characteristic structure of the soil profile:
a – studied cryogenic soils; *b* – peat-bog soils; *c* – pale-yellow carbonate soils



Fig. 5. Overview of the sites:
a – intersected cryogenic soils; *b* – peat-bog soils; *c* – pale-yellow carbonate soils



The studied cryogenic soils are characterized by a generally low humus content in the upper level ($0.73 \pm 0.05\%$ on average) with an abrupt characteristic increase in the lower layer due to cryoturbation ($V = 12/56\%$) (Table 1). The clay fraction is relatively homogeneous in the range of 24.0–29.1%, which corresponds to heavy sandy-light loamy soils. The reaction of the medium in the studied levels varies from slightly acidic to slightly alkaline, and there is no characteristic distribution in the levels due to cryoturbation.

The humus content in the upper levels of pale-yellow carbonate soils is generally uniform, and in the underlying level the humus content decreases abruptly. The clay fraction varies from 16.8 to 39.1%

in the upper level and 20–31% in the lower level, which corresponds to light loams with insignificant sandy loam interlayers. The reaction of the medium is typical for pale-yellow carbonate soils – it varies from acidic to alkaline with depth throughout the profile.

In peat-bog soils the total humus content decreases noticeably, and the medium changes from neutral to slightly acidic-acidic with depth. The content of physical clay is from 9 to 29%, which corresponds to sandy and light loamy soils.

The highest humus content is observed in the peripheral parts of the surveyed area in close proximity to the transport and industrial infrastructure facilities on the windward side. With a relative homogeneity of soil and vegetation conditions, the differences in the

Table 1

Results of chemical studies of collected soils

Indicator	Level	Depth, cm	Variation range	Mean and error $\bar{x} \pm S_x$	Coefficient of variation $V, \%$
Homogeneous high-frost cryogenic soils					
Humus, %	T	7...24	0.60...0.83	0.73 ± 0.05	12
	Cr	24...43	0.42...2.44	1.29 ± 0.36	56
pH (aqueous)	T	7...24	6.8...7.1	7.00 ± 0.06	2
	Cr	24...43	6.1...7.6	6.93 ± 0.27	8
pH (salt)	T	7...24	3.9...4.6	4.25 ± 0.01	7
	Cr	24...43	4.5...6.7	5.13 ± 0.46	18
Physical clay, %	T	7...24	22.3...26.7	24.0 ± 0.9	7
	Cr	24...43	24.0...36.7	29.10 ± 2.62	18
Pale-yellow carbonate soils					
Humus, %	A _{1K}	2...26	0.95...8.53	1.9 ± 0.7	116
	B _K -BC _K	26...53	0.2...3.6	0.8 ± 0.3	119
pH (aqueous)	A _{1K}	2...26	5.1...5.9	5.60 ± 0.09	6
	B _K -BC _K	26...53	6.2...7.1	6.85 ± 0.08	4
pH (salt)	A _{1K}	2...26	4.1...5.9	4.10 ± 0.17	4
	B _K -BC _K	26...53	4.1...4.4	4.25 ± 0.04	12
Physical clay, %	A _{1K}	2...26	16.8...39.1	30.50 ± 2.14	27
	B _K -BC _K	26...53	20.2...40.0	27.05 ± 1.34	22
Peat-bog soils					
Humus, %	O	5–14	0.8...5.8	2.36 ± 0.80	77
	T	14–36	0.1...1.3	0.80 ± 0.22	61
pH (aqueous)	O	5–14	5.6...7.3	6.76 ± 0.30	9
	T	14–36	5.5...6.2	6.00 ± 0.11	4
pH (salt)	O	5–14	4.1...5.5	4.6 ± 0.2	11
	T	14–36	3.6...4.0	3.84 ± 0.06	4
Physical clay, %	O	5–14	21.5...28.3	25.12 ± 1.10	10
	T	14–36	9.0...29.9	22.20 ± 3.14	32

Note. Designations of soil levels are given in accordance with the 2004 soil classification.



humus content can be characterized by an increase in the content of not only humus, but also a non-humic part of organic matter due to the input of the man-made impact [16]. The latter is reflected in the shift of the soil medium towards acidic one and increased migration properties with a natural increase in the concentration of HM in the future [17].

The HM content is relatively homogeneous (Table 2); practically no sharp peaks are observed in the sample, and the increased content is noted for all the studied HM (except for As and Hg). Accumulation occurs in the upper levels for Ni, Cu, less frequently for Cd, and in the lower levels mainly for Cd, Pb, and Zn. Nevertheless, such differences are weakly contrast. An increasing contrast of metal accumulation in soil levels will indicate an increase in the man-made load and landscape transformation.

According to the average values, the HM content is higher in lower levels. Analyzing the nature of HM accumulation, we can say that the upper levels accumulate HM mainly through the mechanism of their sorption by organic components under the conditions of weakly acidic medium and weak drainage – mainly oxygen sorption physical and chemical barriers are formed. The lower levels are characterized by accumulation under the conditions of neutral and weakly alkaline medium, and weak development of gley processes in the soil profile for these depths is noted in the form of bluish spots and leather coatings. Thus,

the conclusion about the formation of gley alkaline physical and chemical barriers in above-permafrost levels is fair [14]. The HM content in the upper layer in the descending order can be written in the following form: $Pb > Zn > Ni > Cu > Cd > As > Hg$.

For the lower layers the record is identical, and only the concentrations of individual elements change. At the same time, the content of Pb, Zn, Cu in peat-bog soils is higher than in pale-yellow soils and cryogenic soils. This is due to the higher humus content in the soil profile and geochemical specifics (Fig. 6).

Considering very homogeneous spatial distribution of HM in the soil surface layer both from the windward and leeward sides, it can be concluded that there is no or hard-to-diagnose (by available methods) man-made impact as such, the exception being a few test sites sampled in the zone of direct adjoining to the waste dump. Here, maximum concentrations of the studied HM are recorded. However, considering the metallogeny of the area, this may also have a predominantly natural origin, since the ratio of ore elements is preserved. Other authors also come to similar conclusions for cryolithic zone landscapes adjacent to mining areas [3]. The increased content of organic matter in soils in these areas is also noted in comparison with the other samples. No own studies have been conducted on the structure of emissions on the territory of the enterprise.

Table 2

Results of studies of HM in collected soils

Indicator	Level	Variation range	Mean and error $\bar{x} \pm S_x$	Coefficient of variation V, %	Coefficient of variation $n = 5$
pH	Upper	5.2...8.1	7.00±0.14	10	-
	Lower	6.1...8.1	7.09±0.10	7	
Arsenic As	Upper	Less than 0.05			Less than 0.05
	Lower	Less than 0.05			
Cadmium Cd	Upper	0.65...4.00	1.52±0.18	62	1.04
	Lower	0.53...3.80	1.52±0.14	48	
Mercury Hg	Upper	Less than 0.005			Less than 0.005
	Lower	Less than 0.005			
Lead Pb	Upper	31...120	56±4	33	50
	Lower	39...155	58±5	43	
Copper Cu	Upper	3.22...21.90	6.80±0.87	68	9
	Lower	2.8...28.9	7.77±1.40	93	
Nickel Ni	Upper	16.9...28.6	22.9±0.5	12	21
	Lower	19.2...37.0	24.00±0.74	16	
Zinc Zn	Upper	18.6...51.0	35.6±2.1	31	34
	Lower	18.6...52.0	36.6±2.0	28	

Analysis of state reports of the Republic of Yakutia showed that the structure of emissions is dominated by gases, 50–65% of which is carbon monoxide.

The correlation analysis shows that there is a correlation between HM concentrations at the significance level of < 0.05 and humus (Fig. 7). Positive correlations are observed between humus and Cd, Pb, and Zn. Synergism among the studied HM is reflected in the following pairs: Pb-Cd, Zn-Pb, and Zn-Cu.

The values of concentration coefficients of the HM content in the soil cover, exceeding the background, are observed for Cd, Pb, Ni, Zn throughout the sample, and for Cu the background is exceeded in 87 % of cases, more often in the upper levels. The basis of the structure of concentration coefficients is cadmium, and lead and nickel to a lesser extent. The values of the total pollution indicator vary from 2 to 10 (see Fig. 3), the average value being 6.

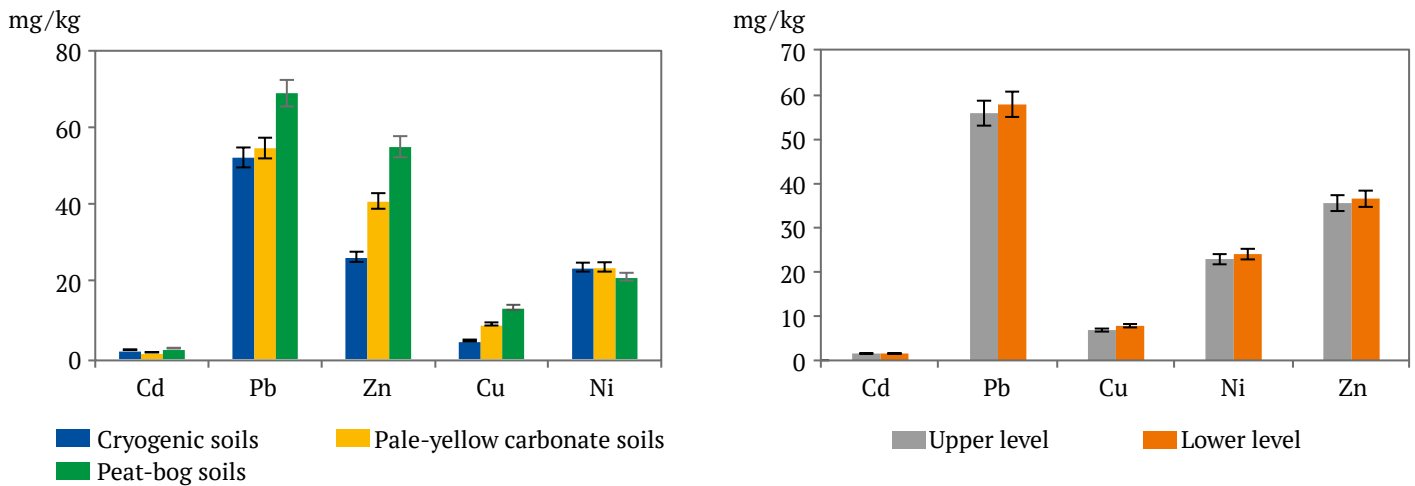


Fig. 6. Distribution of the heavy metals content in soils depending on the soil type (left) and soil level (right)

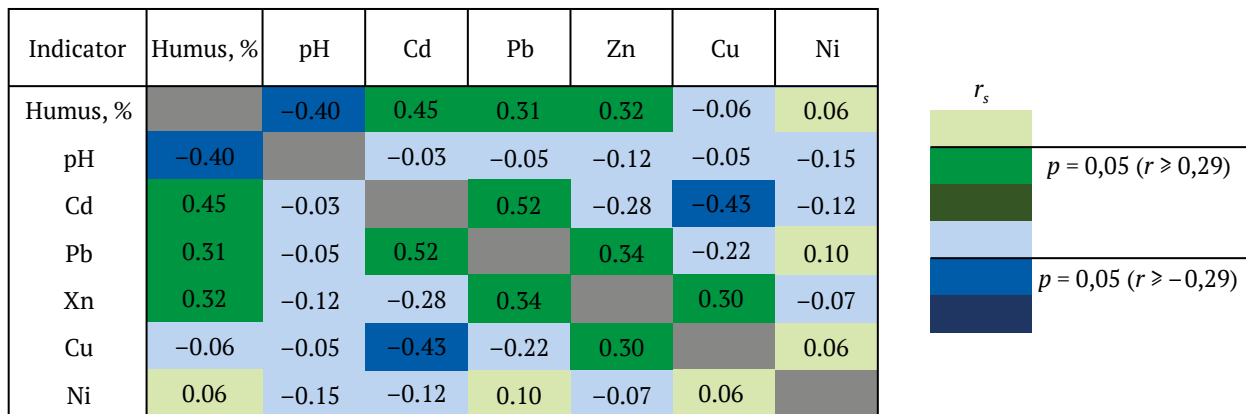


Fig. 7. Spearman's rank correlation coefficients between humus and heavy metals

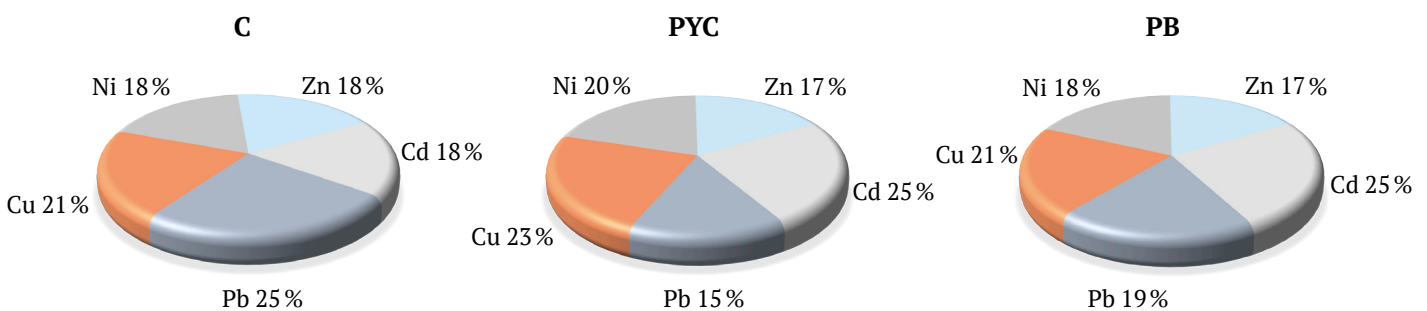


Fig. 8. Structure of Z_c in the studied soils:
C – cryogenic soils; PYC – pale-yellow carbonate soils; PB – peat-bog soils



According to criteria [12], the territory can be ranked according to one pollution level, “Permissible” (100% of the territory). It is important to note that the total pollution indicator was developed for soils of residential areas, and it is not quite correct to apply it to natural areas (including those subject to technogenesis); it can serve as a reference and information indicator, the application of the current gradations in accordance with the RD is conditional, and the impact should be assessed with the help of complex geoenvironmental studies [16].

The structure of the total pollution indicator differs for the group of soils under study (Fig. 8). Pale-yellow carbonate soils are characterized by the predominance of cadmium and nickel, and cadmium has the highest concentration coefficients ($CC_{max} - 5.4$ units). In peat-bog soils, cadmium and copper also demonstrate a high share in the structure of the total pollution indicator. This may be due to the higher content of organic compounds and the predominance of humic substances in the profile of these soils. In the studied cryogenic soils, it is difficult to identify certain regularities in the content of HM due to the absence of clear differentiation of the content of chemical elements in the profile of these soils. Lead prevails in the structure of the total pollution indicator.

The homogeneous distribution of HM concentrations in the upper level relative to the lower level can also indicate the absence or minor occurrence of the man-made component in the studied area – only in the areas adjacent to the waste dump, the accumulation factor increases by 1.7–3.2 times.

The features of the HM chemical elements distribution in the soil cover can be characterized by metallogenic features of the territory itself, and to a lesser extent by the presence of the HM under study in the structure of diamond mining emissions [17]. It is important to note that the territory under study belongs to the Vilyui-Markha system of deep faults. In general, the formation of geochemical anomalies in the form of dispersion halos of predominantly siderophilous (Fe, Ni, Co) and chalcophilous (Zn, Cd, Cu, Pb, S) elements is characteristic of the depositional environment in the area of such structures [18]. The insignificant contribution of man-made impact in the structure of the total soil pollution indicator is indeed confined to the territories adjacent to the mining and processing facilities. This may be due to both the metallogeny of the area and the prevalence of calms, and atmospheric transport with the prevalence of the northwestern winds is expected at a considerable distance from these facilities [19].

The man-made supply of heavy metals as a result of mining operations will be accompanied by an increase in the share of the most mobile forms of these elements. As shown by numerous geoenvironmental studies, the largest share of elements in soils is strongly associated with its mineral and organomineral components. In this connection the interest was directed to the study of the migration ability of the studied elements in the most mobile form (water-soluble) (Fig. 9). Establishment of the predominant forms of metals and their referencing to natural organic ligands can substantiate the forecast of changes in the environmental situation and change the list of priority pollutants [18].

Despite the fact that in a water-soluble extract a small fraction (up to 2%) of the total organic carbon in soil and approximately the same similar fraction of the gross metal content (up to 2.5%) are mobilized, it is this fraction that is the most mobile in ecosystems and is able to be included in the biological cycle.

According to the thermodynamic modeling data, the studied elements were divided into two groups: mainly associated with fulvic acids (Cu, Cd, Pb) and in the form of free ions (Zn and Ni). Free ions are the most accessible form for inclusion of metals in the biological turnover. It is also the most toxic one. Thus, when entering the cryolithic soils in the surveyed area without taking into account the hazard class, nickel and zinc will be mobile elements to the maximum. Cadmium will be more mobile in pale-yellow carbonate and cryogenic soils. Copper is the most firmly associated with natural organic substances in all types of soils. A part of zinc and nickel in peat bog soils is weakly associated with the organic matter. Under changing geochemical conditions, they can be transferred both to the form of free ions and to the form more firmly associated with humic substances.

By the share of mobility of water-soluble forms of heavy metals, the studied types of soils form the following series: pale-yellow carbonate < cryogenic soils < peat-bog soils.

Thus, pale-yellow carbonate soils, which dominate at this area, have the lowest environmental capacity in relation to heavy metals. However, considering the relief, it can be assumed that when the territory of pale-yellow carbonate soils is drained by precipitation, a significant share of soluble forms of metals will go to the territory with stagnant humidification (peat-bog soils), where the toxicity of metals will be partially leveled.

At present, it is proposed to rate the soil cover for the HM content in accordance with the existing maximum permissible concentrations (MPC), and in their absence – with the approximate permissible

concentrations (APC). This proposal is questionable, since MPC/APC do not take into account the regional biogeochemical features of the territory. In the absence of the established MPC/APC it is proposed to use the established regional background, but it has been calculated not in all regions and not for all soils.

Due to the long-term functioning and evolution of the soil cover in the conditions of a relatively close location of the operating mining and processing complex, the obtained data on the gross HM content can be used as background values for further research and control of the soil cover condition during monitoring and production control.

Based on the results of the soil survey, the background values for the studied soils were calculated. The distribution of HM in the peat-bog soil and pale-yellow carbonate soil samples obeys the Gauss's law. With such distribution, background values can be determined as the mathematical expectation of a normally distributed sample, considering tripled standard deviation. To determine the background values of the HM content in cryogenic soils, the sample volume was insufficient, moreover, cryoturbation processes in the soil profile predetermine the complex conditions of chemical elements distribution in the soils themselves.

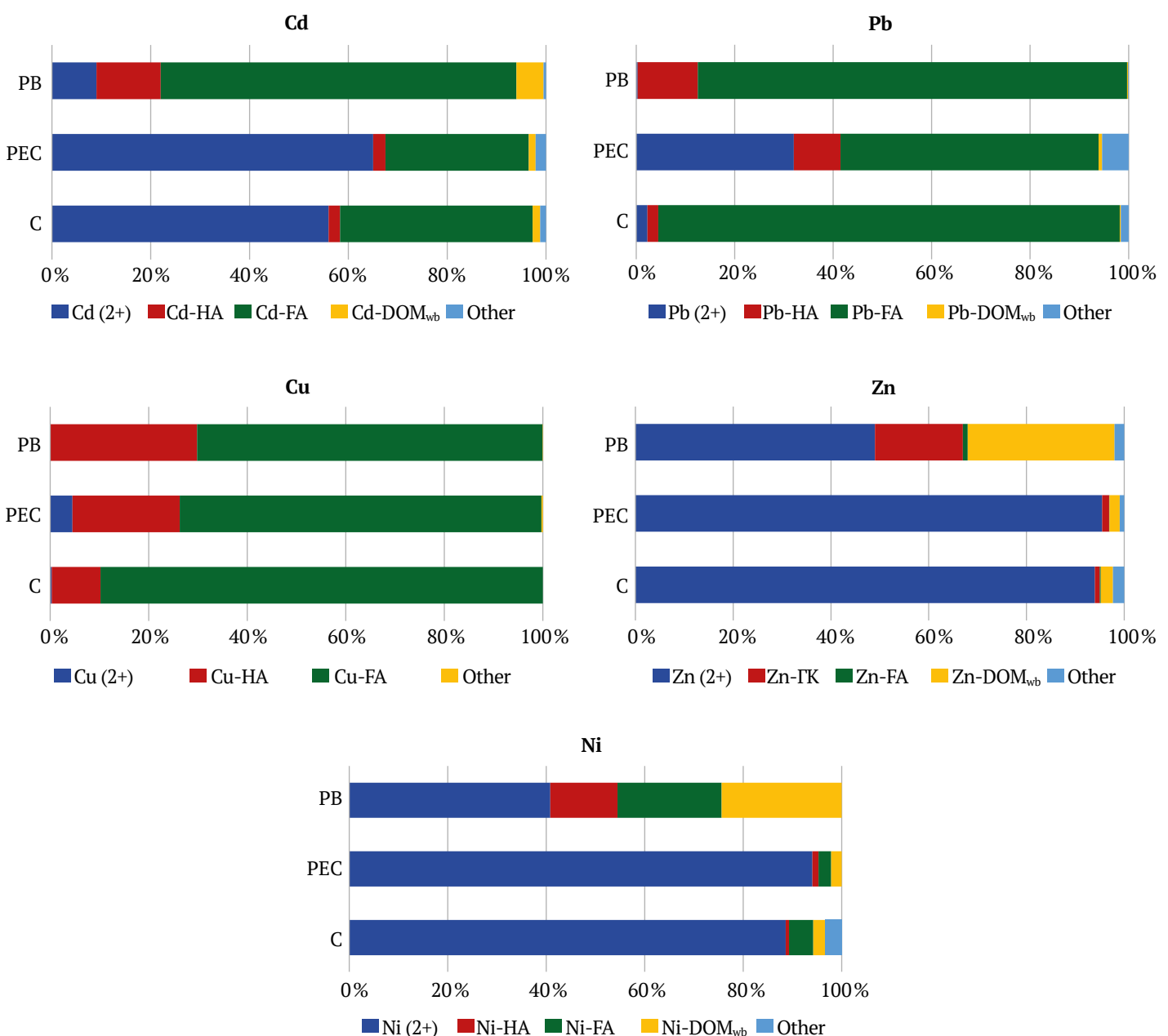


Fig. 9. Speciation of heavy metals in the water-soluble fraction of soils: C – cryogenic soils; PEC – pale-yellow carbonate soils; PB – peat-bog soils; Me-HA – complexes with humic acids; FA – complexes with fulvic acids; Me-DOM_{wb} – weakly (electrostatically) bound to dissolved organic matter (Donnan phase)



Table 3

Calculation of background values for pale-yellow carbonate and peat-bog soils

HM	Min	Max	Mathematic expectation	Calculated background and + 3σ
Peat-bog soils, n = 18				
Arsenic As	Less than 0,05			
Cadmium Cd	0.8	4.0	2.0	5
Mercury Hg	Less than 0.005			
Lead Pb	31.0	72.0	51.0	81.0
Copper Cu	5.9	10.3	8.0	13
Nickel Ni	19.2	28.5	23.0	32
Zinc Zn	18.6	50	31.0	80
Pale-yellow carbonate soils, n = 26				
Arsenic As	Less than 0.05			
Cadmium Cd	0.53	3.50	1.0	3
Mercury Hg	Less than 0.005			
Lead Pb	39.0	107.0	53.0	102
Copper Cu	3.31	28.9	10.0	32
Nickel Ni	16.9	37.0	24.0	37
Zinc Zn	24.0	52	41	67

Due to the absence of data on the background content for further studies, it is proposed to establish the fact of true pollution and its dynamics using the obtained data on the upper boundary of the background content of HM in peat-bog and pale-yellow carbonate soils (Table 3).

For this territory, it is recommended to carry out local environmental monitoring of the state of natural landscapes in the zone of direct mining operations. The gross content of HM can be used as an estimate of the general condition of the territory, while the impact determination requires a transition to HM mobile forms in the “soil–phytocenosis–zoocenosis” system. The test sites should be located, considering the wind rose at the most typical biotopes, and the most typical species, such as *Larix Gmelinii*, *Vaccinium vitis-idaea*, *Vaccinium uliginosum*, *Cladonia stellaris*, should be taken for sampling of plant organs. At the same time, it is recommended to determine the fact of impact or its absence only during comprehensive studies.

Conclusion

The results of the study show a high content of cadmium, lead, nickel and copper in the soil cover in the immediate vicinity of diamond mining operations.

The analysis of concentration coefficients shows that the upper levels accumulate HM by their sorption by humus under the conditions of a weakly acidic medium and weak drainage on the oxygen sorption physical and chemical barrier. Lower levels are characterized by accumulation under the conditions of a neutral and weakly alkaline medium in the soil profile on a pale-yellow alkaline physical and chemical barrier in suprapermafrost levels. The geochemical representation of a number of HM in the soil cover of the surveyed area is characterized as: $Pb > Zn > Ni > Cu > Cd > As > Hg$. Correlation series of HM were compiled, which reflect positive dependencies between humus and Cd, Pb, Zn, as well as the occurrence of synergism in the Pb–Cd, Zn–Pb, Zn–Cu pairs. The territory can be ranked by one pollution level, “Permissible”. An increase in the HM content in the soil cover occurs as it approaches the mine sites of the mining and processing complex.

Pale-yellow carbonate soils have the lowest buffering capacity in relation to heavy metals among the studied soils based on the abundances of their easily mobile species. Among the studied pollutants the greatest tendency to binding by natural organic ligands was revealed for such elements as lead and copper. Zinc and nickel will actively migrate in the ionic



form. Cadmium occupies an intermediate position in terms of the ratio of ionic and organically bound forms.

The data presented in the study, due to the absence of similar studies, can be used in monitoring

the state of the soil cover in the diamond mining zone within the Nakyn kimberlite field, within the boundaries of the SPZ of mining and processing complexes, and as target indicators for the subsequent reclamation of disturbed lands.

References

1. Gololobova A. G., Legostaeva Ya. B. Ecogeochemical monitoring of soil cover on diamond mining site in Western Yakutia. *Bulletin of the Tomsk Polytechnic University. Geo Assets Engineering*. 2020;331(12):146–157. (In Russ.) <https://doi.org/10.18799/24131830/2020/12/2948>
2. Demkova L., Jezny T., Bobulska L. Assessment of soil heavy metal pollution in a former mining area – before and after the end of mining activities. *Soil & Water Research*. 2017;12(4):229–236. <https://doi.org/10.17221/107/2016-SWR>
3. Elsukova E. Yu., Opekunova M. G., Opekunov A. Yu. Technogenic transformation of heavy metal streams in soils in regions under influence of copper-nickel production. *International Research Journal*. 2019;(12):118–124. (In Russ.) <https://doi.org/10.23670/IRJ.2019.90.12.024>
4. Vysotskaya N. A., Piskun E. V. The Main Factors of Adverse Environmental Impact of Potash Production and Methods of Environmental Protection. *Mining Science and Technology (Russia)*. 2019;4(3):172–180. (In Russ.) <https://doi.org/10.17073/2500-0632-2019-3-172-180>
5. Sorokina O. A., Kisselev V. I. Chemical pollution of soils in the area of development of Dzhaldinskoy alluvial and ore deposits of gold (Amur region). *Ecology and Industry of Russia*. 2005;(7):24–28. (In Russ.)
6. Basova I. A., Ivatanova N. P., Kopylov A. V. Assessment of the ecological state of soils in regions of developed mining industry. *Proceeding of Tula State University. Natural Sciences*. 2012;(1–2):14–16. (In Russ.)
7. Gololobova A. G., Legostaeva Ya. B. The stability of frozen soils in conditions of development of mining industry. In: *17th International Multidisciplinary Scientific GeoConference, SGEM 2017. Water Resources, Forest, Marine and Ocean Ecosystems Conference Proceedings*. Albena, Bulgaria. 2017;17:655–662.
8. Legostaeva Ya., Popov V., Kozlova I. et al. Tectonic and eco-geochemical situation of the Nakyn Kimberlite Field. In: *Geology and Mineral Resources of the North-East of Russia: Materials of the XI All-Russian Scientific and Practical Conference*. April 5–7, 2021. Yakutsk: North-Eastern Federal University Publ. House; 2021. Pp. 388–390. (In Russ.) https://doi.org/10.52994/9785751331399_2021_103
9. Zvereva V. P., Frolov K. R., Lysenko A. I. Formation of mine drainage in the Far Eastern region and its impact on the ecosphere and public health. *Mining Science and Technology (Russia)*. 2022;7(3):203–215. <https://doi.org/10.17073/2500-0632-2022-3-203-215>
10. Serebryakov E. V., Gladkov A. S., Koshkarev D. A. Three-dimensional structural-material models of the formation of the Nurbinskaya and Botuobinskaya kimberlite pipes. *Geodynamics & Tectonophysics*. 2019;4(4):899–920. (In Russ.) <https://doi.org/10.5800/GT-2019-10-4-0448>
11. Kilizhekov O. K., Tolstov A. V. New opportunities for the growth of diamond reserves in the Sredne-Markhinsky district of Yakutia. In: *Proceedings of the Workshop. Diamond Deposits: Formation Processes, Localization Patterns, Forecasting and Prospecting Methods. Materials of the Meeting*. Novosibirsk; 2016. Pp. 54–60. (In Russ.)
12. Yershov Y. I. Cryogenic soils on the trappean rocks of Central Siberia. *Eurasian Soil Science*. 2022;55(6):695–709. <https://doi.org/10.1134/S1064229322060059> (Orig. ver.: Yershov Y. I. Cryogenic soils on the trappean rocks of Central Siberia. *Pochvovedenie*. 2022;(6):657–672. (In Russ.) <https://doi.org/10.31857/S0032180X22060053>)
13. Motuzova G. V. *Soil resistance to chemical effects*. Moscow: Moscow State University Publ. House; 2000. 57 p. (In Russ.)
14. Legostaeva Ya. B., Shadrina E. G., Soldatova V. Yu., Dyagileva A. G. Ecogeochemical and bioindication assessment of transformation of ecosystem in process drafting of primary deposits of diamonds in Yakutia. *Modern Problems of Science and Education*. 2011;(6). (In Russ.)
15. Feklistov P. A. Estimation of the impact area of the Nyurbinsk diamond deposit road rotational settlement Nakyn-Industrial zone by means of bioindication. *Arctic Environmental Research*. 2012;(3):48–53. (In Russ.)



16. Jaishankar M., Tseten T., Anbalagan N. et al. Toxicity, mechanism and health effects of some heavy metals. *Interdisciplinary Toxicology*. 2014;7(2):60–72. <https://doi.org/10.2478/intox-2014-0009>
17. Gololobova A.G., Legostaeva Ya.V. Influence of mining and processing activities on frozen soils of the khannya-nakyn interfluves (Western Yakutia). In: *Geology and Mineral Resources of the North-East of Russia: Materials of the XI All-Russian Scientific and Practical Conference*. April 5–7, 2021. Yakutsk: North-Eastern Federal University Publ. House; 2021. Pp. 367–370. (In Russ.) https://doi.org/10.52994/9785751331399_2021_97
18. Dinu M.I., Shkinev V.M. Complexation of metal ions with organic substances of humus nature: methods of study and structural features of ligands, and distribution of elements between species. *Geochemistry International*. 2020;58(2):200–211. <https://doi.org/10.1134/S0016702920020032> (Orig. ver.: Dinu M.I., Shkinev V. M. Complexation of metal ions with organic substances of humus nature: methods of study and structural features of ligands, and distribution of elements between species. *Geohimiya*. 2020;65(2):165–177. (In Russ.) <https://doi.org/10.31857/S001675252002003X>)
19. Gololobova A.G., Legostaeva Ya.V. Heavy metals in cryozems of Western Yakutia. In: *19th International Multidisciplinary Scientific GeoConference, SGEM 2019. Water Resources. Forest, Marine and Ocean Ecosystems Conference Proceedings*. Albena, Bulgaria. 2019;19(3.2):239–246.

Information about the authors

Anton S. Titov – Environmental Engineer, EKOSTANDART LLC. “Technical solutions”, Moscow, Russian Federation; ORCID [0009-0005-0157-4609](https://orcid.org/0009-0005-0157-4609); e-mail Titov.A@ecostandard.ru

Andrey S. Toropov – Cand. Sci. (Geolog. and Mineral.), Researcher at the Faculty of Chemistry, Lomonosov Moscow State University, Moscow, Russian Federation; ORCID [0000-0001-7759-2831](https://orcid.org/0000-0001-7759-2831), Scopus ID [57693206900](https://scopus.org/57693206900); e-mail torop990@gmail.com

Received 11.12.2023

Revised 11.03.2024

Accepted 15.03.2024



POWER ENGINEERING, AUTOMATION, AND ENERGY PERFORMANCE


Research paper

<https://doi.org/10.17073/2500-0632-2024-03-254>

UDC 621.31:622

**Reliability analysis of open-pit power supply system components**R. V. Klyuev   

Moscow Polytechnic University, Moscow, Russian Federation

 kluev-roman@rambler.ru**Abstract**

In the field of designing power supply systems of open pits an important role is attributed to the problems of components reliability analysis, which can be solved by integrated application of different analysis methods for individual types of electrical equipment and network devices in power supply systems. The purpose of the work is to establish optimal parameters for an open-pit mine power supply at mining and processing complexes, and to conduct research that allows a technical and economic model of the system to be created. It has been established that mathematical statistics provides a number of methods for establishing the homogeneity (or heterogeneity) of the population of random variable values. When analyzing the data of failure statistics of electrical equipment, the method of comparative estimate of two sample averages (compared to the method of comparing the empirical distribution with the normal distribution or the moving average method) is the most acceptable. The paper presents accident rates of electrical equipment of open-pit substations and network devices of the quarry processed on the basis of data, also presents the relationship between the reliability of the circuit and its elements and shows the influence of protection reliability on the reliability of the circuit. Methods of optimizing open-pit power supply systems are presented, which consist in the use of first-order gradient methods, second-order methods or the so-called quadratic optimization methods, and random search methods. A group of gradient methods is the most widespread for solving nonlinear programming problems, among which the method of steepest descent should be considered primarily. The combination of random search with the penalty function method makes it possible to determine conditional extrema for the problem of optimizing the electrical grid and system operation mode. The method of random descent, which consists in determining the minimum of the target function according to an appropriate algorithm, is also considered, in which the direction of motion is generally given by a random vector uniformly distributed over a hypersphere.

Keywords

reliability of components, power supply system, open pit, gradient methods, accident rate, mine substations, random search, target function

For citationKlyuev R.V. Reliability analysis of open-pit power supply system components. *Mining Science and Technology (Russia)*. 2024;9(2):183–194. <https://doi.org/10.17073/2500-0632-2024-03-254>

ЭНЕРГЕТИКА, АВТОМАТИЗАЦИЯ И ЭНЕРГОЭФФЕКТИВНОСТЬ

Научная статья

Анализ надежности элементов системы электроснабжения карьеровР. В. Ключев   

Московский политехнический университет, г. Москва, Российская Федерация

 kluev-roman@rambler.ru**Аннотация**

В области проектирования систем электроснабжения карьеров важная роль отводится вопросам анализа надежности элементов, которые могут быть решены в ходе проведения комплексного применения различных методов расчета отдельных видов электрооборудования и сетевых устройств в системах электроснабжения. Целью работы является установление оптимальных параметров электроснабжения рудника открытых горных работ горно-обогатительных комбинатов, проведение исследований, позволяющих создать технико-экономическую модель системы. Установлено, что математическая статистика дает ряд методов установления однородности (или разнородности) совокупности значений случайной величины. При анализе данных аварийной статистики электрооборудования наиболее приемлемым является метод сравнительной оценки двух выборочных средних (по сравнению с методом сравнения эмпирического распределения с нормальным или методом скользящей средней). В работе приведены обработанные на основе данных аварийности электрооборудования рудничных подстанций и сетевых устройств карьера, также представлены соотношения между надежностью схемы и ее элементами и показано влияние надежности защиты на надежность схемы. Представлены методы оптимизации систем электроснабжения карьеров, заключающиеся в применении градиентных методов первого порядка, методов второго порядка или так называемых квадратичных методов оптимизации, методов случайного



поиска. В качестве наиболее распространенных для решения задач нелинейного программирования используется группа градиентных методов, среди которых в первую очередь следует рассматривать метод наискорейшего спуска. Сочетание случайного поиска с методом штрафных функций дает возможность определять условные экстремумы для задачи оптимизации режима работы электрической сети и системы. Также рассматривается метод случайного спуска, заключающийся в определении минимума целевой функции по соответствующему алгоритму, при котором направление движения в общем случае задается случайным вектором, равномерно распределенным по гипосфере.

Ключевые слова

надежность элементов, система электроснабжения, карьер, градиентные методы, аварийность, рудничные подстанции, случайный поиск, целевая функция

Для цитирования

Klyuev R.V. Reliability analysis of open-pit power supply system components. *Mining Science and Technology (Russia)*. 2024;9(2):183–194. <https://doi.org/10.17073/2500-0632-2024-03-254>

Introduction

Fulfillment of the problems set for the mining industry is impossible without further increase in production efficiency, labor productivity and automation of production processes, increase of the efficiency level of mining production and the use of electrical equipment [1, 2].

The growth of power availability per man leads to an increase in the cost of creating and operating a power supply system (PSS). In this regard, the problems of building an optimal PSS not only for a mining enterprise as a whole, but its individual subsystems as well, solved at the design stage, as well as the problems of building reliability models of a PSS [3, 4] are of particular relevance.

The application of optimization methods in the design practice, including those using artificial intelligence, will significantly improve the designing quality in accordance with the problems of the need to improve the design business on the basis of the wide introduction of scientific achievements into the engineering practice [5, 6].

The achieved scientific and technical progress in the technique and technology of open-pit mining (a high degree of concentration of mining operations, operation of large deep pits, steady growth of the installed capacity of mining machines and power availability per man) poses a number of technical and economic problems of efficiency improvement in the field of designing power supply of open pits, which require urgent solution.

The efficiency of open-pit PSS depends not only on the quality of the equipment used [7, 8], but also on the correctness of design decisions and the quality of design documentation. However, at present PSS's are designed by traditional methods developed for the conditions of open pits of relatively small productivity and depth. Complex interrelationships between system parameters, electrical loads and mining-geometric, technical and technological parameters of modern open pits are taken into account during designing in-

sufficiently. Electrical loads are analyzed on the basis of demand coefficients, and the choice of the power supply scheme is based on the technical comparison of a limited number of options without taking into account the dynamics of mining operations and changes in electrical loads. This does not help to choose its optimal parameters.

When solving technical and economic problems of power supply designing, design institutes cannot widely use the capabilities of computer technology due to the lack of algorithms suitable for specific conditions of open-pit mining. It practically excludes multivariant and optimization analyses, causes deterioration of the quality and increase of terms for design preparation, with an abrupt increase in the scope of design.

The purpose of the work is to establish the optimal parameters of power supply of an open-pit mine within mining and processing complexes (MPC) and to conduct studies that allow investigation of the reliability of PSS individual components in order to further consider the safety of work in the electrical grids of the mining industry [9, 10].

Analysis of existing power supply schemes of open pit mines

The accident rate of individual components of grids and electrical equipment of enterprises depends on many disturbing factors, on the state of installation and repair works performed, various operating conditions, their technical state, etc. [11, 12]. The influence of each of these factors separately is often insignificant and practically imperceptible, but the total effect leads to results fluctuating from case to case. Consequently, accident rates can be considered as a random variable, which is the subject of mathematical statistics and probability theory. Proceeding from the statistical nature of the accident rate phenomenon and from the essence of the probability concept of some event, the quantitative expression of the reliability concept can be formulated as follows:

reliability is the probability that a component or an installation as a whole will operate satisfactorily for a certain period of time. For example, if the duration of emergency downtime of the installation during a year is equal to 8.76 hr, then the probability of its failure is $P = 8.76/8760 = 10^{-3}$, and the reliability is $P' = 1 - 10^{-3}$.

Method of reliability analysis of electrical equipment individual types and network devices

In electrical distribution networks and systems, damage to certain types of components can cause downtime of a part or the whole installation for the time of finding and eliminating the failure (emergency downtime), or for the time of finding the failure and subsequent disconnection of the damaged section (emergency shutdown time) [13, 14].

According to the operational data on the emergency downtime and emergency shutdown duration x of the main types of electrical equipment and network devices used in open pits, the two most important statistical characteristics are determined: the weighted average of argument \bar{x} and standard σ_x .

Comparison of the obtained average values and standards shows that the value of coefficient of variability k for the considered variation series keeps some constant value with maximum deviation of its individual values from the average value up to 4%:

$$k = \frac{\sigma_i}{x_i} \tag{1}$$

Respectively, the following ratio is true practically for all sample distributions:

$$\sigma_i = k\bar{x}_i \tag{2}$$

The obtained ratio indicates the same regularity in distribution of all considered variation series and that we should expect almost a constant value of the

standard of the modifying function argument for all sample distributions.

To reveal the law of distribution of the observed frequencies for the emergency downtime and emergency shutdown time, a quantile plot of the argument distribution for some types of electrical equipment is drawn on the probability paper (Fig. 1).

As the quantile plot shows, the points of values of some distribution functions are grouped near curves resembling a logarithmic curve.

Fig. 2 shows new quantile plots on the log-probability paper. The plot shows that the points are grouped very closely near straight lines, with more or less noticeable deviation of the points from a straight line observed for only up to 5% and above 95% of the quantiles.

For graphic estimation of the obtained deviations of the distribution function values from a straight line (Fig. 3), the curves of permissible values of emergency deviations from the theoretical line with the reliability (probability) of $P = 0.95$ were drawn.

Fig. 3 shows that the permissible value of random deviations from the theoretical line is much higher at values P close to 0 or 100% than at the values close to 50%. Therefore, the observed noticeable deviation of points of the distribution function values from a straight line of up to 5% and above 95% quantiles (see Fig. 2) cannot noticeably change the sample distribution law. In addition, the number of observations within these limits does not exceed 10% of the sample volume. Comparison of the curves for permissible values of random deviations from the theoretical line with the obtained deviations of the values of the sample distribution function from a straight line shows that the latter are within the permissible limits of random deviations at $P = 0.95$ and $n > 250$. Respectively, the emergency downtime and emergency shutdown

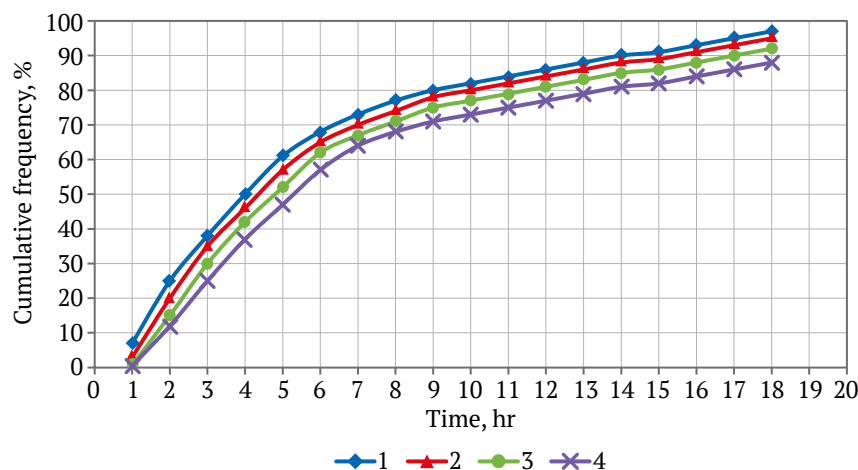


Fig. 1. Quantile plot of distribution of the emergency downtime and emergency shutdown time of open pit excavator cables and networks

time both in case of damaged excavator cables and in case of open-pit network failures is distributed according to the log-normal distribution. According to the result of graphical analysis, sample distributions are adjusted by the equation:

$$\Phi(u) = \frac{1}{\sigma_u \sqrt{2\pi}} e^{-\frac{(u_i - \bar{u})^2}{2\sigma_u^2}}, \quad (3)$$

where $\Phi(u)$ is the distribution function; u_i is the argument of the modifying function; \bar{u} is the mean value of the modified argument; and σ_u is the standard of the modified argument.

The results of analytical evaluation of the discrepancy between sample and theoretical frequencies are: $\lambda_1 = 0.307$ and $P_1 = 0.999$; $\lambda_2 = 0.818$ and $P_2 = 0.52$; $\lambda_3 = 0.448$ and $P_3 = 0.987$; $\lambda_4 = 0.942$ and $P_4 = 0.365$ (indexes P and λ correspond to line numbers given in Figs 1, 2). Random values λ , which are greater than or equal to the observed values, may occur with a probability greater than 0.365, i.e., the difference between

the theoretical and sample distributions is insignificant. Analytical verification confirms the conclusions obtained by graphical analysis.

The slope of a straight line to the quantile plot abscissa axis in case of log-normal distribution is determined by the value of the modifying function argument standard.

The quantile plot (see Fig. 2) shows that the value of the modifying argument standard for all distributions is very stable, since all the straight lines of the plot are within two straight lines insignificantly distant from each other.

The average value of the modifying argument standard for all the distributions under study is $\sigma_u = 0.347$. The maximum deviation of its individual values from the average value is 20.1%, which can be neglected and in the first approximation $\sigma_u = 0.347 = \text{const}$ can be assumed ($\sigma_u = \lg u_{60} - \lg u_{15.9}$, where u_{60} and $u_{15.9}$ are 60% and 15.69% of quantiles respectively).

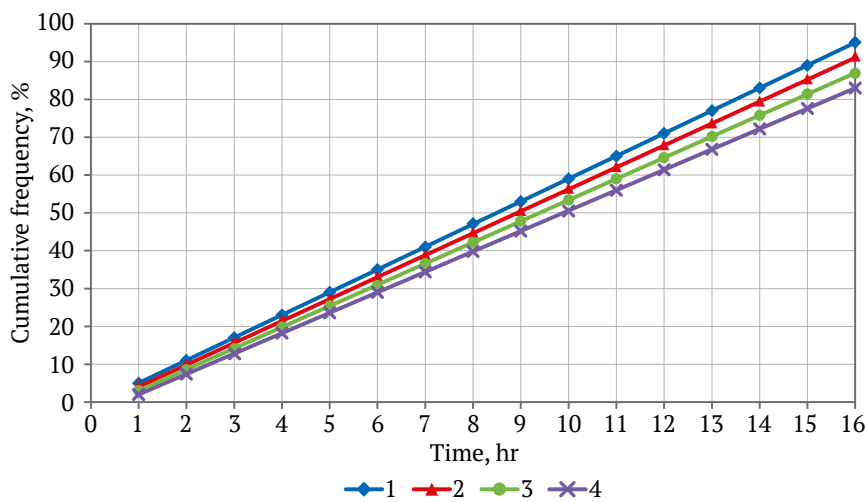


Fig. 2. New quantile plot of distribution of the emergency downtime and emergency shutdown time of open pit excavator cables and networks

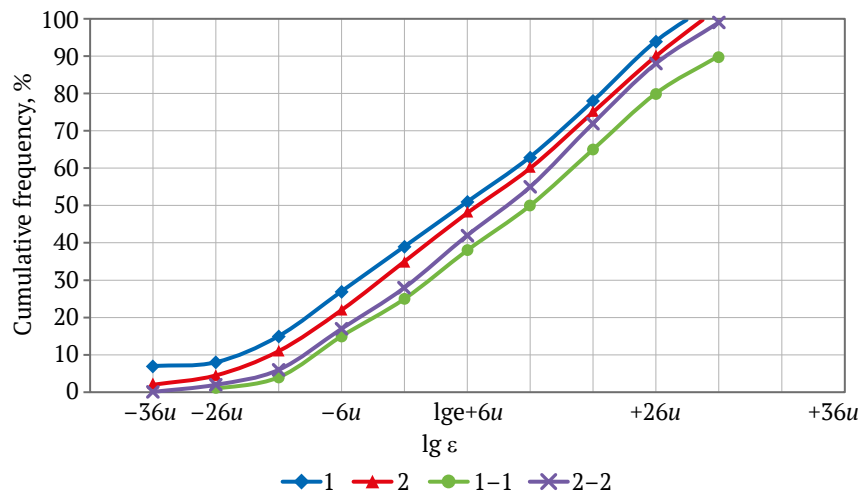


Fig. 3. Curves of permissible random deviations from the theoretical line with the reliability of $P = 0.95$, 1-1 at $n = 100$, 2-2 at $n > 250$



Similar analyses made for all main components of open-pit power supply schemes show that:

1. The emergency downtime and emergency shutdown time is subject to the log-normal distribution.
2. The modifying function argument standard practically maintains a constant value.

When the distribution is log-normal, the following ratio takes place:

$$M(\lg u) = \lg \varepsilon, \quad (4)$$

where $M(\lg u)$ is the mathematical expectation of the logarithm of the observed argument; $\lg \varepsilon$ is the mean value of the modified argument.

The value of $\lg \varepsilon$ is median Me in the modified argument distribution, and the quantiles of the modified value coincide with the modified quantiles of the original value, as long as the modification is performed by a non-decreasing function. Hence, value ε shall be equal to the median in the x distribution. However, the median changes if any values of the argument less than the median change randomly, remaining less than Me under these changes. This property of the median and the fact that the probabilities of occurrence of a certain number of observations to the left and right of the median are equal to each other, allow them to be used to determine the mean values of the argument with relatively small sample sizes.

Based on the known ratio:

$$\lg \bar{x} = \lg \varepsilon + 1.151 \sigma_u^2 \quad (5)$$

the following can be written:

$$\lg \bar{x} = \lg \varepsilon + 0.1387. \quad (6)$$

The obtained equality can be used to determine the average value of the considered failure parameters and to make practically its exact estimate with very insignificant sample sizes, even with $n = 25-25$. At the same time, the obtained mean values are within the confidence limits defined by the accuracy of 0.15 of the mean value determined with the sample sizes exceeding 150–200 and having a reliability practically equal to 0.9. Mean values determined with such accuracy and reliability are quite applicable as input data for determining the quantitative indicators of the electrical grid reliability.

The conducted analyses show that the annual durations of emergency downtime of open-pit electrical equipment are also distributed according to the log-normal distribution and the values of the modified argument standard have deviations not exceeding 20% of the determined standard mean value of $\sigma_u = 0.347$. Respectively, the time of emergency downtime of certain types of electrical equipment and network devices per year can also be calculated by the proposed method without determining their

average damage rate per year with subsequent multiplication by the average duration of emergency downtime.

To determine the reliability index of power supply schemes, it is necessary to know the third failure parameter – the mean value of the number of failures per year of individual types of electrical equipment and network devices.

Determination of the arithmetic mean of the number of failures is not difficult, but determination of the statistical mean necessary to calculate the quantitative reliability indicators is associated with some difficulties (complications) related to the need to take into account the degree of influence of disturbing factors on the failure parameter values.

Individual values of failure parameters, possessing a common mean level, deviations from which appear to be random, constitute a homogeneous population. In this case, the value of their arithmetic mean is the mean in the statistical sense and, expressing the mean level, summarizes random deviations. If a part of their disturbing factors causes a systematic deviation of the values of failure parameters from some level, along with random values, it creates a new level (mean), thus forming a heterogeneous population. The arithmetic mean loses its cognitive meaning when one tries to use it to characterize failure parameter values that make up a heterogeneous population. This is because it is impossible to express the mean level that does not exist in a heterogeneous population by any indicator. In this case, to obtain a statistical mean, it is necessary to divide the heterogeneous population into homogeneous ones and then to determine the mean value for each homogeneous population of failure parameters and, if necessary, to establish the form and measure of correlation between the failure parameter values and disturbing factors.

Mathematical statistics provides a number of methods for establishing the homogeneity (or heterogeneity) of the population of random variable values. When analyzing the data of failure statistics of electrical equipment, the method of comparative estimate of two sample averages compared to the method of comparing the empirical distribution with the normal distribution or the moving average method is the most acceptable

The essence of the recommended method as applicable to the failure data processing is that the sample data for a certain set of disturbing factors determines the value of \bar{x}_1 . After excluding the factors whose influence on the formation of the average level is clarified from the factors population, a new sample is taken and average \bar{x}_2 is also determined. Then the criterion is determined:



$$t = \frac{\bar{x}_1 - \bar{x}_2}{\sqrt{\frac{(n_1 + n_2) \left[\sum (x_1 - \bar{x}_1)^2 + \sum (x_2 - \bar{x}_2)^2 \right]}{n_1 n_2 (n_1 + n_2 - 2)}}} \quad (7)$$

According to the value of t found and the number of degrees of freedom k , probability P is found using the Student's distribution probabilities table. It can be used to expect value t to be numerically equal to or greater than the observed (calculated) value. If $P > 0.95$, the compared averages differ insignificantly and the values of the failure parameters form a homogeneous population. The number of degrees of freedom is determined as the number of independent values of failure parameters. If for some sample of size n_1 the values of failure parameters shall satisfy h conditions linking them, then the number of degrees of freedom is equal to: $k = n_1 - h$.

Accident rates

Accident rates of electrical equipment of open-pit substations and network devices [15, 16], processed on the basis, given in Table 1.

Correlations between reliability of the scheme and its components

Using the provisions of the probability theory and the data given in Table 1, correlations between reliability of the scheme, its individual circuits and components with different connection types were obtained:

– with series connection a failure of each component causes a malfunction of the whole installation and therefore: $P' = 1 - \sum p_i$, $P'' = \sum p_i$;

– with parallel connection, power outage can occur only if all parallel circuits fail, therefore: $P' = 1 - p_1 p_2$, $P'' = p_1 p_2$;

– with mixed connection:

$$P' = (1 - p_1 p_2) \cdot (1 - p_3), P'' = p_1 p_2 + p_3,$$

where p_i is the probability of failures of the scheme individual parallel circuit components; p_1, p_2 is the probability of failures of individual parallel circuits and components; p_3 is the probability of failures of a series circuit or component in case of mixed connection; P', P'' are the reliability and probability of failure of the scheme.

In conclusions of accident rates of individual components and circuits the schemes are considered as events independent of each other.

Influence of protection reliability on scheme reliability

Based on the essence of the probability concept of some event to determine the probability of incorrect action of protection p_3 , it is necessary to take a certain number of protection actuations S for the number of all cases belonging to some particular stochastic test plan, and to take the statistical mean of the number of malfunctions of protection m with the accepted number of actuations for the number of cases favorable to the protection malfunction, i.e.:

$$p_3 = mS. \quad (8)$$

Downtime duration of the busbar system T for incorrect protection functions p_3 can be determined from the expression:

Table 1

Accident rates of electrical equipment of open-pit substations and network devices

Item No.	Name of electrical equipment and network devices	Number of damages per 1 facility, times/year	Probability of emergency shutdown	Probability of emergency downtime
1	Flexible cables	3.65	$0.595 \cdot 10^{-4}$	$13.1 \cdot 10^{-4}$
2	In-pit overhead power lines with excavator number x used for – stripping – offsite dumps – onsite dumps	$y = 4.7 \cdot x + 1.7$ $y = 1.32 \cdot x + 0.87$ $y = 2.5 \cdot x + 0.67$	$0.595 \cdot 10^{-4}$ $0.595 \cdot 10^{-4}$ $0.595 \cdot 10^{-4}$	$13.5 \cdot 10^{-4}$ $4.6 \cdot 10^{-4}$ $6.66 \cdot 10^{-4}$
3	Mobile substations	0.99	$0.595 \cdot 10^{-4}$	$1 \cdot 10^{-4}$
4	Boxes of RVNO and VYaP type	0.228	$0.595 \cdot 10^{-4}$	$0.42 \cdot 10^{-4}$
5	Transformer points within the pit and at dumps	0.111	$0.595 \cdot 10^{-4}$	$0.29 \cdot 10^{-4}$
6	Pit power supply points with disconnection devices	2.3	$0.595 \cdot 10^{-4}$	$2.36 \cdot 10^{-4}$
7	Excavator electrical equipment (upstream of disconnection device)	0.6	$0.595 \cdot 10^{-4}$	$1.1 \cdot 10^{-4}$
8	Daylight surface overhead power line	0.402	$0.595 \cdot 10^{-4}$	$1.3 \cdot 10^{-4}$
9	Overhead power line between substations	0.302	$0.595 \cdot 10^{-4}$	$0.86 \cdot 10^{-4}$
10	Collecting busbars with maximum protection on outgoing feeders in case of incorrect operation of protections for one emergency shutdown of protections	–	$0.35 \cdot 10^{-6}$	–
11	Connections	0.098	–	$0.35 \cdot 10^{-4}$

$$T = np_3t, \tag{9}$$

where n is the total number of failures on feeders outgoing from the busbars; t is the statistical mean duration of busbar downtime during the protection malfunction.

The influence of the protection operation on the scheme reliability is determined from the expression

$$P_n = \frac{T}{8760} = \frac{np_3t}{8760}. \tag{10}$$

Methodology of reliability analysis of schemes

When assessing the reliability of electrical schemes, a special place is taken by substations and distribution points (DP) busbars, whose reliability indicators depend not only on the accident rate of the busbars themselves, but also on the number of failures on feeders outgoing from them and the protections function. Thus, the probability of interruption of power supply to load A (Fig. 4) is influenced not only by the failure of the circuit through which power is transmitted, but also by the failure of other feeders outgoing from busbar 2.

Therefore, bus bars 2 (see Fig. 4) with feeders outgoing from them shall be replaced by another conditional component, for example, a component with an accident rate equal to the sum of the accident rate of the busbars and the probability of coincidence of failures on feeders with protection malfunction. Then, to determine the probability of interruption of power supply to load A, we obtain a design circuit of series-connected components (Fig. 5), from which:

$$P_A = \sum p_i, \tag{11}$$

where p_i is the probability of failure of individual components in the design circuit.

When determining the probability of failure of conditional component III for another receiver, for example, B, the number of emergency disconnections of outgoing feeders may be slightly different than for load A and is due to a difference in the number of failures on the loads A and B feeders. This difference is very small compared to the total number of failures on the outgoing feeders, so in practical calculations it can be neglected and the probability of failure of component III can be assumed to be the same for all receivers (feeders). Further presentation of the methodology for determining the reliability indicator is made on a specific example (Fig. 6).

We determine the reliability indicators of substations 1, 2, 3, 4 and the whole network if:

Variant I

1. The probability of failure of connections between substations is equal to $a, b, c, d,$ and e .

2. The receiver capacities of substations 1, 2, 3, 4 have the following ratios: $N_1 : N_2 : N_3 : N_4 = 2 : 3 : 5 : 2$.

3. The capacity of the connections is equal to: $N_{A-1} = N_{A-3} = N_1 + N_2 + N_3 + N_4, N_{1-2} = N_2 + N_3 + N_4, N_{2-3} = N_1 + N_2$.

4. The reliability of substation operation is equal to 1, the protection at all substations is ideal.

For substation 4, the accident rate of the scheme section from district substation A to substation 3, which has two parallel branches with failure probabilities $b, a + c + d,$ is equal to $b(a + c + d)$. Consequently, the considered scheme for substation 4 can be replaced by the scheme shown in Fig. 7, from which the probability of interruption of power supply to substation 4 is equal to: $P_4 = b(a + c + d) + e$.

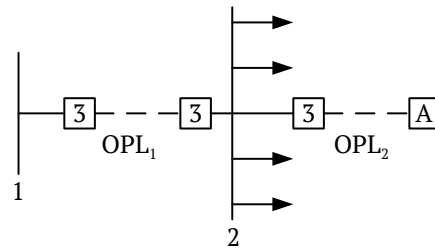


Fig. 4. Design circuit of the electrical grid: OPL – Overhead Power Line

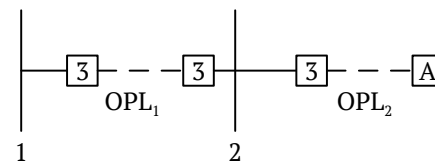


Fig. 5. Design circuit of series-connected components: OPL – Overhead Power Line

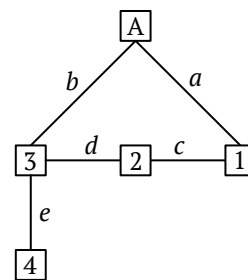


Fig. 6. Example of presentation of the methodology for determining the reliability indicator

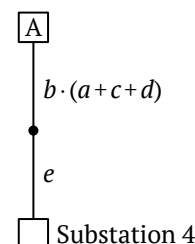


Fig. 7. Replacement of the scheme in Fig. 6

The probabilities of interruption of power supply to substations 1, 2, 3 are equal to: $a(c + b + d)$, $(a + c) \cdot (b + d)$, $b(a + c + d)$ respectively.

Variant II

Let us modify condition 3 and assume that $N_{A-1} = N_1 + N_2 + N_3$, $N_{A-3} = N_1 + N_2 + N_3 + N_4$, $N_{1-2} = N_2 + N_3$, $N_{2-3} = N_1 + N_2$.

The probability of interruption of power supply to substations 1, 2, 3 does not change, but the probability of scheme failure in relation to substation 4 changes significantly, because connection A-1-2-3 to substation 3 in case of failure of connection A-3 is not able to power substation 4. The probability of interruption of power supply to substation 4 is determined by the failure of connections A-3 and 3-4 and is equal to: $P'_4 = b + e$.

Thus, the same scheme with the same loads depending on the capacities of separate scheme sections has different reliability indicators.

Variant III

Let us change condition 2 and accept that $N_1 : N_2 : N_3 : N_4 = 5 : 1 : 2 : 4$.

The values of probabilities of power supply interruption to individual substations do not change, but the capacity of the receivers of each substation, kW·h, does change. Therefore, a change in the ratio between the substation capacities of the scheme under study changes the duration of downtime of the whole scheme receivers. Therefore, the sum of probabilities of power supply interruption to individual substations (receivers without taking into account their capacities) cannot be a reliability indicator of the whole scheme. The capacities of substations (receivers) can be taken into account, if the probability of power supply interruption to substations is brought to the same capacity, for example, to the total capacity of all substations, by multiplying them by the ratio of capacities of individual substations to their total capacity. The obtained new values of the probability of

power supply interruption to individual substations, which have the same significance from the duration of downtime of receivers standpoint, allow modifying the scheme under consideration into a single-line scheme with one conditional receiver, whose capacity is equal to the sum of the capacities of all substations (receivers).

Modification according to the conditions of the considered scheme variants is shown in Fig. 8.

The results of probability calculations for power supply interruption to all scheme receivers, assuming that $a-b-c-d-e$, are equal to:

Variant I – $3 \frac{1}{4} a^2 + \frac{1}{6} a$,

Variant II – $2 \frac{3}{4} a^2 + \frac{1}{3} a$,

Variant III – $3 \frac{1}{12} a^2 + \frac{1}{3} a$.

Thus, the reliability analysis of schemes should be performed as follows:

1. Replace the busbars of substations and distribution substations with conditional components III_i, whose failure probability is determined by the sum of the probability of failures of the busbars themselves and the probability of coincidence of failures on outgoing feeders with protections malfunction.
2. Determine the probability of power supply interruption to each receiver (substation), taking into account the capacities of individual scheme sections. In case of complex schemes, to simplify the calculation, convert them into design circuits for each receiver (substation).
3. Reduce the probabilities of power supply interruption to individual loads to their total capacity and, using the probabilities given, make a design circuit with one conditional load of the total capacity.
4. Determine the probability of power supply interruption to all receivers of the scheme.

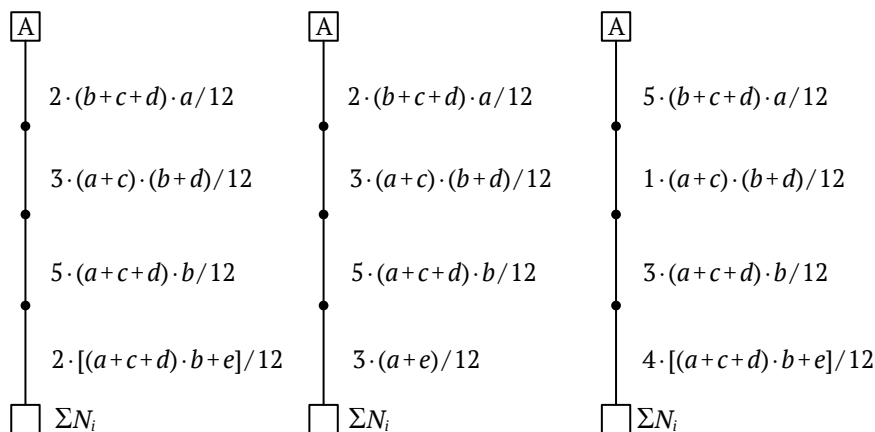


Fig. 8. Modification according to the conditions of the considered scheme variants



Methods of optimizing open-pit power supply systems

The central problem in the development of any CAD subsystem is to determine the optimal parameters of this subsystem. Only in this case the advantages of designing automation can be realized in full [17, 18].

The variety of the content of practical problems reflected in the existing mathematical models is so great that it is usually necessary to investigate many ways to achieve the optimum. None of the optimization methods is universal from the application to any particular problem standpoint, but also does not act in isolation from others.

An optimization problem can be mathematically formulated as follows: there is function F of several variables X_n . These variables are related to each other by k -equations or inequalities of the form:

$$\begin{aligned} W_1(X_1, X_2, \dots, X_n) &\geq 0; \\ \dots & \\ W_k(X_1, X_2, \dots, X_n) &\geq 0, \end{aligned} \tag{12}$$

where W_1, W_k are some functions of variables X_i ($i = 1, 2, \dots, n$).

It is required to find the minimum (maximum) of function F . Three directions for solving the above problem can be distinguished based on the application of:

- first-order gradient methods;
- second-order methods or so-called quadratic optimization methods;
- random search methods.

A group of gradient methods is the most widespread for solving nonlinear programming problems, among which the method of steepest descent should be considered primarily.

The search for the minimum using the method of steepest descent consists in the sequential application of the following expression for the calculation of the main variables:

$$X_j^{(k+1)} = X_j^{(k)} + h \frac{\partial \Phi}{\partial X_j^{(k)}}, \tag{13}$$

where $X_j^{(k+1)}$ are the refined values of the required parameters at the $(k+1)$ -th iteration; $X_j^{(k)}$ is the value of parameters at the k -th iteration; h is the coefficient of the length of increment; $\partial \Phi / \partial X_j^{(k)}$ are the values of particular derivatives from the target function for the main variables at the k -th iteration.

It is convenient to present the values of derivatives at the sequential iteration in the form of a matrix.

The increment length coefficient can be calculated by the formula:

$$h = \frac{\sum_{j=1}^n \left(\frac{\partial \Phi}{\partial X_j} \right)^2}{\sum_{j=1}^n \sum_{k=1}^n \left(\frac{\partial^2 \Phi}{\partial X_j \partial X_k} \frac{\partial \Phi}{\partial X_j} \frac{\partial \Phi}{\partial X_k} \right)}. \tag{14}$$

Let it be necessary to minimize function $U(Z)$ with a continuous gradient under constraints: $W(Z) = 0, Z_{\min} \leq Z \leq Z_{\max}$.

The vector of parameters Z is presented as a set of vectors X and Y (dependent and independent parameters). In this case, the problem can be presented as minimization of an implicit function:

$$U[X(Y), Y] = H(Y). \tag{15}$$

With constraints: $X_{\min} \leq X(Y) \leq X_{\max}, Y_{\min} \leq Y \leq Y_{\max}$, where $X(Y)$ is an implicit function determined by the steady-state condition equation:

$$W(X, Y) = 0. \tag{16}$$

The problem is proposed to be solved in two stages: entering the mode into the permissible region and determining the minimum of the target function in the permissible region.

Let there be a problem of entering the mode into the permissible region. With $Y^{(0)}, X = X^{(0)}$ is calculated from equation (16). Corrections ΔX to initial approximation vector $X^{(0)}$ are determined by the equation:

$$\frac{\partial W}{\partial X} \Delta X = -W, \tag{17}$$

where $\partial W / \partial X$ is the matrix of particular derivative functions.

Based on (15), the gradient is calculated:

$$\frac{\partial H}{\partial Y} = \frac{\partial H}{\partial Y} \Big|_0 = \frac{\partial H}{\partial X} \frac{\partial X}{\partial Y}, \tag{18}$$

where

$$\frac{\partial X}{\partial Y} = \left[\frac{\partial W}{\partial X} \right]^{-1} \frac{\partial W}{\partial Y}. \tag{19}$$

The permissible vector of descent (V) is obtained from the gradient by replacing with zeros the components of the corresponding variables that are on the boundary and tend to go beyond the permissible limits and change the sign of the remaining components.

The following approximation of vector Y :

$$Y^{(1)} = Y^{(0)} + Vt = Y(t), \tag{20}$$

where $t = \min(t_n, t_{ul})$.

Value t_n is determined by the Newton method from expression:

$$V \frac{\partial H}{\partial Y}(t) = 0. \tag{21}$$

Ultimate increment $t_{ul} = \min(t_{iul})$ is the solution of the equation:

$$Z_i[Y(t)] - Z_{iul} = 0, \quad (22)$$

where

$$Z_{iul} = \begin{cases} Z_{iul_{max}} & \text{at } \frac{\partial Z}{\partial t} < 0, \\ Z_{iul_{min}} & \text{at } \frac{\partial Z}{\partial t} > 0. \end{cases} \quad (23)$$

The end of the computational optimization process is controlled by value V , taking into account the changes in vector Y and $И(Y)$ over a number of successive approximations.

The disadvantages of this method include worsening of convergence when approaching the minimum of the target function, as well as the complexity of the algorithm and the labor intensity of its implementation.

To take into account inequality-type constraints when applying gradient methods, it is proposed to use the penalty function method.

In the literature, a network of gradient-based optimization methods is given and their comparative characteristics are provided.

The most powerful optimization method based on the first-order gradient method is designed to solve problems minimizing the function:

$$И = \sum_{i=1}^k И_i(X). \quad (24)$$

Compared to the reduced gradient method, the steady-state equation is written in the form of explicit functions, and the functional constraints are controlled by penalty functions, whereas in the reduced gradient method they are controlled by changing the basis, i.e., by exchanging variables of vectors X and Y .

Optimization methods of the second direction have been widely used in numerous studies.

A method of solving the problem of integrated optimization is known. The basic idea is to modify an initially nonlinear problem with constraints into a sequence of problems without constraints, whose solution approaches the solution of the original problem. The modified problem is solved by the Fletcher–Powell method [19].

Different methods of modifying the original problem are analyzed in scientific papers. The analysis of the Fiacco and McCormick, Zangwill, and Powell [20] methods showed the expediency of the latter two methods as not requiring an initial point satisfying inequality-type constraints.

Using the Zangwill’s transformation corresponding to the application of penalty functions, the following unconstrained function is formulated:

$$F(X) = И(X) + \sum_{i=1}^r r_i \cdot W_i(X)^2 + \sum_{j=1}^p r_j \cdot g_j(X)^2. \quad (25)$$

In equation (25), term $g_j(X)$ representing an inequality-type constraint exists only when this constraint is violated.

According to the Fletcher–Powell method, for quadratic function $f(X)$ the following ratio is true:

$$f(\bar{X} - X) = l_j g(X), \quad (26)$$

where \bar{X} is the point of maximum; l_j is the reverse matrix of the second partial derivatives of function $f(X)$, called the Hesse matrix; $g(X)$ is the vector of the first partial derivatives of function $f(X)$.

The difference in the left-hand side of ratio (26) represents the distance between any point X and the point of minimum. For a non-quadratic function, \bar{X} is not an exact minimum, but this point can be considered as an initial approximation for the sequential iteration by expression (26).

Matrix l_j is obtained iteratively by an algorithm that requires only the first derivatives of the target function. After determining ΔX and a new point of matrix l_j , which was initially singular, matrix l_j is recalculated by adding the coefficient matrices to it:

$$l_j^{(i+1)} = l_j^{(i)} + A^{(i)} + B^{(i)}, \quad (27)$$

where

$$B_{jk}^{(i)} = \frac{(l_j^{(i)} Y^{(i)})_j (Y^{(i)T} l_j^{(i)})_k}{Y^{(i)T} l_j^{(i)} Y^{(i)}},$$

$$A_{jk}^{(i)} = \frac{\Delta X_j^{(i)} \Delta X_k^{(i)}}{\Delta X^{(i)T} Y^{(i)}},$$

$$Y^{(i)} = \frac{\partial f^{(i+1)}}{\partial X} - \frac{\partial f^{(i)}}{\partial X}.$$

The peculiarity of the Fletcher–Powell method is that there is no need to compute the inverse matrix of the second partial derivatives.

The disadvantages of the method include: (1) the Hesse matrix shall be permanently stored in the computer core memory and changed at each step of the algorithm; (2) when solving problems with a large number of variables, changes in matrix l_j may be insufficient to obtain such values of ΔX that would reduce $f(X)$.

To eliminate these disadvantages, the idea of direct estimation of the Hesse matrix is proposed:

$$H \Delta X = g(X), \quad (28)$$

where H is the Hesse matrix.

Equation (28) is solved relative to ΔX using Gauss elimination, which consists in reducing the system to a triangular form. The main disadvantage of the method is its dependence on the choice of the starting point.

Statistical methods for optimizing power supply systems are outlined and have been developed by D.A. Arzamastsev [21]. The formulation of the problem of the electric grid mode complex optimization is con-



sidered. The combination of random search with the penalty function method makes it possible to determine conditional extrema for the problem of optimization of the electrical grid and system operation mode.

In the permissible region of the k -factor space under study, starting point $X^{(0)}$ is chosen with coordinates $X_1^{(0)}, X_2^{(0)}, \dots, X_k^{(0)}$, and the value of target function $T^{(0)}$ is calculated in it. To move to new point $X^{(1)}$ with coordinates $X_1^{(1)}, X_2^{(1)}, \dots, X_k^{(1)}$, a random vector is selected, which is evenly distributed over a hyposphere of radius h with the center in the coordinate origin:

$$\Delta\bar{X}^{(0)} = (\Delta X_1^{(0)}, \Delta X_2^{(0)}, \dots, \Delta X_k^{(0)}). \quad (29)$$

Coordinates of point $X^{(1)}$ are determined by summing up two vectors:

$$\bar{X}^{(1)} = \bar{X}^{(0)} + \Delta\bar{X}^{(0)}. \quad (30)$$

The value of the target function in point $X^{(1)}$ is equal to $T^{(1)}$.

The completed step is considered successful and point $X^{(1)}$ is accepted if the following condition is fulfilled:

$$T^{(1)} < T^{(0)}. \quad (31)$$

Otherwise, point $X^{(1)}$ is not accepted. Once again a random vector is selected and a new attempt to make a successful step is made. The process of transfer from point $X^{(1)}$ to point $X^{(2)}$ is performed in the same way.

The advantage of the random search method is the simplicity of the structure of program implementation on the computer, high reliability and efficiency in solving many nonlinear programming problems. It is the only method capable of solving multiextremal problems. It is especially effective in the absence of analytical expressions for the gradient. At the same time, when approaching the minimum of the target function using the random search algorithm, the number of unsuccessful steps increases, so it is advisable to do refinement near the extremum using some deterministic optimization method, such as gradient.

A variety of the random search method is the random descent method.

When determining the minimum of the target function according to a random descent algorithm, the direction of motion is generally given by a random vector uniformly distributed over a hyposphere.

However, unlike the random search algorithm, the direction is not chosen at every step. In the randomly selected successful direction, a number of working steps are performed until the function starts to increase. At the resulting point, a successful direction is selected again, and descent is performed in that direction until it is exhausted, and so on. Thus, a descent to the region of the required minimum is performed.

Conclusion

The existing power supply schemes of open-pit mines have been analyzed from the standpoint of the accident rate of separate network components and electrical equipment of open pits and the influence of various disturbing factors on it. The analysis for all main components of open-pit power supply schemes showed that the time of emergency downtime and the time of emergency shutdown is subject to the log-normal distribution, and the standard of the modifying function argument practically keeps a constant value. The conducted analyses show that the annual durations of emergency downtime of open-pit electrical equipment are also distributed according to the log-normal distribution and the values of the modified argument standard have deviations not exceeding 20% of the determined standard mean value of 0.347. The method of reliability analysis of schemes for several variants has been developed. It consists in determining the probability of power supply interruption to each receiver (substation), taking into account the capacities of individual scheme sections and individual loads in relation to their total capacity. Methods of optimizing the open-pit power supply systems are presented, which consist in the use of first-order gradient methods, second-order methods or the so-called quadratic optimization methods, and random search methods. A group of gradient methods is the most widespread for solving nonlinear programming problems, among which the method of steepest descent should be considered primarily. The method of random descent, which consists in determining the minimum of the target function according to an appropriate algorithm, is also considered, in which the direction of motion is generally given by a random vector uniformly distributed over a hyposphere.

References

1. Pirogov G.G. The principles of opening ore deposits in the development on the basis of underground mining complexes. *Scholarly Notes of Transbaikal State University. Series Physics, Mathematics, Engineering, Technology*. 2017;12(4):73–79. (In Russ.) <https://doi.org/10.21209/2308-8761-2017-12-4-73-79>
2. Kaplunov D.R., Lomonosov G.G. Main problems of subsoil development during underground mining of ore deposits. *Gornyi Zhurnal*. 1999;(1):42–45. (In Russ.)
3. Tugai Yu.I., Gai A.V., Stachniuk S.V. The model's construction of power system reliability based on using Monte Carlo simulation. *Agrotekhnika i Energoobespecheniye*. 2015;1(5):96–107. (In Russ.)



4. Ershov S.V., Demyanov D.V. The definition of indicators of system of power supply enterprise. *Izvestiya Tula State University. Technical Science*. 2017;(12–1):118–125. (In Russ.)
5. Corrigan C.C., Ikonnikova S.A. A review of the use of AI in the mining industry: Insights and ethical considerations for multi-objective optimization. *The Extractive Industries and Society*. 2024;17:101440. <https://doi.org/10.1016/j.exis.2024.101440>
6. Yaakoubi Y., Dimitrakopoulos R. Learning to schedule heuristics for the simultaneous stochastic optimization of mining complexes. *Computers & Operations Research*. 2023;159:106349. <https://doi.org/10.1016/j.cor.2023.106349>
7. Suslov N.M., Chernukhin S.A., Suslov D. N. Increasing energy efficiency of walker dragline. *News of the Ural State Mining University*. 2020;(3):131–139. (In Russ.) <https://doi.org/10.21440/2307-2091-2020-3-131-139>
8. Klyuev R.V., Bosikov I.I., Gavrina O.A., Lyashenko V.I. Assessment of operational reliability of power supply to developing ore mining areas at a high-altitude mine. *Mining Science and Technology (Russia)*. 2021;6(3):211–220. (In Russ.) <https://doi.org/10.17073/2500-0632-2021-3-211-220>
9. Petrov V.L., Pichuev A.V. Hazard assessment of asymmetric modes for leakage current flowing through insulation in underground mine electrical grids. *Energy Safety and Energy Economy*. 2022;(5):15–22. (In Russ.)
10. Klyuev R.V., Golik V.I., Bosikov I.I., Gavrina O.A. Ensuring electrical safety of a mountain quarry by choosing selective relay protection in the electrical networks with the voltage above 1 kV. *Occupational Safety in Industry*. 2021;(9):31–37. (In Russ.) <https://doi.org/10.24000/0409-2961-2021-9-31-37>
11. Pelipenko M.V., Balovtsev S.V., Aynbinder I.I. Integrated accident risk assessment in mines. *Mining Informational and Analytical Bulletin*. 2019;(11):180–192. (In Russ.) <https://doi.org/25018/0236-1493-2019-11-0-180-192>
12. Kulikova E.Yu., Balovtsev S.V. Risk control system for the construction of urban underground structures. In: *IOP Conference Series: Materials Science and Engineering. International Conference on Construction, Architecture and Technosphere Safety (ICCATS 2020)*. 6–12 September 2020, Sochi, Russia. 2020;62(4):042020. <https://doi.org/10.1088/1757-899X/962/4/042020>
13. Cabral E.A., Tofoli F.L., Sampaio R.F., Leão R.P.S. Reliability assessment applied in the design of an industrial substation in the context of Industry 4.0. *Electric Power Systems Research*. 2024;231:110365. <https://doi.org/10.1016/j.epsr.2024.110365>
14. Singh K., Kalra Sh. Reliability forecasting and accelerated lifetime testing in advanced CMOS technologies. *Microelectronics Reliability*. 2023;151:115261. <https://doi.org/10.1016/j.microrel.2023.115261>
15. Jia Q., Fu G., Xie X. et al. Enhancing accident cause analysis through text classification and accident causation theory: A case study of coal mine gas explosion accidents. *Process Safety and Environmental Protection*. 2024;185:989–1002. <https://doi.org/10.1016/j.psep.2024.03.066>
16. Li W., Wang L., Ye Zh. et al. A dynamic combination algorithm based scenario construction theory for mine water-inrush accident multi-objective optimization. *Expert Systems with Applications*. 2024;238(A):121871. <https://doi.org/10.1016/j.eswa.2023.121871>
17. Pevzner L.D., Kiselev N.A. Automatic control system for walking dragline excavator digging. *Mining Science and Technology (Russia)*. 2022;7(1):57–65. <https://doi.org/10.17073/2500-0632-2022-1-57-65>
18. Sokolov A.A., Orlova L.G., Bashmur K.A. Ensuring uninterrupted power supply to mining enterprises by developing virtual models of different operation modes of transformer substations. *Mining Informational and Analytical Bulletin*. 2023;(11–1):278–291. (In Russ.) https://doi.org/10.25018/0236_1493_2023_111_0_278
19. Yokoyama K., Yoshii A., Adachi T., Kasai R. Application of Fletcher-Powell's optimization method to process/device simulation of MOSFET characteristics. *Solid-State Electronics*. 1982;25(3):201–203. [https://doi.org/10.1016/0038-1101\(82\)90108-3](https://doi.org/10.1016/0038-1101(82)90108-3)
20. Sieniutycz S., Jeżowski J. 1 – Brief review of static optimization methods. In: *Energy Optimization in Process Systems and Fuel Cells*. 3rd Edition. Elsevier; 2018. Pp. 1–41. <https://doi.org/10.1016/B978-0-08-102557-4.00001-3>
21. Misrikhanov M.Sh., Rusina A.G. Innovative approach to solving regime problems in managing electric power systems. *Vestnik of Ivanovo State Power Engineering University*. 2012;(3):22–27. (In Russ.)

Information about the author

Roman V. Klyuev – Dr. Sci. (Eng.), Assistant Professor, Professor of the Department of Engineering and Technology of Mining and Oil and Gas Production, Moscow Polytechnic University, Moscow, Russian Federation; ORCID [0000-0003-3777-7203](https://orcid.org/0000-0003-3777-7203), Scopus ID [57194206632](https://scopus.org/57194206632); e-mail kluev-roman@rambler.ru

Received 13.03.2024

Revised 17.04.2024

Accepted 10.05.2024